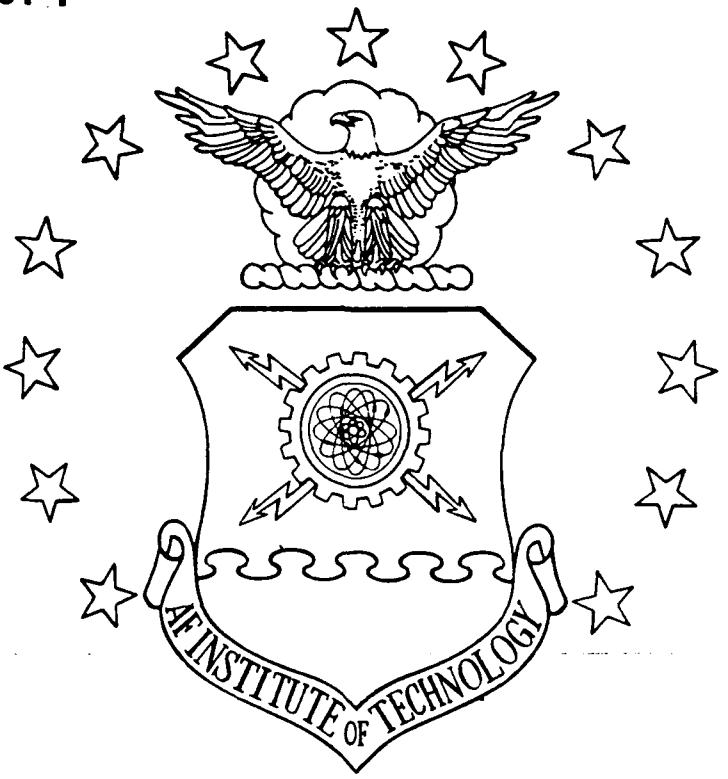

DEFECTS ASSOCIATED WITH THE INCORPORATION OF GERMANIUM IN GALLIUM ARSENIDE

DISSERTATION

Kevin J. Keefer
Captain, USAF

AFIT/DS/ENP/90-1

DEPARTMENT OF THE AIR FORCE
AIR UNIVERSITY
AIR FORCE INSTITUTE OF TECHNOLOGY

Wright-Patterson Air Force Base, Ohio

AFIT/DS/ENP/90-1

DEFECTS ASSOCIATED WITH THE INCORPORATION OF GERMANIUM IN GALLIUM ARSENIDE

DISSERTATION

Kevin J. Keefer
Captain, USAF

AFIT/DS/ENP/90-1

Approved for public release; distribution unlimited.

AFIT/DS/ENP/90-1

DEFECTS ASSOCIATED WITH THE INCORPORATION OF GERMANIUM IN GALLIUM ARSENIDE

DISSERTATION

Presented to the Faculty of the School of Engineering
of the Air Force Institute of Technology
Air University
In Partial Fulfillment of the
Requirements for the Degree of
Doctor of Philosophy

Kevin J. Keefer, B.S., M.S., M.S.
Captain, USAF

June, 1990

AFIT/DS/ENP/90-1

DEFECTS ASSOCIATED WITH THE INCORPORATION OF GERMANIUM IN GALLIUM ARSENIDE

Kevin J. Keefer, B.S., M.S., M.S.

Captain, USAF

Approved:

Yung Kee Yeo, chairman 25 May '90

Robert L Hengehold 25 May '90

Edward S. Kolesar 25 May '90

Donald C. Reynolds 25 May 90

25 May 1990

Interim Dean, School of Engineering

Acknowledgments

This dissertation was completed with the support and encouragement of many people. I would like to thank Dr. Yung Kee Yeo and Dr. Robert L. Hengehold for assistance and encouragement rendered; thanks also for assistance provided by Jeff Cavins (who also developed important computer software for data collection and reduction), Gernot Pomrenke, Jose Colon, Bill Evans, Leroy Cannon, Greg Smith, Rick Patton and Walt Pemberton. I especially wish to thank my wife, Julie, and daughter, Ann, for their love, support and sacrifice during this challenging program. I also thank God for bringing these and others to my assistance.

Kevin J. Keefer

Table of Contents

List of Figures

List of Tables

List of Symbols

Symbol	Definition	Page
E_g	Bandgap Energy	2-1
ϵ	Static Dielectric Constant	2-2
CCC	Central Cell Correction	2-5
LEC	Liquid Encapsulated Czochralski	2-7
PL	Photoluminescence	2-13
SPL	Selective Pair Luminescence	2-13
LO	Longitudinal Optic	2-22
TO	Transverse Optic	2-22
TA	Transverse Acoustic	2-22
R_p	Projected Range	2-39
LO_1	LO Raman Peak	4-8
m-lines	Modal Lines	4-8
EMA	Effective Mass Acceptor	4-21

Abstract

Above and below bandgap excitation studies were performed on GaAs samples implanted with Ge to assess the nature of impurities and defects associated with the incorporation of this element. In addition, dual implanted GaAs samples ({Ge+Ga} and {Ge+As}) were also investigated to further facilitate the characterization and identification of probable stoichiometric defects. The luminescence results are presented for samples implanted with various doses of ions spanning 1E13–1E15 cm^{-2} at an energy of 120 keV, and annealed for 15 minutes at a temperature of 900°C.

The above-gap excitation luminescence of Ge-only and {Ge+Ga}-implanted layers was seen to be critically dose-dependent. At doses of 1E13–3E13 cm^{-2}, a broad band dominated the luminescence spectrum in the 1.47–1.42 eV range, and it was assigned as the Q band, which was assigned previously to similar luminescence activity in Si-doped GaAs. At higher doses (1E14–1E15 cm^{-2}), however, the Q band was no longer observed for the Ge-only implanted samples, whereas evidence for transitions involving the Ga_{As} double acceptor at ~1.445 eV was collected for the {Ge+Ga}-implanted samples. The luminescence resulting from {Ge+As} dual implanted samples showed no Q band nor Ga_{As}-related transitions. The absence of the Ga_{As} double acceptor is expected, based on stoichiometric arguments, upon implantation with As.

Below-gap excitation, in conjunction with temperature-dependent studies, enabled resolution of the broad Q band into high- and low-energy components. The low-energy component, located at about 1.447 eV, was assigned to the Ga_{As} double acceptor and determined to originate mainly from a combination of (e, Ga_{As}) transitions with some contribution from (D^o, Ga_{As}) transitions occurring amongst distant pairs. The high-energy component, which peaked at ~ 1.456–1.458 eV,

was also mainly due to $(D^{\circ}, \mathrm{Ga_{As}})$ transitions, which were described according to a close donor-acceptor pairs model. This newly derived model assumed that the relatively strong binding energy of the $\mathrm{Ga_{As}}$ double acceptor allowed increased numbers of $(D^{\circ}, \mathrm{Ga_{As}})$ transitions to occur amongst relatively close pairs. Thus, the $(D^{\circ}, \mathrm{Ga_{As}})$ pair luminescence was able to take place over a sufficiently broad energy range such that its peak could, in fact, occur at higher energy than the $(e, \mathrm{Ga_{As}})$ luminescence. The sensitivity of the Q band's intensity and exact spectral position seemed to depend on the relative concentrations of $\mathrm{Ga_{As}}$ double acceptors and donors. These concentrations, in turn, would likely depend greatly on ion doses and the combinations of Ge (an amphoteric impurity), Ga and As.

Below-gap excitation provided other supplementary pieces of information about the samples under investigation. Acceptor excited states associated with Ge were definitely observed to arise from the implantation of the element. In addition, the apparent excited states of the g and $\mathrm{Mn_{Ga}}$ acceptors were observed for the first time from selective pair luminescence data. The $1S_{3/2} - 2S_{3/2}$ energy splitting associated with the $\mathrm{Mn_{Ga}}$ acceptor was determined to be about 87.4 meV. Finally, a relatively new peak at $\sim$1.467 eV, best seen with below-gap excitation, was determined to arise from D°-A° pair recombinations, but whose exact origin is otherwise not known at present.

DEFECTS ASSOCIATED WITH THE INCORPORATION OF GERMANIUM IN GALLIUM ARSENIDE

I. Introduction

Increased effort is being expended on the characterization and implementation of new compound semiconductor materials and their ternary modifications to supplement, and in some cases replace, the older silicon (Si) technology. This thrust is being sustained by the Air Force's continuing high speed signal processing requirements and desire for the development of monolithically integrated optoelectronic circuits. Particular attention has been focused on gallium arsenide (GaAs), and rightly so. The effective mass of electrons in GaAs is only 7% of that in Si, leading to higher operating speeds for GaAs devices. GaAs also has a direct bandgap that is larger than the indirect gap of Si, making it especially useful for operation at higher temperature and for optoelectronic devices such as light-emitting diodes and lasers. Some of the electronic and physical properties for GaAs are provided in Table 1.1. Additional effort has been expended on the study of the ternary and quartenary relatives of GaAs, including $Al_xGa_{1-x}As$ and $In_{1-x}Ga_xAs_{1-y}P_y$, for their use in microwave and optoelectronic devices.

A difficulty is encountered with the use of compound semiconductors. Since compound semiconductors consist of two or more elements with possibly widely different vapor pressures, it is difficult to grow stoichiometrically perfect crystals. In addition, dissociation takes place at temperatures well below the melting point when anneal stages are required during device fabrication. To prevent dissociation, encapsulants are used, or the anneal is performed under a controlled atmosphere.

Table 1.1. Properties of GaAs [11]

Parameter	$T \rightarrow 0$K	$T = 300$K
Lattice Constant (Å)	...	5.65325
Crystal Density (g/cm^3)	...	5.3174
Linear Thermal Expansion Coefficient (K^{-1})	0	5.73×10^{-6}
Specific Heat (mJ/gK)	0.043	327
Band Gap (eV)	1.519	1.424
Static Dielectric Constant	12.40	12.85
Electron Effective Mass (m_o)	0.067	0.063
Light-hole Effective Mass(m_o)	0.082	0.076
Heavy-hole Effective Mass(m_o)	0.51	0.50
TO Phonon Energy (meV)	33.81	33.25
LO Phonon Energy (meV)	36.57	36.13

Nevertheless, stoichiometric defects such as vacancies, interstitials and antisites are common in the III-V semiconductor materials.

It is important that intentional doping of the III-V materials, to obtain *n*- or *p*-type electrical behavior, not be affected by stoichiometric defects. Such defects may affect device properties by their intrinsic electrical behavior. The defect may act as a donor or acceptor. Examples of such defects in GaAs are arsenic (As) localized at a gallium (Ga) site (As_{Ga}) and Ga localized at an As site (Ga_{As}). These antisite defects, in fact, act as deep double donors and acceptors, respectively. In addition, defects can affect the properties of a device by interacting directly with the dopants. Defects, such as As or Ga vacancies (V_{As} or V_{Ga}), may create complexes with the dopants, thus compensating their simple donor or acceptor behavior. The presence of these vacancies also provide sites for the dopant to occupy, thus insuring donor and/or acceptor activation. The role that these interactions play seems especially intriguing in the case of amphoteric dopants such as carbon (C), Si or germanium (Ge) which otherwise could create *n*- or *p*-type layers. An investigation of these defects, then, is principally motivated by the fact that such defects can affect carrier concentrations and ultimately threshold voltages in field effect transistors, light-emitting diodes and semiconductor lasers. Also, these defects can act as nonradiative recombination centers to degrade the internal quantum efficiency of optoelectronic devices.

The present research was concerned mainly with defects found in the III-V material, GaAs, following the incorporation of the Group IV element, Ge. Ge is important to consider because of its availability as a dopant in GaAs. Its amphoteric nature has been used to advantage for routine growth of p/n junctions by molecular beam epitaxy (MBE) [53:5781]. In fact, Ge, as a dopant in MBE GaAs layers, is more amphoteric than other Group IV elements (including Si and tin (Sn)), and dopant densities in excess of 10^{19} cm^{-3} have been attained [1:629]. In addition, Ge doping has been used to produce ohmic contacts to *n*-type GaAs which are stable,

reliable and reproducible [53:5781]. However, it was demonstrated early that GaAs *implanted* with Ge, rather than chemically doped with this element, exhibited very complicated electrical behavior [15, 80].

It was discovered that the *n*- or *p*-type activity of Ge-implanted GaAs depended on several parameters such as ion dose, implant temperature and anneal temperature. Yeo *et al.* [80] performed room temperature implants at an energy of 120 keV with doses ranging from 5E12 to 3E15 cm^{-2}. Anneals were conducted for 15 minutes at 700°–950°C. It was found that the implanted layer was *p*-type for doses of $\sim$ 1E14 cm^{-2} or below. This was true for all anneal temperatures. The implanted layer was *n*-type for doses greater than or equal to 1E15 cm^{-2} and all anneal temperatures. For the intermediate dose of 3E14 cm^{-2}, the implanted layer was *n*- or *p*-type depending upon the anneal temperature. The layer was *p*-type for anneals up to and including 900°C, and *n*-type for anneals at 950°C. Chan *et al.* also found that layers were *n*- or *p*-type depending upon the dose or anneal temperature when using room temperature implants. However, the dose and anneal temperature dependence disappeared when the implants were performed at 100°C or -100°C (all layers were *n*- or *p*-type, respectively). Additional studies by Pedrotti *et al.* [53] and Yeo *et al.* [81], with dual implantation of either {Ge+Ga} or {Ge+As} demonstrated that the aforementioned effect that the implant dose and anneal temperature had on the electrical behavior could be modified. The Ga enhanced *p*-type activity, and the As enhanced *n*-type activity.

To try to improve the understanding of the physical processes in GaAs layers implanted with Ge, it is necessary to apply additional experimental techniques. One such technique is photoluminescence. The technique, using above bandgap excitation, has already been applied to Ge-implanted layers in a study by Yu [83]. It was discovered that, in addition to the conventional shallow transitions for the Ge impurity in GaAs, deeper transitions at $\sim$ 1.4 eV were also observed. As will be discussed in future chapters, many possible defect centers (all of which involve

stoichiometric defects) have been speculated to contribute to luminescence at ~ 1.4 eV in GaAs. To add to the complexity, the ~ 1.4 eV luminescence may be broad, making assignment difficult.

In this research, the techniques of both above and *below* bandgap excitation of Ge-implanted GaAs layers are used to facilitate identifying impurities and defect centers which subsequently arise from the incorporation of Ge. Below bandgap (or below-gap) excitation has been used mainly for the technique of selective pair luminescence. As will be shown, this technique provides an excellent means of identifying shallow, hydrogenic impurities, especially acceptors, in GaAs. In this study, below-gap excitation will also be used to alter oscillator strengths of transitions involving the defect centers to improve spectral resolution. This, in turn, will improve the potential for identification. Dual implanted layers ({Gc+Ga} and {Ge+As}) are also investigated to further assist in the characterization and identification of probable stoichiometric defects. One such defect given particular scrutiny is the Ga_{As} double acceptor.

II. Background

Energy States in Semiconductors

Many of the electrical and optical properties of semiconductor materials derive from the basic notion that the materials' electronic energy structure includes bands of allowed energy levels. Ashcroft and Mermin [3:Ch 9-11] present derivations of these bands. Approximations such as the tight-binding, nearly free-electron and Orthogonalized Plane Wave methods, and combinations thereof, may be applied depending upon the particular material. The following sections will expand upon this basic property by looking at the *intrinsic* and *extrinsic* semiconductors in turn.

Intrinsic Semiconductors. The intrinsic (pure) semiconductor is essentially characterized by the energy gap (E_g) separating the top of the highest filled (valence) band and bottom of the lowest empty (conduction) band. In GaAs, the bottom of the conduction band and top of the valence band are spherically symmetric, parabolic and separated in energy by 1.5192 ± 0.0002 eV at 0K [61]. The conduction band minimum (with Γ_6 symmetry) occurs at the same point in k-space ($\vec{k} = 0$) as the valence band maximum, making GaAs a direct bandgap material. A portion of the energy band structure of GaAs is shown in Figure 2.1, where E_c and E_v refer to the energy of the conduction band minimum and valence band maximum, respectively. The valence band maximum for GaAs (with Γ_8 symmetry) consists of two degenerate sub-bands with different curvatures, giving rise to *light* and *heavy* holes. Each sub-band itself has twofold spin degeneracy. Located slightly below this extremal point, is a third sub-band, with a twofold spin degenerate maximum of Γ_7 symmetry, which has been split-off by the spin-orbit interaction. (In the absence of spin-orbit splitting, the valence band would be sixfold degenerate at $\vec{k} = 0$).

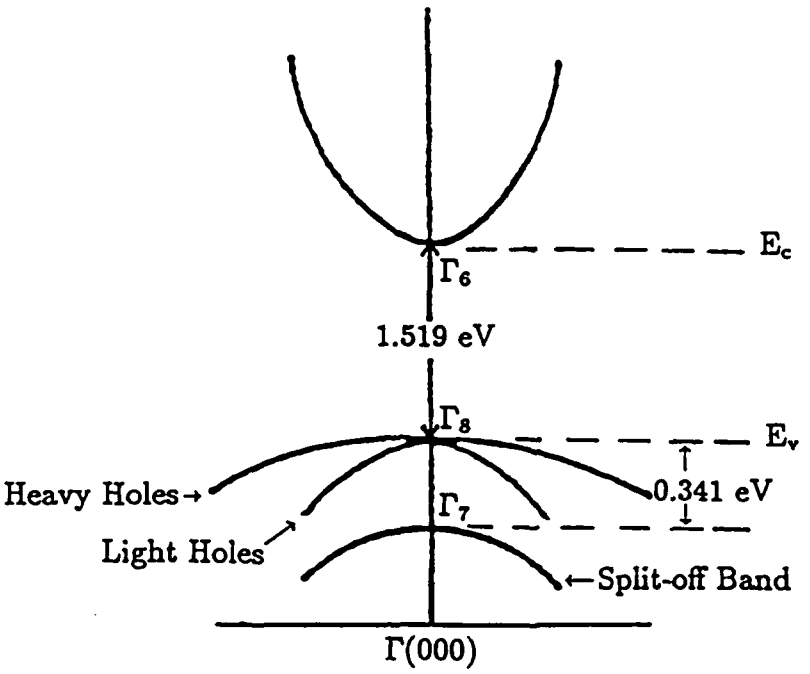

Figure 2.1. Energy Bands in GaAs

Although the population of electrons in the conduction band is zero at 0K, valence band electrons, upon absorption of energy greater than or equal to the energy gap, can be excited into the conduction band. A positive charged hole would be left in the valence band for every electron which transitions to the conduction band. The electron and hole can orbit about each other because of their Coulomb interaction, and would travel throughout the crystal as a pair. This electron-hole pair (free exciton) is nicely modelled using the hydrogen atom.

The hydrogen-like approximation derives appropriate states for the free exciton by accounting for the polarizable crystal background. This is accomplished in two ways. First, the polarizable background screens the charge interaction which requires that the expression for the Coulomb potential be reduced by the static dielectric constant (ϵ). The potential is written

$$V_{\text{Coulomb}} = \frac{-e^2}{\epsilon r} \tag{2.1}$$

where r is the separation distance between electron and hole. Secondly, the masses

of the charged particles are replaced by their respective effective masses. The effective mass accounts for the fact that the particle's dynamics are no longer derived from a free-space momentum, but rather, with the *crystal momentum.* Thus, the overall approach is termed the effective mass approximation. In direct analogy, then, with the hydrogen atom problem, the exciton's ionization energy is given by

$$E_{ex} = \frac{13.6m^*}{m_o n^2 \epsilon^2} \text{ eV} \tag{2.2}$$

where $n = 1, 2, 3, \ldots, \infty$, m_o is the rest mass of the electron, m^* is the reduced effective mass defined as

$$\frac{1}{m^*} = \frac{1}{m_e} + \frac{1}{m_h} \tag{2.3}$$

and m_e and m_h are the electron and hole effective masses, respectively. The ionization energies correspond to the separation between the exciton's ground or excited states and the conduction band. The free exciton's ground state binding energy is calculated to be 5.2 meV using $m_e = 0.067m_o$, $m_h = 0.51m_o$ and $\epsilon = 12.40$ from Table 1.1. Experimental evidence has shown that the exciton's ground state lies 4.2 ± 0.2 meV below the conduction band [61]. There is good agreement between the theory and experiment.

Thus, applied heat, voltage or photons alters the electrical properties of an intrinsic semiconductor by creating electronic levels in the energy gap and electron (hole) populations in the conduction (valence) band. Almost invariably, though, one must resort to adding impurities to the crystal to achieve essential, well controlled, electrical characteristics for a particular application.

Extrinsic Semiconductors. An extrinsic semiconductor, one in which impurity atoms or defects are either non-intentionally or intentionally introduced, presents a more intricate energy structure. An impurity introduced substitutionally, replacing the crystal's atoms, can be classified as a donor or acceptor. This depends upon the relative valency of the impurity and atoms which comprise the

crystal. Donors have a higher chemical valence than the atoms of the host lattice while acceptors are of lower valence. The Ge donor in GaAs, residing on the Ga sublattice, contributes three of its four valence electrons to complete covalent bonds with neighboring As atoms. One electron remains loosely bound to the Ge atom. The Ge acceptor resides on the As sublattice with all four of the Ge's valence electrons being used to complete the covalent bonds with four neighboring Ga atoms. The fifth covalent bond is not complete; the missing electron is interpreted as a hole loosely bound to the Ge atom. Another class of substitutional impurity is deemed isovalent; its valence is equal to that of the replaced host atom. In addition to these relatively simple *substitutional* impurities, there are other defects which may form complex centers. Typical complex centers include interstitial impurities (those that lodge themselves between lattice sites), such as As or Ga interstitials (As_i or Ga_i), and lattice vacancies.

Substitutional Donors and Acceptors. From the above discussion, it can be inferred that the donors may donate electrons to the crystal's conduction band, thereby creating free electrons there. The acceptors, on the other hand, may capture electrons from the valence band (completing the acceptor's covalent bonds with neighboring atoms) and so create free holes there. Subsequent to this release or capture of the electron, the donor or acceptor is said to be ionized. It is appropriate, then, to locate the donor levels just below the conduction band and the acceptor levels just above the valence band in the forbidden energy gap. These states are derived from the interaction of the electron (hole) and impurity's core with proper allowance for the polarizable crystal background. To accomplish this task, one must solve the Schrödinger equation for the Hamiltonian

$$H = H_o + V(\vec{r}) \tag{2.4}$$

where H_o is the single-electron Hamiltonian for the ideal lattice, and $V(\vec{r})$ represents the potential describing the electron (hole) - impurity interaction. The

following paragraphs briefly introduce one to the theory of substitutional donors and acceptors in semiconductors [5, 52, 66]. Particular emphasis is placed on the *simple* donors and acceptors (those that are singly ionizable).

Donors. In many semiconductors, the donor's excess electron is very loosely bound, and thus, located far from the donor center (as verified below). Therefore, two approximations are reasonable. First, the donor center is represented by a point charge ($+e$), and the attractive force between it and the electron is defined by a Coulomb potential modified by the crystal's polarizable background analagous to the free exciton. That is

$$V(\vec{r}) = V_{\text{Coulomb}} = \frac{-e^2}{\epsilon r} \tag{2.5}$$

A more general form for the potential would be

$$V(\vec{r}) = V_c - \frac{e^2}{\epsilon r} \tag{2.6}$$

where V_c is a short-range potential due to the impurity-specific core whose magnitude and shape contributes in part to the so-called central cell correction (CCC). For shallow impurities, the Coulomb approximation works well. The loosely bound electron orbits the positive charged core as shown in Figure 2.2 for the Ge donor center (where the Ge atom occupies a Ga lattice site). The electron's large orbital radius (relative to the lattice constant) also means that when performing a Fourier expansion of an electronic wave function, the dominant wave vectors will be small compared to the reciprocal lattice vector. Therefore, the electron dynamics will be derived from energies near the bottom of the conduction band where the wave vectors are smallest.

Utilizing these approximations with the effective mass approach, enables one to derive a hydrogen-like Schrödinger equation for the donor's localized electronic states in GaAs. The analysis is also simplified because of the nondegeneracy of the conduction band. Solutions to the Schrödinger equation give binding energies

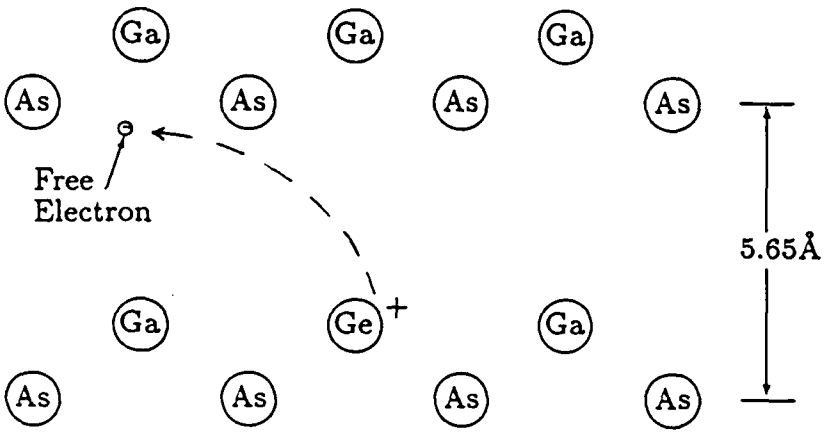

Figure 2.2. Two Dimensional Representation of a Ge Donor in a GaAs Lattice

(referenced to the bottom of the conduction band)

$$E_n = \frac{13.6 m_e}{m_o n^2 \epsilon^2} \text{ eV} \tag{2.7}$$

and effective Bohr radii, a_n, for the orbiting electron of

$$a_n = \frac{a_B \epsilon n^2 m_o}{m_e} \text{ Å} \tag{2.8}$$

where a_B is the Bohr radius of the hydrogen atom.

Using $m_e = 0.067 m_o$ and $\epsilon = 12.40$, the electron in the donor ground and the first excited state has a theoretical ionization energy of 5.9 and 1.5 meV, respectively. Table 2.1 shows that the effective mass theory satisfactorily predicts experimentally observed donor ionization energies in GaAs. The disadvantage of the theory is that it does not differentiate between donor species. A better approximation to the core potential (one which is impurity specific) would help to model the chemical shifts. The agreement between theory and experiment, however, is even better (and to be expected since the core potential drops off and plays a lesser

Table 2.1. Ground State Energies of Selected Donors in GaAs [8:1133]

Donor	E_{1S} (meV)
Ge	6.08
Si	5.81
Sn	5.87
S	6.1
Se	5.87

role) for the case of donor excited states. The ionization energy for an electron in the donor $2S$-state was observed to be 1.44 meV [8:1133]. More recent results collected by Paget and Klein [50] indicated greater discrepancies between theory and experiment. For example, a continuous distribution of donor ground state energies between 5.8 and 12 meV were found in liquid-encapsulated Czochralski (LEC) grown, (apparently un-doped) semi-insulating GaAs. However, Wagner and Ramsteiner [76] have subsequently shown that these large discrepancies were more a function of inadvertant probing of perturbed donor levels.

Lastly, the large effective Bohr radius for the electron in the donor ground state ($a_1 \approx 100$Å) predicted by Eq (2.8) justifies earlier assumptions. The orbit is indeed large relative to the lattice constant of GaAs, which, from Table 1.1, is only about 5.65Å.

Acceptors. As mentioned earlier, a hole is bound to an acceptor in its neutral state. The hole drops into the valence band(s) upon ionization. One may derive the acceptor bound states as was done in the previous section for donor bound states with the effective mass theory using the Coulomb potential screened by the crystal's static dielectric constant. Unfortunately, the situation is quite a bit more complicated for the acceptor case in GaAs as in all zinc-blende-type

semiconductors. One source of complexity arises from the degenerate valence band at the $\vec{k}$=0 extremum. The degeneracy requires consideration of an enlarged set of eigenstates (Bloch functions) satisfying the ideal-lattice Hamiltonian, H_o. In other words, there exists $t > 1$ Bloch functions, ϕ_r, which satisfy the Schrödinger's equation

$$H_o\phi_r = E_o\phi_r \tag{2.9}$$

for $r = 1, 2, \ldots, t$. Derivation of the Schrödinger equation, including the impurity potential, for this degenerate case in the effective mass formalism was performed simultaneously by Kittel and Mitchell [33] and by Luttinger and Kohn [42]. Luttinger [41] pursued the subject further and derived a more compact form for the Schrödinger equation in the two limiting cases of zero and infinite spin-orbit interaction. In the process, he defined the so-called Luttinger parameters; γ_1, γ_2 and γ_3. These are dimensionless constants (also referred to as valence-band parameters) that describe the hole dispersion relation near the center of the Brillouin zone and necessarily are material-dependent [7, 40]. However, it was discovered that even Luttinger's formulations for the Schrödinger equation were difficult to implement in the theoretical calculations.

Baldereschi and Lipari [6, 7, 40] performed additional re-formulations of the acceptor Hamiltonian in which they more fully exploited the strong similarities between impurity centers and atomic and nuclear systems. This allowed use of theorems and techniques developed for angular-momentum theory which enabled easier implementation in theoretical analyses. In addition, Baldereschi and Lipari's approach made possible a meaningful classification of acceptor states, allowing clearer understanding of the acceptor problem. They were the first to write the acceptor Hamiltonian as the sum of a term having strict cubic symmetry and terms which, in addition to having cubic symmetry, are spherically invariant. Noting that the strictly cubic term was small relative to the spherically invariant terms, the former was initially treated as a perturbation and neglected. Thus, the resulting

Table 2.2. Acceptor Energy Spectrum in GaAs Neglecting Cubic Perturbation Term [6:2707]

Eigenstate	Ionization Energy (meV)
$1S_{3/2}$	25.6
$2S_{3/2}$	7.6
$2P_{1/2}$	1.6
$2P_{3/2}$	11.1
$2P_{5/2}$	6.5

Hamiltonian is spherically symmetric and the total angular momentum, $\vec{F} = \vec{L} + \vec{J}$, is a constant of the motion. Accordingly, and of tremendous value, the acceptor eigenstates can be classified analogous to atoms with spin-orbit interaction using the usual hydrogenic quantum numbers. The spin-orbit interaction, of course, introduces a fine structure so that the nS states give rise to $nS_{3/2}$ states and the nP states split into the $nP_{1/2}$, $nP_{3/2}$ and $nP_{5/2}$ states. The theoretical hole ionization energies for these acceptor eigenstates in various semiconductors materials were determined. The results for an acceptor in GaAs, using a static dielectric constant of 12.56, are shown in Table 2.2. By including the cubic perturbation term in the calculation, Baldereschi and Lipari [7] noted that the term lowered the symmetry of the problem such that the acceptor states needed to be classified according to the irreducible representation of the point group O_h. For example, the $S_{3/2}$ states transform like Γ_8^+ and, therefore, are explicitly represented as $nS_{3/2}(\Gamma_8^+)$. Similar explicit representations of the $P_{1/2}$ and $P_{3/2}$ states are used to denote that they transform as Γ_6^- and Γ_8^-, respectively. The inclusion of the cubic perturbation term had a larger effect on the $P_{5/2}$ states as they were split into a twofold degenerate Γ_7^- and fourfold degenerate Γ_8^- state. Thus, the $2P_{5/2}$ state is split into the doublet $2P_{5/2}(\Gamma_7^-)$ and $2P_{5/2}(\Gamma_8^-)$ states. The modified acceptor energy spectrum for

Table 2.3. Acceptor Energy Spectrum in GaAs Including Cubic Perturbation Term [7:1535]

Eigenstate	Ionization Energy (meV)
$1S_{3/2}(\Gamma_8^+)$	25.67
$2S_{3/2}(\Gamma_8^+)$	7.63
$2P_{1/2}(\Gamma_6^-)$	1.60
$2P_{3/2}(\Gamma_8^-)$	11.38
$2P_{5/2}(\Gamma_8^-)$	7.20
$2P_{5/2}(\Gamma_7^-)$	5.33

GaAs that results when the cubic term is included in the calculation, is presented in Table 2.3. Experimental data (resulting from photoluminescence and two-hole spectroscopy) for the $1S_{3/2}$ and $2S_{3/2}$ states of various acceptors in GaAs is presented in Table 2.4 for an initial evaluation of the theory. The acceptor states' classification according to the irreducible representation of the point group O_h is shown in Table 2.3. To simplify the discussion, future acceptor state classification will only be explicitly written/noted for the $2P_{5/2}$ doublet. It is apparent that the theory is unable to account for chemical shifts of the acceptor energy levels. Part of the discrepancy arises from only using the screened Coulomb potential and neglecting any short-range potentials due to impurity-specific cores.

Double Acceptors. From the valency arguments postulated in an earlier section for the simple substitutional impurities, group III elements of the periodic table which substitute on the As site in GaAs may be considered to act as double acceptors. The most extensively studied double acceptor in GaAs is that whose neutral and negatively charged (singly ionized) state is located 78 and 203 meV above the valence band, respectively [63]. Although its identification

Table 2.4. Observed Binding Energies for Various Acceptors in GaAs [4:1051]

Acceptor	$1S_{3/2}$ Binding Energy (meV)	$2S_{3/2}$ Binding Energy (meV)
C	26.0	7.4
Be	28.0	8.2
Mg	28.4	8.3
Zn	30.7	8.9
Si	34.5	9.3
Cd	34.7	9.4
Ge	40.4	...

remains a subject of discussion, much evidence favors assignment to the Ga_{As} [46]. Consistent with the simple donors and acceptors discussed above, the most intuitive understanding results from modelling the impurity in terms of its atomic analogue, which for the double acceptor, would be the helium atom. Moore, *et al.* [46] combined this insight, Baldereschi and Lipari's analyses, and the results for double acceptors in another semiconductor material (germanium), to correlate experimental data for the Ga_{As} double acceptor in GaAs with specific electronic energy levels of the impurity depicted in Figure 2.3.

Complex Centers. As mentioned previously, another class of impurities are those that are deemed complex centers. For the purposes of this research, the discussion will be limited to vacancy-impurity complexes or pairs, specifically those of the form $V_{As} - Ge_{As}$. The complex consists of a vacancy paired with a single *nearest-neighbor* substitutional impurity. The most recent theoretical investigation of such vacancy-impurity complexes was conducted by Myles and Sankey [48]. The distinct disadvantage in treating these centers is that the relatively long-ranged Coulomb potential is no longer adequate because of the relatively tightly

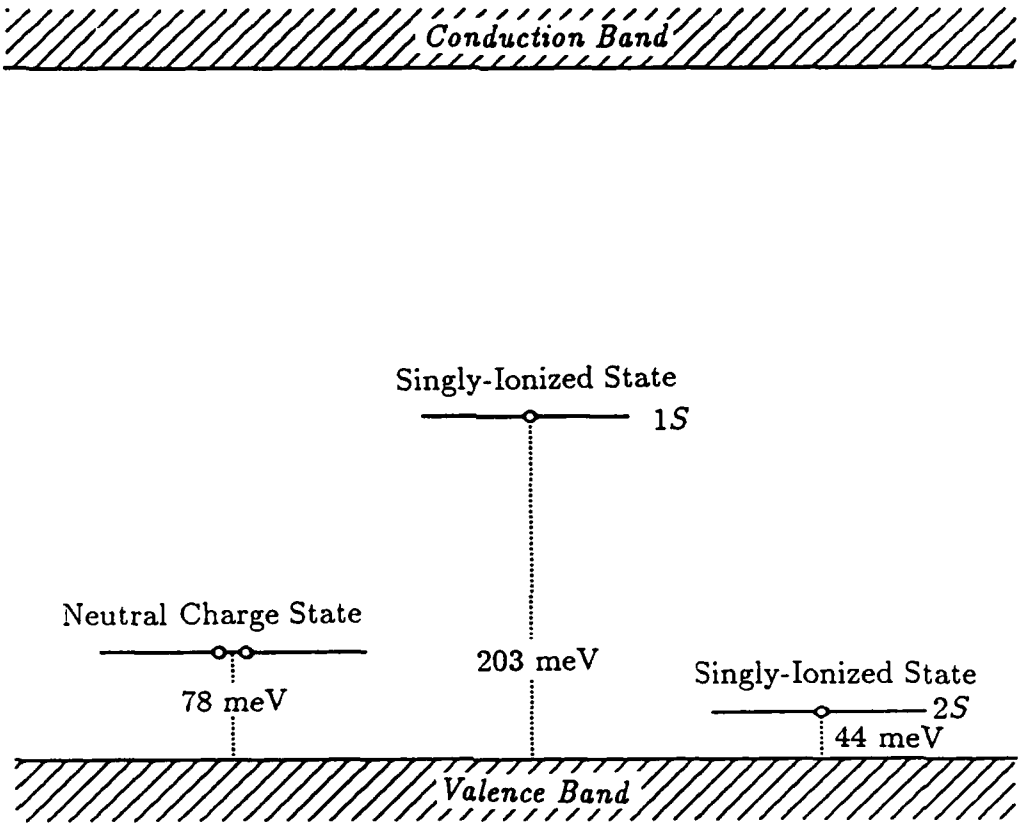

Figure 2.3. Some Electronic Energy Levels of the Ga_{As} [46]

bound electron (hole). Because the bound charge is so tightly bound (and no longer located far from the defect center, as was the case for the simple donors and acceptors described above), the complexes are considered to be localized. Therefore, it is important that the short range, central-cell portion of the defect potential be accurately modelled. In practice, the calculations have been performed from first principles using the tight-binding model to describe both the perfect crystal and the complex [48]. The energy level predictions from these calculations had an uncertainty of a few tenths of an electron volt. Thus, the theoretical work to date has provided only a global view of chemical trends, which, in some cases, may not be sufficient for experimentalists attempting to interpret data. In addition, it has been concluded that the physics of vacancy-impurity complexes remain unclear [48:6822].

Crystal Excitation, Absorption and Emission

Optical characterization relies upon the emission of radiation to investigate impurities and their associated electronic levels described above. There is a variety of techniques which may be employed to investigate these systems. These techniques include optical absorption, photoconductivity, photocapacitance and various types of light scattering [22]. All of the optical techniques have the advantage of being nondestructive. An optical technique that has proven itself useful in the study of many semiconductor materials is that of photoluminescence (PL) [67]. The PL data is obtained with above gap laser excitation. Another closely related luminescence technique employs below gap laser excitation, and it has produced useful results such as selective pair luminescence (SPL), which will be described below. Prior to discussing the radiative transitions which produce the luminescence, it is useful to consider the actual penetration depth of the excitation photon.

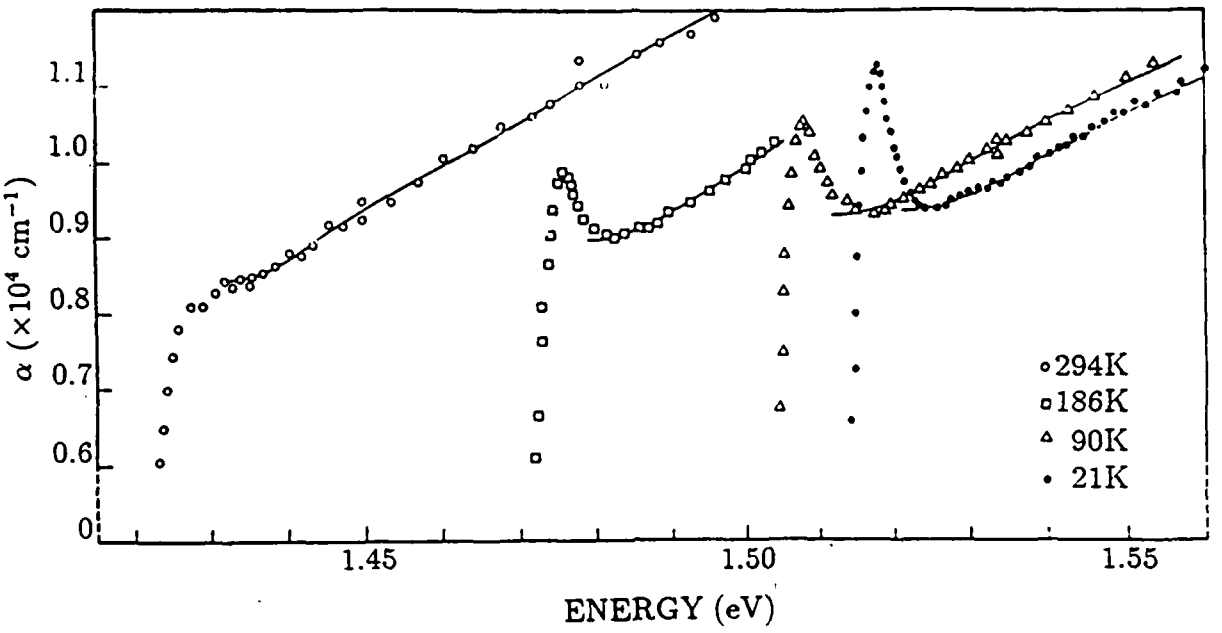

Figure 2.4. GaAs Absorption Characteristics at Various Temperatures [71:771]

Excitation Photon Penetration Depth. The excitation photon flux, F, decreases exponentially with increasing depth of penetration according to the equation [51:87]

$$F(x) = F(0)\exp\left(\frac{-4\pi kx}{\lambda}\right) \tag{2.10}$$

where $F(x)$ is the photon flux at a depth x measured from the surface, $F(0)$ is the flux incident on the surface, k is the extinction coefficient of the solid and λ the photon wavelength. The extinction coefficient may be written in terms of the absorption coefficient, α, as [51:88]

$$k = \frac{\alpha\lambda}{4\pi} \tag{2.11}$$

GaAs absorption data was gathered by Sturge [71:771] and is presented in Figure 2.4. The overall absorption curves have similar shape, especially at the lower temperatures.

Table 2.5. Photon Penetration ($F(x) = 0.37F(0)$) in GaAs at 21K [62:522]

Wavelength (Å)	Extinction Coefficient	Penetration Depth (Å)
4880	0.375	1035
6471	0.145	3550
8100	0.065	9915

The approximate photon penetration depths (the depth at which the photon flux is $1/e$, or ~ 0.37, times the incident flux) for some wavelengths of concern in this investigation are listed in Table 2.5. The respective extinction coefficients are determined from the absorption data collected by Sturge [71] for GaAs at 21K [62:522]. The expression for the temperature dependence of the GaAs bandgap is given by [11:R155]

$$\mathrm{E_g}(T) = 1.519 - \frac{(5.405 \times 10^{-4})T^2}{T + 204} \tag{2.12}$$

Thus, the absorption edge shifts from about 8166 to 8160Å as the temperature decreases from 21 to 2K. Because this shift in the absorption edge of GaAs is small, and the shape of the absorption curves vary little, as was shown in Figure 2.4, the extinction coefficients shown in Table 2.5 are reasonable to use for lower temperatures, such as 2–4K.

For luminescence measurements using below-gap excitation, it is often said that the material is essentially transparent. To verify this, the above calculations could be repeated with knowledge of the extinction coefficients. Unfortunately, such coefficients have been tabulated for temperatures no lower than 90K. However, since the shapes of the GaAs absorption curves in Figure 2.4 vary (with at most a slight increase in the absorption coefficient for below gap photons with decreasing temperature) little with temperature, a reasonable extrapolation of penetration depths at 2–4K might be possible. The extinction coefficients [62:522] (which again were determined from Sturge's absorption data [71]) and calculated penetration

Table 2.6. Below-Gap Photon Penetration ($F(x) = 0.37F(0)$) in GaAs at 90K [62:522]

Wavelength (Å)	Extinction Coefficient	Penetration Depth (μ)
8260	1.55×10^{-2}	4.24
8300	1.44×10^{-3}	45.9
8340	5.08×10^{-4}	131
8380	1.90×10^{-4}	351

depths for below gap photons at 90K (λ greater than $\sim$ 8240Å) are shown in Table 2.6. It is assumed, then, that these penetration depths for 90K provide a reasonable estimate of those at 2–4K, when exciting below the bandgap. Thus, the penetration depth of 8220Å photons (having a wavelength $\sim$60Å larger than that of bandgap photons) at 2–4K will be $\sim$45–50μ (similar to that of the 8300Å photons in Table 2.6).

Photoluminescence. A theoretical treatment of PL is presented by Bebb and Williams [9]. The semiconductor is irradiated with above gap photons, and it subsequently emits radiation in excess of the thermal equilibrium blackbody radiation. PL can be separated into three processes. First, the above gap photons are absorbed, and electron-hole pairs are created. Second, the electron-hole pairs eventually recombine, but not necessarily in the near-surface where they were generated. This is due to the fact that these photo-excited excess carriers have an inhomogeneous spatial distribution within the sample. Therefore, these carriers will have a tendency to diffuse into the sample before recombining, in their attempt to re-establish a uniform distribution. The subsequent and third stage of PL involves the internal emission of photons, resulting from radiative, or a combination of radiative and non-radiative, transitions. These photons escape the sample, if not otherwise absorbed or reflected in the crystal. The absorption coef-

ficient for such photons depends on their energy (wavelength); that is, those with energy below the band gap energy have a smaller absorption probability, and thus, a larger chance of escaping the sample. Possible radiative transitions are discussed below.

Select Radiative Transitions in Semiconductors. As discussed in previous sections, there are many possible impurity states located within the semiconductor's bandgap. The probability that the photo-excited electron-hole pair forms a *free* exciton, which subsequently decays, decreases as the impurity concentration increases. Consequently, the electron and hole recombine increasingly via these impurity states. The following paragraphs examine some representative recombinations [21, 22, 24, 51, 78]. Commonly observed PL transitions are depicted in Figure 2.5.

Exciton-Related Transitions. Exciton-related transitions include both free and bound exciton recombination. When the free exciton decays, the photo-excited electon-hole pair recombines, and a photon is emitted. The electronic states representing the free exciton were calculated to be separated from the conduction band an energy E_{ex}, given by Eq (2.2). Therefore, the emitted photon's energy is given by

$$\hbar\omega_l = E_g - E_{ex} \tag{2.13}$$

Recalling that the free exciton's states all lie within ~ 4 meV of the conduction band in GaAs, it is not surprising that it is very difficult to distinguish all of them. These states can be resolved by using the Zeeman effect [49]. The free exciton will thermally dissociate with increasing temperature, and thus, the associated transition luminescence will decrease.

The recombination energy of a bound exciton can be approximated by

$$\hbar\omega_l = E_g - E_{ex} - E_b \tag{2.14}$$

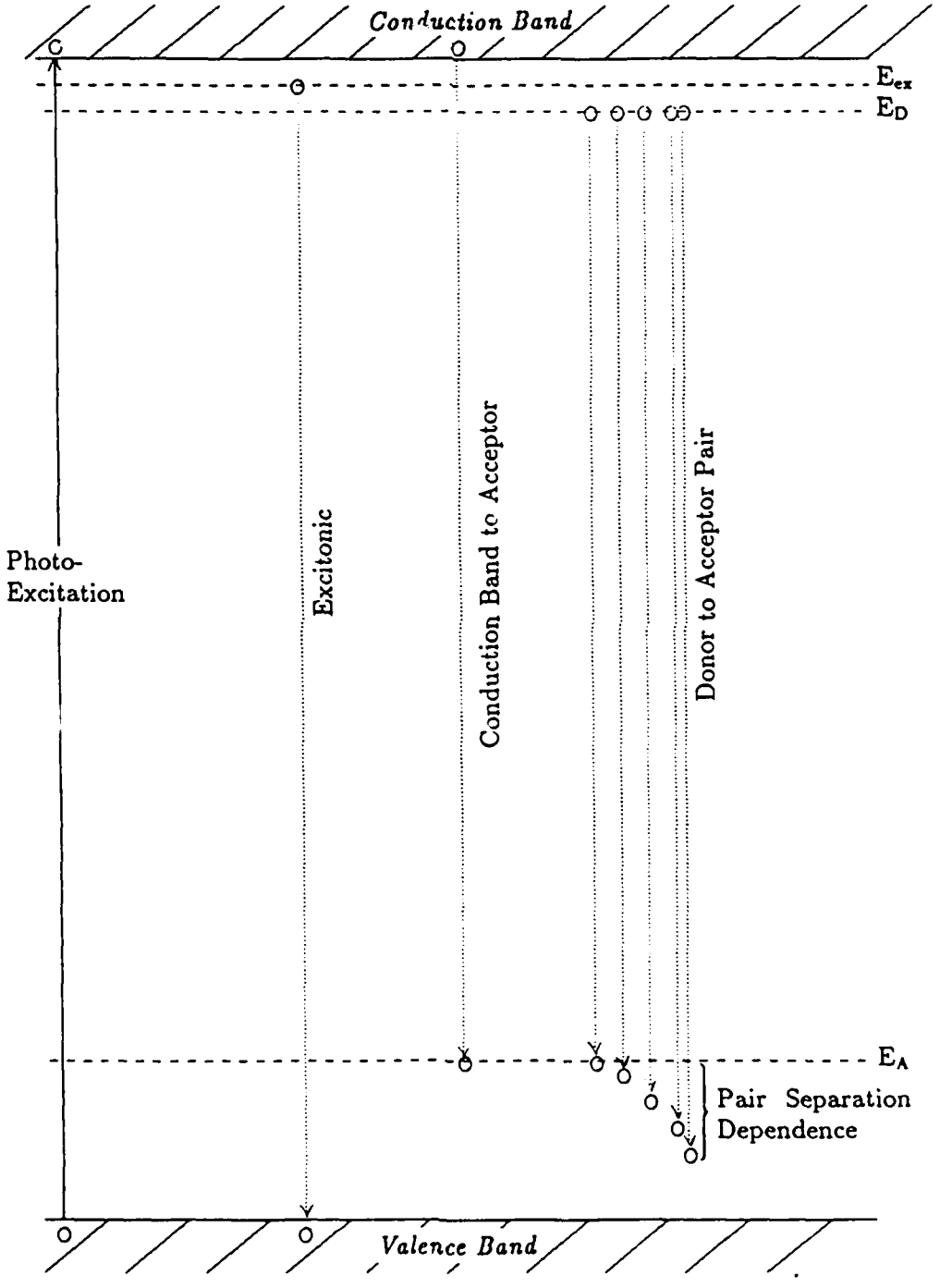

Figure 2.5. Commonly Observed PL Transitions in Semiconductors

where E_b refers to the energy binding the free exciton to the impurity. E_b has been determined to be a function of the ratio of the host crystal's electron to hole effective mass [64, 65]. This binding energy is normally given in terms of the acceptor or donor impurity's ionization energy. The impurity can manifest itself in many forms, including both ionized and neutral donors and acceptors. However, Williams and Bebb [78:349–351] have concluded that the exciton bound to an ionized acceptor has not been demonstrated in GaAs; the non-existence of which coincides with theory. The bound exciton emissions differ from those of the free exciton in that they are much narrower [51:116]. Their intensity can also be expected to decrease with increased temperature, as the complex thermally dissociates into a free exciton and the impurity.

Band-Impurity Transitions. The band-impurity, or bound-to-free (*B-F*), and free-to-bound (*F-B*) transitions include those of an electron from a donor to a valence band hole (D^o,*h*), and from the conduction band to a hole bound to an acceptor (*e*,A^o), respectively. The recombination emits a photon with energy given by

$$\hbar\omega_l = E_g - E_i \tag{2.15}$$

where E_i refers to the ionization energy of the impurity; donor or acceptor. The emission peaks broaden with increased impurity concentrations. This results from broadening of the impurity level itself and has been observed at concentrations as low as 10^{16} cm^{-3} [51:9]. If the impurity concentration becomes sufficiently large, the broadened level forms a continuum of states with the conduction or valence band [51:9]. In this situation, the band-impurity transitions become much less probable, and their associated luminescence peaks are hard to identify [51:133–134].

Donor-Acceptor (D^o-A^o) Pair Transitions. In addition to the above transitions, the photoexcited electron-hole pairs may recombine by first photo-neutralizing ionized donors and acceptors, which are, necessarily, present

in any real semiconductor. That is

$$e^- + D^+ \rightarrow D^\circ$$
$$h^+ + A^- \rightarrow A^\circ$$

To re-establish thermal equilibrium, the electron at the neutral donor may recombine radiatively with a hole at a neighboring neutral acceptor, such that

$$D^\circ + A^\circ \rightarrow D^+ + A^- + \hbar\omega_l$$

where $\hbar\omega_l$ is given by

$$\hbar\omega_l = \mathrm{E_g} - (\mathrm{E_A} + \mathrm{E_D}) + \frac{e^2}{\epsilon R} + J(R) \tag{2.16}$$

and $\mathrm{E_A}$ and $\mathrm{E_D}$ are the ionization energies of the acceptor and donor, respectively. The screened Coulomb interaction, represented in the third term, arises because the donor and acceptor return to an ionized state when equilibrium has been regained. The distance separating the pair is R. Finally, $J(R)$ is a higher-order, non-coulombic term accounting for the overlap of the donor and acceptor wavefunctions. It is non-negligible only for small R.

The luminescence spectrum should consist of several sharp peaks, corresponding to the discrete values of R which are allowed by the periodically spaced lattice sites of the crystal. The value of R depends upon which sub-lattice the donor and acceptor occupy. Both donor and acceptor occupy the same sub-lattice for Type I pairs, and, in this case, R has discrete values given by [21:15]

$$R_m = a_\circ \left(\frac{m}{2}\right) \tag{2.17}$$

where m is the *shell* index number and $a_\circ$ the lattice constant. (The index numbers refer to the concentric radial shells containing the various lattice positions of one pair member about the other, in order of increasing radii, with $m = 1$ being the closest possible pair separation, $m = 2$ the next closest, and so on [21:15]). Certain

values of m are not allowed, corresponding to $m = 4^x(8y + 7)/2$ (x is an integer greater than zero, and y an integer greater than or equal to zero), or 14, 30, 46, 56, 62, and so on [21:15–16]. For Type II pairs, where the donor and acceptor occupy different sub-lattices, R has discrete values given by

$$R_m = a_o \left(\frac{m}{2} - \frac{5}{16}\right)^{1/2} \tag{2.18}$$

where m can now be any integer greater than or equal to one [21:16]. Unfortunately, the discrete luminescence structure is difficult to observe for semiconductors like GaAs. For GaAs, $E_A + E_D$ is not sufficiently large to allow bound states to be observed according to Eq (2.16) for small R (shell number, m) [22:119]. The allowed transitions, involving pairs with relatively large R, are not easily resolved, because the separation between discrete peaks (corresponding to transitions with pair separations R_m and R_{m+1}) may become smaller than 0.1 meV [22:119].

To identify D^o-A^o pair transitions in semiconductors such as GaAs, one must rely on other characteristic features of such transitions. These include a shift of the corresponding luminesence band to higher energies with increased excitation intensity. This characteristic can be explained using the expression for the rate, W, of D^o-A^o pair recombination (tailored for GaAs) given by [78:339]

$$W(R) \propto \exp(-CR) \tag{2.19}$$

where C is a constant proportional to the Bohr radius of the shallowest member of the pair [24:175]. From Expression (2.19), distant pair recombination is slower, and therefore, will saturate rapidly with increased excitation intensity. Thus, increasing the excitation intensity will result in an increased proportion of close pair recombinations, causing the D^o-A^o pair band to shift to higher energies.

An additional characteristic of D^o-A^o pair transitions is their shift to higher energies with increasing temperature, especially between $\sim$15 and $\sim$35K for GaAs [21:59–60]. This can be attributed to thermal ionization of the shallower member

of the pair which, for GaAs, is the donor. The thermally released electron may recombine directly with the acceptor. As will be shown later, a (e, A^o) recombination in GaAs produces luminescence of greater energy than that of the associated D^o-A^o pair recombination. Thus, a higher-energy (e, A^o) transition occurs instead of the typically lower-energy D^o-A^o pair transition. The temperature-induced shift of the D^o-A^o pair transition may also result when the thermally released electron becomes bound to another donor which is closer to a neutral acceptor. There would be an increased chance of D^o-A^o pair recombination rather than continued thermal ionization of the electron in view of Expression (2.19). Consequently, on average, as the temperature is increased, one would expect the number of distant pair recombinations to decrease, resulting in a shift of the D^o-A^o pair band to higher energies. As the temperature continues to increase, fewer and fewer donors will be able to capture the released electrons, and the D^o-A^o pair band will gradually disappear in favor of the (e,A^o) peak.

Phonon-Assisted Transitions. As mentioned previously, GaAs is a direct gap material. Therefore, transitions between states do not require the assistance of phonons to conserve momentum. Nonetheless, phonons still may play an active role in the direct gap material's recombination processes. Because substitutional impurities are part of the vibrating lattice, it can be determined that photons released via recombinations involving the impurity will be Doppler-modulated by the crystal's characteristic vibrational quanta (phonons) [28:44–45]. Any number of these quanta may be associated with a transition, and thus, several lower-energy replicas of the *zero-phonon* peak may be observed. As reported in Table 1.1, the longitudinal (LO) and transverse optical (TO) phonon have corresponding energies of ~ 36.6 and ~ 33.8 meV, respectively. Another phonon interaction observed in the GaAs luminescence is that involving the transverse acoustic (TA) phonon, with a corresponding energy spanning 8.2 to 9.0 meV [69:46–47].

Photoluminescence Spectrum of GaAs. Table 2.7 presents several transition peaks that have been observed in GaAs PL and provides their assignment.

Luminescence Centers at ~ 1.4 *eV.* In addition to the simple substitutional centers giving rise to the recombinations shown in Table 2.7, another group of more complex, localized centers are thought to give rise to PL at ~ 1.4 eV. As will be discussed in Chapter IV, PL due to the Ga_{As} double acceptor occurs in this region. However, the PL probably originates from other centers as well; including those involving additional stoichiometric defects such as vacancies and interstitials.

Early investigations attributed PL at ~ 1.4 eV to these additional centers. Jeong *et al.* [31] presented their own and others' evidence that allowed them to conclude that a peak at 1.42 eV, observed only in Si-doped GaAs crystals, was due to $V_{As} - Si_{As}$ complexes. This evidence included the following:

1. The intensity of the 1.42 eV peak was much higher in samples grown by liquid phase epitaxy (LPE) relative to that in boat-grown samples. Electrical measurements indicated that Si substituted more likely on the As sites in the LPE samples, while Si atoms occupied a higher proportion of Ga sites in the boat-grown samples. Thus, it was concluded that the 1.42 eV peak was related to Si atoms on As sites.

2. When samples exhibiting the 1.42 eV peak were subjected to a heat treatment of 800°C for two hours (after having first been sealed in a fused-silica ampoule) with an excess As environment, the peak completely disappeared. The excess As vapor pressure decreased the V_{As} defect population, thus signifying this defect's role in the creation of the peak.

3. Enhancement of the 1.42 eV peak occured after isochronal anneal (performed without a protective cap for the sample) above 500K. It was stated that

Table 2.7. Some Transition Peaks in GaAs PL [56:Ch 12]

Recombination	Peak Energy (eV)
Free exciton (F,X)	1.515–1.5153
Exciton bound to neutral donor (D^o,X)	1.5141
Neutral donor to valence band (D^o,h)	1.5141, 1.5133
Exciton bound to ionized donor (D^+,X)	1.5133
Exciton bound to neutral acceptor (A^o,X)	1.5124
Conduction band to C acceptor (e, C_{As})	1.4932
Conduction band to Be acceptor (e, Be_{Ga})	1.4923, 1.4915
Conduction band to Mg acceptor (e, Mg_{Ga})	1.4911
Conduction band to Zn acceptor (e, Zn_{Ga})	1.4894, 1.4888
Neutral donor to C acceptor (D^o, C_{As})	1.4892
Neutral donor to Mg acceptor (D^o, Mg_{Ga})	1.4875
Neutral donor to Zn acceptor (D^o, Zn_{Ga})	1.4854
Conduction band to Si acceptor (e, Si_{As})	1.4850
Conduction band to Cd acceptor (e, Cd_{Ga})	1.4848
Neutral donor to Si acceptor (D^o, Si_{As})	1.4816
Conduction band to Ge acceptor (e, Ge_{As})	1.4782, 1.4790
Neutral donor to Ge acceptor (D^o, Ge_{As})	1.4745
Mn_{Ga}-related	1.4089
Cu_{Ga}-related	1.3578

when the V_{As} defect migrates during anneals above 500K, it is able to form a complex with Si atoms on As sites. Subsequently, the 1.42 eV peak is observed to increase in intensity.

An investigation by Itoh and Takeuchi [29] was significant in that As implantation was used to assess the stoichiometry of melt-grown GaAs samples, heavily doped with Si, that were subjected to an 800°C anneal for one hour (without a protective encapsulant). A band which peaked near 1.4 eV (observed after the anneal and only in samples doped with Si) was seen to decrease in intensity if the Si-doped layers were implanted first with As and then annealed. As a control, it was discovered that initial implantation of argon (Ar), instead of As, did not have the same affect on the 1.4 eV band's intensity. This evidence helped to substantiate the authors' conclusion that the 1.4 eV band was associated with the V_{As} defect. Ultimately, the band was attributed to the $V_{As} - Si_{As}$ complex.

Data was also gathered by Swaminathan *et al.* [72] on a PL feature in the $\sim$1.4 eV region, which was identified as the Q band. The Q band appeared only in heat-treated (at 830°C) n^+, (that is, heavily Si-doped) substrates.. (The band did not appear in heat-treated semi-insulating Cr-doped substrates). The band's spectral position, half-width and intensity varied from sample to sample. The luminescence peaked at 1.423–1.454 eV, and it had a spectral half-width of 25–50 meV. Luminescence data was presented for the sample in which the Q band was located at the lower end of this spectral range. This sample was successively etched at one minute intervals in a sulfuric acid:hydrogen peroxide:water (20:1:1) solution (H_2SO_4:H_2O_2:H_2O). After the first minute (or after removing a layer $\sim 1\mu$ in thickness), the Q band was observed to have shifted to $\sim$1.462 eV. The band's upward energy trend continued after successive etches.

Additional characteristics were noted for the Q band [72]. As the excitation intensity was increased, the Q band increased to higher energies. This suggested that the band was associated with D^o-A^o pair recombinations. The energy shift was

found to be ~ 12 meV per decade change of excitation intensity. It was concluded that this large shift might result from heavy compensation in the layers from which the band originated. The association of the Q band with D°-A° pair recombination is not a straightforward interpretation based upon the temperature-dependent PL results. The band shifted to lower energies and decreased in intensity as the temperature was increased. This temperature-induced shift to lower energies is exactly opposite that expected for the D°-A° pair recombination. The investigators did not note this divergence. Thus, higher-temperature PL measurements were interpreted based on the D°-A° pair assignment. A higher-energy band evolved at 60K (so that at 80K its peak position was 1.470 eV) and was assigned to Q-related $F - B$ transitions. The acceptor, with ionization energy determined to be $\sim 40 \pm 5$ meV, was concluded to be most likely Si_{As}. The donor which was believed to participate in the lower-temperature Q band PL, whose ionization energy was determined to be $\sim 35 \pm 10$ meV, was difficult to assign.

Swaminathan *et al.* [72] recognized that nonstoichiometric As-deficient layers would remain (after the volatile As evaporated) after heating essentially unprotected GaAs in an open tube at high temperatures. Defects believed to exist in the As-deficient layers included V_{As}, Ga_i, and the Ga_{As}. Swaminathan *et al.* noted (from the general observations made by Kröger [37:9]) that non-metal vacancies and metal interstitials should act as donors in compound semiconductors. Thus, it was proposed that, if the V_{As} and Ga_i behaved as donor(s), then one or both could participate in the D°-A° pair recombinations which contributed to the Q band emission. The above works by Jeong *et al.* and Itoh and Takeuchi would favor the participation of the V_{As}. However, the Q band was not determined to be sufficiently broad to warrant the conclusion that the V_{As} defect was involved. As to the involvement of the Ga_i, the authors determined the data did not allow a firm conclusion.

The Q band was further characterized in luminescence studies by Pomrenke *et*

Table 2.8. Q Band Energy as a Function of Depth in Si-Implanted GaAs [54:417]

Depth (Å)	Peak Energy (eV)
Surface	1.415
580	1.440
1060	1.462

al. [54]. It was shown that the band could also originate from layers implanted (as opposed to chemically doped) with Si and subsequently annealed for relatively short times (15 minutes as opposed to 3.5 hours in the above research by Swaminathan *et al*). Referencing Itoh and Takeuchi [29] and Swaminathan *et al.* [72], the Q band was speculated to originate from complexes such as $V_{As} - Si_{As}$ and $Ga_i - Si_{As}$. The Ga_{As} was proposed as an additional recombination center, because its associated transition energy (1.44 eV) [84] lies in the same spectral region as that of the Q band, and this antisite is a native defect originating from annealed GaAs.

Applying PL profiling techniques in their investigation, Pomrenke *et al.* [54] found that the Q band shifted to higher energies as successive layers were etched away (somewhat similar to what was observed by Swaminathan [72:156–157]). This is shown in Table 2.8, where the Q band energies are approximated from the spectral data for a sample implanted with Si, at a dose of 3E13 cm^{-2} and annealed at 950°C. The shift was explained, in part, via multiple recombination sources. The existence of multiple recombination sources, in turn, were based on studies of the distributions of various defects in ion-implanted layers [17, 43]. Thus, it was speculated that at the surface, the Q band of relatively low energy arose mainly from V_{As} defects. As one etched deeper into the sample, to the mean projected range of the Si ion implant (which for these samples was 1025Å) and beyond, the relatively higher energy band resulted from recombinations involving the Ga_i. These conclusions should be accepted with caution. Samples exhibiting the Q band

Table 2.9. Q Band Energy as a Function of Si-Implant Dose [54:418]

Si Dose (cm^{-2})	Q Peak Energy (eV)
1E13	1.474
1E14	1.441
1E15	1.355

were annealed at temperatures greater than or equal to 750°C. Unfortunately, the analyses in references [17] and [43] do not adequately consider the effects which high temperature anneal has on the defect distribution.

Pomrenke *et al.* [54] also discovered that the band's peak energy shifted with implant dose and anneal temperature. The dose dependence of the band's spectral position is shown in Table 2.9 for an anneal of 900°C (where the data for the 1E14 cm^{-2} implant is taken from cathodoluminescence). For the anneal temperature dependence [54:416–417], when the sample was annealed between 750 and 800°C, the band originated at low energies ($\sim$1.39–1.40 eV for a 3E13 cm^{-2} implant). At anneal temperatures of 800°C and above, a higher-energy Q band was observed ($\sim$1.465 eV for a 3E13 cm^{-2} implant).

It was concluded by Pomrenke *et al.* [54] that the relative contribution of multiple recombination centers to the shifting Q band PL was determined, not only by the depth into the material, but also the implant dose and anneal conditions. It was also believed that a secondary source for the Q band's fluctuating nature may result from irregular fluctuations of the electrostatic potential. As explained by Swaminathan *et al.* [72], based on work by Pankove [51:151], D^o-A^o pair recombination in impure heavily compensated GaAs occurs due to tunneling-assisted transitions between spatially separated upper (donor) and lower (acceptor) states. The D^o-A^o pair peak position, in this case, is expected to depend on the magnitude of the fluctuating electrostatic potential which, in turn, varies with the

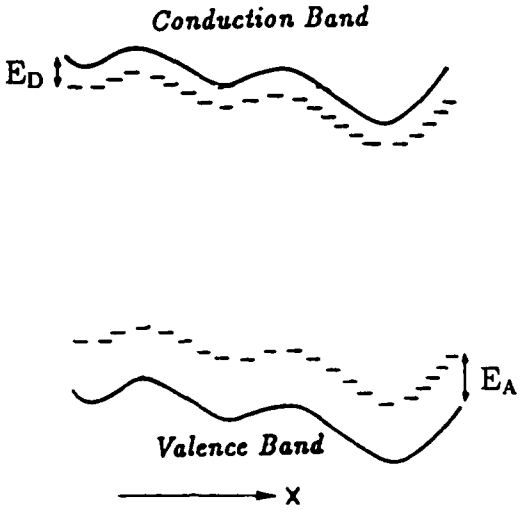

Figure 2.6. Perturbed Energy Level Structure as a Function of Position [51:151]

relative concentrations of impurities and defects, or, in other words, the relative amount of compensation [54, 72]. (As shown in Figure 2.6, local fluctuations in the electrostatic potential perturbs both the band structure and the associated impurity levels as a function of position [51:151]).

Photoluminescence Spectrum of GaAs:Ge. GaAs layers doped with Ge, either chemically or by implantation, exhibit PL due to the standard recombination processes including $(e, \mathrm{Ge_{As}})$ and $(D^{\circ},\mathrm{Ge_{As}})$. Therefore, from Table 2.7, PL originating from these processes is expected at 1.4790–1.4782 and 1.4745 eV, respectively. However, the PL of Ge-doped layers often includes contributions from lower-energy transitions as well. These will be discussed below. It should be noted at the outset that luminescence results for GaAs dually implanted with {Ge+Ga} or {Ge+As} have not been reported in the literature.

Centers at $\sim$*1.4 eV in GaAs:Ge.* In an early study by Kressel *et al.* [36], where GaAs was chemically doped with Ge, it was concluded that Ge

actually introduces two separate acceptor centers. The shallower of the two (which produced a PL peak at 1.479 eV at a temperature of 77K) was attributed to the simple substitutional Ge_{As} acceptor. The deeper acceptor level, at ~ 70 meV above the valence band, was associated with a Ge atomic complex. This assignment was probably deduced based on a study of GaAs chemically doped with Si [35]. There the Si was also observed to give rise to two acceptor levels, the deeper of the two occurring at ~ 100 meV above the valence band. It was argued that the ~ 70 meV acceptor produced both a PL peak at 1.44 eV in *p*-type material, and a peak at 1.395–1.405 eV in *n*-type material (with all measurements taken at 77K). In any case, the ~ 70 meV acceptor's assignment was not conclusive.

Williams and Elliott [79] studied the proposed Ge atomic complex further. In their investigation, the Ge impurity gave rise to a PL band which peaked at 1.454 eV at 20K, corresponding to the ~ 70 meV acceptor observed above by Kressel *et al.* [36]. The band was only seen in samples which contained Ge. It was also noted that the band was not seen in samples grown under As-rich conditions. In addition, the sample exhibiting the 1.454 eV band was believed to have been grown under Ga-rich conditions. These observations suggested that the defect giving rise to the 1.454 eV band involved both Ge and the V_{As} defect, and possibly, the Ga_i defect. It was presumed that complexes of Ge and the V_{As} defect, or Ge and the Ga_i defect, were occurring. The Ga_i complex was less favored, in part, because there was a lack of strong evidence in the literature for its existence. On the other hand, there was some evidence in the literature for the existence of V_{As} complexes, including V_{As}-Zn_{Ga} and V_{As}-Cd_{Ga} [27]. However, the PL bands originating from the V_{As}-Zn_{Ga} and V_{As}-Cd_{Ga} complexes shifted to higher energy with increasing sample temperature [27:829]. The 1.454 eV band observed by Williams and Elliott shifted rapidly to *lower* energy with increasing temperature. Thus, associating V_{As}-Ge_{As} complexes with the 1.454 eV luminescence band may be suspect. Nevertheless, the complex was modelled as producing two levels between

which the transitions occur. (Single-level models were not justified in light of the observations). Subsequently, it was conceptualized that the electron was mainly associated with the Ge_{As} acceptor in the complex's ground state and with the V_{As} defect in the excited state. Indeed, a vacancy-impurity complex, such as the proposed V_{As}-Ge_{As} complex, has been considered as an acceptor (in this case the Ge_{As} acceptor) bound by a Coulomb force to a nearest neighbor V_{As} donor [27:830]. The center is assumed to be localized and would not be expected to exhibit conventional D°-A° pair recombination.

Bafleur *et al.* [5] have conducted a relatively recent study of GaAs chemically doped with Ge. The growth process was molecular beam epitaxy (MBE). Notably, two distinct peaks (at 1.45 and 1.41 eV) in the $\sim$ 1.4 eV range were observed after intentionally doping the layers with Ge (indicating that Ge plays a role in the centers from which the peaks originate). The investigators summarily claim that both peaks shift to lower energy parallel to the band gap as the sample temperature is increased. A closer look at the data, however, seems to suggest that the peak at 1.45 eV actually shifts slightly to higher energy as the temperature increases from 20–40K, and then begins to shift to lower energy as the temperature is increased further. This behavior is indicative of D°-A° pair recombination. In fact, excitation intensity-dependent data for the 1.41 eV peak also is indicative of D°-A° pair recombination. (However, this conclusion would be suspect, since the temperature-dependent data for the 1.41 eV peak does not indicate D°-A° pair recombination). Nevertheless, the 1.45 eV peak is tentatively attributed to the V_{As}-Ge_{As} complex. This assignment was supported by the work of Williams and Elliott [79] summarized above, and by the slightly increased peak intensity with decreasing As pressure during crystal growth. The origin of the 1.41 eV peak was surmised to include the As_i-Ge_{As} and the As_{Ga}-Ge_{As} complexes, and could not be made more definitive based upon the experimental results. The investigators supported these hypothetical assignments for the 1.41 eV peak, in part, by noting the decreased

relative intensity of the 1.41 eV peak with increased substrate temperature during growth, and the assignments' reasonableness for the excess As growth conditions used.

Centers giving rise to PL at $\sim$1.4 eV have also originated from Ge-implanted GaAs [83]. PL spectra was presented primarily for samples annealed at 800°C for 20 minutes subsequent to the implantation. The samples were encapsulated with silicon nitride prior to anneal.

Yu [83] discovered that implanting Ge at a dose of 5E12 cm^{-2}, produced a peak in the $\sim$1.4 eV range dominated the sample's PL spectrum. The peak shifted from 1.43 to 1.46 eV with increased excitation intensity (to a maximum excitation intensity of $\simeq$3 W/cm^2). The peak shifted $\sim$10 meV per decade change of excitation intensity. This behavior indicates that D^o-A^o pair recombinations contribute to the PL. However, it was also observed that the peak shifted to lower energy as the temperature was increased from 4K, and the emission rapidly quenched at temperatures greater than 25K. From discussions above, typical D^o-A^o pair recombination will shift to higher energy as the temperature is increased from approximately 15 to 35K. Thus, the excitation intensity- and temperature-dependent PL data seem to contradict each other. Yu noted that bands exhibiting similar excitation intensity- and temperature-dependent behavior have been ascribed to D^o-A^o pair transitions, modified by the random-impurity potential created in an impure compensated crystal [82]. Thus, the 1.43–1.46 eV emission band was assigned to modified (D^o, Ge_{As}) pair transitions. The compensated layers of reference [82] were believed to originate from the presence of V_{As} defects. Likewise, the compensation mechanism in the layers having the 1.43–1.46 eV PL was believed to involve defects such as the V_{As} defects. Finally, excitation wavelength-dependent emission spectra (depth profiling of the PL) in the $\sim$1.4 eV range indicated that the 1.43–1.46 eV PL activity originated from the near-surface region ($\sim$0–300Å).

At a Ge implant dose of 3E13 cm^{-2}, Yu [83] found that a new luminescence

peak at $\sim$1.435 eV appeared. In contrast to the 1.43–1.46 eV band, the $\sim$1.435 eV peak did not shift with changes in the excitation intensity. Notably, the $\sim$1.435 eV peak's temperature behavior was similar to that of the 1.43–1.46 eV band. Associating a high concentration of V_{As} defects with the *p*-type activation in the Ge-implanted layers, it was deemed reasonable that a complex of the V_{As} defect and Ge_{As} acceptor would form and give rise to the 1.435 eV peak. Depth profiling of the $\sim$1.435 eV peak indicated that the luminescence originated from the near-surface region ($\sim$0–500Å).

At higher Ge implant doses, the PL features already mentioned were no longer seen by Yu [83]. (The dominant feature in the PL spectrum of the sample implanted at a dose of 1E14 cm^{-2} is a band at $\sim$1.38 eV). No detailed explanation is offered for this behavior. It is suggested that at the higher implant doses, a large concentration of Ge_{Ga} donors and V_{Ga} defects, as well as Ge_{As} acceptors, is expected. This may explain the absence of the bands mentioned above which were believed to result from the presence of V_{As}.

Selective Pair Luminescence. The advent of the tunable dye laser (and development of the proper dyes) provided an additional optical diagnostic tool for semiconductor material characterization. One of the better known and recent applications of this laser technology is that of selective excitation of D°-A° pairs, alternately referred to as selective pair luminescence (SPL). The technique and characteristics of the associated luminescence is described below [22, 24].

The SPL technique is described as site selection spectroscopy. Under nonselective excitation, using the conventional PL technique, the D°-A° pair recombination appears as a broadband for materials such as GaAs. As previously described, the band is really a collection of unresolved, sharp peaks corresponding to D°-A° pair transitions with many distinct pair separations, R_m, given by Eq (2.17) or (2.18). Because of the relatively short lifetime of excited donor and acceptor states,

radiative pair decay occurs predominantly between ground states of the donor and acceptor [73]. Under selective excitation, the laser excitation or pump is tuned to an energy such that

$$\hbar\omega_p = \mathrm{E_g} - (\mathrm{E_D} + \mathrm{E_A^*}) + \frac{e^2}{\epsilon R_m} + J^*(R_m) \tag{2.20}$$

where $\mathrm{E_A^*}$ represents the energy of an acceptor's excited state (such as $E(2P_{3/2})$ or $E(2S_{3/2})$) relative to the valence band, R_m denotes a specific pair separation, and $J^*(R_m)$ is the non-coulombic interaction term for the donor - excited acceptor pair having a separation of R_m. Thus, in Figure 2.7, which was adapted from that presented by Henning [24:177], the pump photon of energy $\hbar\omega_p$ selectively excites D^o-A^o pairs with separations of R_1, R_2 and R_3. The electron is excited from a $2P_{3/2}$, $2S_{3/2}$ and $1S_{3/2}$ acceptor state, respectively, to the associate donor's ground state. Holes in the excited acceptor states quickly relax to the acceptor ground state and may then recombine with electrons originally pumped to the donor ground state. The photons subsequently emitted have energy

$$\hbar\omega_l = \mathrm{E_g} - (\mathrm{E_D} + \mathrm{E_A}) + \frac{e^2}{\epsilon R_m} + J(R_m) \tag{2.21}$$

In principle, then, one should observe several sharp lines for a given pump photon energy, $\hbar\omega_p$, corresponding to the discrete set of combinations (R_m, $\mathrm{E_A^*}$) defined by Eq (2.20) and shown in Figure 2.7. By subtracting Eq (2.21) from Eq (2.20), one is left with

$$\hbar\omega_p - \hbar\omega_l = \mathrm{E_A} - \mathrm{E_A^*} - (J(R_m) - J^*(R_m)) \tag{2.22}$$

Thus, in the limit of large pair separations R_m (where $J^*(R_m)$and $J(R_m)$ become negligible), one can determine the energy separating the acceptor's ground and excited states by noting the energy difference of the pump photon and the sharp spectral lines. If the acceptor ground state energy is known, this technique allows one to derive the acceptor's excited state energy spectrum. (Although the treatment has concentrated on the acceptor states, a similar derivation is possible for the donor ground and excited states).

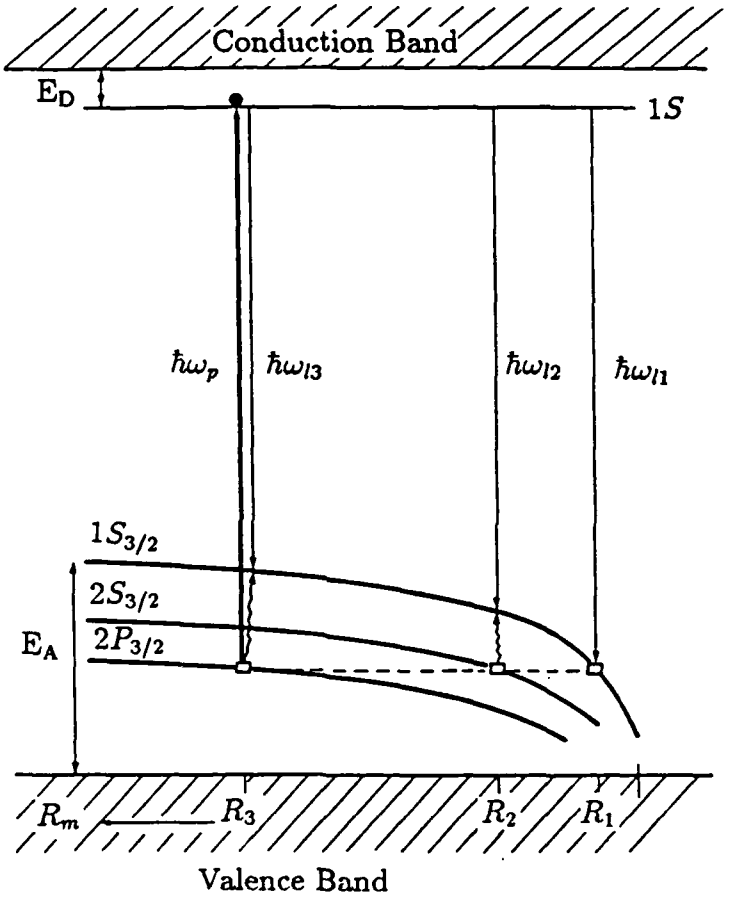

Figure 2.7. SPL Process [24:177]

As a general rule, the SPL structure are seen to be superimposed on the broad D°-A° pair recombination background; specifically on the background's high-energy side. The background's low-energy side corresponds to recombination involving the more distant pairs (reference Eq (2.16)). From expression (2.19), the rate of distant D°-A° pair recombination is relatively slow. Thus, the site selection of distant pairs, which give rise to the lower-energy luminescence, ultimately does not produce sharp SPL structure because the excitation has a greater opportunity to migrate to other non-selectively excited D°-A° pairs. In fact, Tews *et al.* [73] noted that it is important that the pump photon be chosen to site select pairs with not too large a pair separation. On the other hand, too small a pair separation will restrict the number of available donors and acceptors for eventual pair formation, recombination and subsequent radiative luminescence [73]. Even if one is careful in this regard, a broad luminescence background may still persist, making resolution of the SPL structure more difficult. One source is the fact that the pump photon's energy is such that [73]

$$\hbar\omega_p > \mathrm{E_g} - (\mathrm{E_D} + \mathrm{E_A}) \tag{2.23}$$

Therefore, ground state D°-A° pairs with a small distribution of pair separations will be created in conjunction with the selectively excited pairs. Hence, recombination will still occur amongst some random pairs, producing a broad background upon which the SPL will be superimposed.

There are several characteristic features of SPL structure. Typically, the experiment is conducted several times, collecting the luminescence resulting from each of several pump photon energies, $\hbar\omega_p$. This assists in verifying that the observed luminescence is indeed SPL. From Eq (2.22), the sharp SPL structure should spectrally shift with the pump photon energy at large pair separations. This information alone is not sufficient verification. Unfortunately, Raman lines, whose origins include the cryostat windows and the semiconductor sample itself, also shift with the laser pump photon. Further verification results from observation

of a decreasing $\hbar\omega_p - \hbar\omega_l$ value when one samples pairs with smaller and smaller R_m (where the third and fourth terms on the right side of Eq (2.22) are now significant). In addition, one should note the appearance and disappearance of the sharp line structure as one tunes the pump photon to lower energy. The SPL structure should fall somewhere within the energy region defined by the corresponding D^o-A^o pair recombination band observed in PL. A final method of assessing the nature of sharp line structure involves performing temperature-dependent studies. Naturally, the D^o-A^o pair-related SPL structure should disappear as the sample temperature is increased. Cavins *et al.* [14] observed that the intensity of the SPL structure and the D^o-A^o pair PL have similar temperature-dependent behavior [14]. In fact, the SPL was shown to persist through 20K [14:2117].

SPL in GaAs. The SPL technique has been applied to GaAs for several years, and tabulated results are still evolving for the excited state spectrum of acceptors and donors. It should be noted that there are still no published SPL results for Ge-implanted GaAs. Typically, the SPL results are presented in terms of the energy separating the donor or acceptor ground state and the several corresponding excited states, or, as was shown above, $\hbar\omega_p - \hbar\omega_l$.

The energy spectrum for several acceptor states in GaAs derived from SPL are tabulated in Table 2.10 where all energies are in meV. The ground state energies were established by Ashen *et al.* [4:1051].

In early SPL studies of GaAs, it was believed that sharp structure corresponding to the excited states of donors were not observed, because these states were located so close to the conduction band, and thus, easily thermally ionized [26]. Recent studies have, in fact, been able to resolve donor-related SPL structure and $1S \rightarrow 2S$ energy splittings have been found to range from $\sim$ 4.5–6.2 meV [50, 76]. An identification for the donor impurity, with which these electronic transitions were associated, was not provided.

Table 2.10. Ground State Energies and Ground/Excited State Energy Splittings, Determined from SPL, for Several Acceptors in GaAs (Energies in meV) [4, 13, 32, 34]

	C_{As}	Mg_{Ga}	Zn_{Ga}	Si_{As}	Ge_{As}
$1S_{3/2}$	26.0	28.4	30.7	34.5	40.4
$1S_{3/2} - 2P_{3/2}$	15.2	17.0	19.2	23.5	26.1
$1S_{3/2} - 2S_{3/2}$	18.4	20.1	21.7	25.1	28.3
$1S_{3/2} - 2P_{5/2}(\Gamma_8)$	19.4	21.0	23.1	27.3	30.1
$1S_{3/2} - 2P_{5/2}(\Gamma_7)$	21.3	···	25.2	29.6	31.6
$1S_{3/2} - 3S_{3/2}$	22.4	···	26.2	30.8	34.0

Ion Implantation

Ion implantation involves the introduction of various atomic species into a solid substrate by bombarding the substrate with high energy ions. The technique essentially accelerates ions with a potential from an ion source to the target. An intermediate mass separating magnet removes unwanted impurities. Advantages to using ion implantation for device fabrication include good uniformity and reproducibility, improved control of dopant distribution (both the dopant concentration and thickness of the doped layer) and the potential to selectively dope designated regions of materials using appropriate masks [47:109]. Depth distribution and damage related to ion implantation will be discussed below.

An important consideration in semiconductor fabrication is the depth distribution of the implanted ion. Gibbons, *et al.* [23] have generated tables of depth distributions for a variety of implanted ions in GaAs. In addition, they provide a review of the methodology used to derive these tables, some of which is described here. For ion implantation, the ion's depth profile is a function of the chosen implant energy and the integrated beam current, which is essentially the ion dose,

ϕ. (The ion dose is expressed in units of ions/cm^2). In most instances, the profile or range distribution is roughly Gaussian in shape, as shown in Figure 2.8. The distribution is characterized by a mean projected range, R_p , and its standard deviation, σ_p. These parameters may be theoretically predicted from the ion mass, energy and dose, using the Lindhard, Scharff and Schiott (LSS) calculation. The LSS theory models the collisions and interactions experienced by the implanted ion as it moves through the substrate. Implanted ions may become channelled along one of the axes of the crystal lattice. If channelling occurs, the implant will lodge itself deeper in the substrate than predicted by the LSS theory. This is usually not desired for controlled experimental situations and thus the ions are implanted off-axis.

The disorder produced by the implanted ion as it pushes through and comes to rest in the substrate, is important to consider since both the substrate's electrical and optical characteristics may be affected. The disorder includes both crystal vacancies and interstitially located atoms. Experimental and theoretical investigations have been conducted to determine the relative position of an implanted ion distribution and its related damage distribution [43]. Heat treatment subsequent to implantation is an effective means of restoring the crystalline order. The appropriate treatment depends on the amount of damage. The amount of damage depends on such factors as the dose and identity of the ion that is implanted [2].

GAUSSIAN APPROXIMATION OF IMPURITY CONCENTRATION, $N(X_p)$:

$$N(X_p) = \frac{\phi}{\sigma_p\sqrt{2\pi}} \exp\left[-\frac{(X_p - R_p)^2}{2\sigma_p^2}\right]$$

where ϕ is ion dose/cm^2, and X_p is a measured distance along the direction of incident ion beam.

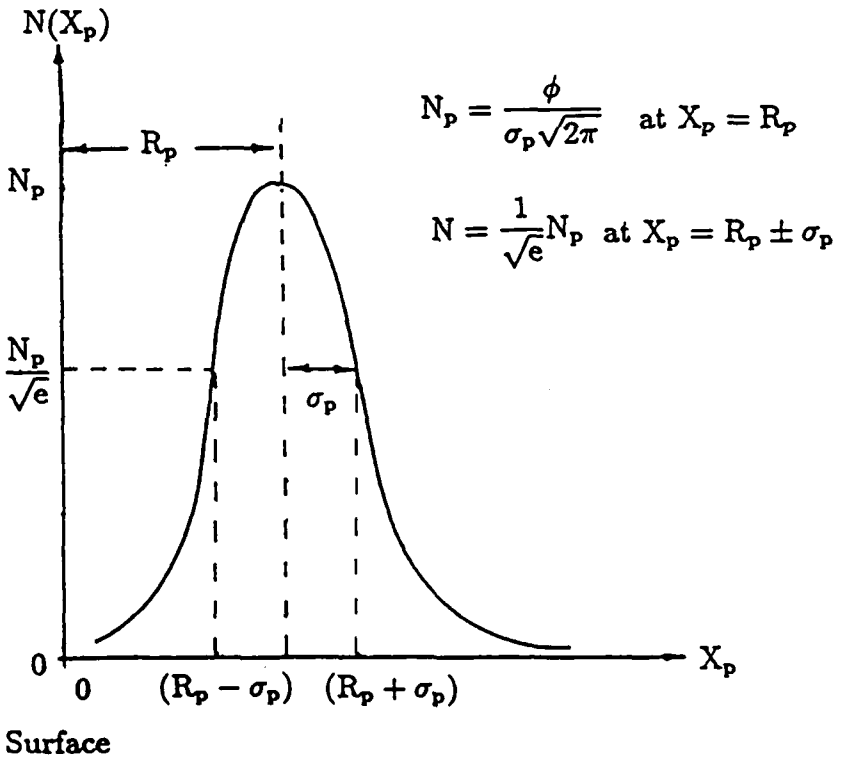

Figure 2.8. Implanted Ion Range Distribution and Associated Statistics

III. Description of Experiment

This chapter describes sample preparation, experimental systems, and associated operating procedures.

Sample Preparation

The processed GaAs samples (unimplanted or implanted) used in this study were obtained from those initially prepared for the investigations of the samples' electrical properties [53, 80, 81]. The electrical investigations were performed at the Air Force Avionics Laboratory. The substrate material, obtained from Crystal Specialties (batch number CS-3820), was semi-insulating Cr-doped GaAs, which was grown by the horizontal-Bridgman technique.

Prior to implantation, the material was flushed with the following in the order listed: 10% acquasol (diluted basic-H solution), deionized water, trichloroethylene, acetone, methanol, and deionized water. This combination insured the removal of organic contaminants and other impurities from the sample's surface. After flushing, the surface was blown dry with nitrogen gas. Subsequent to cleaning, the samples were free-etched for 90 seconds. This step removed any remaining mechanical damage imparted to the surface during the crystal wafer's early fabrication phases. Ideally, one will be left with a damage-free surface. The etchant was a sulfuric acid, hydrogen peroxide and water solution (H_2SO_4 : 30% H_2O_2 : H_2O) in a 3:1:1 ratio by volume. The samples were etched in a teflon beaker which was carefully agitated for the duration to keep bubbles from forming on the sample surface. Bubbles tend to cause a non-uniformly etched sample surface. The free-etching step was normally accomplished just prior to subsequent sample processing to minimize the development of oxides on an otherwise clean surface.

Table 3.1. Implant Schedule for GaAs Samples

	Dose (cm^{-2})			
Ion	1E13	3E13	1E14	1E15
As	X		X	X
Ga	X		X	X
Ge	X	X	X	X
Ge+Ga	X	X	X	X
Ge+As	X	X	X	X

Implantation. Following completion of the above-mentioned clean and etch steps, the samples were ready for implantation. The implantations were accomplished at the Avionics Laboratory using an implanter whose basic design is shown in Figure 3.1. The ion beam, shown in the figure as straight lines connecting the high-voltage terminal to the substrate via the analyzing magnet, was created by a hot-cathode source. The incident beam was directed 7° off-axis with respect to the substrate's ⟨100⟩ crystal axis to minimize channeling effects. The implant schedule included that presented in Table 3.1. An unimplanted sample was also studied to act as one of the controls for the experiment. The implantations were made at an energy of 120 keV at room temperature. From the calculations of Gibbons *et al.* [23], it is found that R_p for the Ge ions is 457Å. The dual implants shown in Table 3.1 were carried out sequentially; equal doses of both ions being implanted.

Anneal. Subsequent to implantation, the samples were annealed. Before anneal, the samples were cleaned again and then encapsulated with a dielectric coating. The cap discouraged the out-diffusion of the implanted species and decreased the surface decomposition of the GaAs, since As can dissociate from the Ga at a temperature as low as 400°C [55:5]. A silicon nitride (Si_3N_4) dielectric

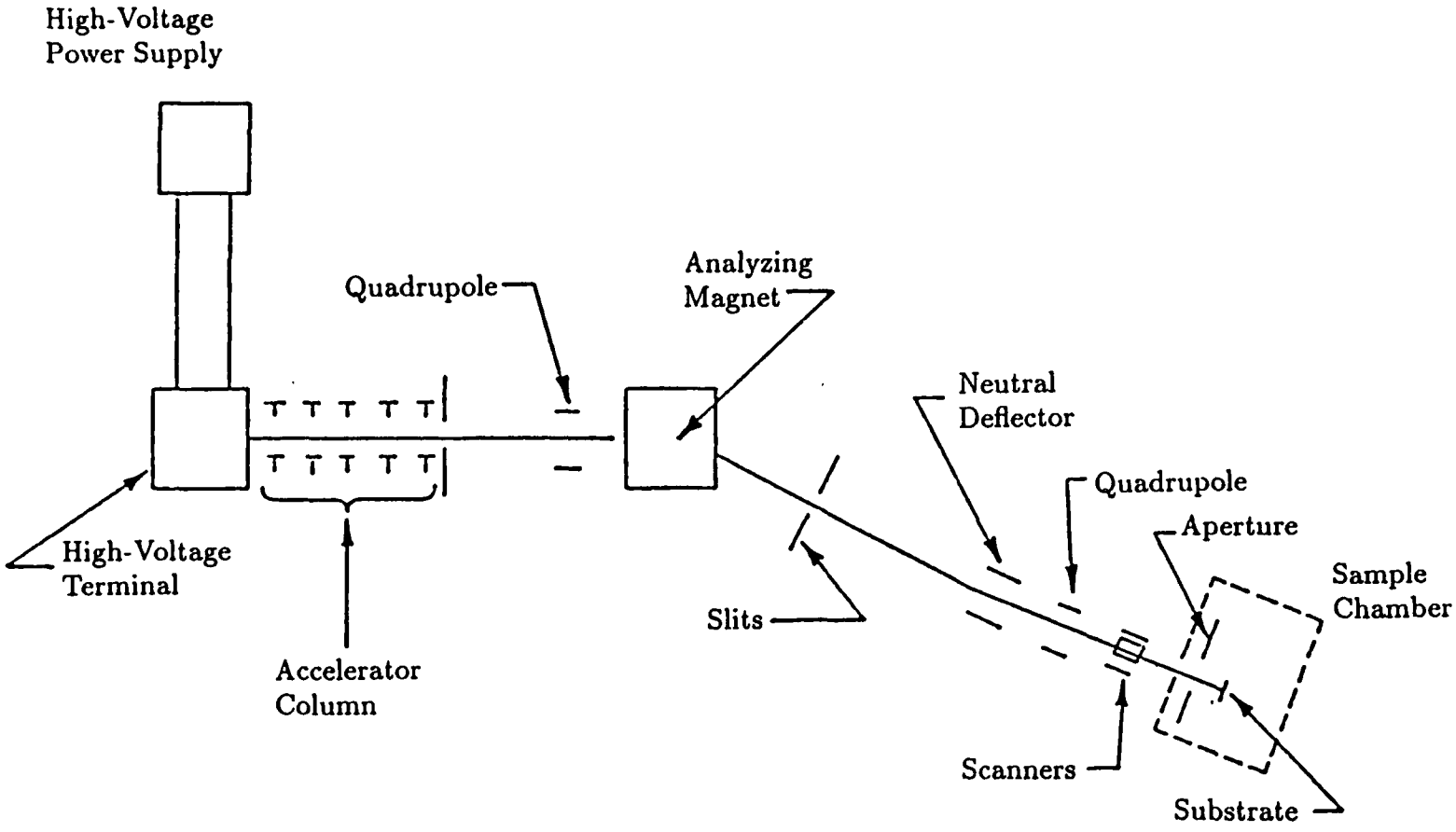

Figure 3.1. Schematic of Ion-Implantion Accelerator [55]

coating was deposited at ~700°C onto the sample's surface in a pyrolytic reactor. The desired encapsulant thickness was 1000Å.

Following encapsulation, the samples were annealed. They were placed in a furnace and annealed in a flowing hydrogen gas ambient for 15 minutes. The data presented in the next chapter were obtained from samples annealed at a temperature of 900°C, unless otherwise noted. To improve the performance of the encapsulants during anneal, many samples were rested cap-side down on a bare GaAs substrate. This procedure prevented the deterioration of the encapsulants caused by the As dissociation and subsequent tendency for it to out-diffuse [81:5786].

After anneal, the encapsulant was removed by soaking the sample in a 48% hydrofluoric acid (HF) solution. The removal of the encapsulant was monitored through its color change: blue, to dark blue, then brown and finally to the silver metallic color of the GaAs surface. The soak lasted about three minutes.

Luminescence Measurements—Systems and Procedures

The luminescence data was gathered using the following procedures and system. The system is depicted in Figure 3.2.

Excitation Source and Optical Detection System. A Spectra Physics Model 171-17 argon ion laser was one of two excitation sources that were used for PL measurements. The argon ion laser was capable of operating in a single- or multi-line mode in the wavelength range of 4545–5145Å. For the PL measurements, it was desirable to operate in the single-line mode. The 4880Å line was used in almost all the PL measurements because it is relatively intense and absorbed relatively well in the implant layer. A Spectra Physics Series 2000 krypton ion laser was used in some early PL measurements. This laser provided a 6471Å line for sample excitation.

For excitations near or below the GaAs bandgap, a Spectra Physics Model

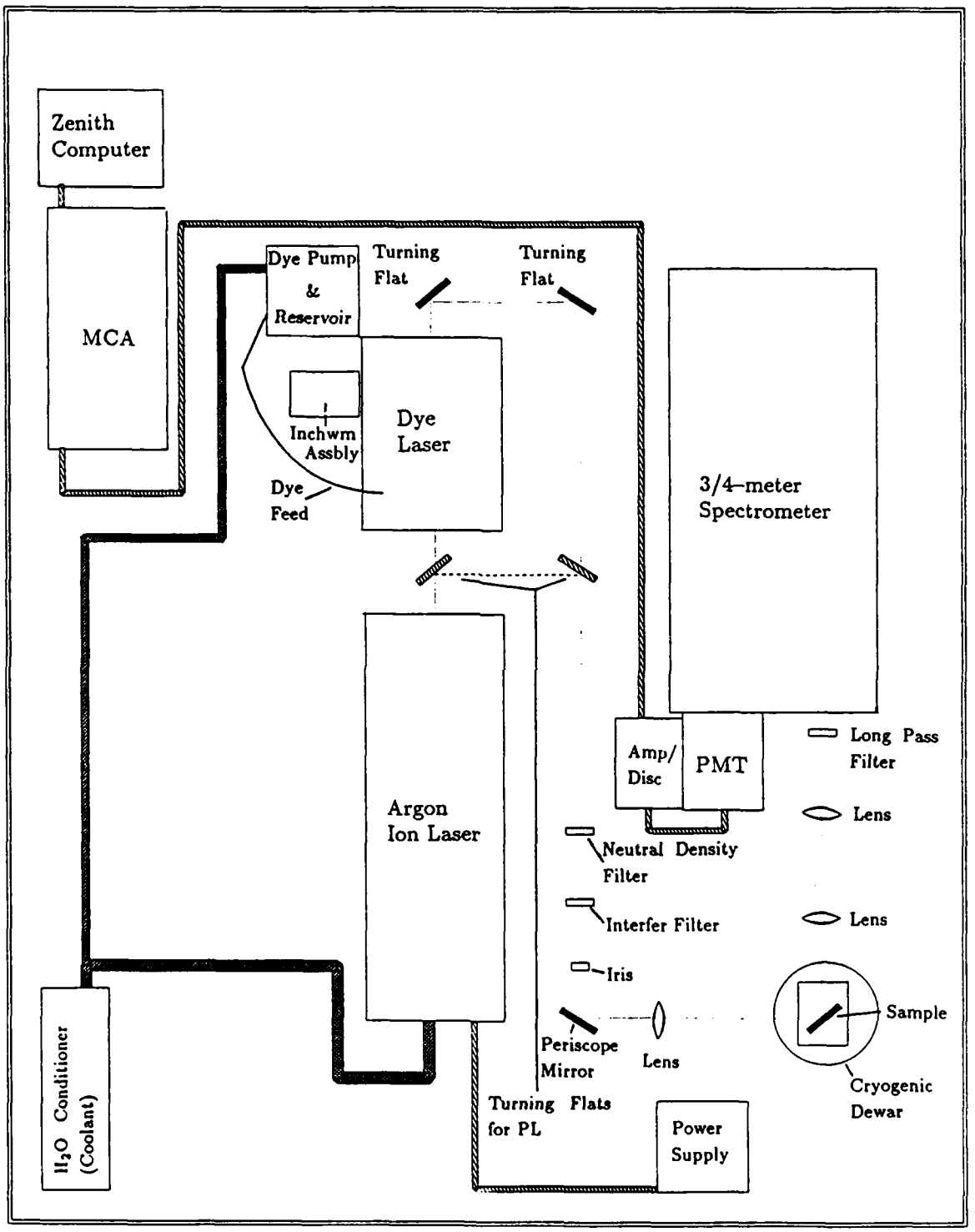

Figure 3.2. Luminescence Measurements System Diagram

Table 3.2. Select Laser Dyes and Spectral Coverage [68]

Dye	Spectral Coverage (Å)
Rhodamine 6G	5700–6550
DCM	6120–7210
LDS 698	6950–7900
LDS 751	7200–8350
LDS 821	7900–9150

375 dye laser was employed. The dye was stimulated with the Model 171-17 argon ion laser operating in the multi-line mode. Typically, three watts of pump power from the argon ion laser generated sufficient dye laser output power for sample excitation. There are a number of dyes available. These provide tunable laser excitation sources over a large spectral range. A list of dyes, and their corresponding spectral coverage, is shown in Table 3.2. The LDS 821 dye provided the required spectral coverage for this research, and it was purchased in crystalline form from Exciton Dyes, Dayton, OH. Sufficient dye was dissolved in 150 ml of propylene carbonate and 850 ml of ethylene glycol to make a two millimole solution. The propylene carbonate acts primarily as a solvent [12:44]. The ethylene glycol provides the proper viscosity such that the dye solution can be directed into a laminar jet through which the argon ion laser pump beam passes. The dye solution is pumped through a nozzle to create the jet. The pressure had to be maintained at 80–100 psi to achieve good laser performance. The dye laser output was tunable via a Spectra Physics three-plate birefringent filter. The excitation energy was selected by rotating the filter with an inchworm assembly mounted, in part, to the dye laser housing.

Several optical components were used to direct and focus the laser radiation onto the sample and to diminish unwanted radiation. Those components preceding

the sample chamber in Figure 3.2 included turning flats and a periscope mirror. The turning flats and periscope mirror were used to direct photons from the argon ion (or, for the case of below-gap excitation, the dye) laser towards the sample chamber. An iris an interference filter also preceded the sample chamber (especially for PL measurements) to reduce the intensity of stray photons and those of improper wavelength. Directly preceding the sample chamber in Figure 3.2 is a focusing lens which was used to insure that the laser spot size on the sample had a diameter of about three millimeters. Thus, typical powers of about 9.5 mW at the sample was equivalent to an intensity of about 135 mW/cm^2. For excitation intensity-dependent measurements, neutral density filters were placed between the excitation source and sample chamber to change the excitation intensity.

The optical radiation emitted by the sample was dispersed by a Spex 1702, 3/4-meter Czerny-Turner spectrometer. To focus the sample luminescence onto the spectrometer's entrance slit, two f6 lenses were placed between the sample chamber and spectrometer as shown in Figure 3.2. A long-pass filter was placed directly in front of the entrance slit for the PL measurements to eliminate additional scattered laser radiation and, therefore, decrease the background noise. The spectrometer dispersion was defined by using a grating blazed for 5000Å (its range of usefulness, therefore, extended from 3400 to 10000Å [30:57]), with 1200 lines/mm. Thus, referring to the spectrometer's user's guide, the dispersion was determined to be between 10.3Å/mm and 8.9Å/mm over the range between 8100Å and 9900Å, respectively. For typical entrance slit widths of 50, 100 and 200μ the resolution would be better than 0.5, 1.0 and 2.1Å (or 0.10, 0.19 and 0.38 meV), respectively.

The final portion of the optical detection system consisted of several components used to collect and record the photon count rate as one scanned across the wavelength spectrum. These included one of two liquid nitrogen cooled photomultiplier tubes (PMTs); RCA C31034 or Thorn EMI 9684B. RCA and Thorn

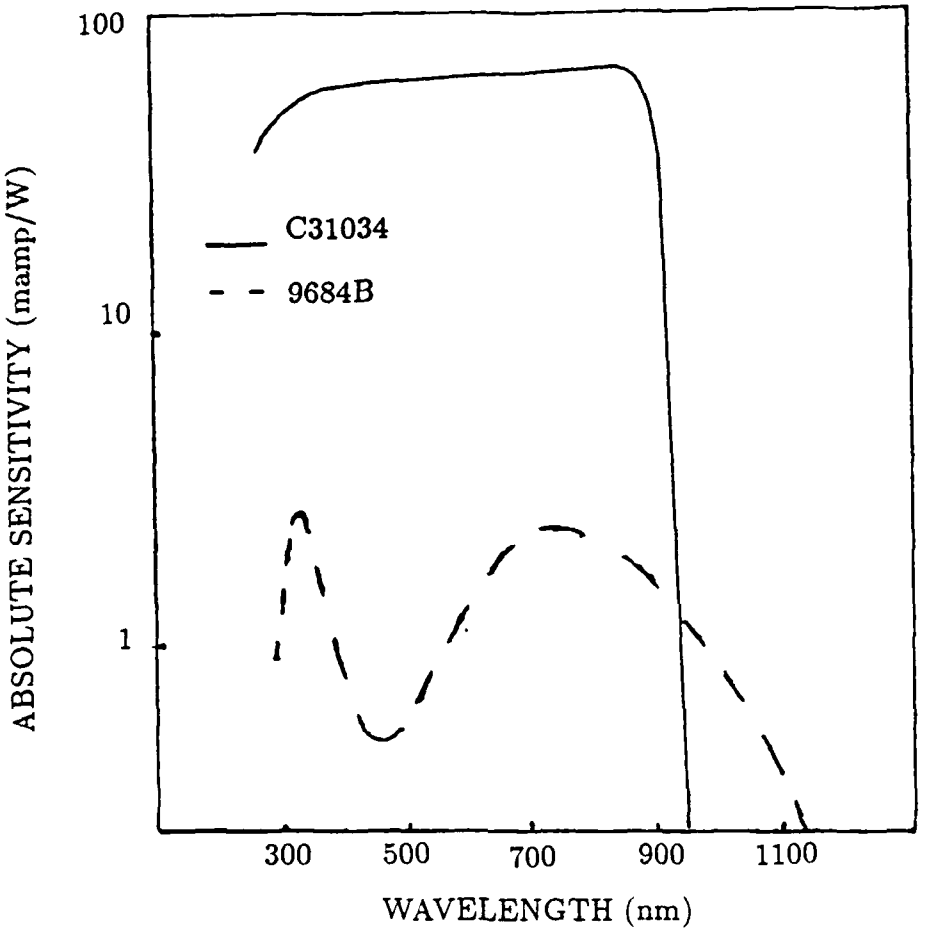

Figure 3.3. RCA C31034 and Thorn EMI 9684B Spectral Response Characteristics [58, 74]

EMI product catalogs provide the following tube characteristics [58, 74]. The RCA C31034 has a GaAs photocathode, with a flat, high gain response in the visible and near infrared regions. The tube's response decreases rapidly at energies below $\sim$1.4 eV. The Thorn EMI 9684B has a Silver-Ogxide-Cesium (AgOCs) photocathode. Its response is not as flat, nor does it exhibit the high gain of the RCA tube. However, the Thorn EMI tube is responsive to photons of lower energy than is possible with the RCA tube. Representative response curves for these tubes are shown in Figure 3.3.

The output pulses at the anode of the PMT, resulting from photons strik-

ing the photocathode, were processed with a Princeton Applied Research, Model 1121A, Amplifier-Discriminator. As its name implies, this piece of equipment provided the high-voltage across the cathode and anode of the PMT, and it also defined thresho ds to enhance the signal-to-noise ratio. The amplified signal which came from the anode was dispatched to the Tracor Northern multi-channel analyzer (MCA). The MCA's channel advance was made synchronous with the spectrometer's scan rate via an interface box. Scan rates, corresponding channel advance rates, as well as the number of channels in which data was collected, were chosen based on the total run time, signal intensity, and resolution. The run time was determined by the length of time allotted per channel and the number of angstroms that one wished to scan. The dwell time allotted to each channel was determined, in turn, by the signal's intensity. Generally, if the signal intensity is small, it is advantageous to increase the dwell time. Finally, the resolution of the MCA was just the number of angstroms covered in the run divided by the number of channels allotted to the run. This *electronic* resolution was always kept at least as good as the spectrometer's resolution. Typical runs were designed to last from 15 to 30 minutes. Dwell times ranged from 125 milliseconds to 2.5 seconds per channel and the *electronic* resolution ranged from 0.1736 to 0.868Å per channel. After collecting the data at the MCA, it was down-loaded to a floppy disk for storage and data reduction.

Sample Environment. To decrease the occurrence of non-radiative transitions, the sample's temperature was made as low as possible. A particularly useful cryogenic tool was the Janis Research Company's Detachable Tail Research Dewar. A schematic of the dewar and associated support equipment is shown in Figure 3.4.

The dewar consisted of a liquid nitrogen and liquid helium reservoir with capacities of 4 and 2.5 liters, respectively. Both reservoirs were surrounded by vacuum walls which acted as good insulators. The liquid nitrogen, at 77K, effectively served to provide a cold external environment for the liquid helium so that

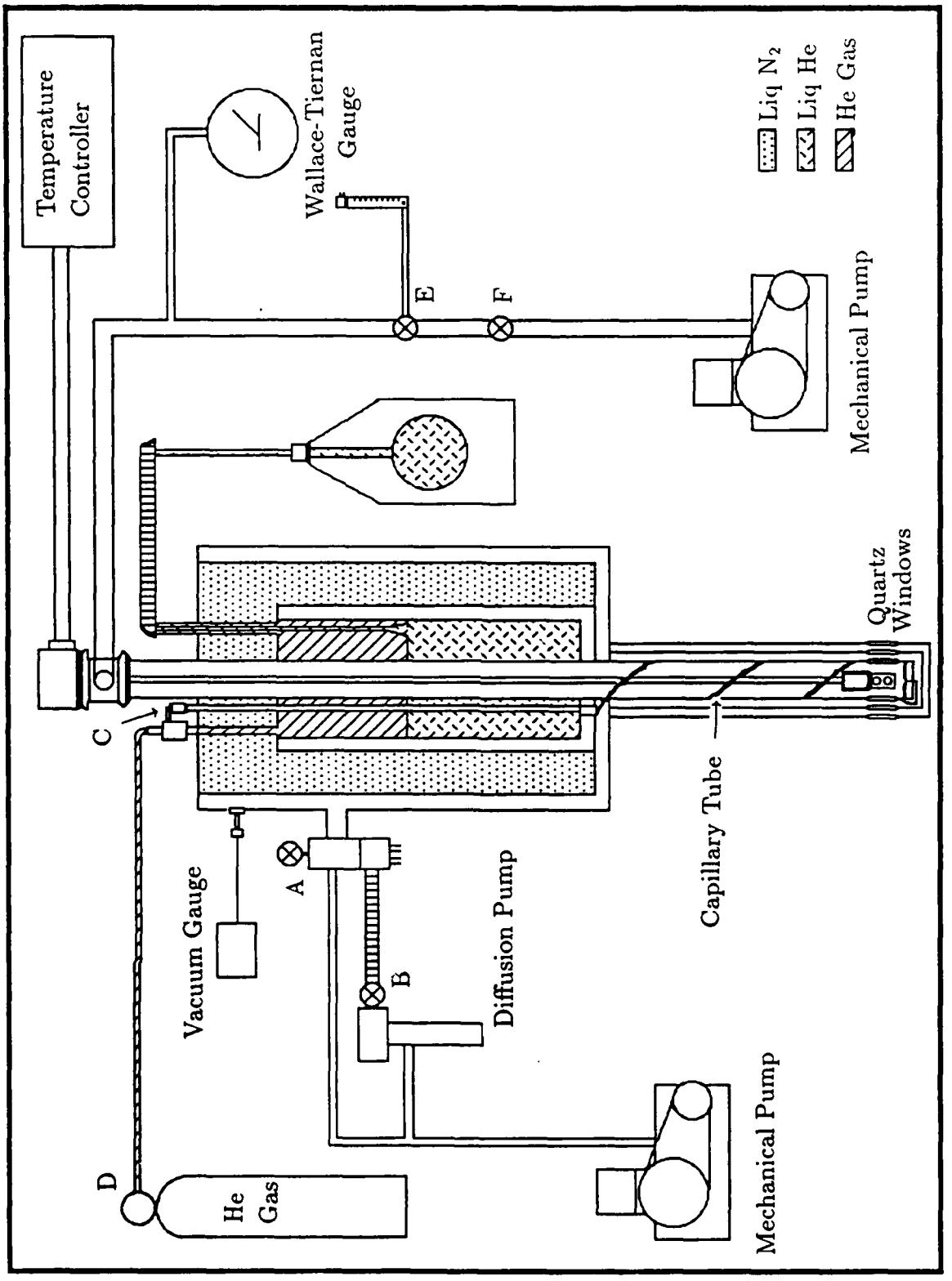

Figure 3.4. Cryogenic System

it would not boil away immediately. Just-vaporized helium came into contact with the sample to cool it to temperatures as low as about 5K. To lower the sample's temperature to 4.2K (the boiling point of helium), the sample would have to be immersed in the turbulent, boiling helium. This was found to interfere with the outgoing luminescence, degrading the intensity and statistical quality of the data, and ultimately, the measurement's resolution. To overcome this problem and, in fact, attain temperatures lower than 4.2K, it was necessary to control the helium's vapor pressure. This was done with a conventional mechanical pump. By pumping on the sample column, and thus, the liquid helium, the helium's vapor pressure was decreased to a range which spanned 25 to 30 mm of Hg (which is below helium's lambda-point of 37.8 mm of Hg [77:368]), as measured by a Wallace-Tiernan pressure gauge. By immersing the sample in the resulting *superfluid, non-boiling* liquid helium, the sample's temperature was reduced to between 2.0 and 2.1K [77:116,368].

To prepare a quasi-thermally stable environment at very low temperatures, the following procedures should be implemented using the cryogenic system of Figure 3.4:

1. Evacuate the dewar's outer jacket to $50–100\times10^{-6}$ torr by turning the butterfly valve at A so that the mechanical pump is open to the outer jacket.
2. Further evacuate the dewar's outer jacket to 10^{-6} torr, by turning the valve at A so that the mechanical pump is no longer open to the outer jacket. Next, open the valve at B so that a diffusion pump now evacuates the jacket.
3. Just prior to the addition of liquid nitrogen to its reservoir, it is imperative that all air, including water vapor, is purged from the helium space and sample chamber. Thus, the needle valve at C and valve at D should be opened. The needle valve controls the flow through the capillary tube, which connects the helium reservoir and sample chamber. By opening the valve

at D, the helium reservoir, sample chamber and capillary tube become filled with helium. Then, open the valve at E to the flowmeter. As soon as a positive flow of helium is indicated at the flowmeter, close the valves at E (also insure that the valve at F is closed to the mechanical pump) and D in the order listed. If this purge is not conducted, air or water vapor in the system will freeze, possibly inhibiting sample cooling.

4. Remove one-half of the split cover at the top of the dewar and add liquid nitrogen. The level of liquid nitrogen should be continuously checked (even after transferring liquid helium in the following step) to ensure that the entire helium reservoir is covered.

5. Transfer the liquid helium to the helium reservoir following one last helium purge as described in step 3 above. The hose that runs to the helium bottle should be removed from the helium reservoir's exhaust tube, and the valve at E should be opened to the flowmeter prior to transferring the liquid helium. The helium reservoir is full when an opaque plume exits the reservoir's exhaust tube.

6. Cool the sample to the desired temperature. Adjust the valves at E and G to maintain a stable temperature throughout the run.

7. If cooling to 2K, first allow the sample to cool to 5–10K. Then, insure that the valves at E and F are closed to the flowmeter and mechanical pump, respectively, and that the needle valve at C is slightly open. Turn on the mechanical pump and slowly open the valve at F so that it can pump on the helium space. Monitor the Wallace-Tiernan gauge. The pressure should drop rapidly at first and then stabilize in the vicinity of helium's lambda point (37.8 mm of Hg). If the pressure is not dropping to the lambda point, open the valve at F further. If the pressure does not stabilize and continues to drop rapidly, stop opening the valve at F. The pressure should stabilize, and if below 37.8 mm of Hg, it will increase slowly. Carefully adjust the

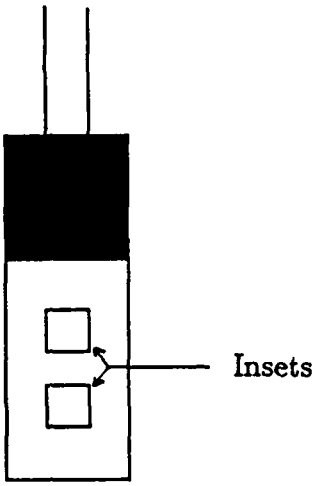

Figure 3.5. Sample Finger

needle valve at C and valve at E to immerse the sample in superfluid helium and maintain the proper vapor pressure (temperature).

The samples were mounted onto the sample finger; a copper block which has good thermal conductivity. The copper block is shown in Figure 3.5. A temperature sensing diode and heater were connected to the copper block. The Lakeshore Cryotronics temperature controller monitored the sample temperature and provided power for the heater if needed. The temperature controller was very useful for temperature-dependent PL studies. The samples were mounted into the insets shown in Figure 3.5. A small amount of silver paste (a mixture of silver and vacuum grease) was placed in one corner of each inset to provide a good thermal and strain-free contact between the samples and the copper block. (The paste was easily removed by wiping with a cotton swab). The silver paste was obtained from the Air Force Materials Lab where it is also used in low temperature experiments to mount samples. Each of four samples was subsequently placed into an inset. A

copper mask, with two properly sized and placed apertures, was then fastened to each side of the block. The mask's purpose was to prevent samples, which might become loose, from falling to the bottom of the sample chamber. It should be noted that the samples never lost contact with the sample finger when mounted with the silver paste.

IV. Results and Discussion

Luminescence results are shown mainly for the 1.52–1.42 eV spectral range. A relatively small characterization effort was performed in the 1.42–1.32 eV spectral range. Thus, only a small amount of the 1.42–1.32 eV data will be presented. Absolute peak energies are written to four decimal places in units of eV. (The wavelength to energy conversion was calculated using $E(\text{eV}) = 12395.13/\lambda(\text{Å})$). The fourth digit is subscripted if the run's resolution was poorer than 0.1 meV. The peaks are labelled in many cases according to the symbology of Table 2.7, or, for SPL, the acceptor and associated excited hole state from which the luminescence originates. In addition, the SPL and other sharp structure arising from the below-gap excitation is given an energy value (in units of meV) in parentheses. This indicates the peak's energy relative to the laser excitation energy ($\hbar\omega_p - \hbar\omega_l$). Thus, in most instances, this value also represents the energy separating an acceptor's excited state and associated ground state.

Unimplanted GaAs

The unimplanted sample was only subjected to the standard cleaning procedures described in the previous chapter. The Cr-doped semi-insulating substrate was not etched. This sample was used as one of the controls to establish the as-grown material's characteristics.

Photoluminescence. The as-grown sample's PL is portrayed in Figure 4.1. The peaks are labelled with their absolute energies. The generally poor luminescence could be the result of non-radiative surface recombination centers [51:160,165–165]. In fact, it is reasonable to assume that these centers are more probable in the un-etched (and, therefore, heavily surface-damaged), as-grown sample. The highest energy structure peaks at 1.514_2 eV. From Table 2.7, it may be concluded

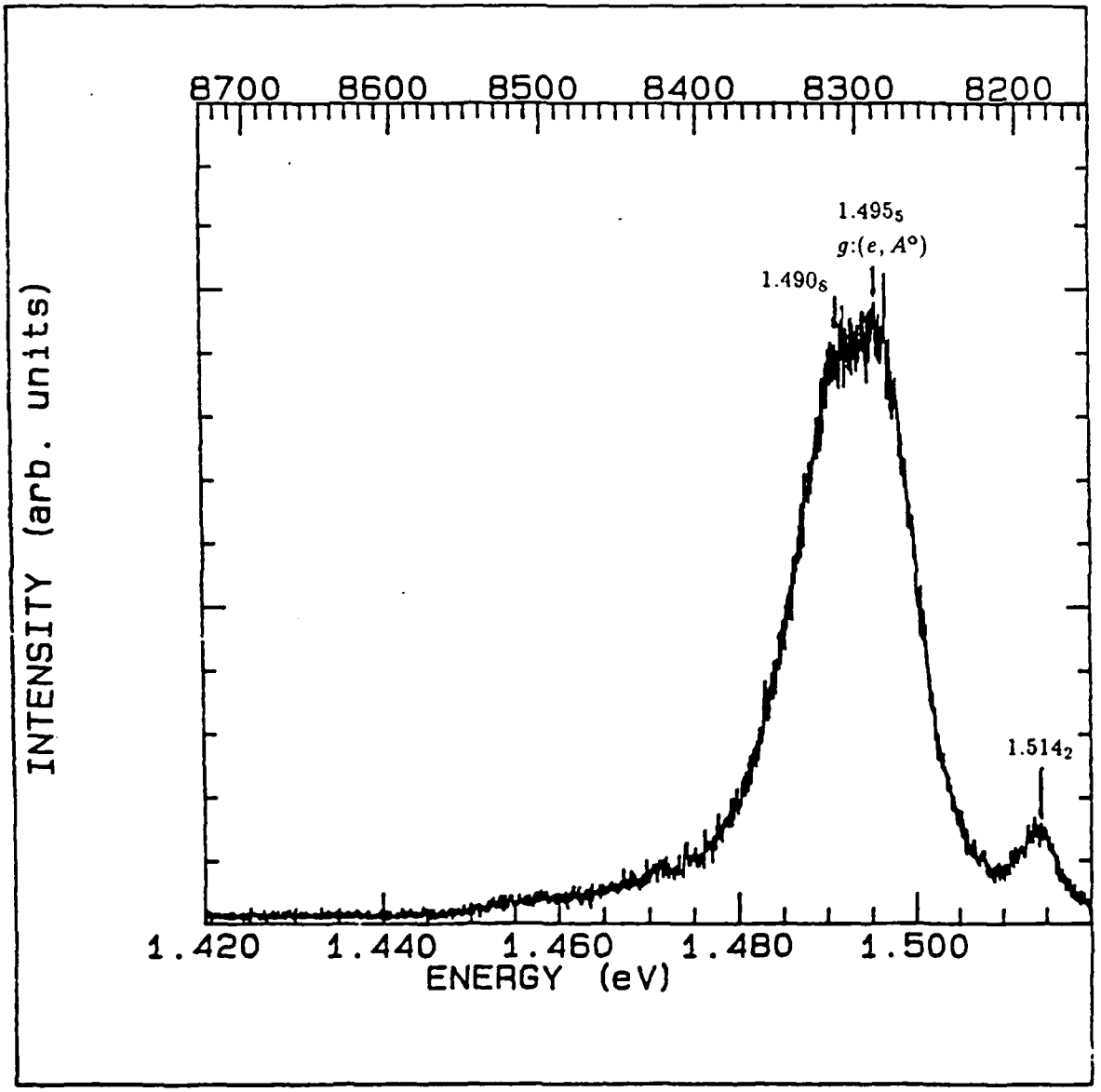

Figure 4.1. As-grown GaAs Spectrum, Exc: 2.5400 eV at 1.34W/cm^2, T=5K

that the PL arises from excitons bound to neutral donors (D°, X) with possible contributions from donor-related B-F (D°, h) transitions. However, the broad, featureless band does not allow discrimination of the particular recombination paths.

The next feature in the sample's luminescence is a more intense, broad band. Again, resolution is poor, making assignment difficult. However, it can be seen that at least two underlying peaks contribute to the band. The band actually peaks at 1.495_5 eV with a shoulder at 1.490_8 eV. The peak at 1.495_5 eV might originate from F-B transitions involving the C_{As} acceptor, (e, C_{As}) [44]. However, referencing Table 2.7, a typical (e, A°) transition energy involving the C_{As} acceptor is 1.4932 eV. The discrepancy is difficult to explain. An alternate assignment is suggested by the following findings. Rao *et al.* [57], observed a (e, A°) emission situated at about 1.496 ± 0.001 eV. It was attributed to a new acceptor whose identity, upon correlation with results published by Contour *et al.*[18], was implied to be that of the g-acceptor. Thus, the 1.495_5 eV peak, shown in Figure 4.1, will be tentatively labelled as g:(e, A°), where the acceptor is understood to be the g-acceptor. The g-acceptor's ground state binding energy has been determined to be ~ 18.5 meV in one instance [70] and 22.9 meV in another [18]. (The 1.5110 eV g line, one of a series of 15 sharp lines first observed in the PL of MBE grown GaAs by Künzel and Ploog [38, 39], is thought to originate from an exciton bound to the g-acceptor [18, 70]).

In addition to the (e, A°) transition, the broad band probably receives contributions from D°-A° pair transitions as well, considering the low sample temperature (~ 5K). From Table 2.7, D°-A° pair transitions involving the C_{As} acceptor have been observed to produce a peak at an energy of 1.4892 eV. This would possibly account for the shoulder at 1.490_8 eV. Nevertheless, based solely on these absolute energies of poorly resolved structures, argument could be made for transitions involving several other impurities including Be, Mg and Zn.

Below-Gap Excitation Luminescence. Figures 4.2 and 4.3 depict the results of below-gap excitation of the as-grown sample. Figure 4.2 is an absolute energy plot. Figure 4.3 plots luminescence intensity versus energy above the ground state (or the peak energy position relative to the laser excitation energy, $\hbar\omega_p - \hbar\omega_l$). The excitation intensity for these runs was predominantly about 140 mW/cm^2; a factor of ten less than the PL run.

Upon excitation at 1.5100 and 1.5081 eV, several sharp peaks are observed to be superimposed upon the non-selectively excited D^o-A^o pair and some (e, A^o) recombination luminescence in the 1.500–1.480 eV range of Figure 4.2. As required for SPL, these structures shift *with* the laser pump line. This behavior is best illustrated in Figure 4.3. It is also seen in Figure 4.3 that the resolution of the SPL is much improved for excitation at 1.5081 eV relative to that at 1.5100 eV. (The structures should disappear with increasing sample temperature. The structures' temperature behavior will be presented in upcoming sections). The energies separating the sharp peaks and the 1.5081 eV laser excitation are $13._9$, $17._1$, $18._2$ and $21._4$ meV. From Table 2.10, the latter two correspond fairly well to the $2S_{3/2} \rightarrow 1S_{3/2}$ transition energy of the hole bound to the C_{As} and Zn_{Ga} acceptors, respectively. The peak at $17._1$ meV from the laser excitation corresponds to the $2P_{3/2} \rightarrow 1S_{3/2}$ transition energy of the hole bound to the Mg_{Ga} acceptor. This confirms the presence of three acceptor impurities whose existence was only tentative from the PL data.

The peak, at $13._9$ meV from the laser excitation, shown in Figure 4.3, persists as the excitation energy is decreased to 1.4998 eV. From Table 2.10, the smallest acceptor excited/ground state separation is that reported for the C_{As} acceptor, $2P_{3/2} \rightarrow 1S_{3/2}$ transition, whose magnitude is 15.1 meV. From discussions in Chapter II, this excited/ground state separation is also too large relative to those reported for donor impurities. Thus, this observed separation does not fit any of the conventional donor or acceptors in GaAs. It has been suggested from

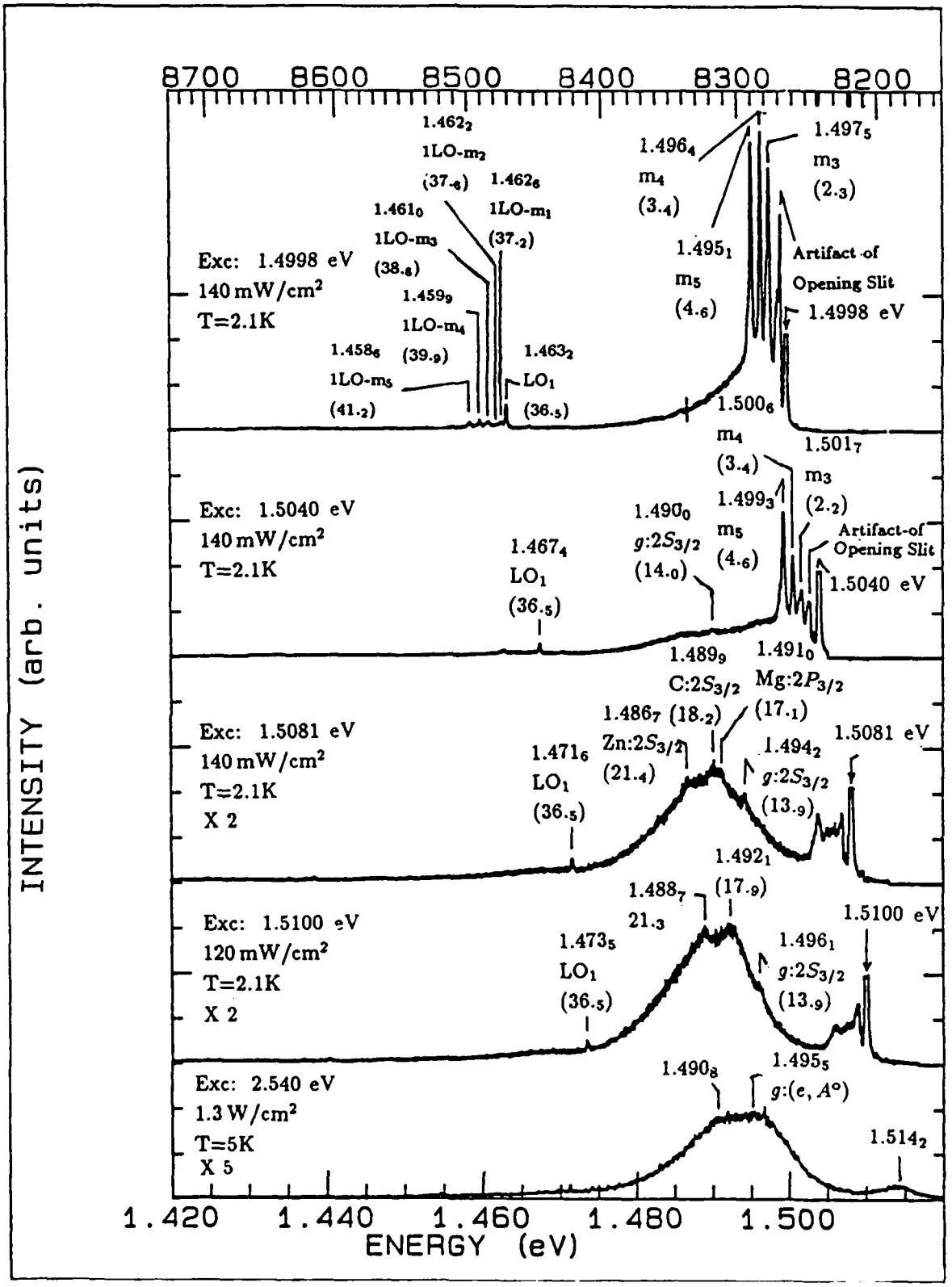

Figure 4.2. As-grown GaAs Spectra, Exc: 2.5400–1.4998 eV, T Mainly 2.1K

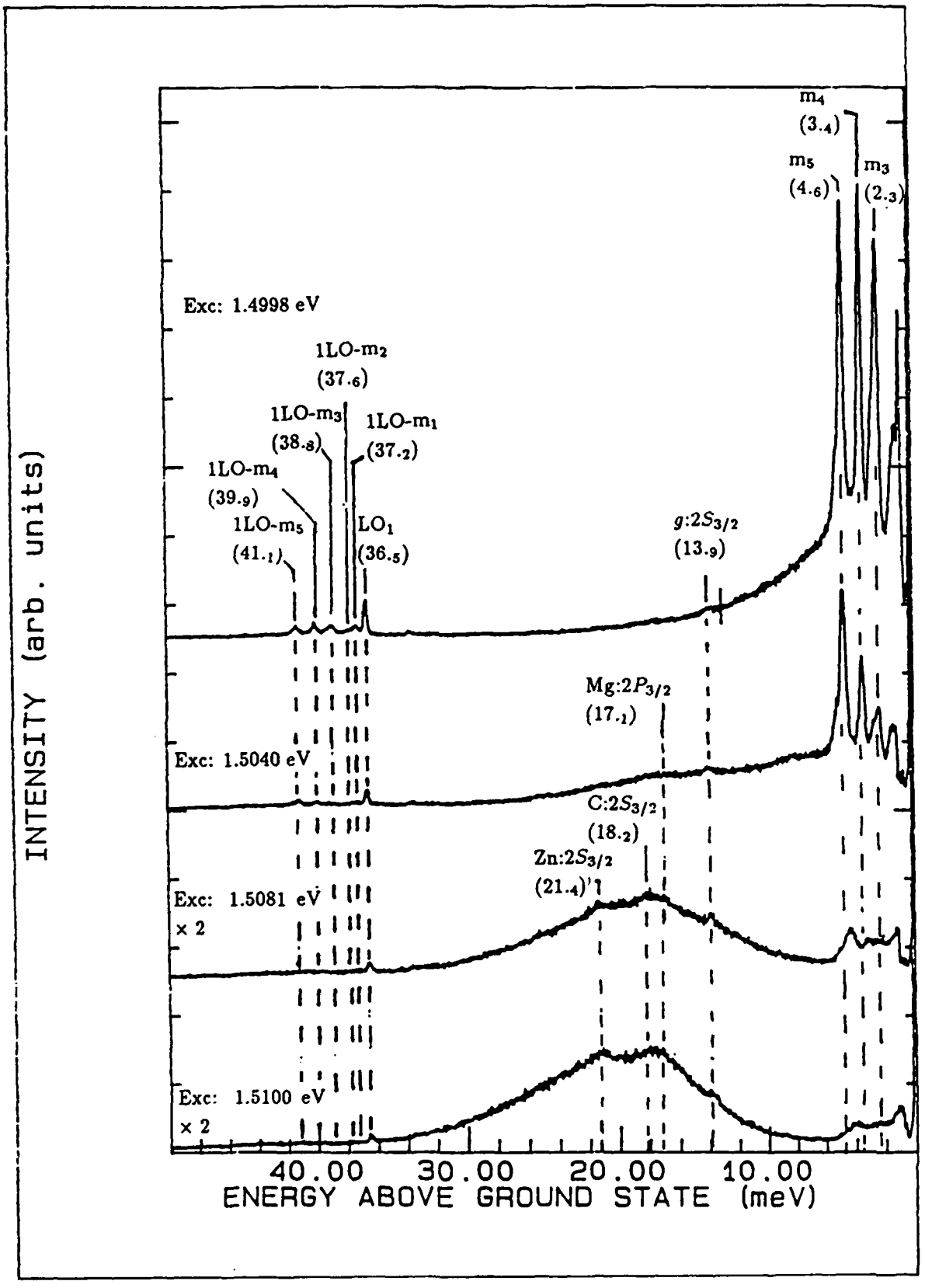

Figure 4.3. As-grown GaAs Spectra, Exc: 1.5100–1.4998 eV, T=2.1K

Table 4.1. The m-lines

Peak	$\hbar\omega_p - \hbar\omega_l$ (meV)
m_1	0.7
m_2	1.1
m_3	2.3
m_4	3.4
m_5	4.6

the PL data that this sample may contain the g-acceptor. To date, the only excited state energies reported for the g-acceptor have been determined by two-hole spectroscopy. Contour *et al.*[18] have found the g-acceptor's $1S_{3/2} - 2S_{3/2}$ energy difference to be 15.8 meV. On the other hand, Steiner *et al.*[70], found this excited/ground state separation to be 14.0 meV. Both of these investigations used MBE-grown GaAs samples. The excited/ground state separation found by Steiner *et al.* agrees very well with that observed in this *SPL* data, resulting from bulk-grown Cr-doped GaAs samples.

In addition to the SPL mentioned above, inspection of Figure 4.3 indicates another group of peaks which are enhanced as one excites the sample with decreasing energies below the bandgap. These peaks all fall within 4.6 meV of the laser line and are enumerated in Table 4.1. (Because of the unimplanted sample's poor luminescence efficiency, the spectrometer slit widths were increased just after sampling the laser pump line. Thus, data within an meV of the laser line was distorted or lost. Data for peaks m_1 and m_2 was deduced from the peaks' LO replicas). The peaks are not caused by deficiencies of the optical system. (The most troublesome deficiencies include laser scattering in the dewar windows and ghosts originating from the spectrometer's grating [24]). This is evidenced by the peaks' LO phonon replicas which are located just to the left of the LO Raman

peak (LO_1) in Figure 4.3. A possible explanation is that these peaks are modes of the dye laser resonantly interacting with electronic states in the GaAs bandgap. In fact, all of the peaks but one are separated by a constant energy (~ 1.2 meV) as would be expected for laser modes. Thus, they will be referred to as the modal lines (m-lines). Further observations will be presented in upcoming sections.

GaAs:As

A portion of the samples were implanted with As-only at 120 keV to act also as a control. The doses, ϕ, were in the range 1E13–1E15 cm^{-2}. The samples were annealed following implantation at 900°C for 15 minutes. Stoichiometrically, these samples are As-rich relative to the as-grown sample. Higher concentrations of V_{Ga}-related defects are assumed present.

Photoluminescence. Figure 4.4 shows the PL for samples implanted with varying doses of As. Immediately apparent is the overall improved PL efficiency that is obtained subsequent to the implantation and anneal of the as-grown substrate. The pre-implant surface etch, described in Chapter III, and the post-implant anneal probably are the main contributing factors.

In all cases, there is exciton-related (and possibly donor-related B-F) recombination occuring in the 1.52–1.50 eV range. At a dose of 1E13 cm^{-2}, a shoulder at 1.5151 eV and peak at 1.5139 eV have emerged from the structureless band observed in the as-grown substrate. From Table 2.7, these can be associated with free excitons and neutral donor bound excitons, respectively. The peak and shoulder gradually disappear with increasing As dose and, finally, at 1E15 cm^{-2} the luminescence in this region looks much like that of the as-grown sample. This may result from insufficient removal of the implant damage at the higher doses.

The implantation and anneal steps appeared to have created dramatic change in the 1.50–1.47 eV range. The relative importance of the transitions has changed

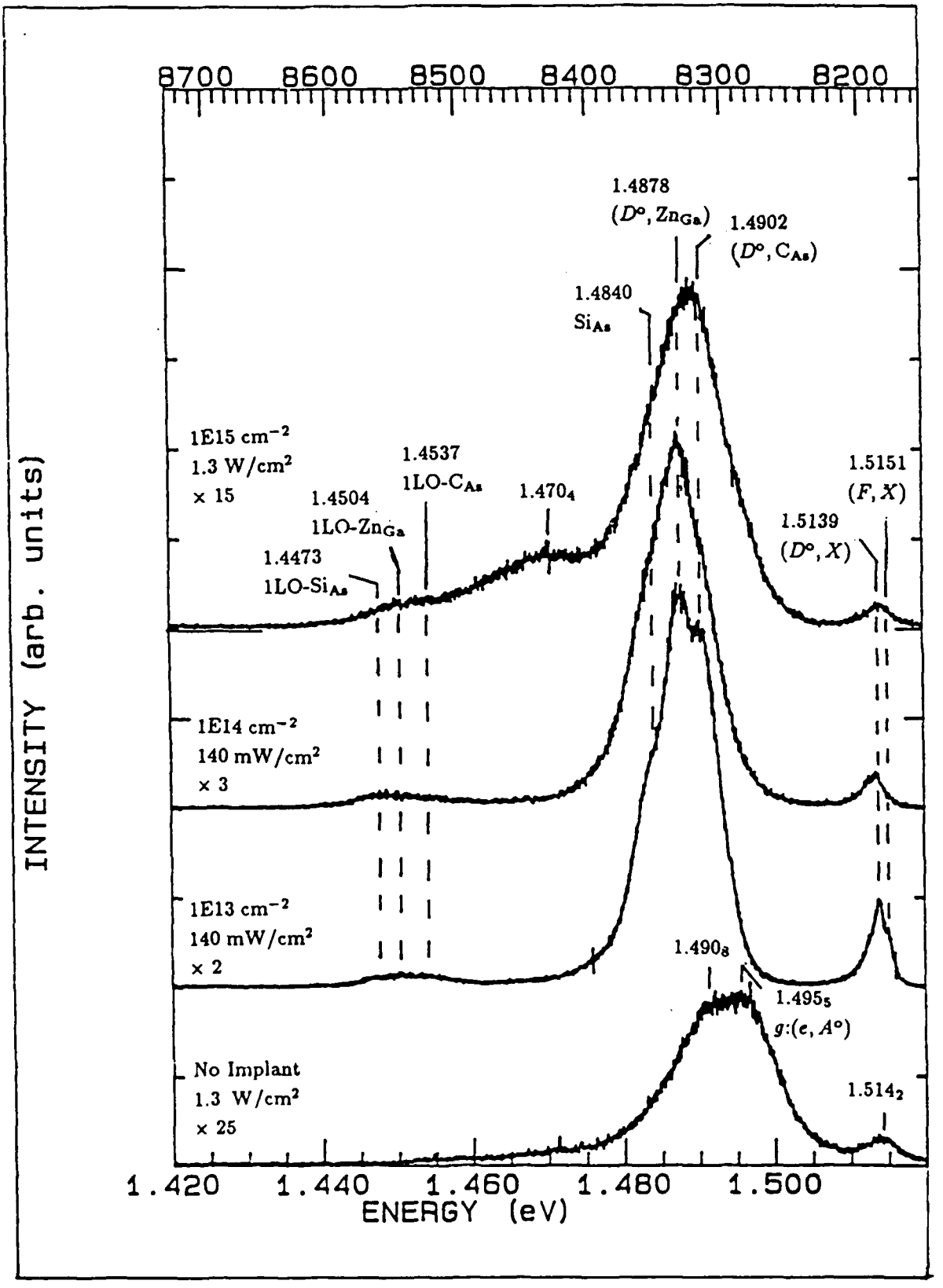

Figure 4.4. GaAs:As, ϕ=1E13–1E15 cm^{-2} Spectra, Exc: 2.5400 eV, T=5K

such that now a peak at 1.4878 eV plays a major role in the PL spectrum of the 1E13 cm^{-2}, As-implanted sample. This transition continues to dominate to the highest dose. In addition, a shoulder at 1.4840 eV is now seen, especially in the 1E13 cm^{-2}, As-implanted sample. The shoulder at 1.490_8 eV in the as-grown, unimplanted sample's PL is now clearly resolved at 1.4902 eV following the implantation at a dose of 1E13 cm^{-2}. The peak at 1.495_5 eV in the as-grown sample's PL has all but disappeared following implantation. From Table 2.7 and the SPL results of the previous section for the as-grown sample, the peak at 1.4902 eV can be attributed to (D^o, C_{As}) pair recombinations. Based solely on Table 2.7, the peak at 1.4878 eV might be assumed to involve (D^o, Mg_{Ga}) pair recombinations. However, the relatively large SPL signal originating from the hole bound to the Zn_{Ga} acceptor (seen in upcoming data) may indicate a larger contribution from (D^o, Zn_{Ga}) pair recombinations. (Thus, although the 1.4878 eV peak in Fig 4.4 is labelled as due to (D^o, Zn_{Ga}) pair recombinations, it is probable that (D^o, Mg_{Ga}) pair recombinations also contribute). The shoulder at 1.4840 eV may originate from Si_{As} acceptors. The Si could have diffused from the protective Si_3N_4 cap into the substrate during the anneal process.

LO phonons were again observed in the region 1.47–1.42 eV. Peaks located at 1.4537, 1.4504 and 1.4473 eV correspond well to LO phonon replicas of formerly assigned C_{As}, Zn_{Ga} and Si_{As} acceptor-related peaks. In addition to the phonon replicas in this region, a band peaks at 1.470_4 in the 1E15 cm^{-2}, As-implanted sample's luminescence. The band was also barely observed in the as-grown sample PL. The literature does not contain much information on the transition giving rise to the band. From Table 2.7, this energy is somewhat small even for the (D^o, Ge_{As}) pair transition. A peak has been observed at 1.468 eV in some samples which also exhibited the ~ 1.496 eV transition [57] and, therefore, apparently is the *g*-acceptor. The peak was speculated to be the result of a new deep acceptor whose identity was unknown. More recently, experiments by van de Ven *et al.*[75] noted

that a new peak at 1.467 eV was observed when horizontal-Bridgman grown GaAs was annealed in an ampoule containing a copper source. The relative intensity of the peak was enhanced by increasing the As pressure in the ampoule during the heat treatment. This is somewhat analogous to the present situation of implanting various doses of As. The authors speculated that $Cu_{Ga} - As_{Ga}$ or $Cu_{Ga} - As_i$ may be involved. Further observations about this new transition will be made in upcoming sections.

1.42-1.32 eV Photoluminescence. PL in the range 1.42–1.32 eV was not characterized for each sample considered in this research. However, such data is presented for the control, 1E13 cm^{-2} As-implanted sample as supplemental information.

As labelled in Figure 4.5, the major luminescence structure in this region is a peak at 1.407_8 eV. From Table 2.7, this may be assigned to recombinations involving the Mn_{Ga} acceptor. Other peaks in the 1.42–1.32 eV spectral range include those at 1.399_1, 1.372_3 and 1.361_9. Recalling the GaAs phonon energies presented in Chapter II, these peaks are assigned as the first TA-phonon replica (1TA), first LO-phonon replica (1LO) and the {1TA + 1LO}-phonon replica of the Mn_{Ga} acceptor-related peak, respectively.

Below-Gap Excitation Luminescence. Excitation at 1.5081 eV was performed on the 1E13 cm^{-2}, As-implanted sample and the results are presented in Figures 4.6 and 4.7. Figure 4.6 compares the luminescence obtained from the as-grown sample with that from the As-implanted and annealed sample. The $2S_{3/2}$ excited state of the g-acceptor is clearly seen in the implanted and annealed sample. On the other hand, that of the C_{As} acceptor and the $2P_{3/2}$ excited state of the Mg_{Ga} acceptor are hard to resolve. These are hard to resolve probably due to the larger background originating from (e, A^o) and non-selectively excited D^o-A^o pair recombination. The stronger $2S_{3/2}$ excited state SPL signal of the Zn_{Ga} acceptor in the

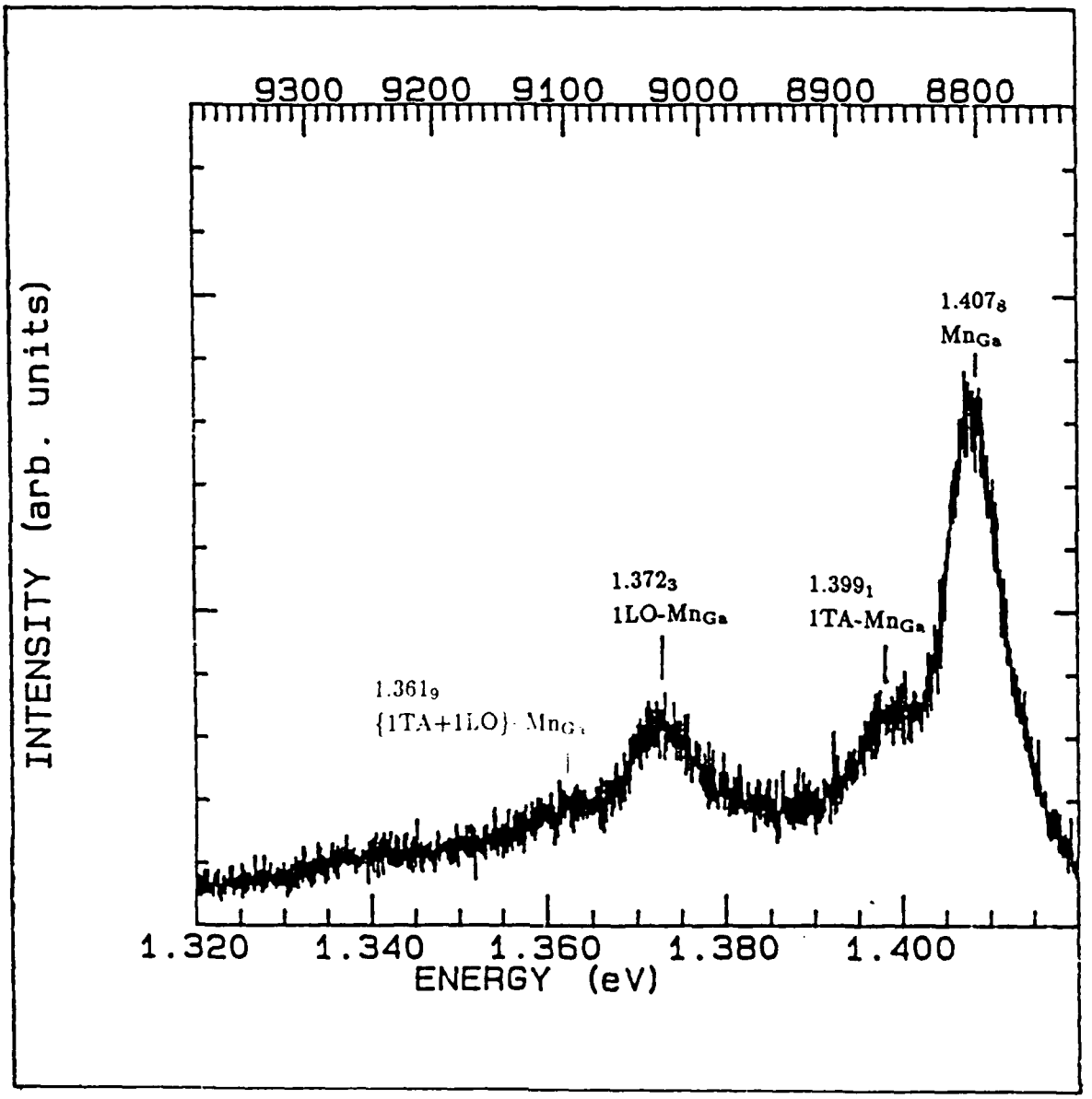

Figure 4.5. GaAs:As, ϕ=1E13 cm^{-2} Spectrum, Exc: 1.9515 eV at 1.3 W/cm^2, T=5K

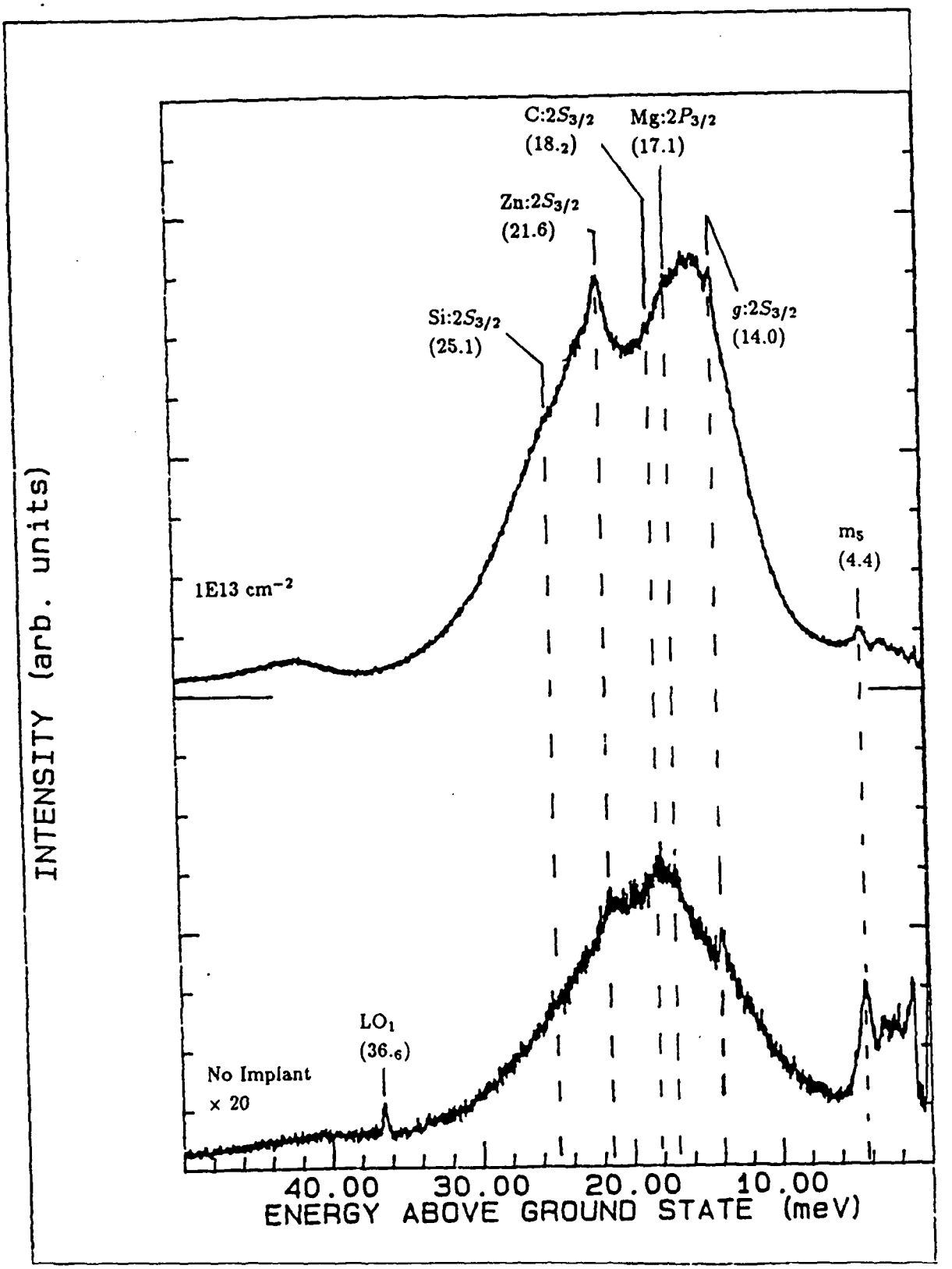

Figure 4.6. GaAs:As, ϕ=1E13 cm^{-2} Spectra, Exc: 1.5081 eV at 140 mW/cm^2, T=2.1K

As-implanted sample corresponds to the emergence of the 1.4878 eV peak (assigned to (D^o, Zn_{Ga}) pair recombinations) in the PL data. A barely discernible signal in the As-implanted luminescence, located at 25.1 meV from the 1.5081 eV laser excitation, corresponds well with the $2S_{3/2} \rightarrow 1S_{3/2}$ transition energy of the hole bound to the Si_{As} acceptor. This confirms the association of the 1.4840 eV peak, observed in this sample's PL, with the Si_{As} acceptor. In addition, one may conclude that (D^o, Si_{As}) pair recombination contributes to the 1.4840 eV luminescence.

A comparison of the above- and below-gap excitation for the 1E13 cm^{-2}, As-implanted sample is shown in Figure 4.7. A significant feature is the appearance of a peak at 1.4662 eV with below-gap excitation. The peak is presumed to be related to the $\sim$1.470 eV peak seen in the PL of the 1E15 cm^{-2} implanted sample in Figure 4.4. The peaks at 1.4577 and 1.4473 eV in the below-gap excitation luminescence of the 1E13 cm^{-2} implanted sample are assigned as LO replicas of higher-energy peaks.

1.42–1.32 eV Luminescence. The below-gap excitation data in the 1.42–1.32 eV spectral region are presented for the 1E13 cm^{-2}, As-implanted sample. These results are contained in Figures 4.8 through 4.11. Figure 4.8 shows the collective effect of decreasing the excitation energy from 1.9515 to 1.4998 eV. Exciting the sample with energies below the bandgap apparently favors recombination via the Cu_{Ga} acceptor relative to the Mn_{Ga} acceptor. At an excitation of 1.4998 eV, a sharp structure at 1.412_4 eV, separated about 87.4 meV from the laser excitation, appears on the high energy side of the Mn_{Ga} acceptor peak.

Pursuing this discovery further, it was found that this structure behaved as SPL. Figure 4.9 shows the structure's behavior when exciting the sample with various energies. Consistent with SPL, the structure tunes with the laser and occurs mainly on the high-energy side of the Mn_{Ga} acceptor-related luminescence, which will be assigned subsequently as due to (D^o, Mn_{Ga}) transitions. The energy sepa-

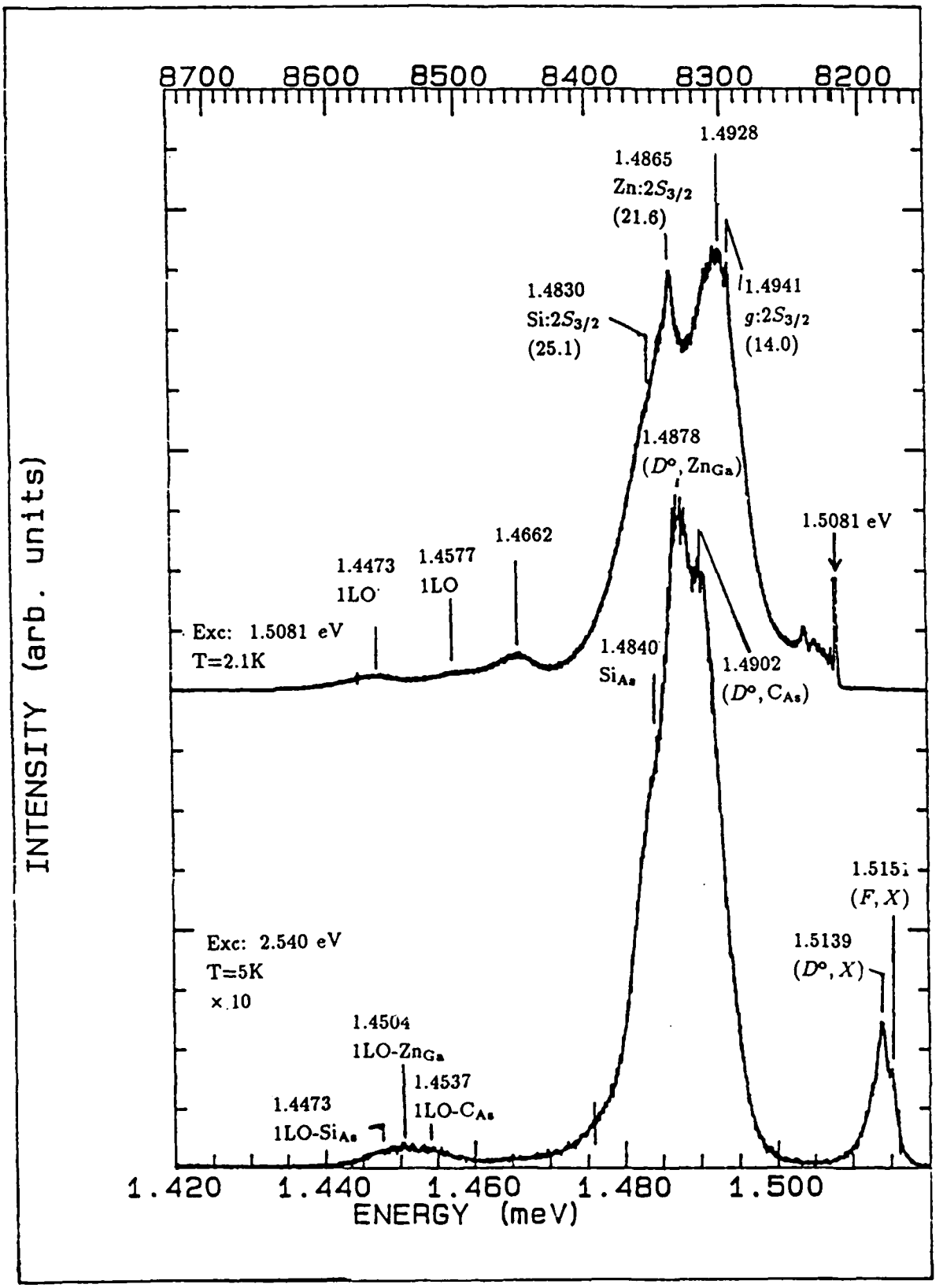

Figure 4.7. GaAs:As, ϕ=1E13 cm^{-2} Spectra, Exc: 2.5400 and 1.5081 eV at 140 mW/cm^2

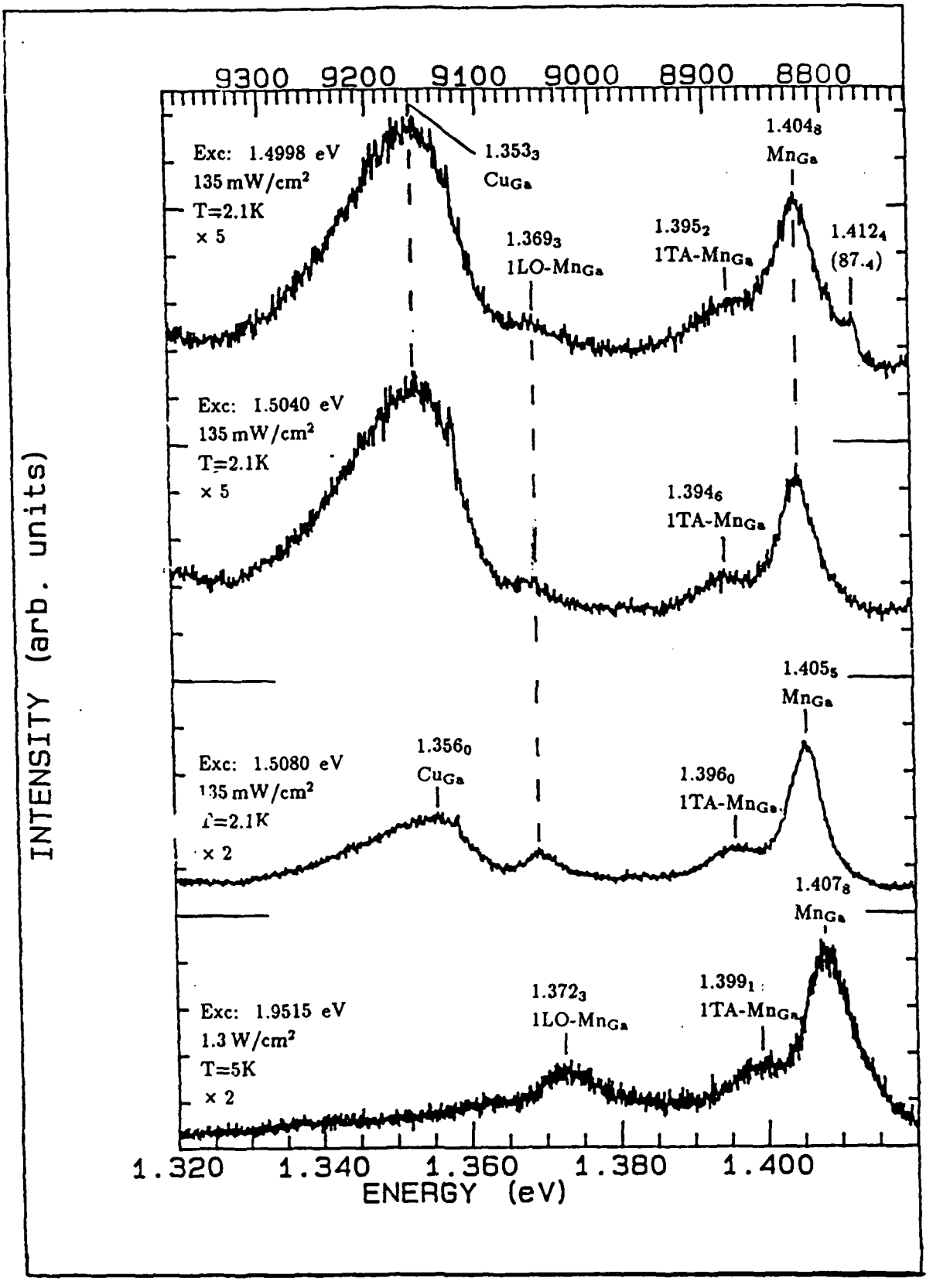

Figure 4.8. GaAs:As, ϕ=1E13 cm^{-2} Spectra, Exc: 1.9515–1.4998 eV, T Mainly 2.1K

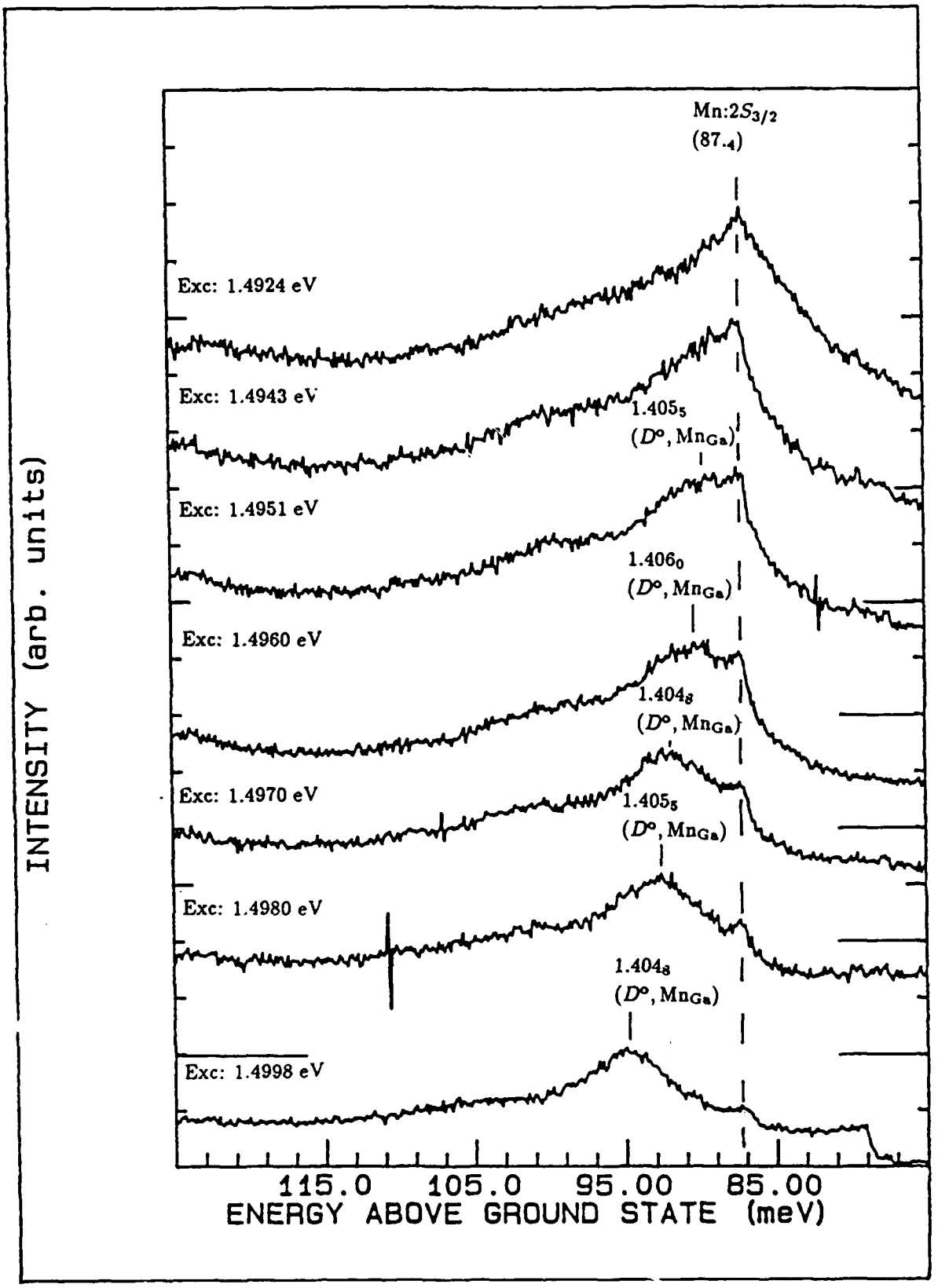

Figure 4.9. GaAs:As, ϕ=1E13 cm^{-2} Spectra, Exc: 1.4998–1.4924 eV at 135–140 mW/cm^2, T=2.1K

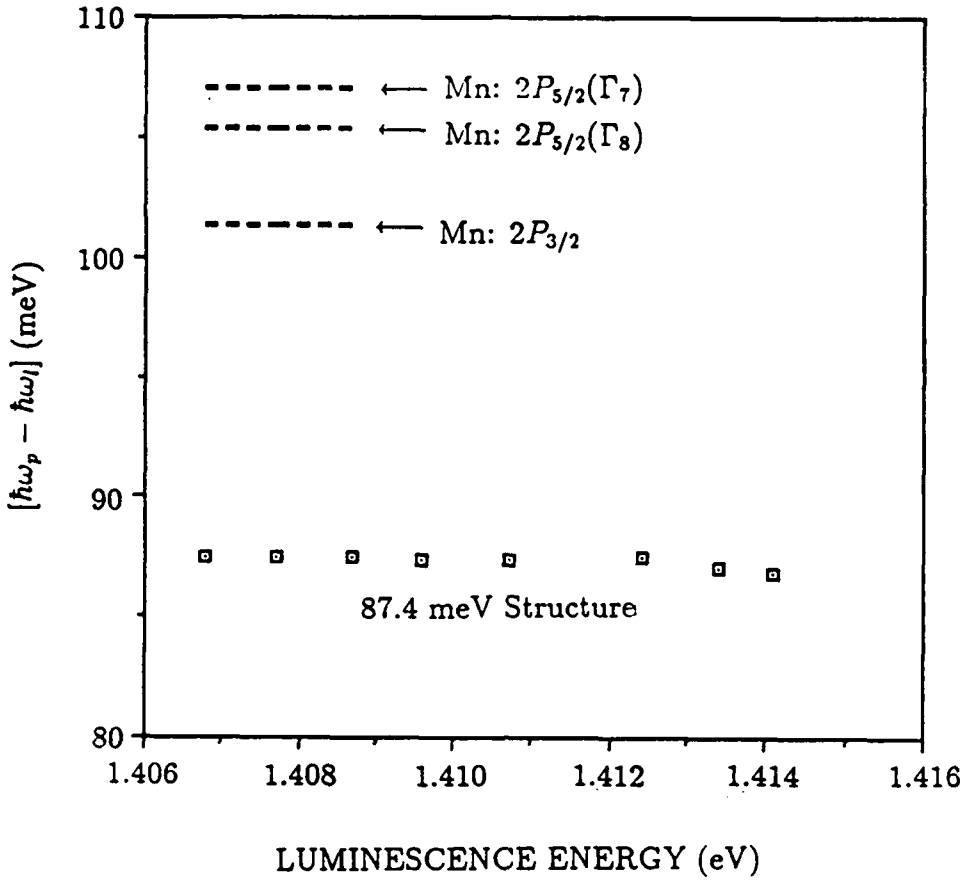

Figure 4.10. Energy Difference Between Laser Pump Line and Mn-related Structure as a Function of Emitted Luminescence Energy

ration ($\hbar\omega_p - \hbar\omega_l$) is relatively constant at about 87.4 meV over a wide range of incident laser pump energies (1.4998–1.4924 eV). This behavior is also shown in Figure 4.10 along with the known excited/ground state separations ($\hbar\omega_p - \hbar\omega_l$) of Mn_{Ga} acceptor hole states (the source of which will be discussed shortly). A slight exception to the constant 87.4 meV separation is at the far right of the plot in Figure 4.10. Here, $\hbar\omega_p - \hbar\omega_l$ is beginning to decrease. At these excitation energies, the selectively excited D^o-A^o pairs have relatively small pair separations. As discussed in Chapter II, the higher-order Coulomb interaction terms of Eq (2.22) become important and effectively decrease the excited/ground state separation (which is manifested as a decreased magnitude for $\hbar\omega_p - \hbar\omega_l$). Finally, Figure 4.11 shows the characteristic SPL temperature behavior for the structure. It is also observed in Figure 4.11 that the broad peak, with an arrow at its maximum and associated

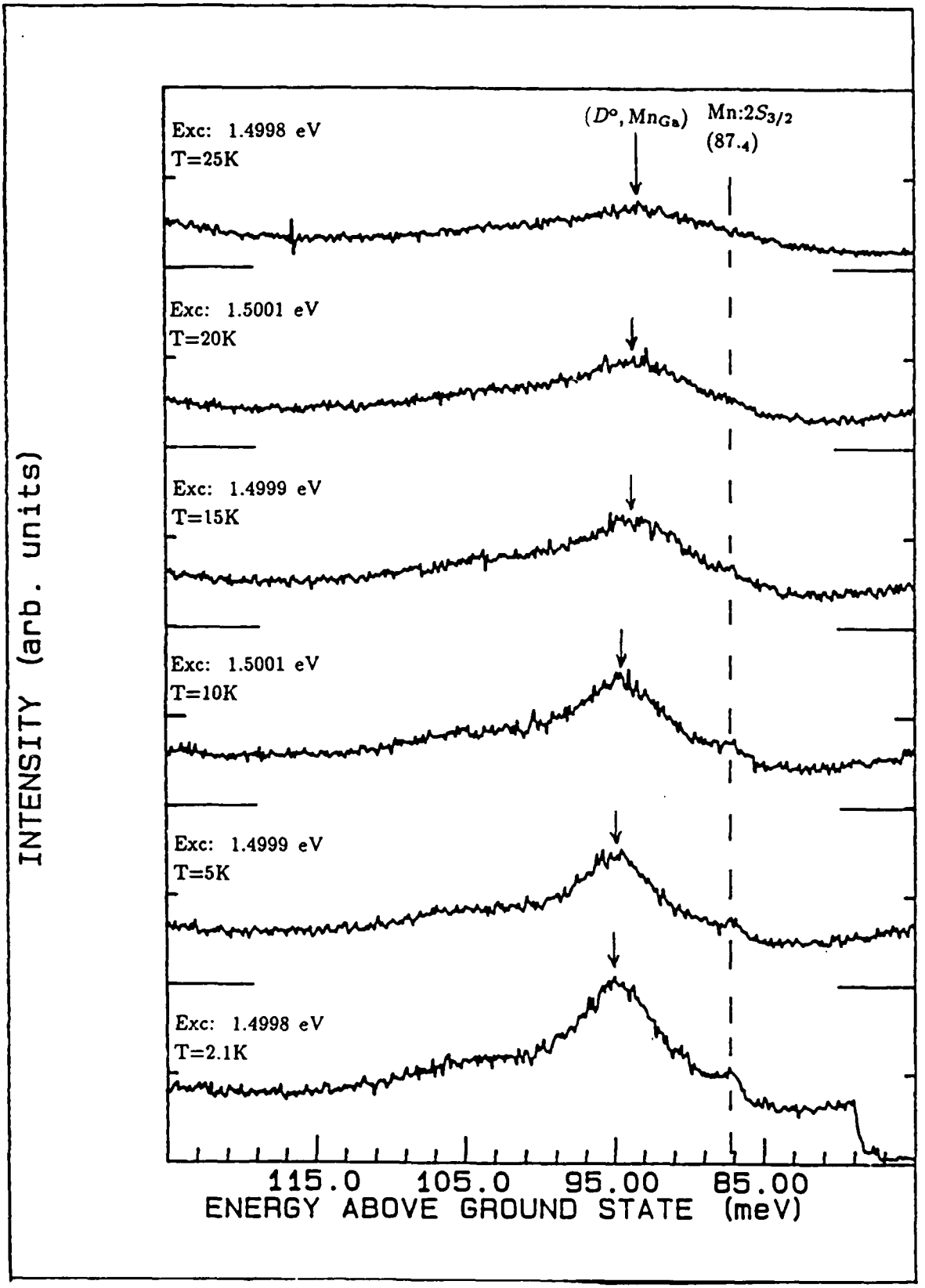

Figure 4.11. GaAs:As, ϕ=1E13 cm^{-2} Spectra, Exc: 1.4998–1.5001 eV at 135 mW/cm^2, T=2.1–25K

with the Mn_{Ga} acceptor, shifts closer to the laser pump line. This is a result of the peak's shift to higher energy, with increasing temperature. The broad peak also disappears rapidly as the temperature is increased to 25K. This indicates, as is already expected from the SPL data, that D°-A° pair recombinations contribute to the peak normally associated with the Mn_{Ga} acceptor.

The location of the apparent excited state (on the high energy side of a D°-A° pair-related peak involving the Mn_{Ga} acceptor) would indicate that it arises from the Mn_{Ga} acceptor. The plausibility of this observation, however, is not straightforward. It implies that Mn, a $3d$ transition-metal, behaves as a conventional shallow acceptor in GaAs. Actually, the question of how the electronic ground state of the neutral Mn_{Ga} acceptor is properly described is quite controversial [60]. Previous experimental evidence has supported both a tight-binding and delocalized configuration (representative of the shallow, hydrogenic, substitutional impurities in semiconductors) for the acceptor hole. The recent electron-spin resonance measurements in [60] further verify the latter, which would allow for an effective-mass type excited state to be observed by the selective excitation technique.

Chapman and Hutchinson [16] provided the first experimental evidence for the delocalized configuration. Their infrared-absorption study discerned three excited-hole states, from which Schneider *et al.* [60] calculated the binding energy of the Mn_{Ga} acceptor ground state. This information (which was already presented in Figure 4.10) and the current SPL result is provided in Table 4.2. If one accepts Chapman and Hutchinson's assignments, the currently observed excited state could be the $2S_{3/2}$ state. This conclusion implies, however, that the $2S_{3/2}$ state is deeper than the $2P_{3/2}$ hole state, which is contrary to findings for the shallower acceptors. Nevertheless, this behavior may result from the relatively strong potential at the Mn_{Ga} acceptor core and the hole's liklihood of being located in the vicinity of this core. The stronger the potential at the core, the larger the magnitude of the CCC. A hole in the $2S_{3/2}$ state has a *much* greater probability of

Table 4.2. Bound Hole States for the Mn_{Ga} Acceptor in GaAs

Hole State	Binding Energy (meV)	Excited/Ground State Separation (meV)
$1S_{3/2}$	113	0
Proposed $2S_{3/2}$	25.6	87.4
$2P_{3/2}$	11.7	101.3
$2P_{5/2}(\Gamma_8)$	7.7	105.3
$2P_{5/2}(\Gamma_7)$	6	107

being found in the vicinity of the core than one in the $2P_{3/2}$ state. Shanabrook *et al.* [63], have deduced from two hole transitions in GaAs [4] that the magnitude of the CCC for any given hole state (and given impurity core) appears to be proportional to the amplitude of the state's wavefunction at the core. Thus, an unusually large CCC for the relatively deep Mn_{Ga} acceptor may have drawn the $2S_{3/2}$ state further into the gap compared to the $2P_{3/2}$ state.

A final step in the analysis is to estimate (using effective mass theory) the transition energy for the hole bound to the Mn_{Ga} acceptor when going from the ground state to the proposed excited state, and compare this energy with that observed experimentally [63]. (The following methodology, used for the determination of the subject transition energy, was borrowed from reference [63]). The proposed $2S_{3/2}$ excited state was determined from the SPL data to be separated from the ground state by about 87.4 meV. From Table 4.2, the ground state binding energy was calculated to be 113 meV (in other words, the ground state is located 113 meV above the valence band). Baldereschi and Lipari [7] calculated the ground state energy for the effective mass acceptor (EMA) as 25.67 meV. The magnitude of the CCC for the ground state of the Mn_{Ga} acceptor is then given by

$$\begin{aligned} \mathrm{CCC}(1S_{3/2}) &= E(1S_{3/2}) - E[1S_{3/2}(\mathrm{EMA})] \\ &= 113 - 25.7 = 87.3\,\mathrm{meV} \end{aligned}$$

Baldereschi and Lipari [6] also calculated the amplitudes of the $1S_{3/2}$ and $2S_{3/2}$ wave functions at the Coulomb core. The ratio of the wavefunctions' amplitudes is 7.7. Therefore, from the discussion in the previous paragraph, it is reasonable to approximate the CCC for the $2S_{3/2}$ state of the hole bound to the Mn_{Ga} acceptor as

$$CCC(2S_{3/2}) = [CCC(1S_{3/2})]/7.7 = 11.3\,\text{meV}$$

Thus, the binding energy for the $2S_{3/2}$ state is estimated to be

$$\begin{aligned} E(2S_{3/2}) &= E[2S_{3/2}(\text{EMA})] + CCC(2S_{3/2}) \\ &= 7.6 + 11.3 = 18.9\,\text{meV} \end{aligned}$$

Finally, the hole transition energy for the $2S_{3/2} \rightarrow 1S_{3/2}$ transition would be

$$E(1S_{3/2}) - E(2S_{3/2}) = 113 - 18.9 = 94.1\,\text{meV}$$

The calculated transition energy is within 8% of the value determined from SPL. The techniques employed here have produced what appears to be the first experimental evidence for the $2S_{3/2}$ excited state of the hole bound to the Mn_{Ga} acceptor.

GaAs:Ga

Samples were implanted with Ga-only, with doses ranging from 1E13–1E15 cm^{-2} at an energy of 120 keV, to serve as another control set. The samples were annealed following implantation at 900°C for 15 minutes. Stoichiometrically, these samples are Ga-rich relative to the as-grown sample. Thus, it is assumed that higher concentrations of V_{As}-related defects will be present.

Photoluminescence. Figure 4.12 shows the PL for samples implanted with various doses of Ga. As was the case for the As-implanted samples, there is an overall improved luminescence efficiency that is obtained subsequent to the implantation and anneal of the as-grown substrate.

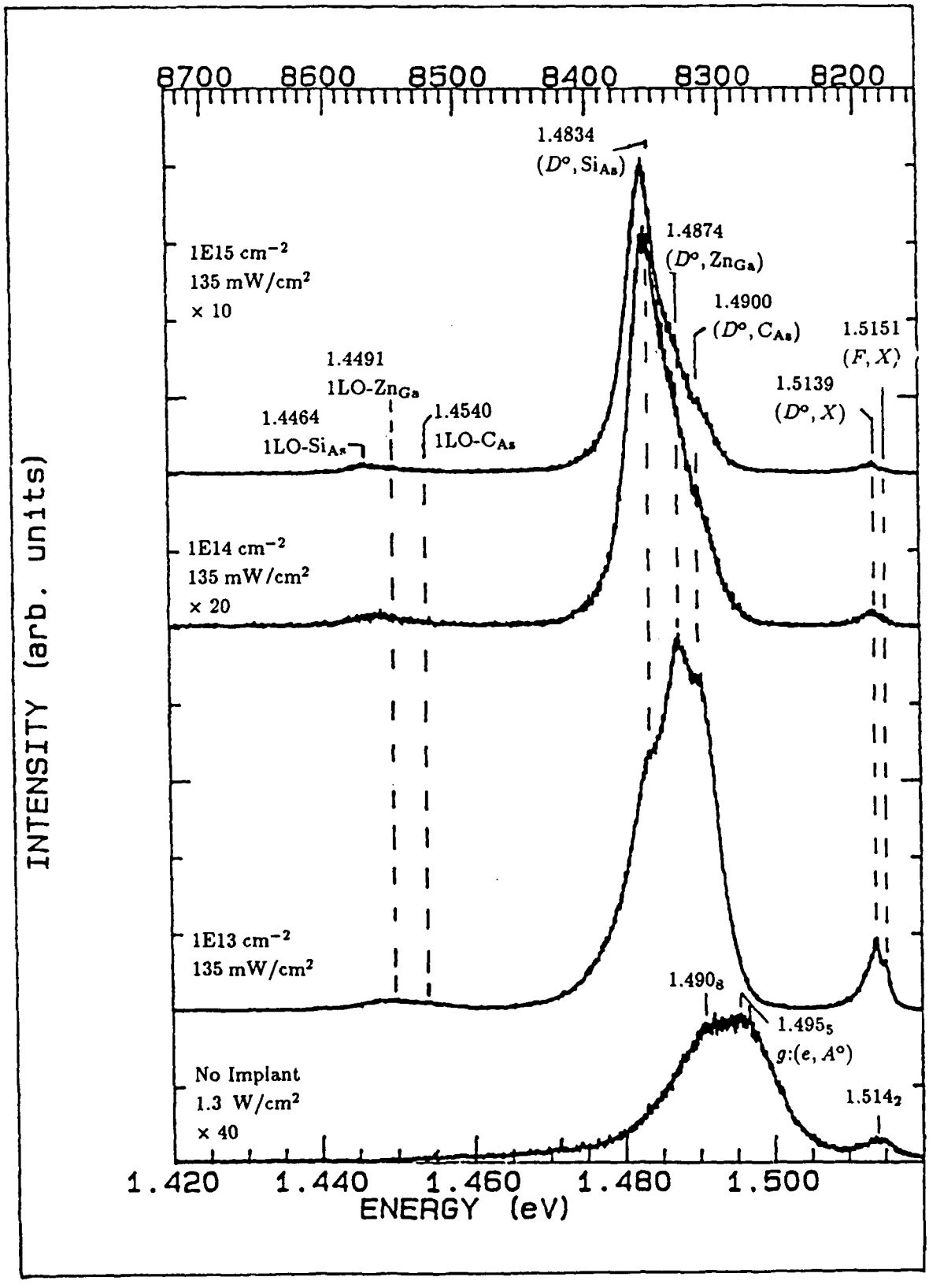

Figure 4.12. GaAs:Ga, ϕ=1E13–1E15 cm^{-2} Spectra, Exc: 2.5400 eV, T=5K

The Ga-implanted samples' luminescence peaks (and their associated behavior), observed in the 1.52–1.50 eV spectral range, are almost identical to those of the As-implanted samples (shown in Figure 4.4). At a dose of 1E13 cm^{-2}, a peak at 1.5139 eV and shoulder at 1.5151 eV have again clearly emerged from the band. As before, these may be associated with neutral donor bound excitons and free excitons, respectively. The peak and shoulder gradually disappear with increasing Ga dose and, finally, at the 1E15 cm^{-2} dose, the PL in this region looks much like that of the as-grown sample. Again, the damage created by the high implant dose appears to have not been completely removed by the anneal.

Similar to the case for the As-implanted samples, there is quite a dramatic change in the 1.50 -1.47 eV PL after implanting Ga and performing the subsequent anneal. In addition to the emergence of the peak at 1.4874 eV after the 1E13 cm^{-2} Ga-implant, shoulders are clearly seen at 1.4900 and 1.4834 eV. These peak energies are very close to those noted for the As-implant PL. Noting this (and the SPL involving the Si_{As} acceptor shown in upcoming discussions) these features are attributed to D^{o}-A^{o} pair recombinations involving Zn_{Ga}, C_{As} and Si_{As} acceptors, respectively. Again, the Si impurity probably originates from the Si_3N_4 cap used during the anneal. At higher doses, the features at 1.4874 and 1.4900 eV have all but disappeared. However, the shoulder at 1.4834 eV has now become a clearly resolved peak. These results indicate that the higher doses of Ga, which are assumed to cause higher concentrations of V_{As} defects, have improved the relative activation of the Si_{As} acceptor, which contributes directly to the 1.4834 eV peak. (In fact, larger concentrations of V_{As} defects will provide more As sites for the Si to occupy).

In the 1.47–1.42 eV range, the dominant features are the LO replicas of the transitions observed in the 1.50–1.47 eV range. The $\sim$ 1.470 eV peak is not discerned here either because the states giving rise to the peak are not present, or the associated transition's oscillator strength is relatively very small when exciting

the sample with above-gap photons (as was shown in Figure 4.7 for the sample implanted with As at a dose of 1E13 cm^{-2}).

Below-Gap Excitation Luminescence. Luminescence resulting from subjecting the Ga-implanted samples to below bandgap excitations is shown in Figures 4.13 and 4.14. Figure 4.13 illustrates the effects of tuning the excitation source from 2.5400–1.5080 eV. By changing the excitation energy from 2.5400 eV to 1.5300 eV, luminescence in the 1.52–1.50 eV range has increased in intensity relative to that in the 1.50–1.47 eV range. Transitions at 1.5141 and 1.5124 eV are clearly enhanced. From Table 2.7, these may be assigned to neutral donor and acceptor bound excitons, respectively. Also resolved is a shoulder at 1.5111 eV which, from earlier discussions, may be assigned to an exciton bound to the g-acceptor, (g,X). By decreasing the excitation energy to 1.5098 eV, one is now able to observe sharp structures at 1.4958, 1.4916 and 1.4882 eV. These peaks' relative positions with respect to the laser line indicates that they are due to SPL involving the g, C_{As} and Zn_{Ga} acceptors' $2S_{3/2}$ hole state, respectively. Another significant observation is that the transition giving rise to a peak at 1.4671 eV is enhanced. Again, this is presumed to be related to the peak at $\sim$1.470 eV previously observed. After tuning the dye laser to 1.5080 eV, the previously noted SPL structure shifts accordingly. Also, additional structure at 1.4927 and 1.4828 eV are resolved. The peaks are separated 15.3 and 25.1 meV from the laser pump line, respectively. From Table 2.10, these can be assigned as SPL involving the C_{As}, $2P_{5/2}$ and Si_{As}, $2S_{3/2}$ hole states.

Figure 4.14 shows the net effect of Ga-implantation and anneal on luminescence excited at $\sim$1.508 eV. The structure associated with the Si, $2S_{3/2}$ hole state is clearly enhanced for the implanted and annealed substrates. This observation is consistent with the PL data for these samples. It is also seen in the figure that the relative intensity of a broad background at about 1.492 eV increases with the Ga dose. In absolute terms, this energy corresponds to (e, C_{As}) transitions.

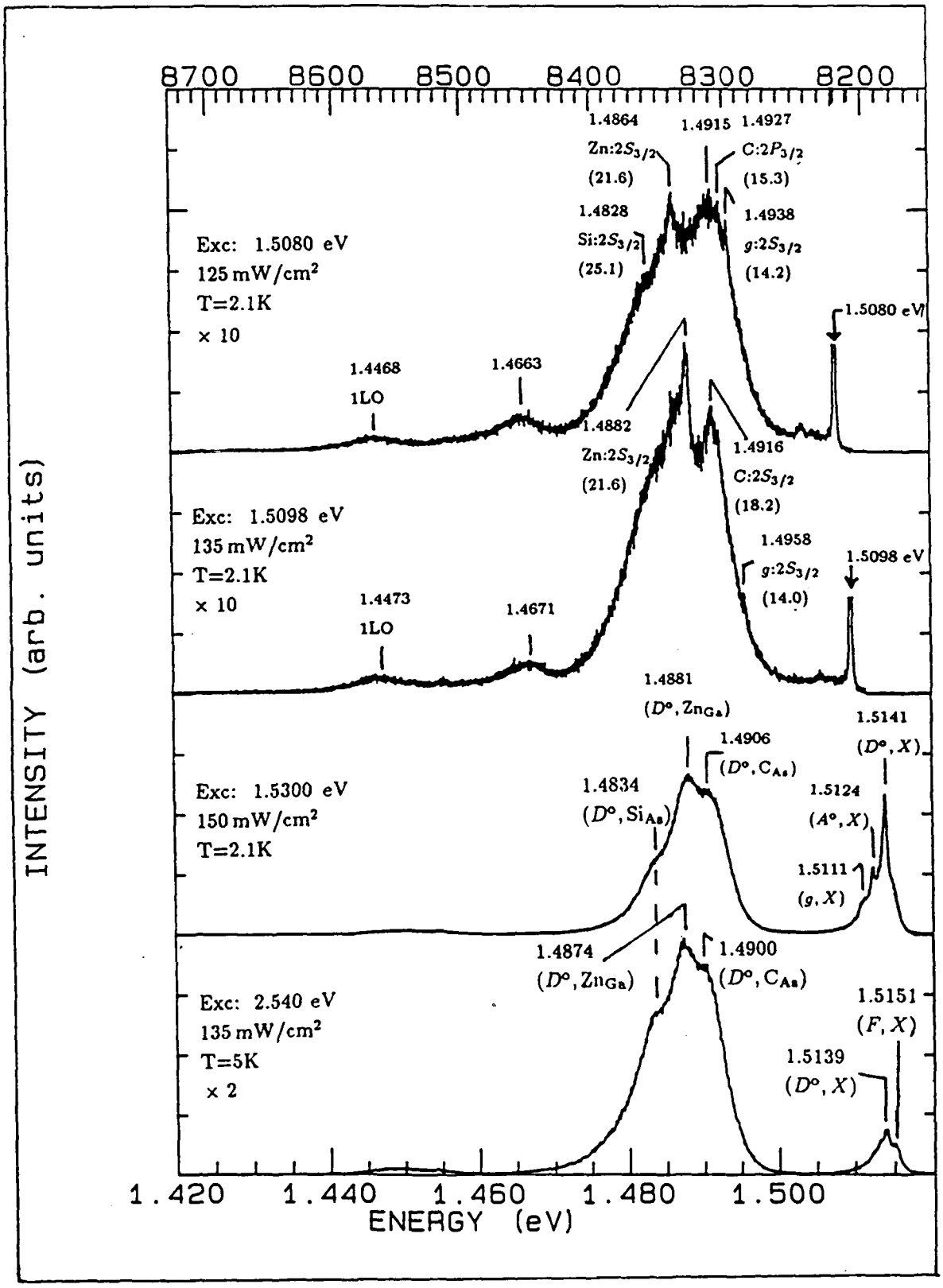

Figure 4.13. GaAs:Ga, ϕ=1E13 cm^{-2} Spectra, Exc: 2.5400–1.5080 eV, T Mainly 2.1K

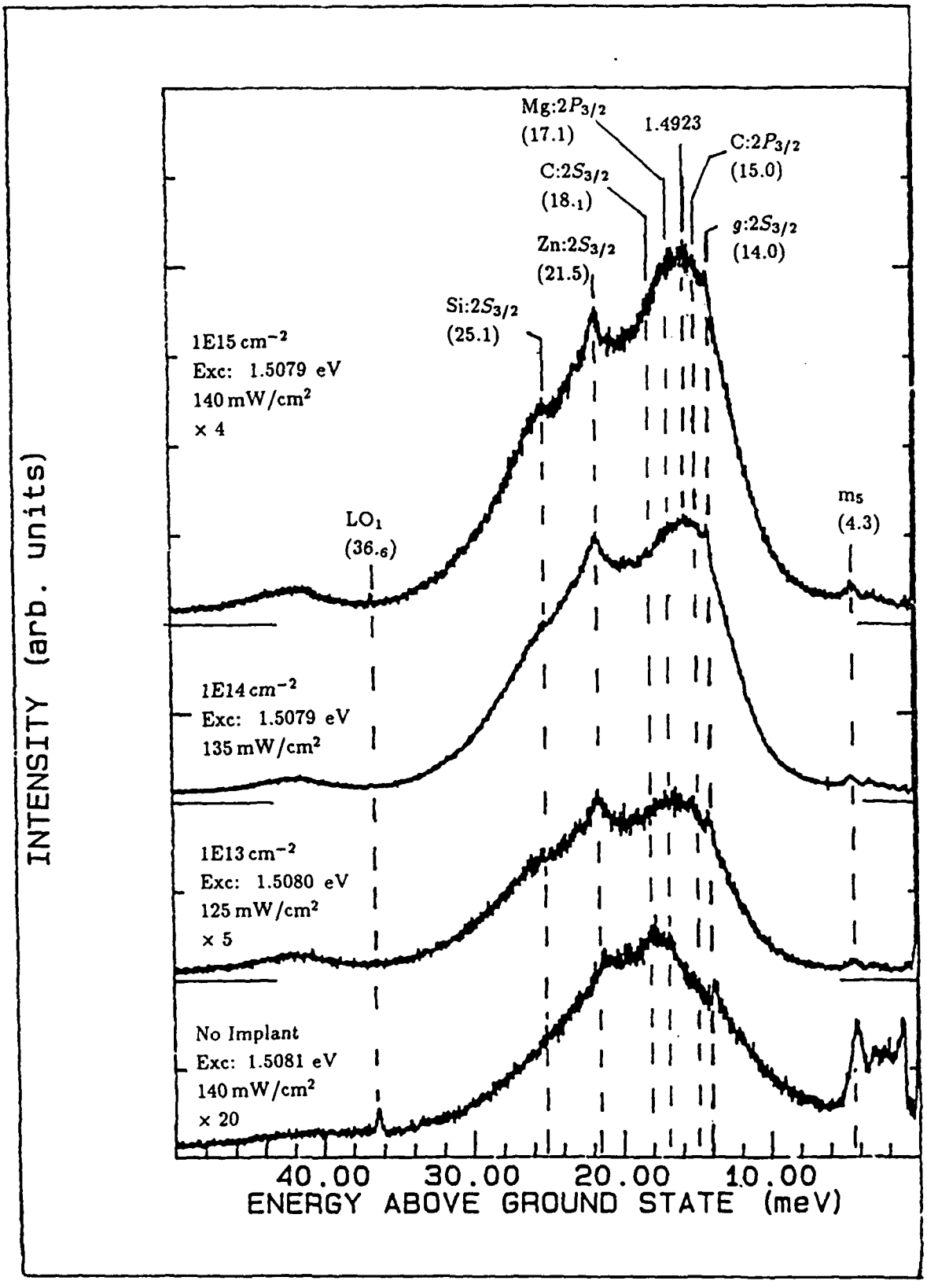

Figure 4.14. GaAs:Ga, ϕ=1E13-1E15 cm^{-2} Spectra, Exc: 1.5079-1.5081 eV, T=2.1K

GaAs:Ge

The luminescence for samples implanted with Ge in the dose range of 1E13–1E15 cm^{-2} is presented below. All samples were annealed at 900°C for 15 minutes.

1E13 cm^{-2} Implant.

Photoluminescence. PL from the sample implanted with Ge, at a dose of 1E13 cm^{-2}, is shown in Figure 4.15. The spectra were obtained by varying the 2.5400 eV (4880Å) excitation intensity from 135 $\mu W/cm^2$ to 140 mW/cm^2. PL in the 1.52–1.50 eV is almost undetectable. Peaks, shown to range from 1.474_2–1.4767 eV, emerge dominant in the 1.50–1.47 eV range. These were not observed in the control samples. All other PL in this range originates from acceptors whose presence was already noted in the control samples (as-grown and/or As- and Ga-implanted). The new peak can be assigned to recombinations involving the hole bound to the Ge_{As} acceptor. The peak's shift toward higher energy with increasing excitation intensity, plotted in Figure 4.16, indicates that the peak is mainly due to (D^o, Ge_{As}) pair recombinations. One would also suspect (as will be verified below) that the PL peak may receive contributions from (e,Ge_{As}) transitions as well. The dominant luminescence feature for this sample occurs in the 1.47–1.42 eV range. The broad peak shifts to higher energy with excitation intensity (behaving as though D^o-A^o pair transitions were involved), at a rate much faster than that of the $\sim$1.475 eV peak, which is also shown in Figure 4.16. The broad peak's sudden appearance subsequent to the Ge-implantation indicates that Ge plays a role.

By varying the sample's temperature, as shown in Figure 4.17, further observations can be made. From 5–25K, the peak at $\sim$ 1.475 eV shifts to higher energy with increasing temperature. As the temperature is increased beyond 25K, the peak remains stationary. This behavior, along with the temperature variation of the GaAs bandgap, is shown in Figure 4.18. Furthermore, the peak's intensity remains strong even at a temperature of 35K. This supports the earlier specula-

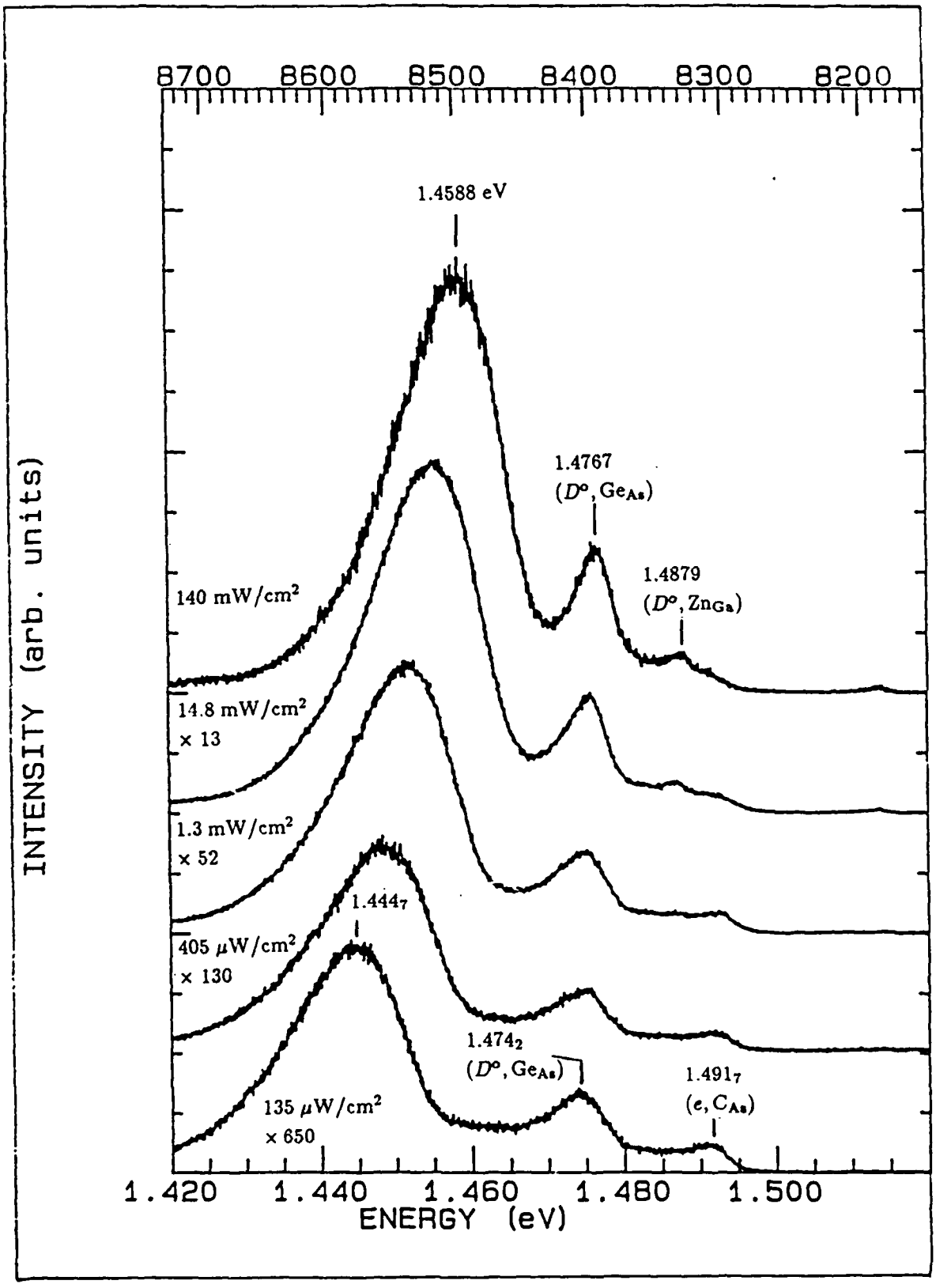

Figure 4.15. GaAs:Ge, ϕ=1E13 cm^{-2} Spectra, Exc: 2.5400 eV at 135 μW/cm^2 - 140 mW/cm^2, T=2.1K

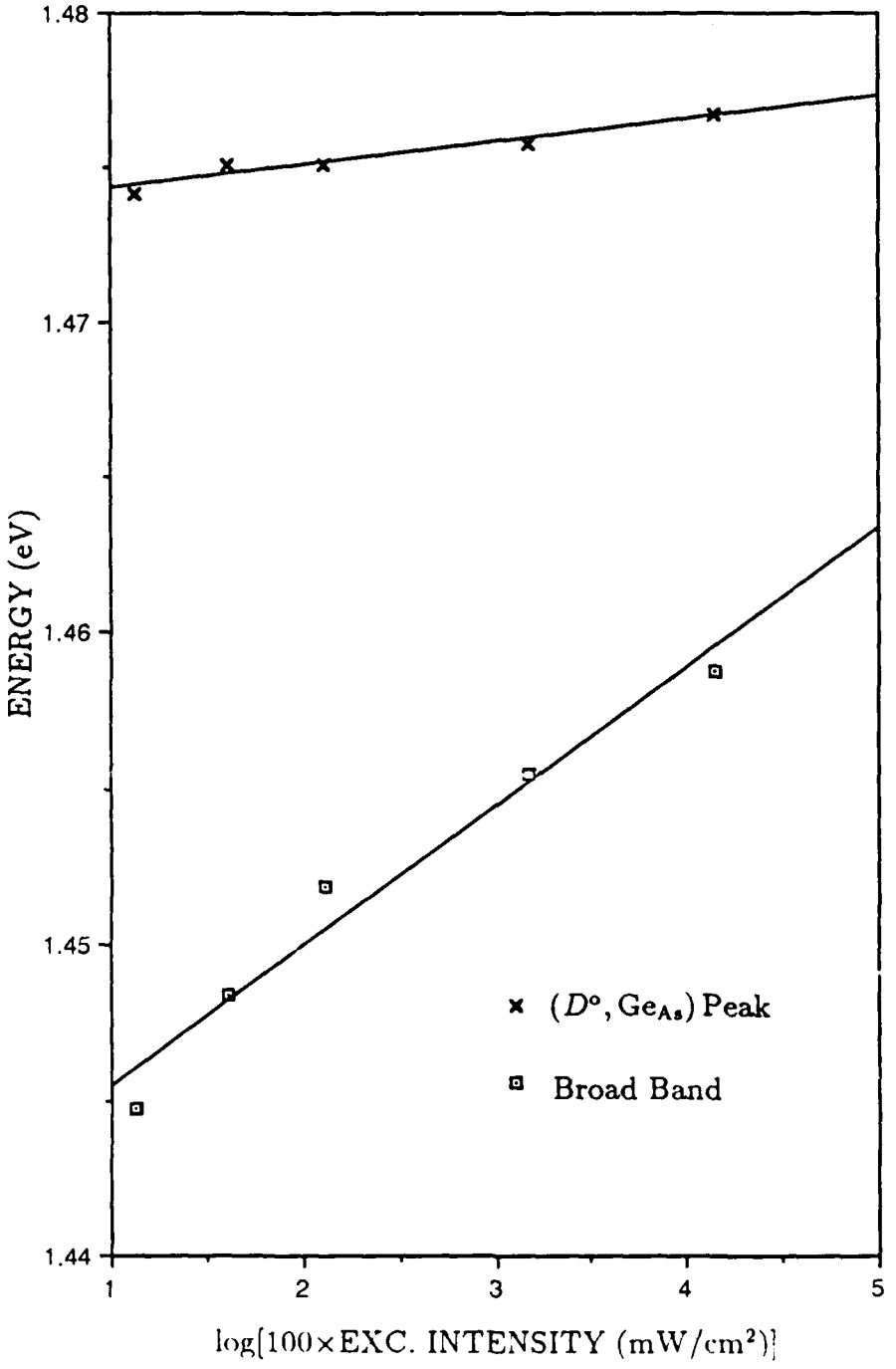

Figure 4.16. GaAs:Ge, ϕ=1E13 cm^{-2}, Peak Energies as a Function of Excitation Intensity

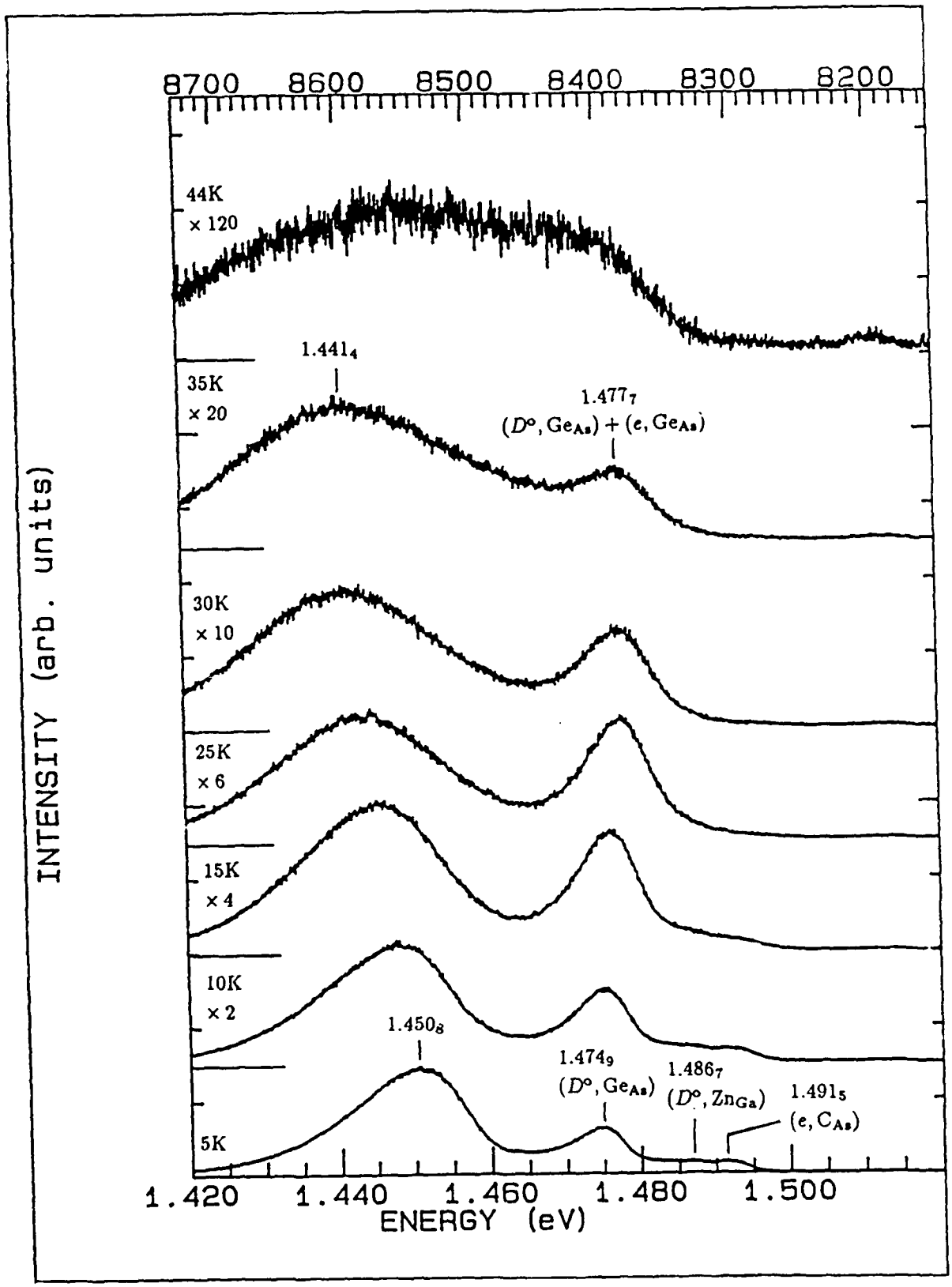

Figure 4.17. GaAs:Ge, ϕ=1E13 cm^{-2} Spectra, Exc: 2.5400 eV at 1.35 mW/cm^2, T=5–44K

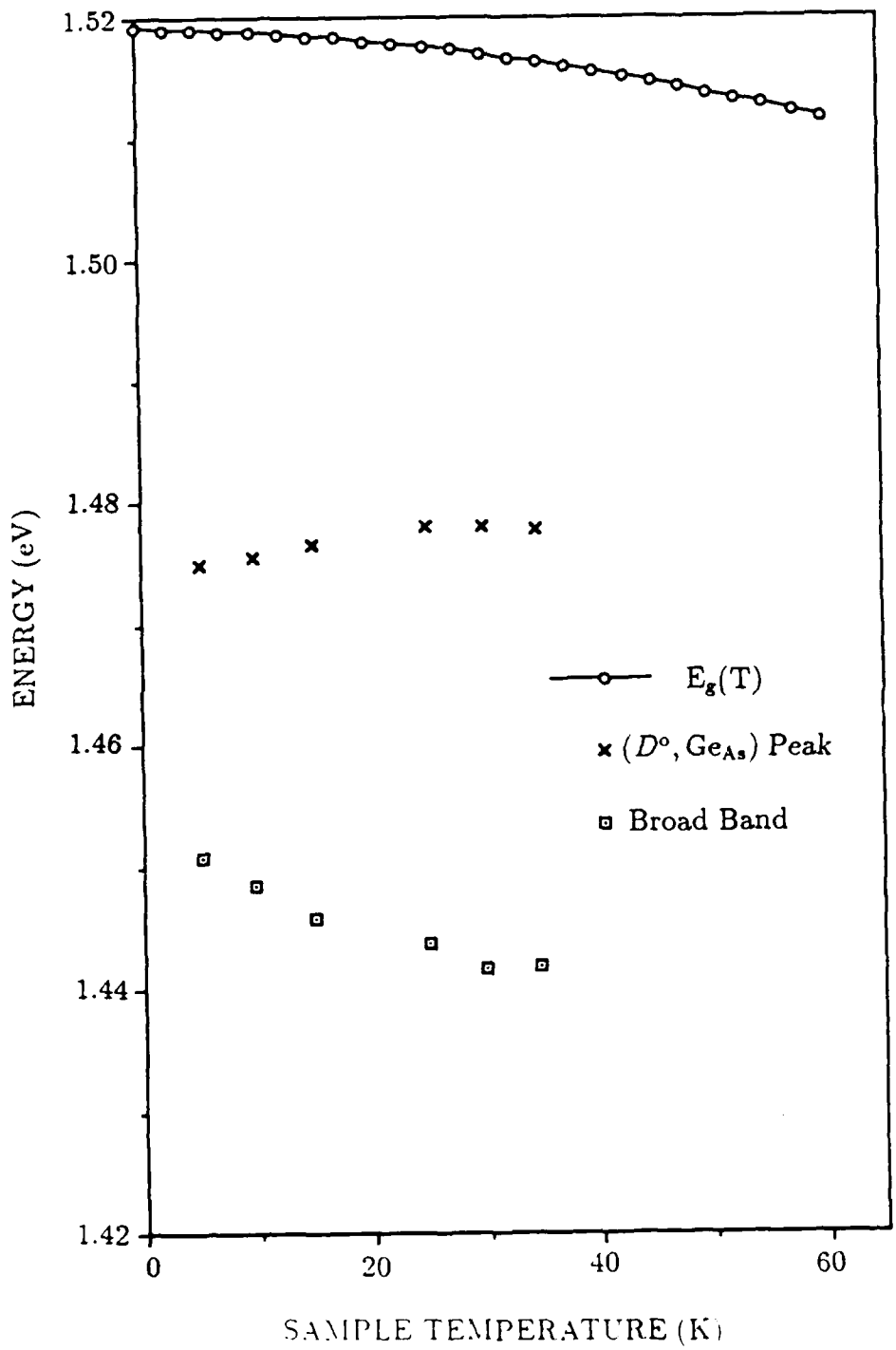

Figure 4.18. GaAs:Ge, ϕ=1E13 cm^{-2} Luminescence Peak Energies as a Function of Temperature

tion that (e,Ge_{As}) transitions also contribute to the peak. The broad band in the 1.47–1.42 eV range behaves differently than does the $\sim$1.475 eV peak at temperatures lower than 30K. That is, the band's maximum shifts to lower energy as the temperature is increased through 30K. This behavior is not characteristic of D^o-A^o pair transitions and contradicts the conclusion made from the intensity-dependent study. A few other observations can be made. The first concerns the shape of the band. At low temperatures, the band has a definite low-energy tail. At 25K, the shape is almost symmetric. Increasing the temperature further, shows the onset of a high-energy tail. Secondly, from 5–25K, the broad band's intensity decreases at a faster rate than that of the $\sim$1.475 eV peak. Above 25K, just the opposite is observed. Finally, the band's excitation intensity- and temperature-dependent shifts and absolute spectral position are very similar to the results reported in the literature for the Q band [54, 72]. Thus, it will tentatively be referred to as the Q band.

Below-gap Excitation Luminescence. The luminescence obtained with excitation energies below the bandgap is shown in Figures 4.19 through 4.22.

The luminescence shown in Figure 4.19 illustrates the effect of decreasing the excitation energy from above, to just below, the bandgap. When shifting from 2.5400 to 1.5300 eV (just above-gap) excitation, the peaks observed in the As- and Ga-implanted control samples (especially the (D^o, Zn_{Ga}) peak at $\sim$1.487 eV) increase in intensity relative to those seen subsequent to Ge-implantation. In fact, the Q band observed in the 1.47–1.42 eV range also decreases in intensity relative to the $\sim$1.475 eV peak, such that the LO replica of the $\sim$1.475 peak is just resolved on the low-energy tail of the band. It is believed that these changes in relative intensities are caused in part by the changes in the relative penetration depth of the excitation photons. From Eq (2.10), it can be determined that approximately 50% of the 2.5400 eV photon flux is absorbed within the mean projected range for the Ge-implant (R_p=457Å). This compares to less than 5% of the 1.5300 eV

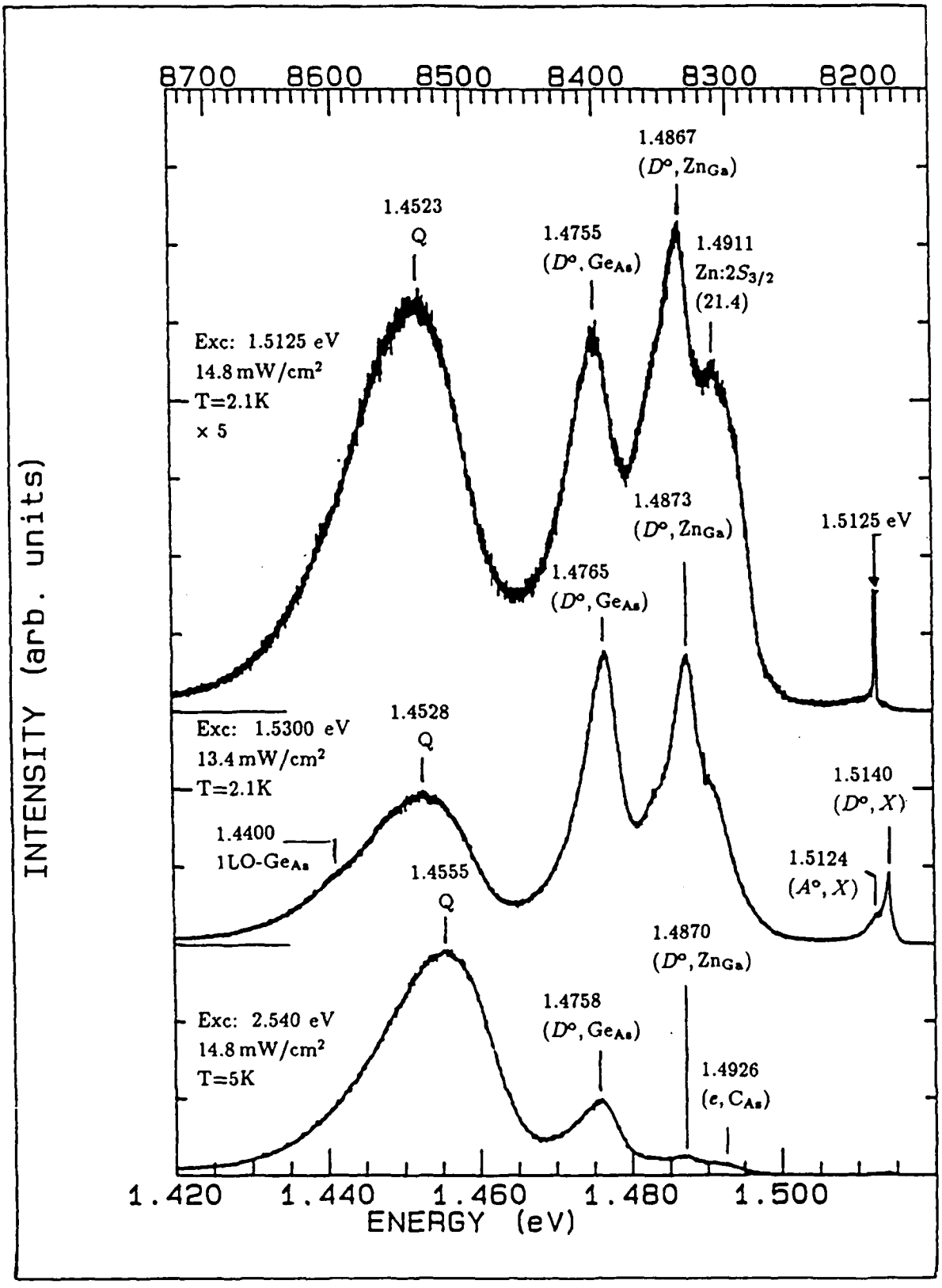

Figure 4.19. GaAs:Ge, ϕ=1E13 cm^{-2} Spectra, Exc: 2.5400–1.5125 eV, T Mainly 2.1K

photon flux. If the change in penetration depth were the major mechanism, it would allow one to also conclude that the depth distribution of the defect(s) giving rise to the Q band is shallower than that of the Ge_{As} acceptor which gives rise to the $\sim$1.475 eV peak. By tuning the laser to 1.5125 eV, one observes signs of selective excitation. Although only one hole excited state is observed (which is associated with the Zn_{Ga} acceptor), the other peaks are clearly shifting to lower energy. This selective screening of the D^o-A^o pair distribution was predicted. It is notable that the Q band similarly shifts to lower energy even though its D^o-A^o pair nature is far from conclusive. The relative peak intensities have become more complex upon excitation at 1.5125 eV. The intensity of the (D^o, Ge_{As}) peak at $\sim$1.475 eV has continued to decrease relative to that of the (D^o, Zn_{Ga}) peak at $\sim$1.487 eV. However, the Q band is now more intense than the (D^o, Ge_{As}) peak. It is difficult to reconcile this behavior with the observations made when the excitation energy was changed from 2.5400 to 1.5300 eV.

Figure 4.20 shows the results of stepping the excitation energy down to 1.5000 eV. Already at 1.5100 eV excitation, the peaks at $\sim$1.475 and $\sim$1.487 eV have virtually disappeared. SPL originating from the g, C_{As} and Zn_{Ga} acceptors' $2S_{3/2}$ hole state is now observed at 1.4959, 1.4920 and 1.4883 eV, respectively. The Q band is now located at 1.4502 eV. As the excitation source is tuned to lower energy, this band continues to shift to lower energy (as if a D^o-A^o pair distribution is being selectively screened by the laser excitation) and its intensity decreases rapidly. (At 1.5000 eV excitation, the band peaks at 1.4439 eV). A band at $\sim$1.46 eV has also emerged in the process. The center which gives rise to the $\sim$1.470 eV peak (especially) in the As- and Ga-implanted samples' luminescence data (see Figures 4.4, 4.7 and 4.13) may be involved here. In addition, the 1.46 eV band could receive contributions from the LO phonon replica of the luminescence occuring in the 1.50–1.48 eV region. (At 1.5000 eV excitation, sharp structure superimposed upon the band are assigned to the LO Raman peak (LO_1) and LO replica of one

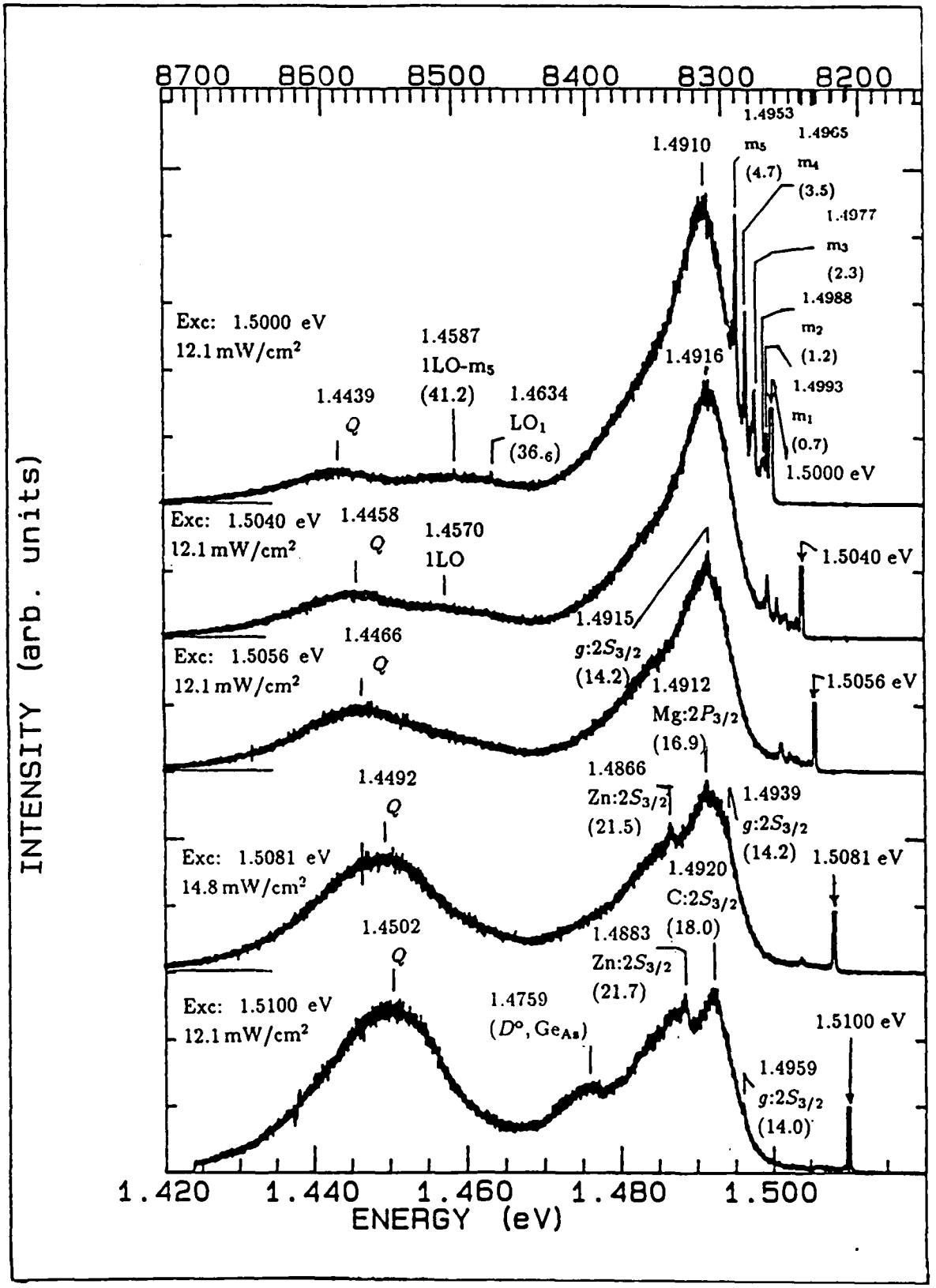

Figure 4.20. GaAs:Ge, ϕ=1E13 cm^{-2} Spectra, Exc: 1.5100–1.5000 eV at Mainly 12.1 mW/cm^2, T=2.1K

of the m-lines).

Focusing attention on the Q band, the selective nature of the below gap excitation can be used to an advantage. In Figure 4.21, rather striking behavior is observed for the band by varying the intensity of the ~ 1.508 eV excitation source. At the lowest excitation intensity, the band is characteristically broad and centered at 1.4492 eV. Increasing the intensity to about 75 mW/cm^2, the band changes shape. In fact, it now appears that at least two peaks make up the band, with the absolute maximum of the band occuring at 1.4541 eV. This observation is also evident at an intensity of about 120 mW/cm^2, where a low-energy shoulder at about 1.4452 eV is now labelled for reference. This change occurred without significant concurrent change in the samples' 1.49 eV luminescence. (Significant relative increases in intensities in the 1.49 eV luminescence would encourage the increase in luminescence at 1.454 eV because of LO phonon activity). The excitation intensity-dependent PL studies (Figure 4.15) indicated rapid shifts in the band's spectral position. With the improved resolution in Figure 4.21, a portion of the observed PL shift may be due to changes in the relative importance of competing recombination processes involving one or many impurity centers.

Employing temperature dependent studies provides further evidence for these competing processes. The results shown in Figure 4.22 were obtained by exciting the sample with ~ 1.5080 eV photons at $\sim$130–135 mW/cm^2. An underlying peak at ~ 1.449 eV is clearly present on the low-energy side of the now assymetric Q band. By increasing the temperature, the underlying peak seems to merge with the band. The Q band has also effectively shifted to lower energy as observed in the temperature dependent PL studies (Figure 4.17). Upon decreasing the excitation intensity to ~ 4 mW/cm^2 in Figure 4.23, the de-convolution of the Q band is improved. The temperature dependent studies now indicate that higher-energy luminescence, which peaks at ~ 1.458 eV, disappears quite rapidly with temperature, (as might be expected for D^o-A^o pair recombination) leaving a narrower, ~ 1.448

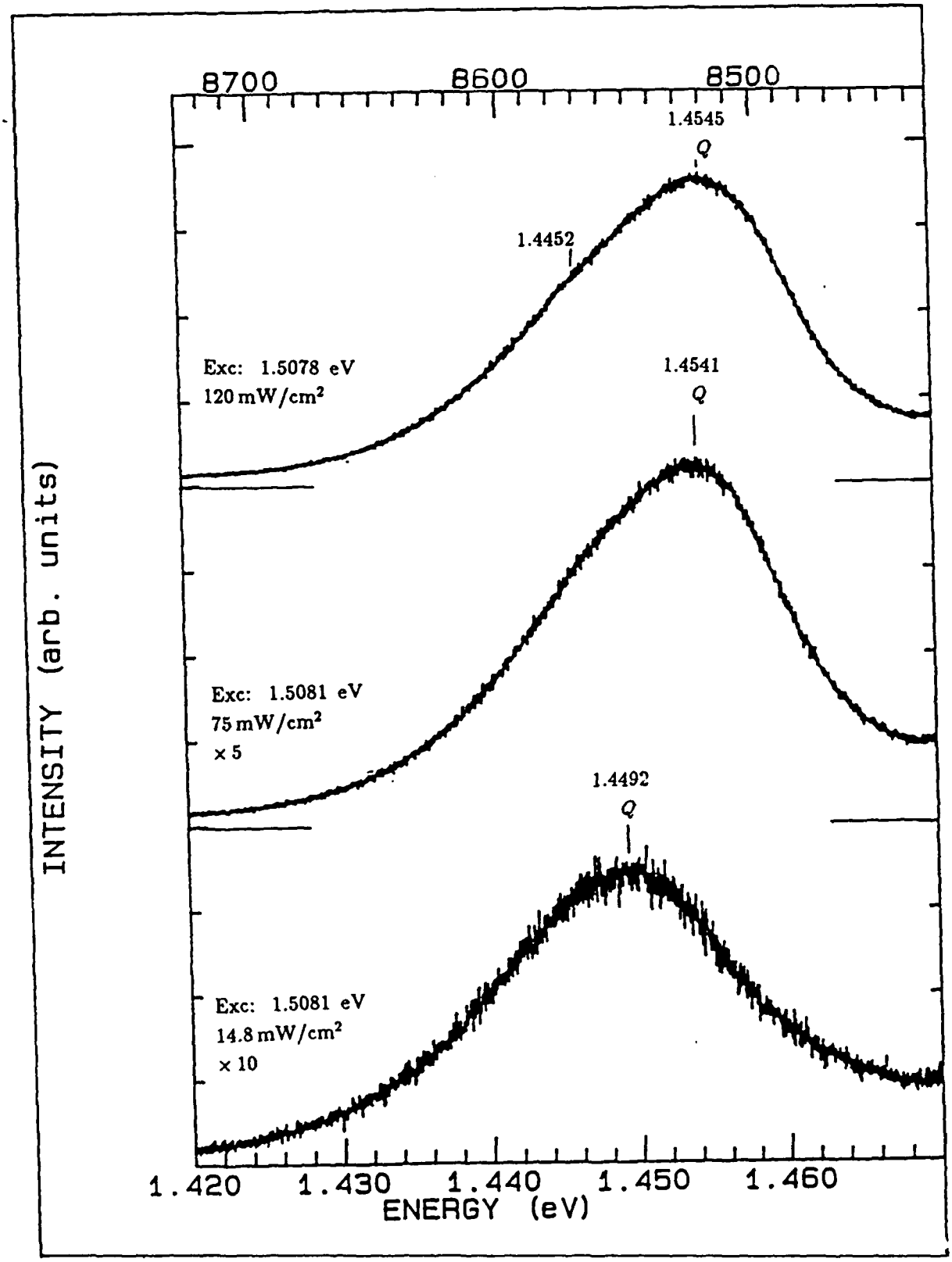

Figure 4.21. GaAs:Ge, ϕ=1E13 cm^{-2} Spectra, Exc: 1.5078–1.5081 eV at 14.8–120 mW/cm^2, T=2.1K

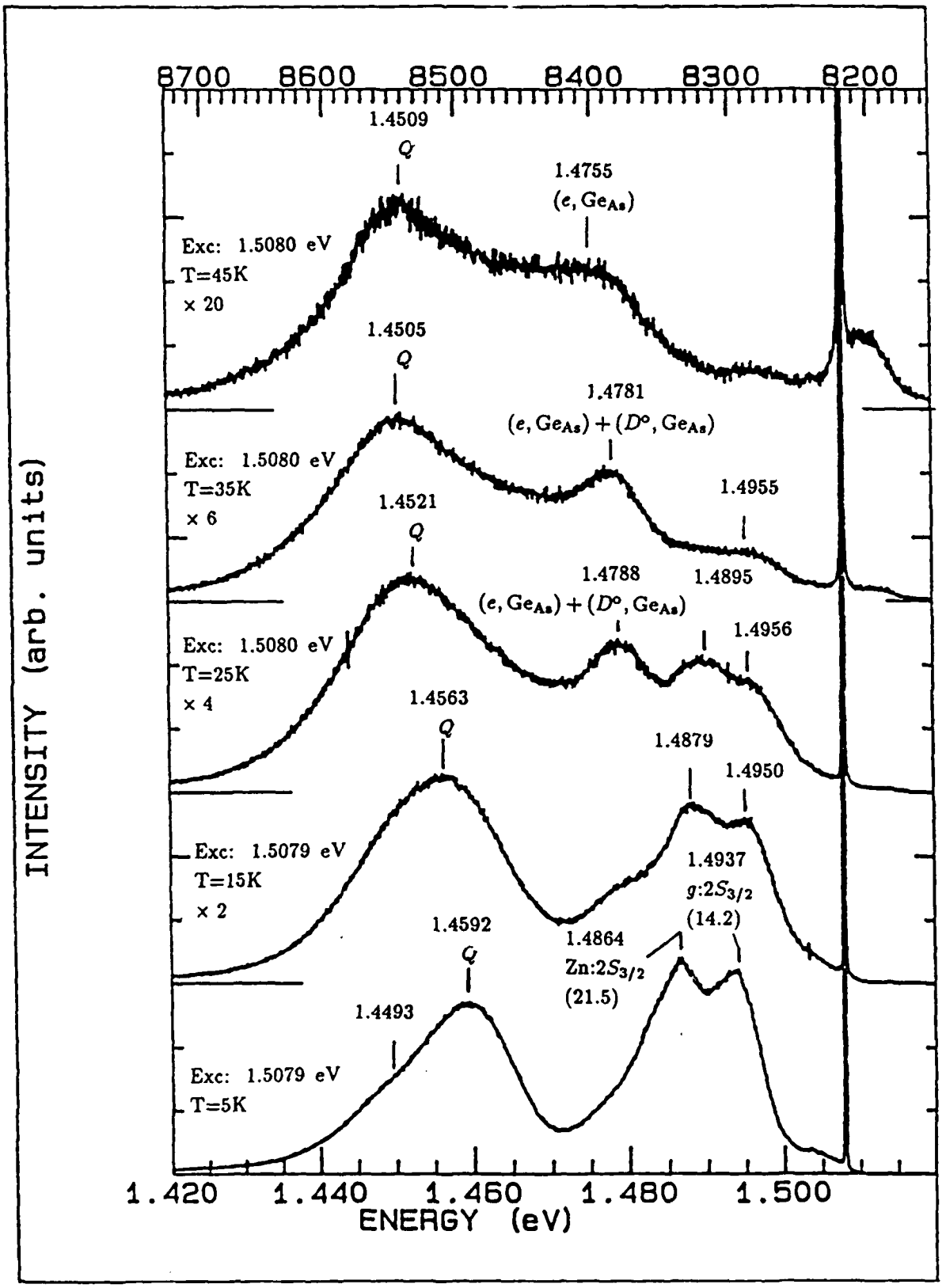

Figure 4.22. GaAs:Ge, ϕ=1E13 cm^{-2} Spectra, Exc: 1.5079–1.5080 eV at 130–135 mW/cm^2, T=5–45K

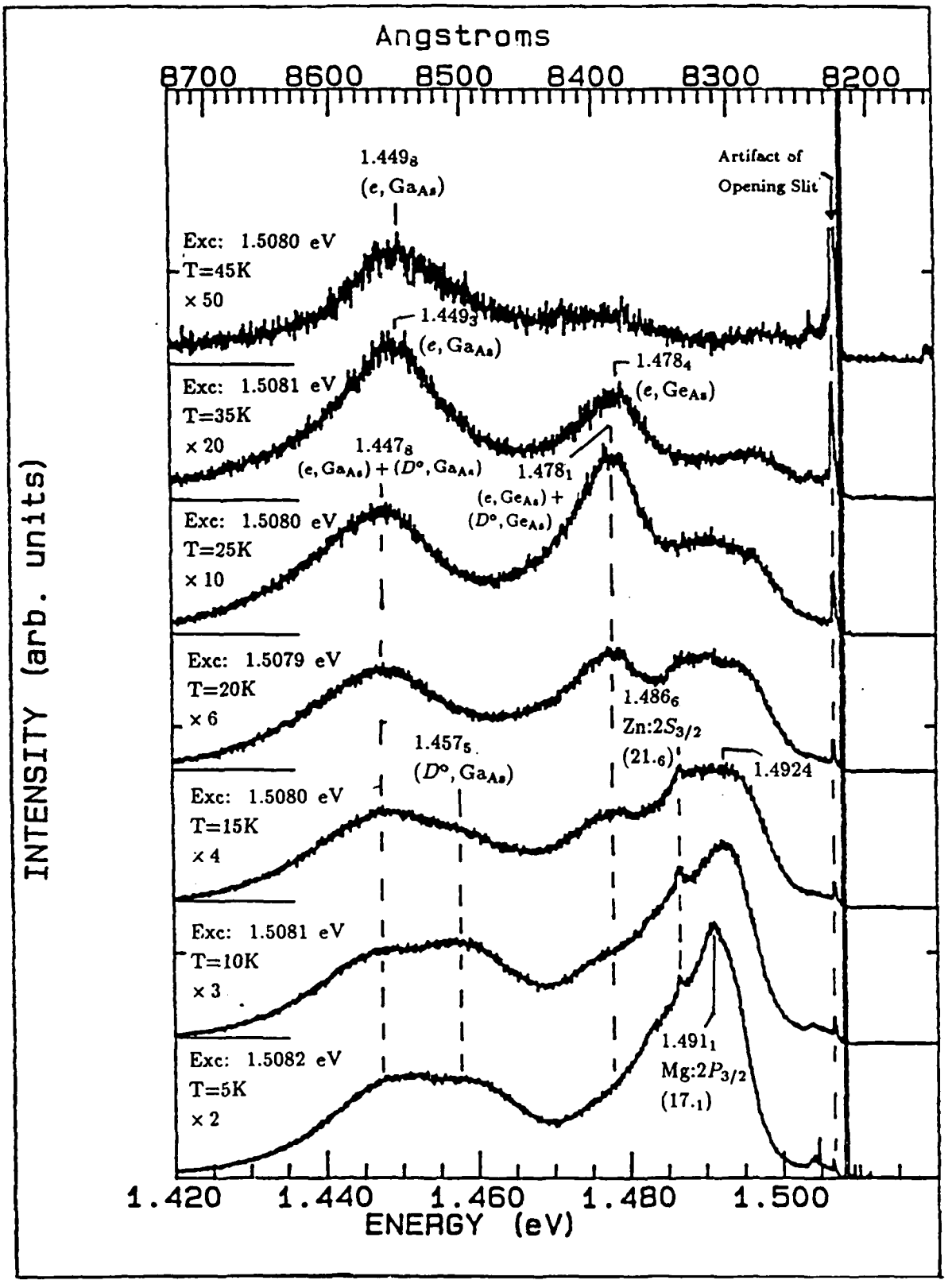

Figure 4.23. GaAs:Ge, ϕ=1E13 cm^{-2} Spectra, Exc: 1.5079–1.5082 eV at 4 mW/cm^2, T=5–45K

eV band at 20K. The remaining narrower band shifts slightly to higher energy as the temperature is further increased to 35K. This also is indicative of contributions from conventional D°-A° pair recombinations. The narrow band remains as the temperature is increased through 45K; a temperature at which the luminescence would no longer be expected to originate from D°-A° pair recombinations. Thus, the peak at 1.449_8 eV (at 45K) is believed to be due to (e,A°) recombinations.

Such narrow band emission in the $\sim$1.44 eV range has been reported in the literature. An early PL investigation by Yu and Reynolds [84], of GaAs grown by the liquid encapsulated Czochralski (LEC) technique from Ga-rich melts, attributed an emission line at 1.441 eV to the Ga_{As} double acceptor paired with another impurity or defect. Certainly, the Ga richness favors such an assignment. The 1.441 eV D°-A° pair band was observed to shift to higher energy as the temperature was increased in the range 4–35K. However, it was soon discovered that Ga richness was not a necessary condition for the creation of the $\sim$1.44 eV peak in PL [10:1786]. In one of the most recent reviews, conducted by Moore, et al. [46], the Ga_{As} double acceptor was still viewed as the most likely source of the 1.441 eV PL peak.

However, there have been other studies which contend that the Ga_{As} double acceptor was responsible for luminescence at a somewhat higher energy. In an implantation study by Dansas [20] (with Ga and boron (B) implants), luminescence at $\sim$1.45 eV was assigned to the Ga_{As} double acceptor. The B double acceptor, B_{As}, seemed to give rise to luminescence in the 1.438–1.443 eV range. The higher-energy assignment by Dansas is in agreement with a recent study on defects in annealed, horizontal-Bridgman grown GaAs, where an emission at 1.448 eV was attributed to the Ga_{As} double acceptor [75]. The absence of the 1.438–1.443 eV peak in this investigation coincides with the fact that smaller amounts of B are incorporated into the crystal during Bridgman growth relative to that during LEC growth [25]. The study was also significant because it apparently was one of the first studies

which showed the presence of an ~ 1.44 eV peak in the PL of GaAs grown by methods other than LEC [45]. (In fact, the ~ 1.44 eV peak was also discovered at about the same time in GaAs layers grown by molecular beam epitaxy [45]). Tentatively, the ~ 1.448 eV band observed in Figure 4.23 will be attributed to the Ga_{As} double acceptor.

Because the Q band in PL remained unresolved, even at intensities of less than 200 $\mu W/cm^2$ (in Figure 4.15), the existence of multiple peaks giving rise to the band was difficult to ascertain. However, it is apparent from the current results that the Ga_{As} double acceptor may be involved in the so-called Q band. In addition, evidence has been presented for the existence of temperature sensitive, higher-energy luminesence peaking at ~ 1.458 eV attributed to D^o-A^o pair recombination. This evidence is essential to understanding the contradictory excitation intensity- and temperature-dependent PL results presented earlier. The rapid disappearance of the higher-energy component of the Q band's PL appears to have produced the band's apparent shift to lower energy as the temperature was increased from 5K in Figure 4.17.

Close Pairs Model for Q Band. The following model attempts to explain the Q band luminescence, observed in the Ge-implanted sample, which was described in previous sections. In addition, the model provides an assignment for the acceptor giving rise to the ~ 1.458 eV D^o-A^o pair luminescence (of Figure 4.23).

The temperature-dependent luminescence of Figure 4.23 indicates a rapid decrease in the intensity of the ~ 1.458 eV band, and a shift of the luminescence peak at ~ 1.448 eV to higher energy as the temperature is increased from 25 to 35K. As mentioned before, the behavior of both peaks is indicative of D^o-A^o pair recombination. In addition, the acceptor giving rise to the ~ 1.448 eV peak has been assigned as the Ga_{As}. There still remains the task of identifying the acceptor which participates in the higher-energy D^o-A^o pair luminescence peaking at ~ 1.458

eV. As already noted, Dansas [20] assigned relatively high-energy PL to the Ga_{As} double acceptor. The Ga_{As} was associated with PL which peaked at energies as high as 1.455 eV [19, 20]. Thus, for the moment, it is hypothesized that the luminescence which peaks at 1.448 eV and 1.458 eV originates from transitions involving the Ga_{As} double acceptor. However, in accepting this hypothesis, one has implicitly assigned the $\sim$1.458 eV low-temperature luminescence to (D^o, Ga_{As}) pairs. Recalling that the peak at 1.449_8 eV in Figure 4.23 was assigned to (e,Ga_{As}) transitions, one is left with the situation of (D^o, Ga_{As}) pair luminescence at both lower and higher energy than (e,Ga_{As}) luminescence. Typically, in a semiconductor such as GaAs, (e,A^o) luminescence is observed only at higher energy than the associated D^o-A^o pair luminescence. For the hypothesis to remain valid, the low-temperature (D^o, Ga_{As}) pair luminescence would have to be taking place over a sufficiently broad energy range such that its peak could, in fact, occur at higher energy than the (e,Ga_{As}) luminescence. (Recombinations at distant (D^o, Ga_{As}) pairs are also assumed to be occurring, but to a lesser extent. These contribute to the D^o-A^o pair luminescence in the vicinity of the $\sim$ 1.448 eV peak). This is possible if there were a large number of transitions at relatively close (D^o, Ga_{As}) pairs in this sample. These relatively close pair transitions may occur if there are large concentrations of Ga_{As} double acceptors and a sufficient number of donors in this sample. The challenge is to account for the atypical observation of relatively close pair recombination in relationship to the discussion in Chapter II of the attributes of D^o-A^o pair transitions in semiconductors such as GaAs.

It is appropriate to recall the discussion in Chapter II on D^o-A^o pair recombination and the accompanying luminescence, which was described by Eq(2.16):

$$\hbar\omega_l = \hbar\omega_{D^o-A^o} = E_g - (E_A + E_D) + \frac{e^2}{\epsilon R} + J(R) \qquad (4.1)$$

Relatively close pair recombination is not dominant in many cases compared with distant pair recombination, because the sum of E_A and E_D is too small for common shallow impurities in GaAs. Therefore, the relatively distant pair recombination is

dominant and $e^2/\epsilon R$ and $J(R)$ are not significant. Subsequently, Eq (4.1) can be simplified to

$$\hbar\omega_{D^o-A^o} \simeq (E_g - E_A) - E_D \tag{4.2}$$

This luminescence energy is less than that resulting from (e,A^o) recombinations which, from Eq(2.15), is given by

$$\hbar\omega_{F-B} = E_g - E_A \tag{4.3}$$

However, the neutral charge state of the Ga_{As} double acceptor has an E_A of 78 meV which is much larger than a typical E_A of $\sim$ 30–35 meV. Therefore, closer pair recombinations can be dominant and $e^2/\epsilon R$ (and possibly even $J(R)$) becomes non-negligible. Thus, combining Eqs(4.1) and (4.3), one obtains

$$\hbar\omega_{D^o-A^o} = \hbar\omega_{F-B} + (\frac{e^2}{\epsilon R} + J(R) - E_D) \tag{4.4}$$

If the second and third terms on the right side of Eq(4.4) are sufficiently large (that is, if there are sufficiently close pairs which may recombine) and there are adequate numbers of these close pair recombinations, it is plausible that the D^o-A^o pair luminescence may be peaked at higher energies than the associated (e,A^o) luminescence.

This close D^o-A^o pairs model successfully explains the Q band luminescence observed for the Ge-implanted sample at a dose of 1E13 cm^{-2}. The excitation intensity-dependent studies, shown in Figure 4.15, are validated by the fundamental component of the model: D^o-A^o pairs. In addition, the distribution of pairs as a function of the donor-acceptor separation has been hypothesized to be peaked at relatively close pairs. Thus, from D^o-A^o pair recombination theory [21:60], it can be inferred that the associated close pair luminescence intensity would be especially sensitive to increasing temperature. Subsequently, the close pairs model accounts for the rapid disappearance of the high-energy luminescence at $\sim$ 1.458 eV as the temperature is increased from 5–20K in Figure 4.23. The rapid decrease in the

1.458 eV luminescence intensity, in turn, explains the temperature shift shown for the Q band in Figure 4.17. Further details associated with the close pairs model are contained in Appendix A.

3E13 cm^{-2} Implant. The PL for the sample implanted with Ge at a dose of 3E13 cm^{-2} is shown in Figure 4.24. The supposed Q band, at 1.4521 eV, is shifted to lower energy relative to that in the 1E13 cm^{-2}, Ge-implanted sample. Taking into account the close pairs model, one could speculate that the dominant (D^o, Ga_{As}) transitions in the 3E13 cm^{-2}, Ge-implanted sample occur amongst pairs whose separation is not as close. This could result from a diminished concentration of Ga_{As} double acceptors. The peak at 1.4761 eV, is assigned to (D^o, Ge_{As}) recombinations. It is also observed to have shifted to lower energy at the higher dose.

By exciting the sample just above bandgap at 1.5300 eV, as shown in Figure 4.25, several peaks observed in the control samples' (that is, the As- and Ga-implanted samples') spectra again increase in intensity relative to those seen subsequent to Ge-implantation. Especially noticeable is the (D^o, Zn_{Ga}) peak at 1.4882 eV. The Q band also decreases in intensity relative to the 1.4774 eV (D^o, Ge_{As}) peak (so that the LO replica of the 1.4774 eV peak is just resolved on the low-energy tail of the Q band). Again, it is believed that these changes in relative intensities are caused in part by the decreased absorption of the excitation photons and relative depth distribution of the respective centers. Finally, the Q band is observed to shift slightly to lower energy while the higher energy peaks (such as the (D^o, Ge_{As}) peak), shift to higher energy when decreasing the excitation energy from 2.5400 to 1.5300 eV. This observation was also made for the 1E13 cm^{-2}, Ge-implanted sample. It may be that the number of (e, A^o) recombinations, involving the shallower acceptors (such as Ge_{As}), is increased for excitation at just above bandgap.

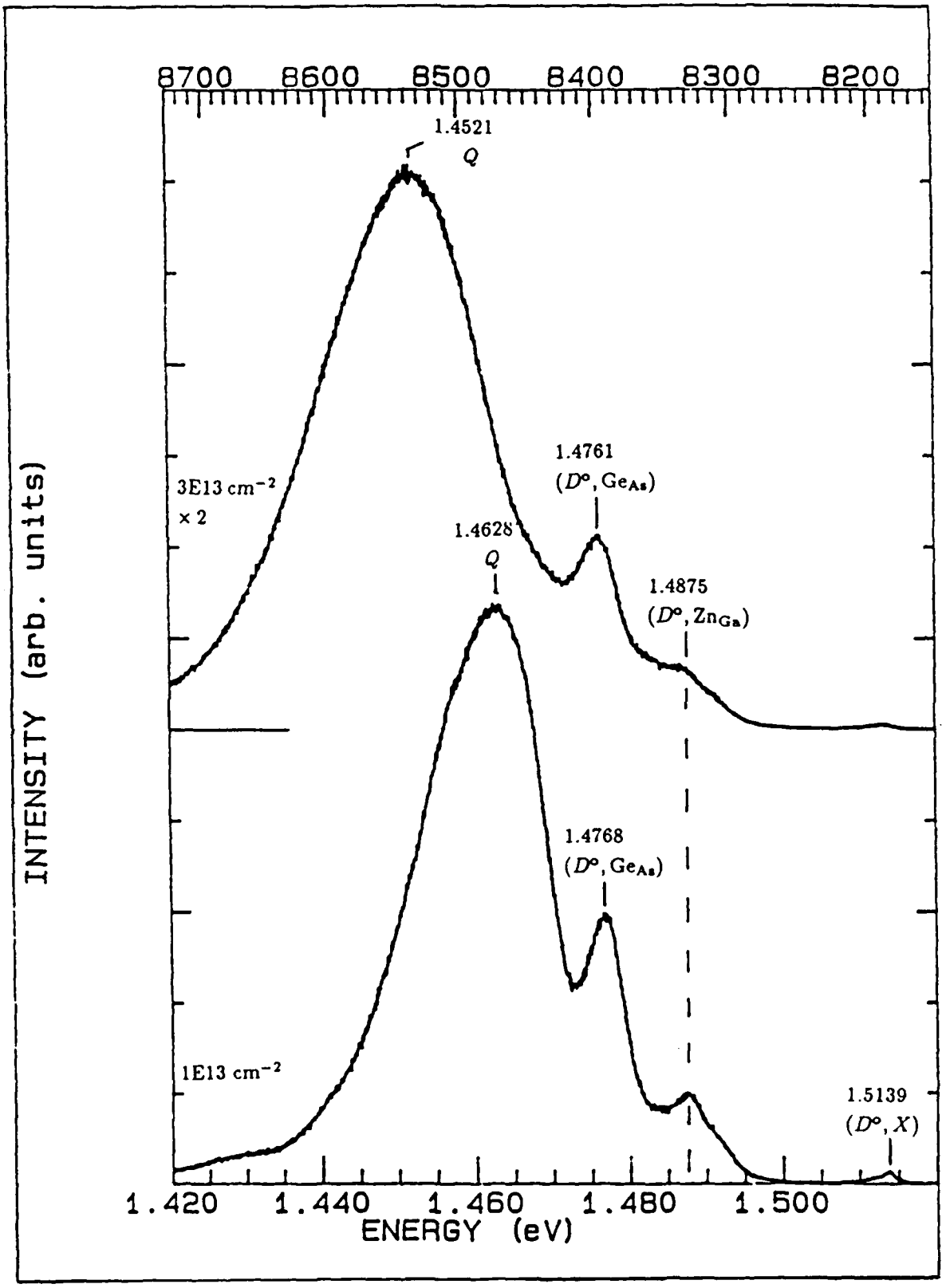

Figure 4.24. GaAs:Ge, ϕ=1E13-3E13 cm^{-2} Spectra, Exc: 2.5400 eV at 135 mW/cm^2, T=5K

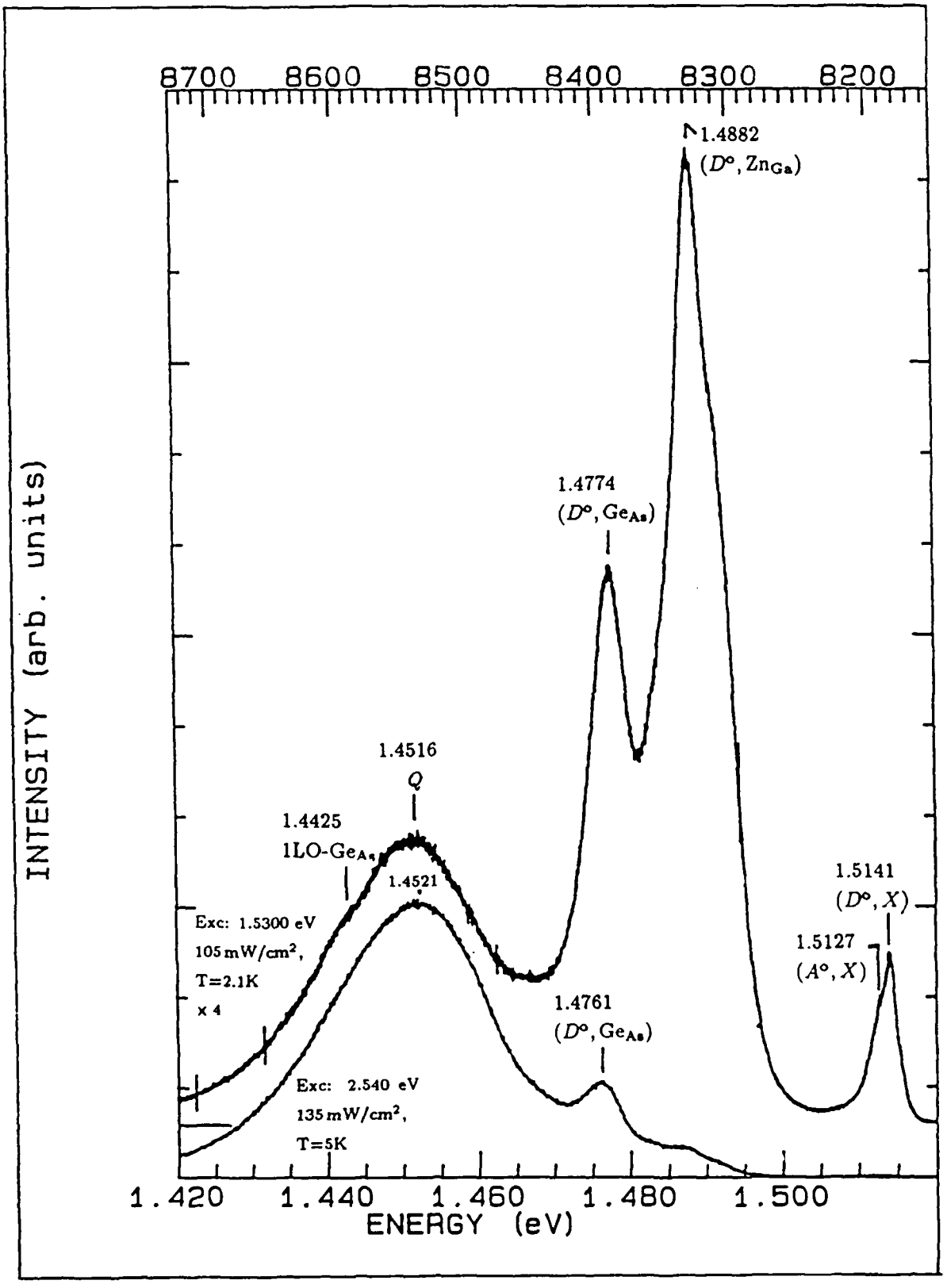

Figure 4.25. GaAs:Ge, ϕ=3E13 cm^{-2} Spectra, Exc: 2.5400-1.5300 eV

The selective excitation data for the 3E13 cm^{-2}, Ge-implanted sample is shown in Figure 4.26. The luminescence in the 1.52–1.47 eV range looks very similar to that for the respective excitations of the 1E13 cm^{-2}, Ge-implanted sample shown in Figure 4.20 (albeit the power intensities on the samples are different). A minor exception to this observation is the resolution of SPL which originated from the $2P_{3/2}$ hole state of the Si_{As} acceptor. The structure at 1.4868 eV is offset from the 1.5100 eV laser pump line by 23.3 meV. From Table 2.10, this offset corresponds very well with the $1S_{3/2} \rightarrow 2P_{3/2}$ transition energy of the hole bound to the Si_{As} acceptor. The luminescence for the 3E13 cm^{-2} and 1E13 cm^{-2}, Ge-implanted samples in the 1.47–1.42 eV range is also similar. Apparent LO replicas, especially of the $\sim$1.4925 eV peak, appear at $\sim$1.4560 eV, and the peak intensity for the Q band-related recombination(s) occurs at $\sim$ 1.447 eV. Upon excitation below-gap, this peak does not continue to shift to lower energies with decreased excitation energy as much as does the corresponding peak in the 1E13 cm^{-2}, Ge-implanted sample. This may partly result from the larger laser intensity placed on the 3E13 cm^{-2}, Ge-implanted sample. More importantly, as noted from the PL data for this sample, there could be a smaller concentration of Ga_{As} double acceptors. This would, in turn, mean that a majority of the (D^o, Ga_{As}) transitions occur amongst pairs having slightly greater pair separations (according to the close pairs model above).

1E14–1E15 cm^{-2} Implants. Figure 4.27 shows the cumulative dose-dependent PL for the Ge-implanted samples. The presence of the $\sim$1.476–1.477 eV peak throughout indicates continued activation of the Ge_{As} acceptor. According to the electrical data reported earlier, the lower dose implants created p-type samples, and n-type activity was clearly measured at a Ge dose of 1E15 cm^{-2}. Although increased Ge_{Ga} (donor) site activation is a probable cause, it is difficult to firmly correlate this hypothesis with the PL shown in Figure 4.27. Nonetheless, one noticeable feature in the PL of the sample implanted at a dose of 1E15 cm^{-2} is

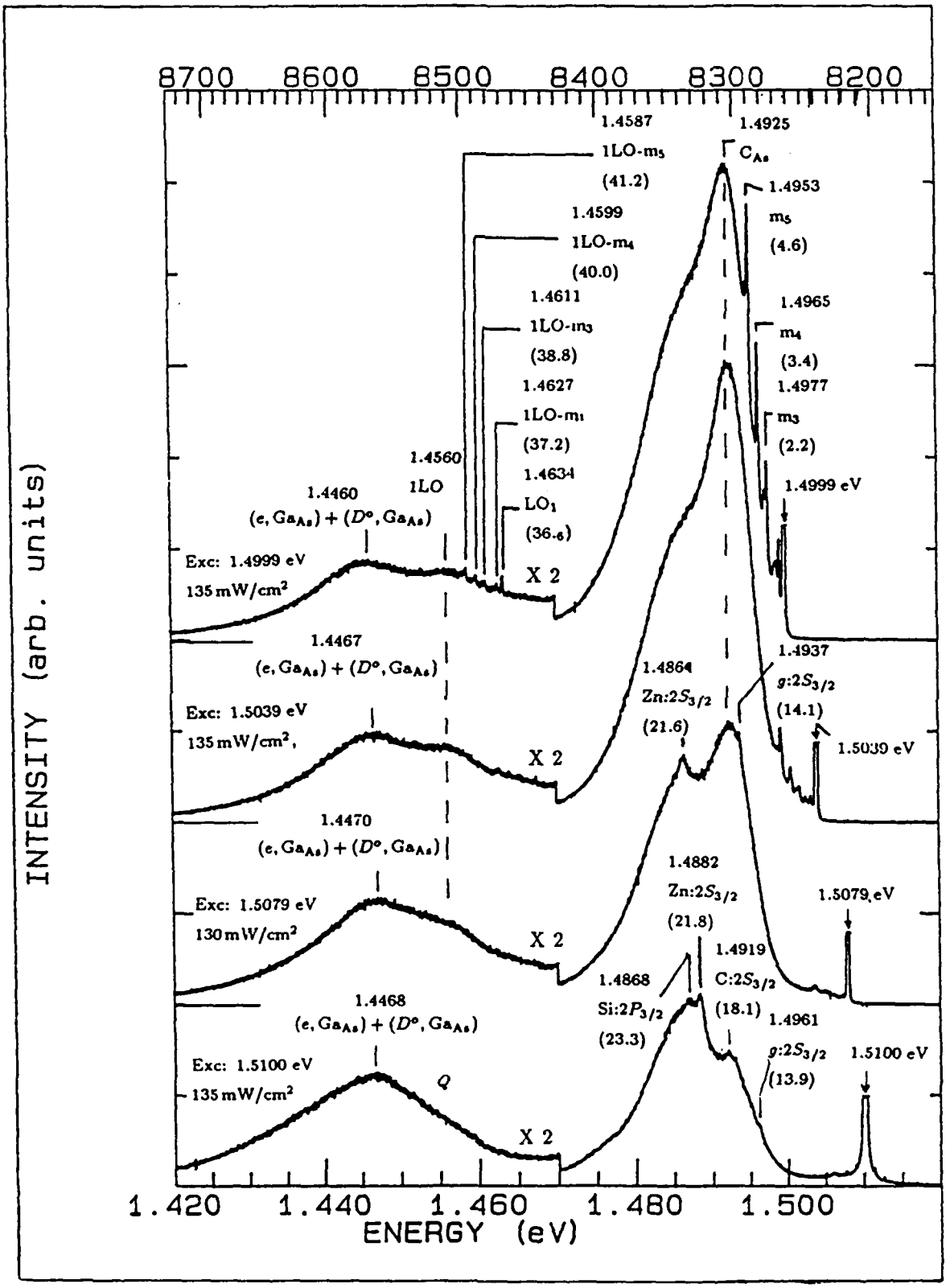

Figure 4.26. GaAs:Ge, ϕ=3E13 cm^{-2} Spectra, Exc: 1.5100–1.4999 eV at 130–135 mW/cm^2, T=2.1K

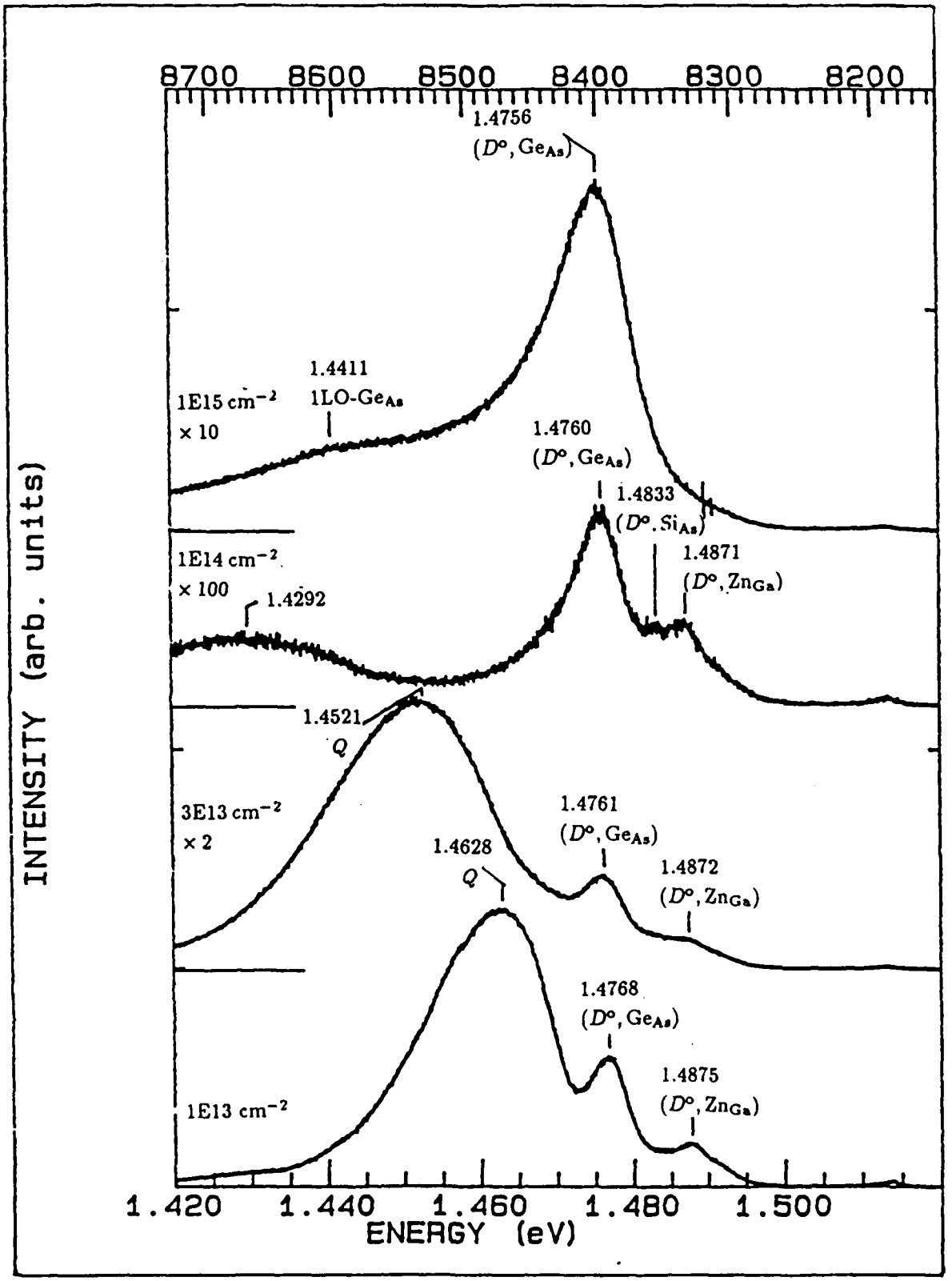

Figure 4.27. GaAs:Ge, ϕ=1E13–1E15 cm^{-2} Spectra, Exc: 2.5400 eV at 135 mW/cm^2, T=5K

the apparent disappearance of the $(D^{\circ}, \mathrm{Zn_{Ga}})$ peak. This may signify a decreased activation of the $\mathrm{Zn_{Ga}}$ acceptor which would correlate with an increased activation of the $\mathrm{Ge_{Ga}}$ donor.

For the PL in the 1.47–1.42 eV range, the Q band has either shifted dramatically to lower energy ($\sim$1.429 eV) and become much broader, or disappeared altogether, when the Ge dose is increased to 1E14 cm^{-2}. This shift with the implant dose is congruent with the Q band behavior in Si-implanted GaAs (presented in Chapter III). Unfortunately, the trend to lower energy does not seem to continue at a still higher dose of 1E15 cm^{-2}. Although not presented here, data for the 1E15 cm^{-2}, Ge-implanted sample was collected to energies as low as 1.30 eV using an S1 PMT. There was no indication of Q band PL in the measured spectrum. Pomrenke *et al.* [54] observed that the Q band continued to shift to lower energies as the Si dose was increased through 1E15 cm^{-2}. (As summarized in Table 2.9, the Q band was located at 1.355 eV for a Si dose of 1E15 cm^{-2}). It is also noted in the 1.47–1.42 eV energy range that the $\sim$1.476 eV band has quite an extensive low-energy tail for the 1E15 cm^{-2}, Ge-implanted sample. The tail decreases dramatically at $\sim$1.441 eV which also corresponds to the location where one would expect to see the LO replica of the dominant $(D^{\circ}, \mathrm{Ge_{As}})$ peak. Thus, LO phonon PL contributes to the low-energy tail.

Data for the $\sim$1.5300 eV excitation is presented in Figure 4.28. As previously observed, the relative oscillator strengths for the exciton-related transitions and transitions involving most impurities found in the as-grown substrate are generally enhanced. Also, an interesting trend is seen to persist through an implant dose of 1E14 cm^{-2}. The relative intensity of the $(D^{\circ}, \mathrm{Ge_{As}})$ peak at $\sim$1.476–1.477 eV decreases with increasing Ge dose, while the p-type activation efficiency was seen to remain relatively constant over this dose range [80:199]. However, the trend does not continue after an implant dose of 1E15 cm^{-2}. Coincidentally, electrical type-conversion occurred between Ge-implant doses of 1E14 and 1E15 cm^{-2} [80]. It is

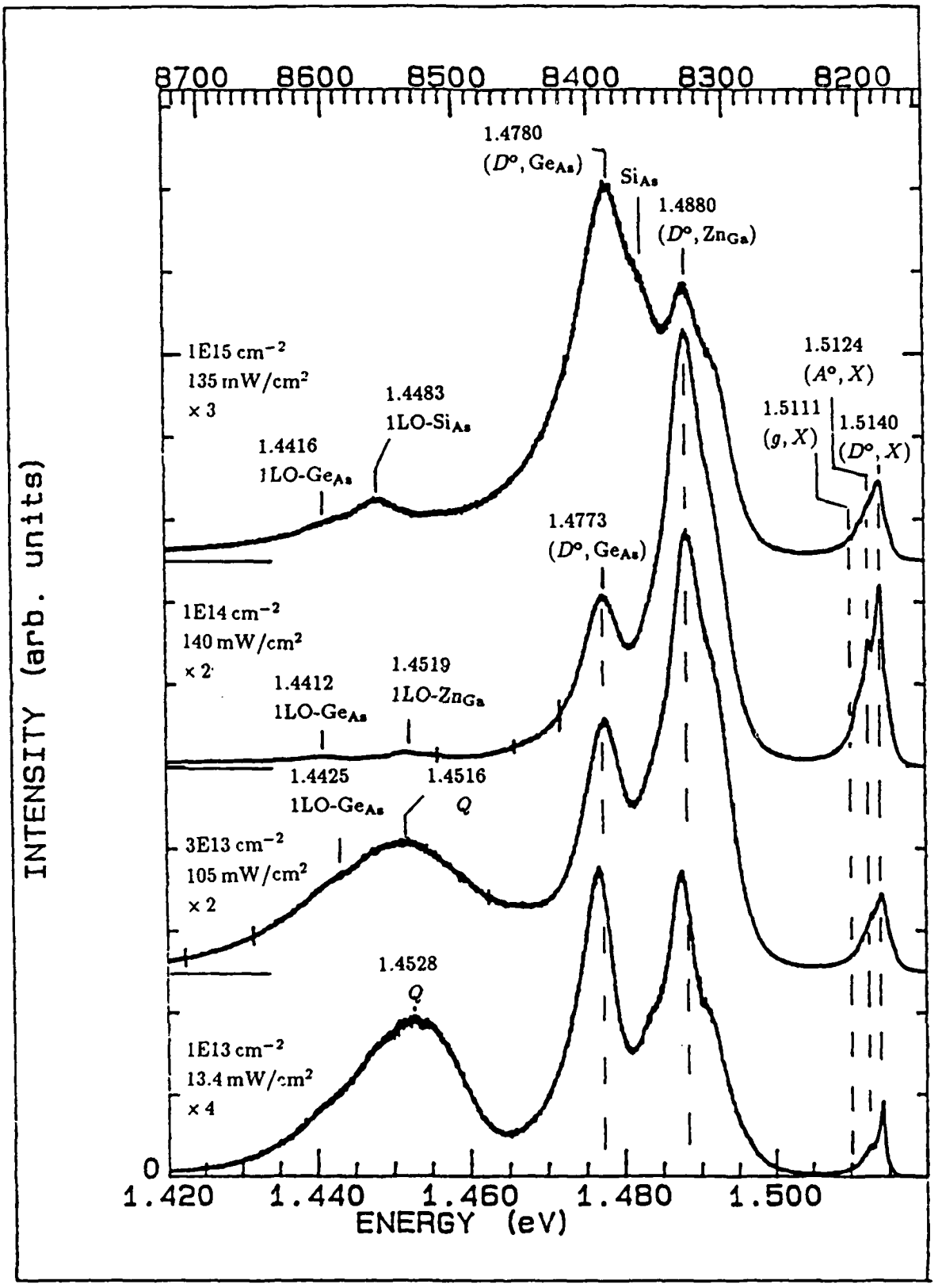

Figure 4.28. GaAs:Ge, ϕ=1E13–1E15 cm^{-2} Spectra, Exc: 1.5299–1.5300 eV, T=2.1K

also observed in Figure 4.28 that the $\sim$1.429 eV band, seen in the 1E14 cm^{-2}, Ge-implant PL of Figure 4.27, no longer appears to exist. In addition, the 1.5299 eV excitation of the 1E15 cm^{-2}, Ge-implanted sample has created conditions favorable for the resolution of a high-energy shoulder (between 1.480 and 1.485 eV) to the 1.4780 eV peak. This probably originates from the Si_{As} acceptor. Also, the low-energy tail associated with the $\sim$1.476 eV peak in the 1E15 cm^{-2}, Ge-implanted sample's PL of Figure 4.27 has disappeared under 1.5299 eV excitation. Underlying peaks are now resolved. The peak at 1.4483 eV could be the LO replica of the high-energy shoulder to the 1.4780 eV peak. The low-energy shoulder of the 1.4483 eV peak is believed to be the LO replica of the 1.4780 eV peak. Noting the relative intensities of the 1.4780 eV peak and its high-energy shoulder, however, shows that the 1.4483 eV peak has a somewhat large intensity. This could result from contributions from recombinations involving the Ga_{As} double acceptor.

Figure 4.29 shows luminescence with $\sim$1.508 eV excitation. The data is presented relative to the laser pump line. Several sharp structures overlay the broad background within 30 meV of the laser line. At the highest implant dose, a structure separated 26.1 meV from the laser line is just resolved. From Table 2.10, this corresponds to the $1S_{3/2} \rightarrow 2P_{3/2}$ transition energy for the hole bound to the Ge_{As} acceptor. Indeed, the best SPL signal for the Ge_{As} acceptor is seen for the 1E15 cm^{-2}, Ge-implanted sample. Coincidentally, this sample is the only one exhibiting a band (probably associated predominantly with the non-selectively excited D^o-A^o pairs) upon which the Ge_{As} acceptor SPL signal may be superimposed. This point is elaborated upon in the following paragraph.

The composite excitation energy variation for the 1E15 cm^{-2}, Ge-implanted sample is presented in Figure 4.30. By tuning the excitation source from 1.5299 to 1.5081 eV, clear trends are seen. First, it is noted that the 1.4756 eV peak, corresponding mainly to (D^o, Ge_{As}) pair transitions, shifts to 1.4780 eV after exciting the sample at 1.5299 eV. As speculated previously, the near gap excitation

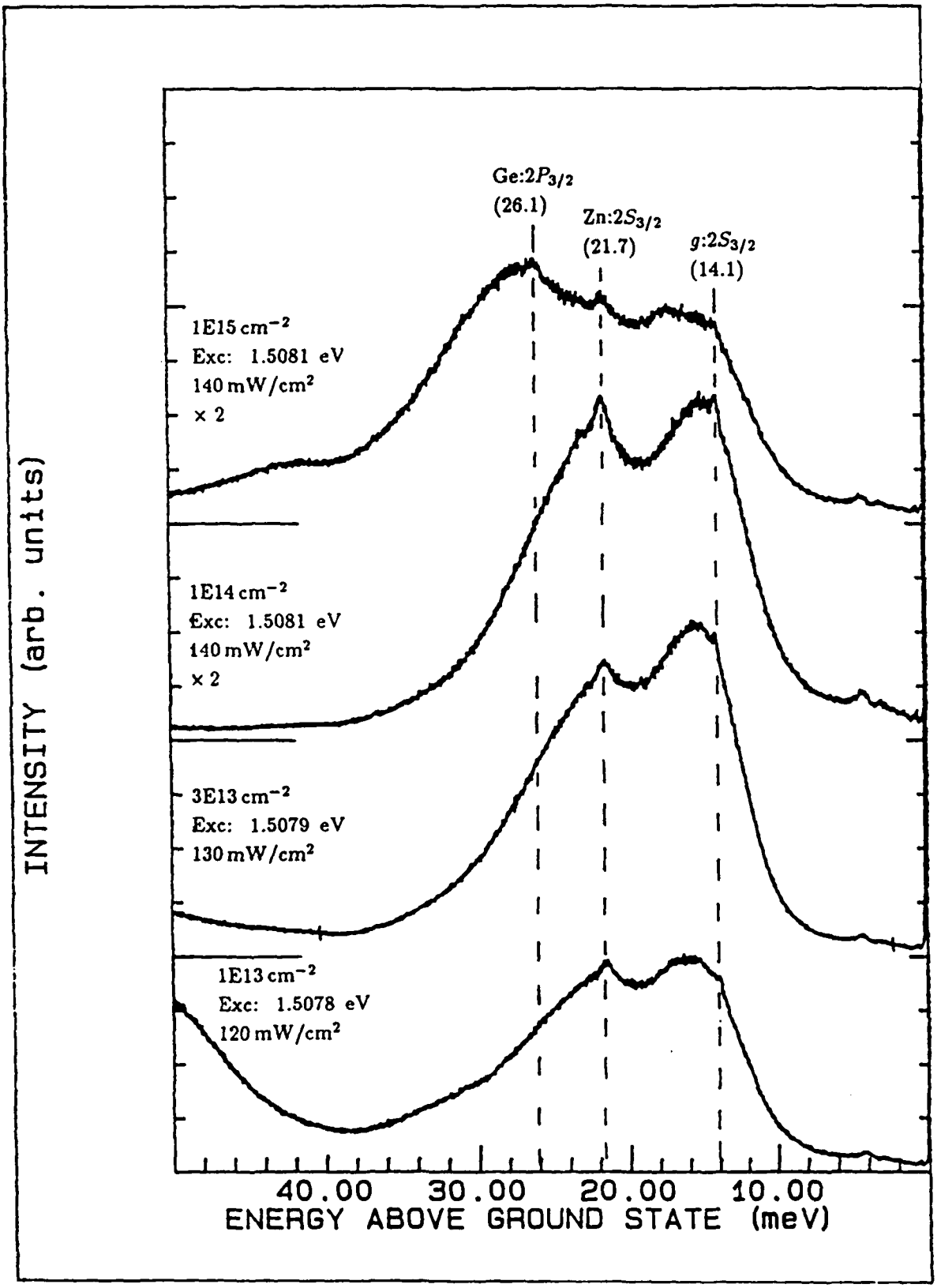

Figure 4.29. GaAs:Ge, ϕ=1E13–1E15 cm^{-2} Spectra, Exc: 1.5078–1.5081 eV, T=2.1K

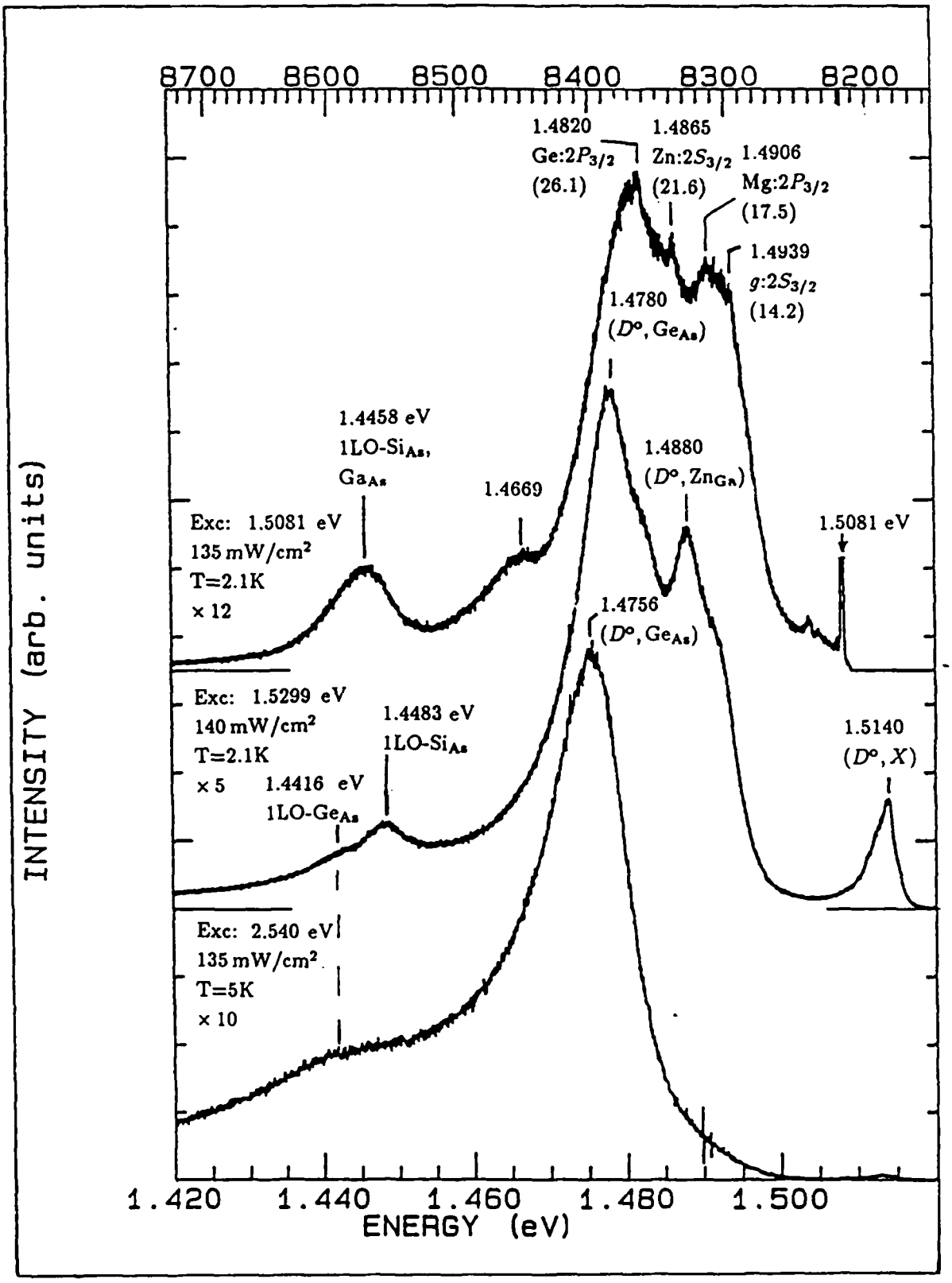

Figure 4.30. GaAs:Ge, ϕ=1E15 cm^{-2} Spectra, Exc: 2.5400–1.5081 eV at 135–140 mW/cm^2, T=2.1K

at 1.5299 eV may be increasing the number of (e, Ge_{As}) transitions. In addition, the 1.5299 eV excitation has produced conditions favorable for the creation of a high-energy shoulder to the 1.4780 eV peak, which (as discussed above) probably originates from recombinations involving the Si_{As} acceptor. At an excitation of 1.5081 eV, it appears that the high-energy shoulder is now fully resolved at the expense of the 1.4780 eV peak. The new peak, upon which the Ge_{As} acceptor's SPL is superimposed, is positioned at $\sim$1.482 eV, which correspond closely to the (D^{o}, Si_{As}) transition energy.

Also shown in Figure 4.30 is the onset of the $\sim$1.467 eV peak, subsequent to exciting the sample below-gap at 1.5081 eV. In addition, a band centered at 1.4458 eV is also observed. The band may originate from recombinations involving both the Ga_{As} double acceptor and LO phonon replicas of higher energy transitions.

GaAs:Ge+Ga

The luminescence for samples implanted with Ge and Ga in the dose range of 1E13–1E15 cm^{-2} is presented below. All samples were annealed following implantation at 900°C for 15 minutes. Stoichiometrically, these samples are Ga-rich relative to the as-grown and Ge-implanted samples. Thus, higher concentrations of V_{As} are assumed available for Ge activation and/or complexing with other impurities.

1E13 cm^{-2} Implant. PL from these {Ge+Ga}-implanted layers is shown in Figure 4.31. The spectra were obtained by varying the 2.5400 eV excitation intensity from about 670 $\mu W/cm^2$ to 140 mW/cm^2. The results are very similar to the case of the sample implanted with Ge-only, at an ion dose of 1E13 cm^{-2}, presented earlier in Figure 4.15. An unresolved band peaks at $\sim$1.470 eV at the lowest excitation intensity. After increasing the excitation intensity to about 140 mW/cm^2, the band appears to peak at $\sim$1.476 eV (resolution is difficult because

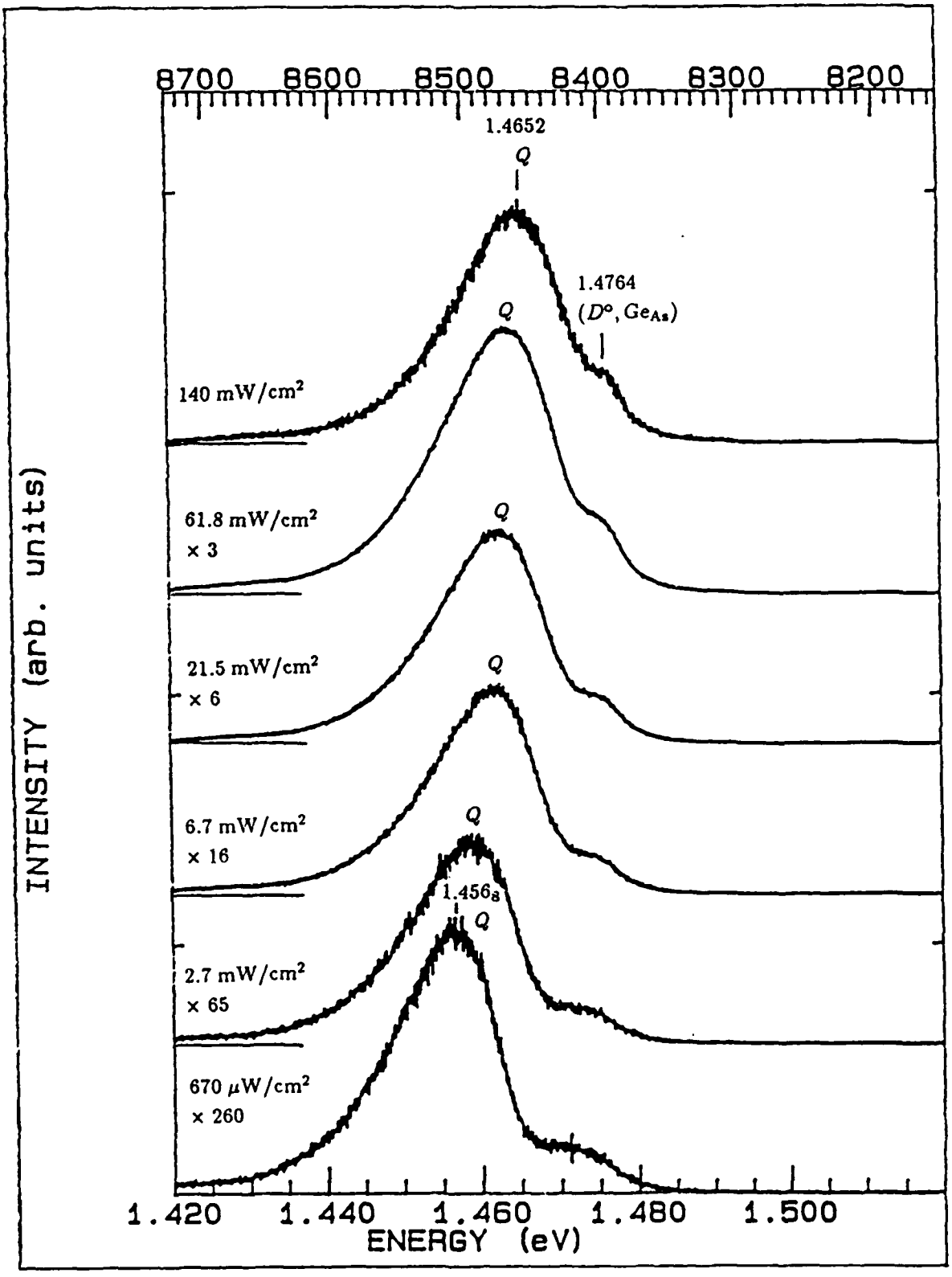

Figure 4.31. GaAs:{Ge+Ga}, ϕ=1E13cm^{-2} Spectra, Exc: 2.5400 eV at 670 μW/cm^2 - 140 mW/cm^2, T=2.1K

of the very intense, broad, lower-energy peak). The shift is indicative of D^o-A^o pair transitions. Although the band is at a somewhat low energy (at the lowest excitation intensities) relative to typical (D^o, Ge_{As}) peaks (according to Table 2.7), the acceptor, nevertheless, is assumed to be Ge_{As} . The PL peaks in the 1.48–1.495 eV range (originating from acceptors whose presence was already noted in the PL data of the unimplanted and Ga-implanted control samples) are not observed in this doubly implanted sample, whereas they were observed in the PL data of the 1E13 cm^{-2}, Ge-only implant in Figure 4.15. The apparent increase in the intensity of the (D^o, Ge_{As}) peak relative to this 1.48–1.495 eV luminescence in the {Ge+Ga}-implanted sample may be an indication that the excess V_{As} environment has enabled increased activation of the Ge_{As} acceptor. Indeed, the electrical measurements reported previously indicated that there was improved Ge_{As} acceptor activation in the {Ge+Ga}-implant relative to the Ge-only implant [53]. The luminescence in the 1.47–1.42 eV range is dominated by a broad, intense band which is assigned again as the Q band. The band exhibits excitation intensity-dependent energy shifts similar to those observed for the Q band in the 1E13 cm^{-2}, Ge-only implanted sample. This behavior is shown in Figure 4.32.

By varying the sample's temperature as shown in Figure 4.33, further observations may be made. The poorly resolved band (peaking at about 1.472_3 eV at 5K) due to Ge_{As} acceptors, shifts to higher energy as the temperature is increased to 30K. Above this temperature, the band's position stabilizes and then starts to shift to lower energy with increasing temperature. This behavior is indicative of (D^o, Ge_{As}) transitions at the low temperatures (already concluded from the excitation intensity-dependent study presented above) which disappear in favor of (e, Ge_{As}) transitions as the temperature is increased above 30K. The broad band in the 1.47–1.42 eV range, which has been labelled Q, shifts to lower energy with temperature as was observed for the band in the Ge-only implant of Figure 4.17. The band's shift is presented in Figure 4.34. Again, the band's excitation intensity-

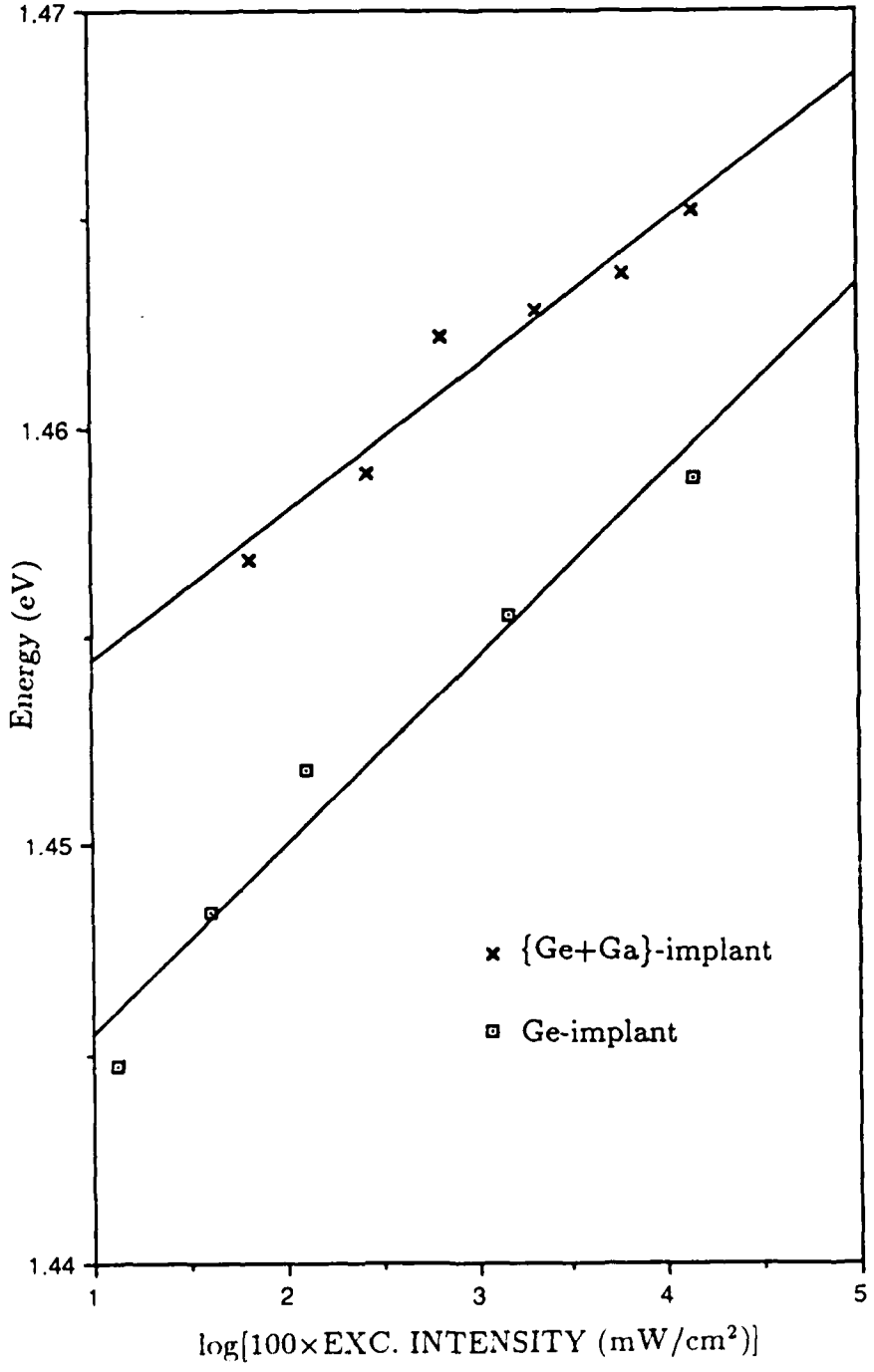

Figure 4.32. GaAs:Ge and GaAs:{Ge+Ga}, ϕ=1E13 cm^{-2}, Q Band Peak Energies as a Function of Excitation Intensity

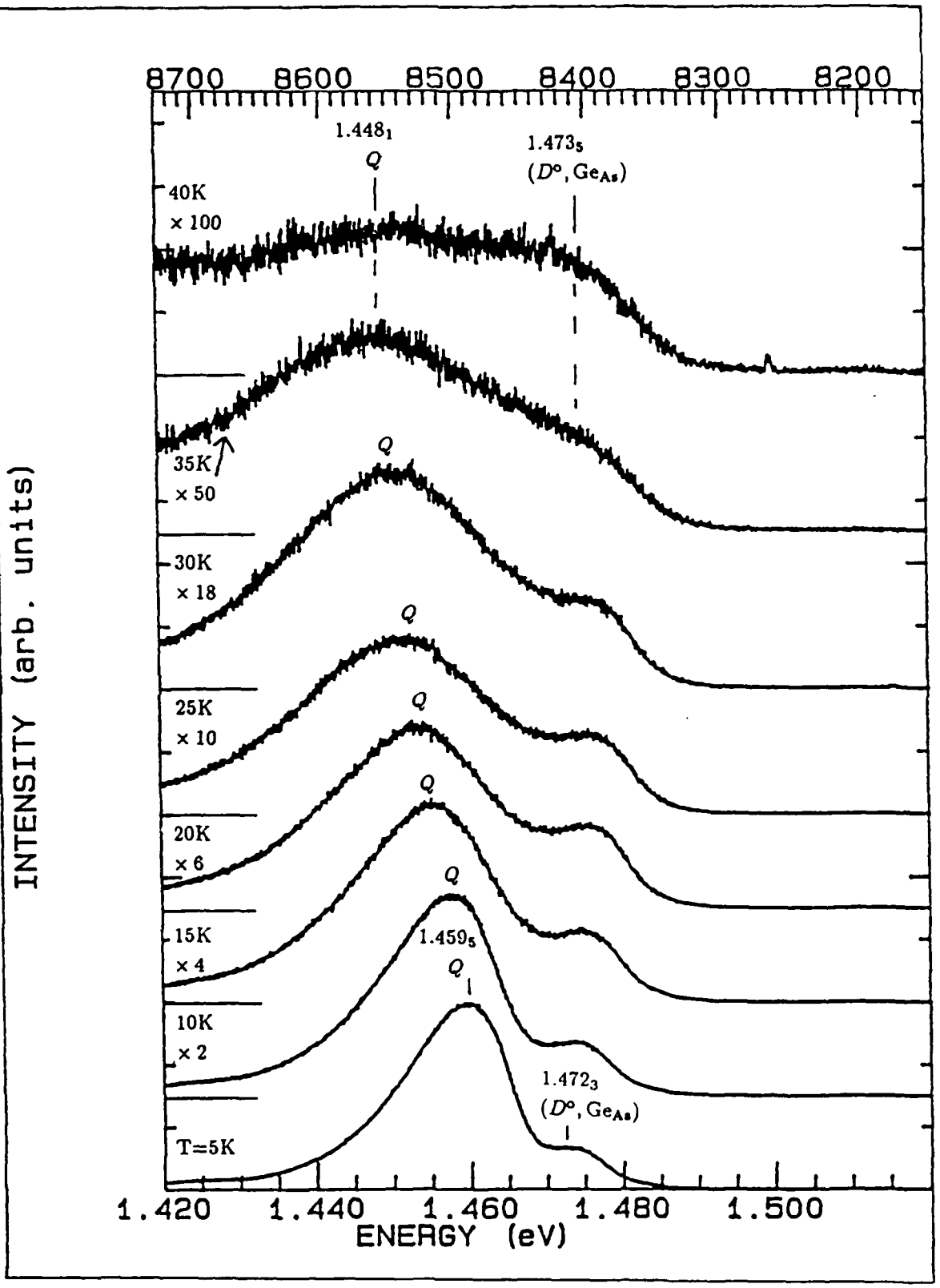

Figure 4.33. GaAs:{Ge+Ga}, ϕ=1E13 cm^{-2} Spectra, Exc: 2.5400 eV at 2.7 mW/cm^2, T=5–40K

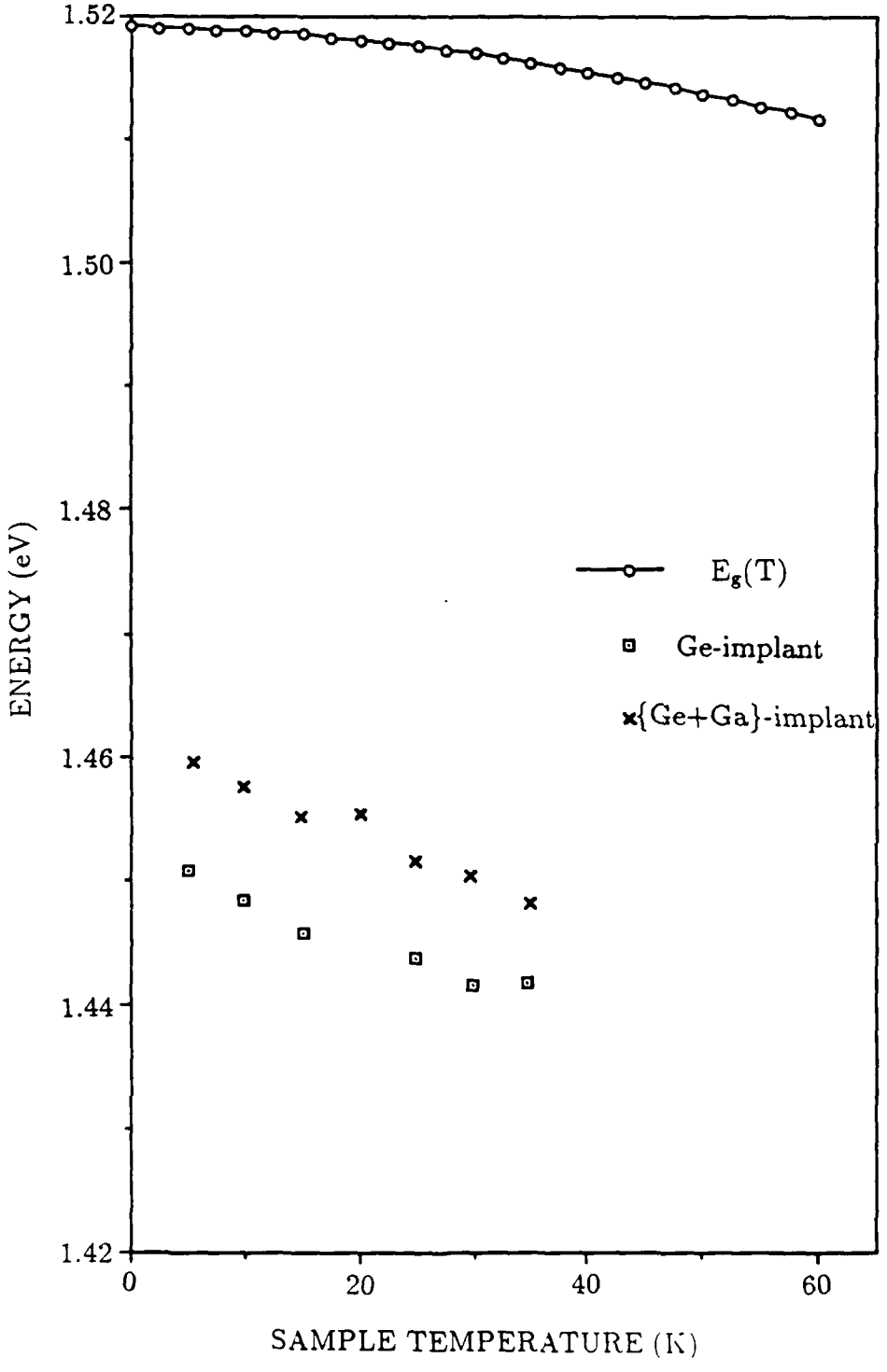

Figure 4.34. GaAs:Ge and GaAs:{Ge+Ga}, ϕ=1E13 cm^{-2}, Q Band Peak Energies as a Function of Temperature

and temperature-dependent shifts and absolute spectral position are very similar to PL results reported in the literature for the Q band.

The analysis can be extended by collecting the luminescence resulting from below-gap excitation. Figure 4.35 shows the cumulative results for several excitation energies. A notable feature is the SPL observed at 26.0 meV from the laser line which corresponds well to the $2P_{3/2} \rightarrow 1S_{3/2}$ transition energy for the hole bound to the Ge_{As} acceptor. In addition, the band, assigned as Q in the PL, shifts to lower energy, and a low-energy shoulder at $\sim$1.446 eV emerges as the excitation energy is decreased to 1.5079 eV. (The band's shift to lower energy was also observed in Figures 4.19, 4.20, 4.25 and 4.26 for the 1E13–3E13 cm^{-2}, Ge-implanted samples). However, by decreasing the excitation energy from 1.5079 to 1.4995 eV, a portion of the luminescence seemingly shifts slightly to higher energy (to $\sim$1.462 eV), decreases in intensity and broadens. This behavior may result from both the selective screening of the D^o-A^o pairs contributing to luminescence in this region, and the resolution of an underlying peak (not related to Q band luminescence) at $\sim$1.462 eV. Looking back at Figure 4.13, one notes that the Ga-implanted sample (which acts as an effective control for this {Ge+Ga} implanted sample) was seen to have PL at $\sim$ 1.470 eV. This, in conjunction with the fact that the Ga-only implanted sample does not satisfy the general conditions necessary for the onset of Q band luminescence, implies that at least a portion of the luminescence in the 1.46 eV range, at the lowest excitation energies of Figure 4.35, is no longer Q band luminescence. One remaining feature to be noted in Figure 4.35 is that the shoulder observed under 1.5079 eV excitation at $\sim$1.446 eV is now resolved to peak at about 1.4455 eV. Analogous to the Ge-only implanted results, the luminescence here is attributed to (e, A^o) and distant D^o-A^o pair transitions involving the Ga_{As} double acceptor.

A temperature-dependent study of the luminescence obtained from the sample implanted with {Ge+Ga}, at a dose of 1E13 cm^{-2}, using $\sim$1.508 eV excitation

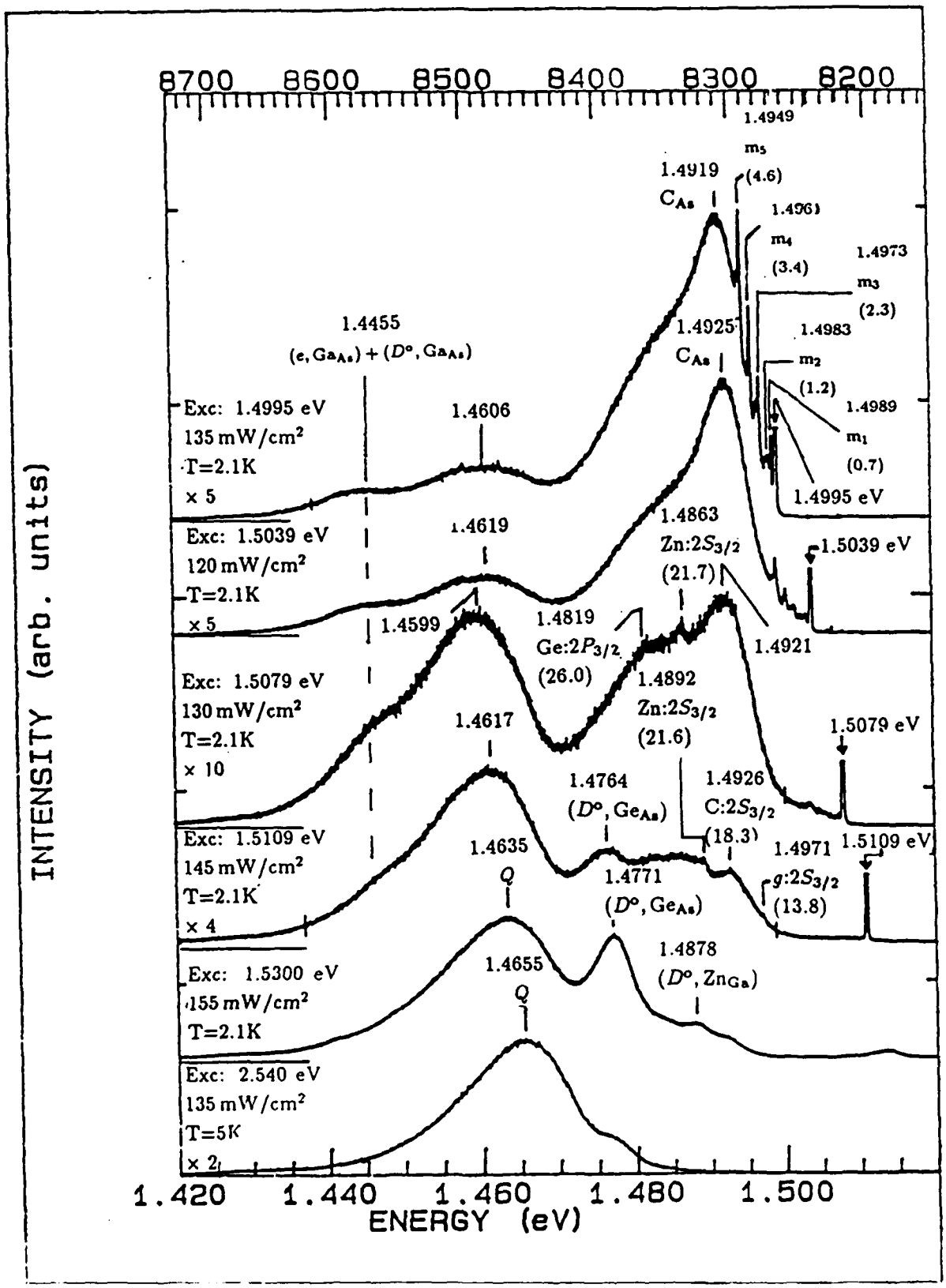

Figure 4.35. GaAs:{Ge+Ga}, ϕ=1E13 cm^{-2} Spectra, Exc: 2.5400–1.4995 eV, T Mainly 2.1K

was performed. This study is similar to that conducted for the 1E13 cm^{-2}, Ge-implanted sample shown in Figures 4.22 and 4.23. The results obtained under relatively low excitation intensity are shown in Figure 4.36. The SPL structure, which has been assigned to the $2P_{3/2}$ state of the hole bound to the Ge_{As} acceptor, remains at temperatures as large as 20K. Luminescence in the 1.47–1.42 eV range de-convolves, similar to the temperature-dependent data for the 1E13 cm^{-2}, Ge-implanted sample in Figure 4.23. (In fact, contrary to data collected for the Ge-only implanted sample, this de-convolution is also observed in the excitation energy-dependent studies shown previously in Figure 4.35.) At 2.1K and an excitation intensity of about 13.4 mW/cm^2, the Q band peaks at 1.455_7 eV with a just-resolved low-energy shoulder. At 5K, a high-energy shoulder appears at 1.463_3 eV, and the 1.455_7 eV peak has shifted slightly to higher energy. At 10K, a peak at 1.447_3 eV, which previously was only observed as a shoulder to the 1.455_7 eV peak, is clearly resolved. This peak shifts slightly to higher energy with increasing temperature so that at about 40K it is located at 1.449_5. As previously discussed, the absolute spectral position of the 1.447_3 eV peak leads one to conclude that the Ga_{As} double acceptor is involved. The 1.477_3 eV peak's temperature behavior indicates that mainly (D^o, Ga_{As}) transitions are occurring at the low temperatures which disappear in favor of (e, Ga_{As}) transitions as the temperature is increased to 40K. Also at 10K, a band is seen to peak at 1.462_0 eV. The band at $\sim$1.456–1.457 eV has seemingly disappeared. However, it is believed that some of this band's luminescence is unresolved in the 1.462_0 eV peak. For 15–20K, the recombinations which give rise to the $\sim$1.456–1.457 eV luminescence are believed to have diminished even more. The strongly temperature-dependent behaviour is very similar to that of the $\sim$1.458 eV peak in Figure 4.23. The remaining luminescence features in this spectral range at temperatures of 15–20K are the Ga_{As}-related peak and the familiar peak at $\sim$1.467 eV, which appears to shift to higher energy with temperature. This peak is that which was just discernible as a shoulder at 1.463_3

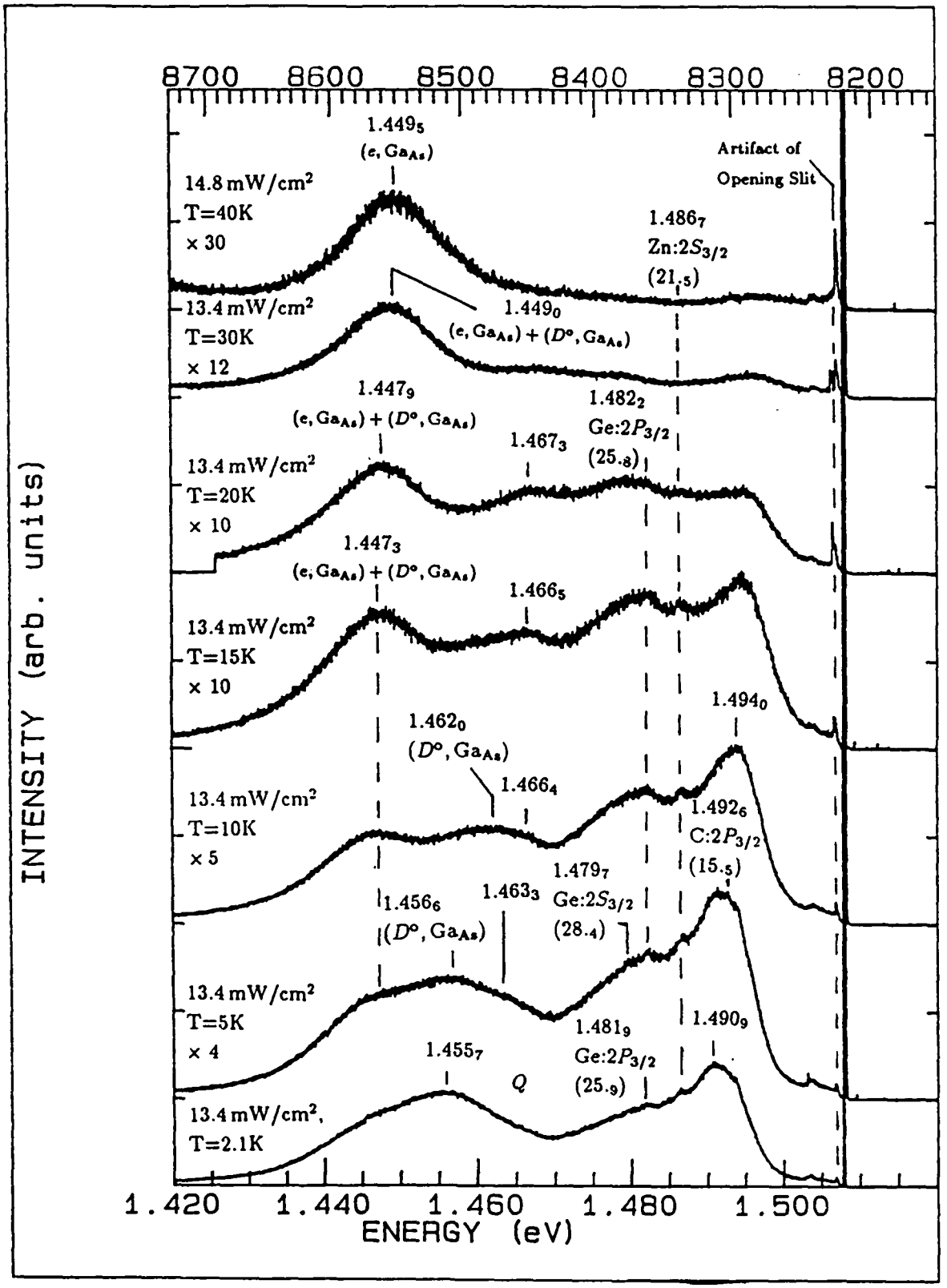

Figure 4.36. GaAs:{Ge+Ga}, ϕ=1E13 cm^{-2} Spectra, Exc: 1.5078–1.5082 eV at Mainly 13.4 mW/cm^2, T=2.1–40K

eV in the 5K luminescence.

Once again, below gap excitation combined with the temperature-dependent studies has brought some insight into the recombination mechanisms giving rise to the Q band which was also observed in the {Ge+Ga}-implanted sample's PL. The results have again demonstrated that it is very likely that the Ga_{As} double acceptor plays a major role. The Q band, observed in both the 1E13 cm^{-2}, Ge-only and {Ge+Ga}-implanted samples, has behaved very consistently. Thus, the close pairs model (developed for the Q band results collected from the Ge-only implanted sample), which assumes large concentrations of Ga_{As} double acceptors that make close pairs with donors, may again be invoked to explain the Q band luminescence seen for the {Ge+Ga}-implanted sample. The resolution of the extremely temperature sensitive peak, lying in the region of $\sim$ 1.456–1.457 eV, is fundamental to both understanding the contradictory excitation intensity- and temperature-dependent PL results and, ultimately, to acceptance of the close pairs model. However, the results differed from those of the 1E13 cm^{-2}, Ge-implanted sample because a peak at $\sim$1.467 eV was also observed to possibly contribute to the Q band's luminescence of the {Ge+Ga}-implanted sample in Figure 4.36. The peak's absolute spectral position is approximately that of the peak observed in the unimplanted, Ga-only, and As-only implanted control samples (1.466–1.470 eV, especially with below-gap excitation, such as $\sim$1.508 eV). It is interesting to note that the $\sim$1.467 eV peak was hardly observed in any of the luminescence arising from the Ge-only implanted samples, except the highest implant dose.

3E13 cm^{-2} Implant. The PL for the sample implanted with {Ge+Ga}, at a dose of 3E13 cm^{-2}, is shown in Figure 4.37. The peak at 1.4764 eV, due mainly to (D^o, Ge_{As}) transitions, is now clearly observed. The shift of the supposed Q band to lower energy relative to the 1E13 cm^{-2} implant case, is partially responsible. The Q band's shift to lower energy as the {Ge+Ga}-implant dose is increased from 1E13 to 3E13 cm^{-2} was also observed for the Ge-only implants as shown

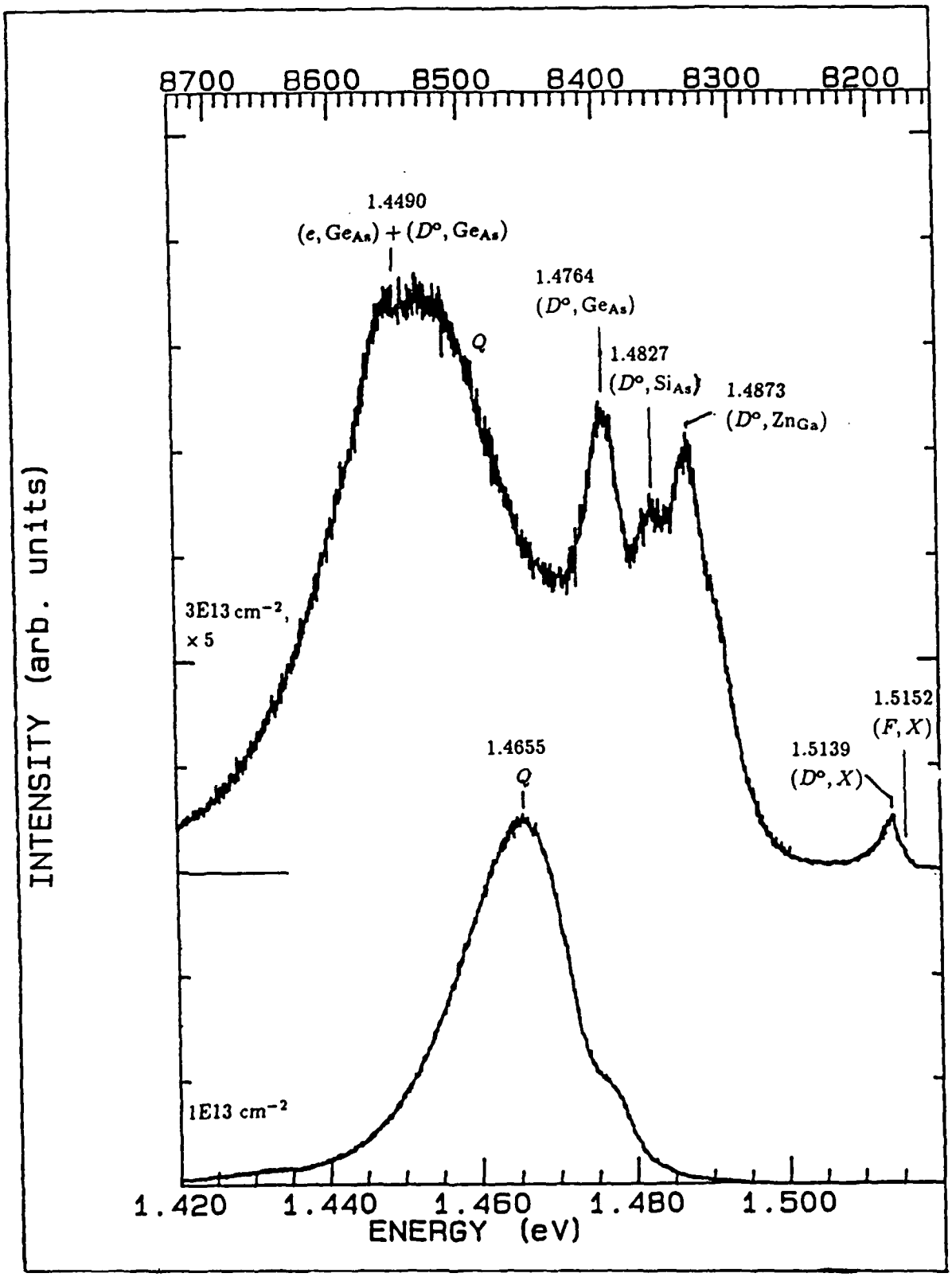

Figure 4.37. GaAs:{Ge+Ga}, ϕ=1E13–3E13 cm^{-2} Spectra, Exc: 2.5400 eV at 135 mW/cm^2, T=5K

again in Figure 4.38. Again, taking into account the close pairs model, one could speculate that a majority of the (D^o, Ga_{As}) transitions occur amongst pairs with not as close a pair separation in the 3E13 cm^{-2}, {Ge+Ga} dual implanted sample relative to those in the 1E13 cm^{-2} dual implanted sample. A similar argument could explain the overall shift of the Q band to lower energy as a function of the implant ion(s) and increasing dose, as shown in Figure 4.38. This could result from a diminished concentration of Ga_{As} double acceptors in the samples implanted with the higher dose. This, in turn, may result from a corresponding increase in Ge activation on the As site (in competition with the activation of Ga on the As site), which is especially reasonable for the Ge-only implanted samples relative to the {Ge+Ga} dual implanted samples. The decreased proportion of close pair transitions in the 3E13 cm^{-2}, {Ge+Ga}-implanted samples is also supported by the resolution of a peak at ~ 1.4490 eV (in Figure 4.37) near the maximum of the Q band which is located at ~ 1.454 eV. The ~ 1.4490 eV peak corresponds closely to that peak which has been previously seen to underlie the Q band only under below-gap excitation (see, for example, Figures 4.35 and 4.36); conditions which are not as favorable to the close pair recombinations. Thus, from the prior data and analysis, it is believed that the peak at ~ 1.4490 eV is due mainly to (e, Ga_{As}) transitions with some contribution from (D^o, Ga_{As}) transitions occurring amongst distant pairs. This is the only sample whose PL exhibited evidence for the contribution of (e, Ga_{As}) transitions to Q band luminescence.

The sample was characterized further by tuning the excitation source to lower energies as shown in Figure 4.39. At 1.5300 eV excitation, much of the Q band is observed to have disappeared. The remaining PL in the 1.47–1.42 eV region is a peak at 1.4480 eV, again attributable to (D^o, Ga_{As}) and (e, Ga_{As}) transitions. (From previous observations concerning excitation at 1.53 eV, this peak may receive a relatively large contribution from the (e, Ga_{As}) transitions). The change was quite rapid relative to previous observations for similarly excited samples exhibiting the

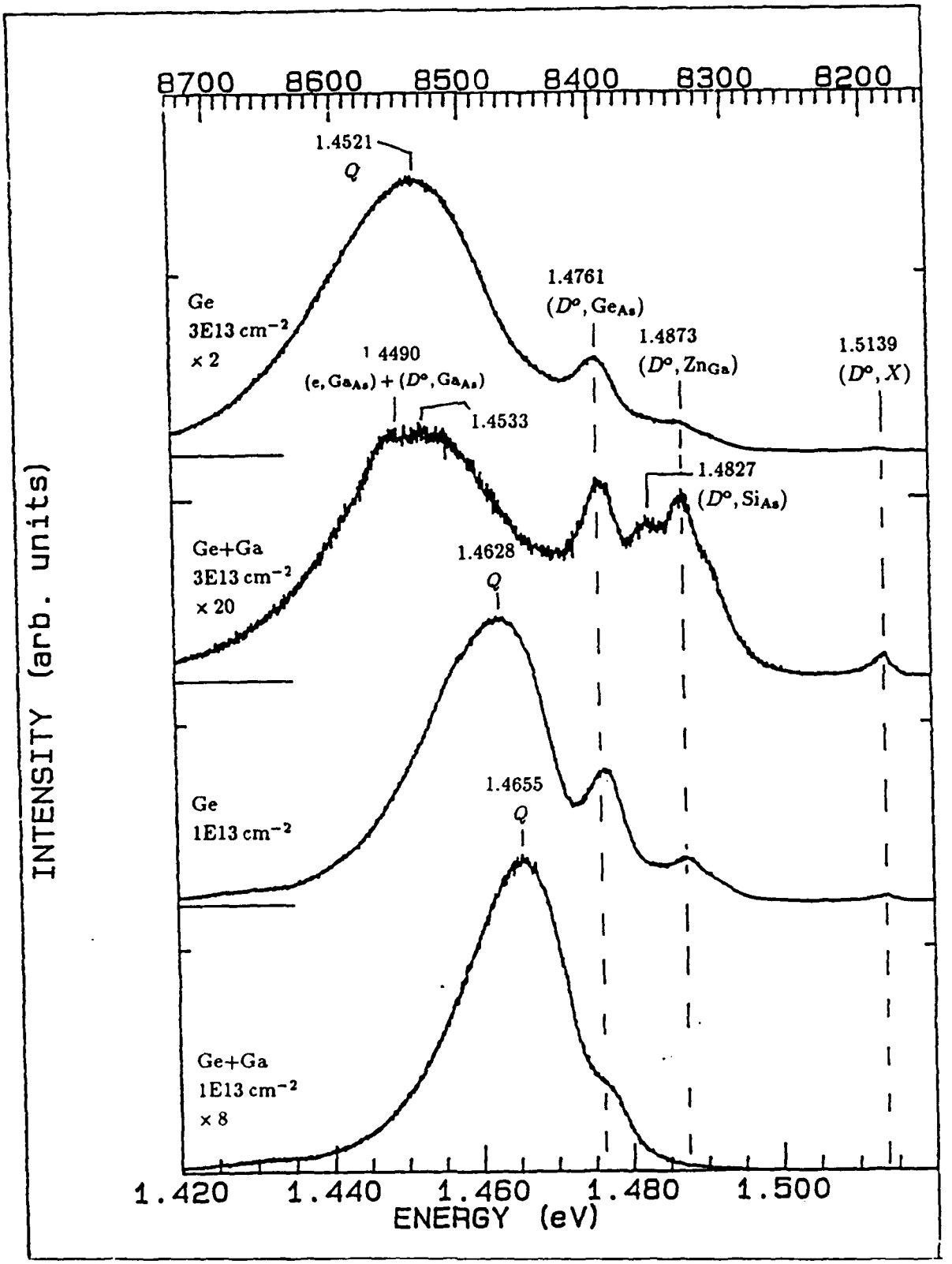

Figure 4.38. GaAs:Ge and GaAs:{Ge+Ga}, ϕ=1E13-3E13 cm^{-2} Spectra, Exc: 2.5400 eV at 135 mW/cm^2, T=5K

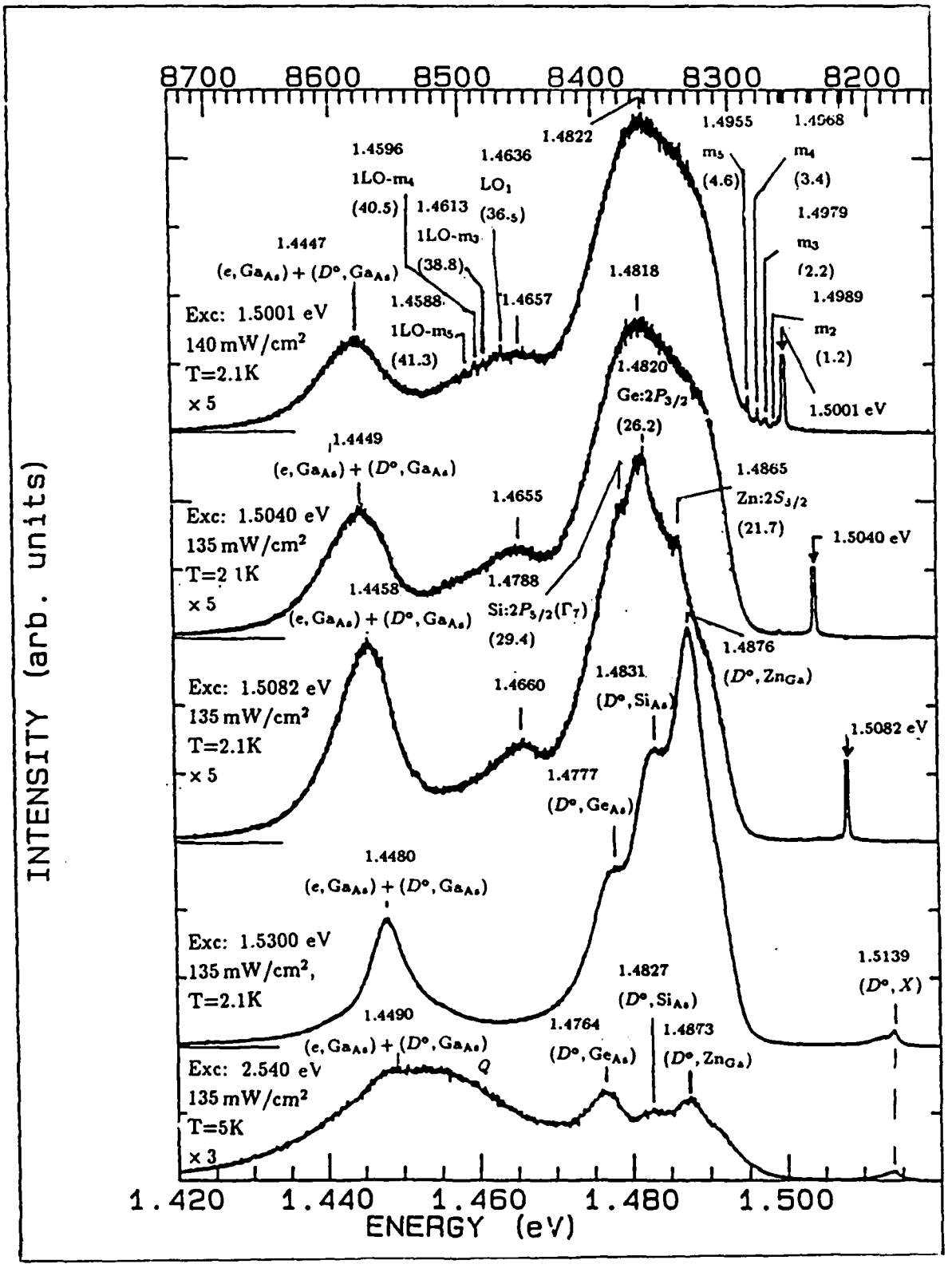

Figure 4.39. GaAs:{Ge+Ga}, ϕ=3E13 cm^{-2} Spectra, Exc: 2.5400–1.5001 eV at Mainly 135 mW/cm^2, T Mainly 2.1K

Q band.

Upon excitation at 1.5082 eV, SPL structure appears in the 1.50–1.47 eV spectral range of Figure 4.39. SPL involving the $2P_{3/2}$ hole state of the Ge_{As} acceptor is much improved over that in the 1E13 cm^{-2} implant case. An additional structure at 29.4 meV from the laser line is also seen. Referring back to Table 2.10, this could originate from the $2P_{5/2}(\Gamma_7)$ state of the hole bound to the Si_{As} acceptor. There is just-resolved evidence for additional SPL structure near the SPL which was associated with the $2P_{3/2}$ hole state of the Ge_{As} acceptor. This is seen somewhat more clearly on an expanded scale in Figure 4.40. By decreasing the excitation intensity by a factor of ten (as presented in Figure 4.40), this SPL structure is better resolved, and is located $27._1$ meV from the laser line. Returning to Table 2.10, the SPL appears to be associated with the $2P_{5/2}(\Gamma_8)$ state of the hole bound to the Si_{As} acceptor. In addition, the decreased excitation intensity has enabled resolution of two more Ge_{As} acceptor excited states. The associated SPL signals are at $28._7$ and $30._1$ meV from the laser line. Referencing Table 2.10, these structures seem likely to be originating from the $2S_{3/2}$ and $2P_{5/2}(\Gamma_8)$ states of the hole bound to the Ge_{As} acceptor, respectively. It is noted from Table 2.10 that the energy associated with the $2S_{3/2} \rightarrow 1S_{3/2}$ transition of the hole bound to the Ge_{As} acceptor has been reported to be 28.3 meV. The small discrepancy may be the result of unresolved contributions from the lower energy signal at 29.4 meV from the laser line, observed at the higher excitation intensity.

The significant changes in the 1.47–1.42 eV range of Figure 4.39, upon excitation below-gap, include the emergence of the band at 1.4660 eV and the shift of the former 1.4480 eV band to 1.4458 eV. The shift of the Ga_{As}-related peak, after excitation below-gap, supports the above parenthetical remark concerning the relative importance of (e, Ga_{As}) transitions at 1.53 eV excitation and now indicates increased contribution of the (D^o, Ga_{As}) transitions. The shift of the 1.4458 eV peak with changing excitation intensity also suggests contributions from (D^o, Ga_{As})

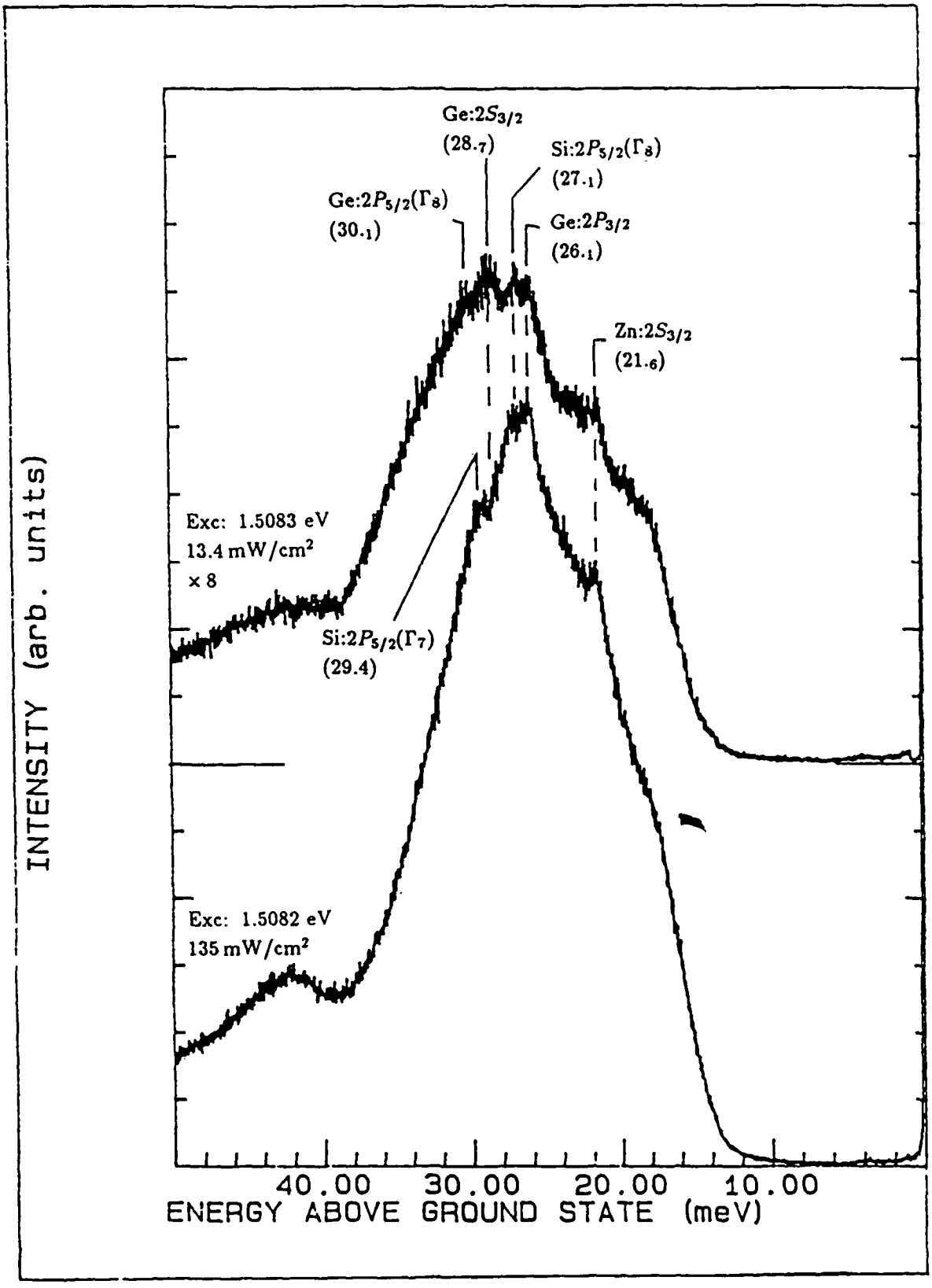

Figure 4.40. GaAs:{Ge+Ga}, ϕ=3E13 cm^{-2} Spectra, Exc: 1.5082–1.5083 eV at 13.4–135 mW/cm^2, T=2.1K

transitions. This behavior is shown in Figure 4.41. As the excitation source is tuned to 1.5040 eV, the SPL structure in the 1.50–1.47 eV range is replaced with a broad featureless band. In addition, the peak now attributed predominantly to $(D^{\circ}, \mathrm{Ga_{As}})$ transitions correspondingly broadens and continues to shift to lower energy. This broadening may indicate that there is some contribution from LO phonon luminescence.

1E14-1E15 cm^{-2} Implants. Figure 4.42 shows the cumulative dose-dependent PL for the {Ge+Ga}-implanted samples. As in the Ge-only implants, the presence of the $\sim$1.475–1.476 eV peak throughout indicates continued activation of the $\mathrm{Ge_{As}}$ acceptor. The relative intensity of this peak does not change with any perceived trend. As observed for the Ge-only implant in the 1.47–1.42 eV range, a large portion of the Q band disappears when the {Ge+Ga} dose is increased to 1E14 cm^{-2}. It appears that the PL which peaks at about 1.4330 eV in the 1E14 cm^{-2} implant is approximately the same shape as that which peaks at about 1.4292 eV in the 1E14 cm^{-2}, Ge-only implant (see Figure 4.27). The only difference is the enhanced resolution of the assigned $(D^{\circ}, \mathrm{Ga_{As}})$ peak at 1.4470 eV in the {Ge+Ga}-implant. A final observation on the 1E14 cm^{-2}, {Ge+Ga}-implant PL is the presence of a just-resolved peak at about 1.4690 eV. This peak appears to correspond to the peak which has appeared in the $\sim$1.466–1.470 eV range in previous samples' luminescence. The peak's presence is significant in that it is rarely observed in above-gap excitation of Ge- or {Ge+Ga}-implanted samples. Concerning the PL of the 1E15 cm^{-2}, {Ge+Ga}-implant, it is seen that the 1.4752 eV peak has quite an extensive low-energy tail. This observation was also made for the 1E15 cm^{-2}, Ge-only implant. The significant difference is the improved resolution of the assigned $(e, \mathrm{Ga_{As}})$ and $(D^{\circ}, \mathrm{Ga_{As}})$ peak in the {Ge+Ga}-implant's PL.

Data for excitation at $\sim$1.5300 eV is presented in Figure 4.43. As previously observed, the signatures of most impurities found in the unimplanted, As-only,

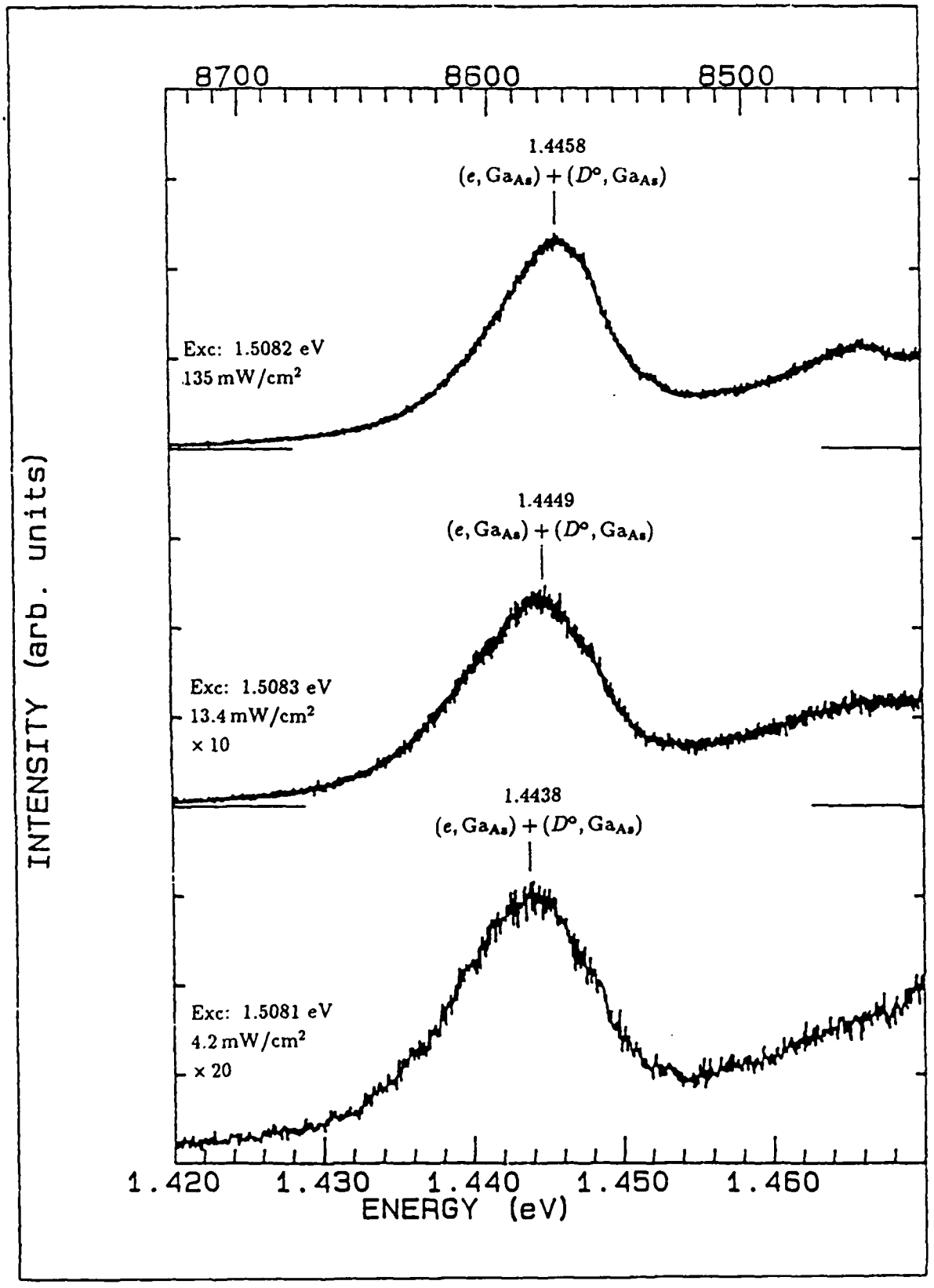

Figure 4.41. GaAs:{Ge+Ga}, ϕ=3E13 cm^{-2} Spectra, Exc: 1.5081–1.5083 eV at 4.2–135 mW/cm^2, T=2.1K

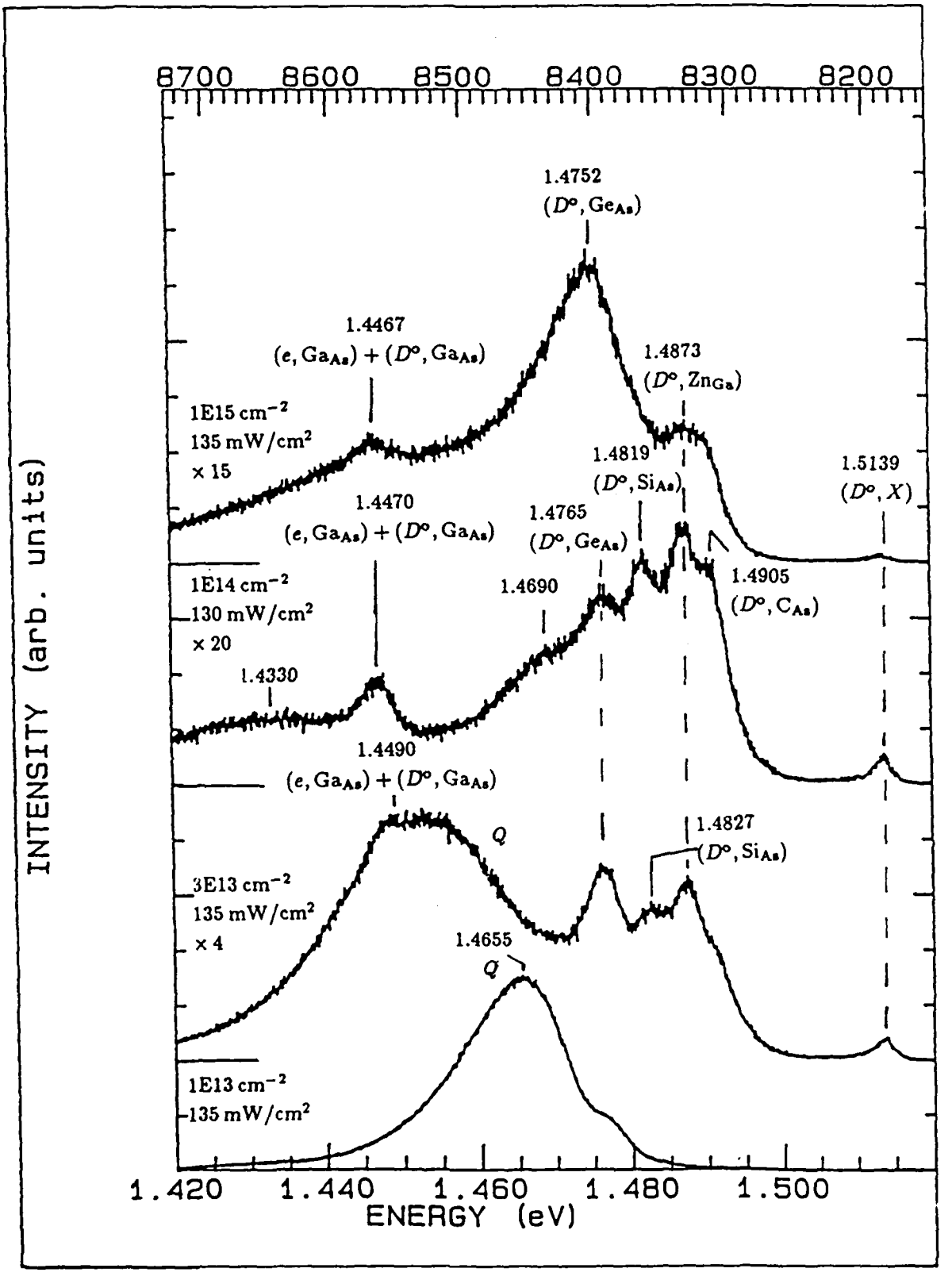

Figure 4.42. GaAs:{Ge+Ga}, ϕ=1E13–1E15 cm^{-2} Spectra, Exc: 2.5400 eV at Mainly 135 mW/cm^2, T=5K

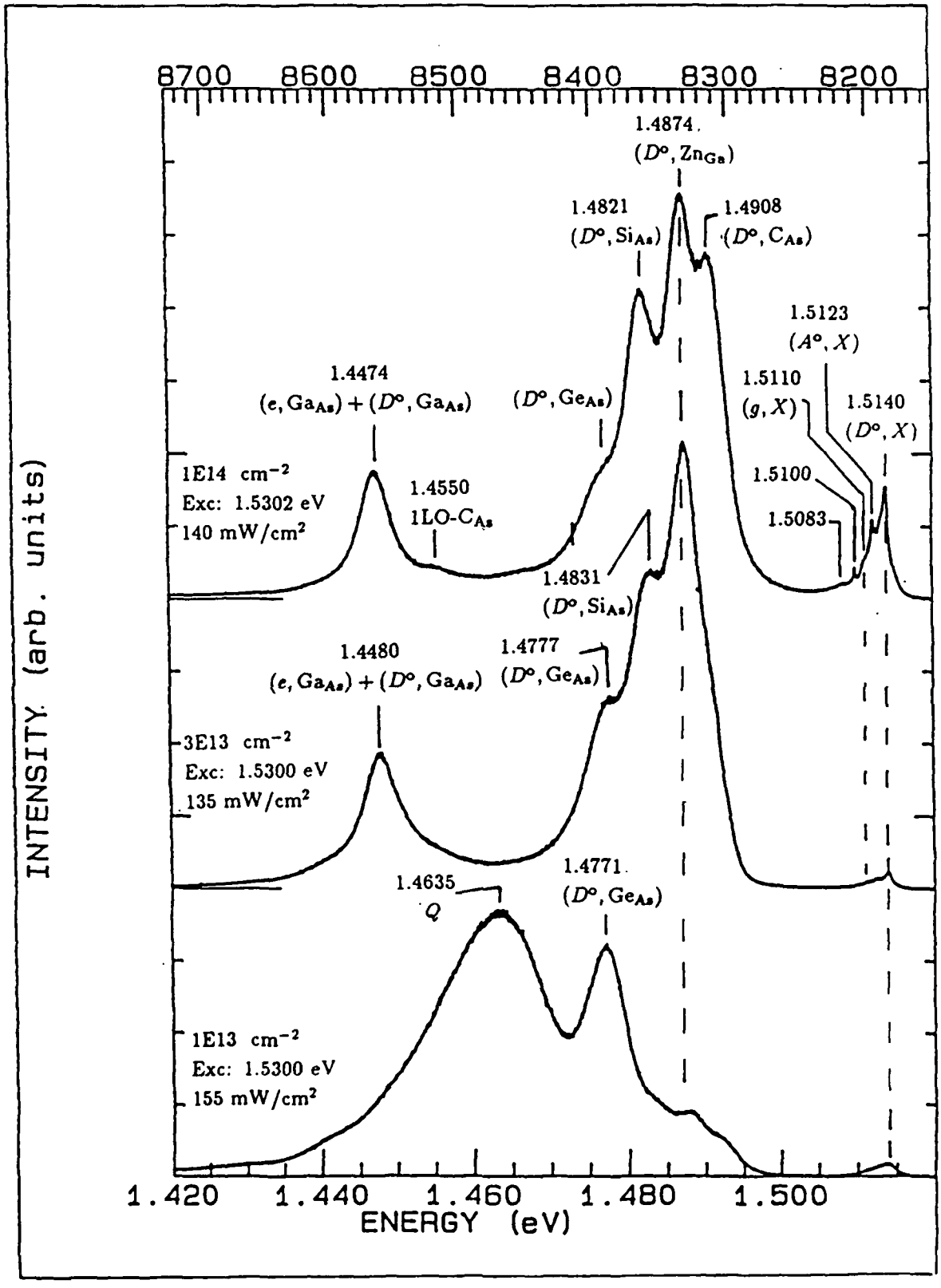

Figure 4.43. GaAs:{Ge+Ga}, ϕ=1E13–1E14 cm^{-2} Spectra, Exc: 1.5300–1.5302 eV, T=2.1K

and Ga-only implanted control samples are enhanced. Also, an interesting trend already seen to persist to doses as large as 1E14 cm^{-2} for the Ge-only implant (shown in Figure 4.28), is repeated for the {Ge+Ga}-implant. That is, the intensity of the Ge-related $\sim$1.477–1.478 eV peak decreases with increasing Ge dose relative to that of the peaks originating from other acceptors. Finally, the 1.4330 eV band, observed in Figure 4.42 for the 1E14 cm^{-2} implant, is now not observed. Like the analogous 1.4292 eV band observed in the 1E14 cm^{-2}, Ge-only implant, this could be an indication of the band's (and hence responsible defect center's) shallow depth distribution.

The analysis is extended in Figures 4.44 through 4.46 by collecting the luminescence resulting from below-gap excitation. Figure 4.44 shows the cumulative dose-dependent luminescence with $\sim$ 1.508 eV excitation. Immediately apparent is the enhanced SPL signal, assigned to the $2P_{3/2}$ state of the hole bound to the Ge_{As} acceptor, for the 1E14 and 1E15 cm^{-2} implants. From the excitation energy-dependent data of Figure 4.45 for the 1E14 cm^{-2} {Ge+Ga}-implant sample, it is seen that this SPL is superimposed upon the luminescence background originating from (D^o, Si_{As}) transitions. It should be recalled that the best indication of SPL associated with the Ge_{As} acceptor in the Ge-only implants also occured for the sample which coincidentally exhibited a (D^o, Si_{As}) band upon which this SPL could superimpose (see Figure 4.30).

Similar to the below-gap excitation of the 3E13 cm^{-2}, {Ge+Ga}-implant, the 1E14–1E15 cm^{-2} implants exhibit significant change in the 1.50–1.47 eV range, upon exciting the samples with below-gap photons. Specifically, Figures 4.44 and 4.45 clearly show the emergence of the band at $\sim$ 1.466 eV. This band's temperature behavior is presented in Figure 4.46. As can be seen, the 1.4663 eV band at 5K shifts slightly to higher energy with increasing temperature. This would indicate that the $\sim$ 1.466 eV band is at least in part attributable to D^o-A^o pair transitions. The rapid decrease in the peak's intensity above 30K supports this

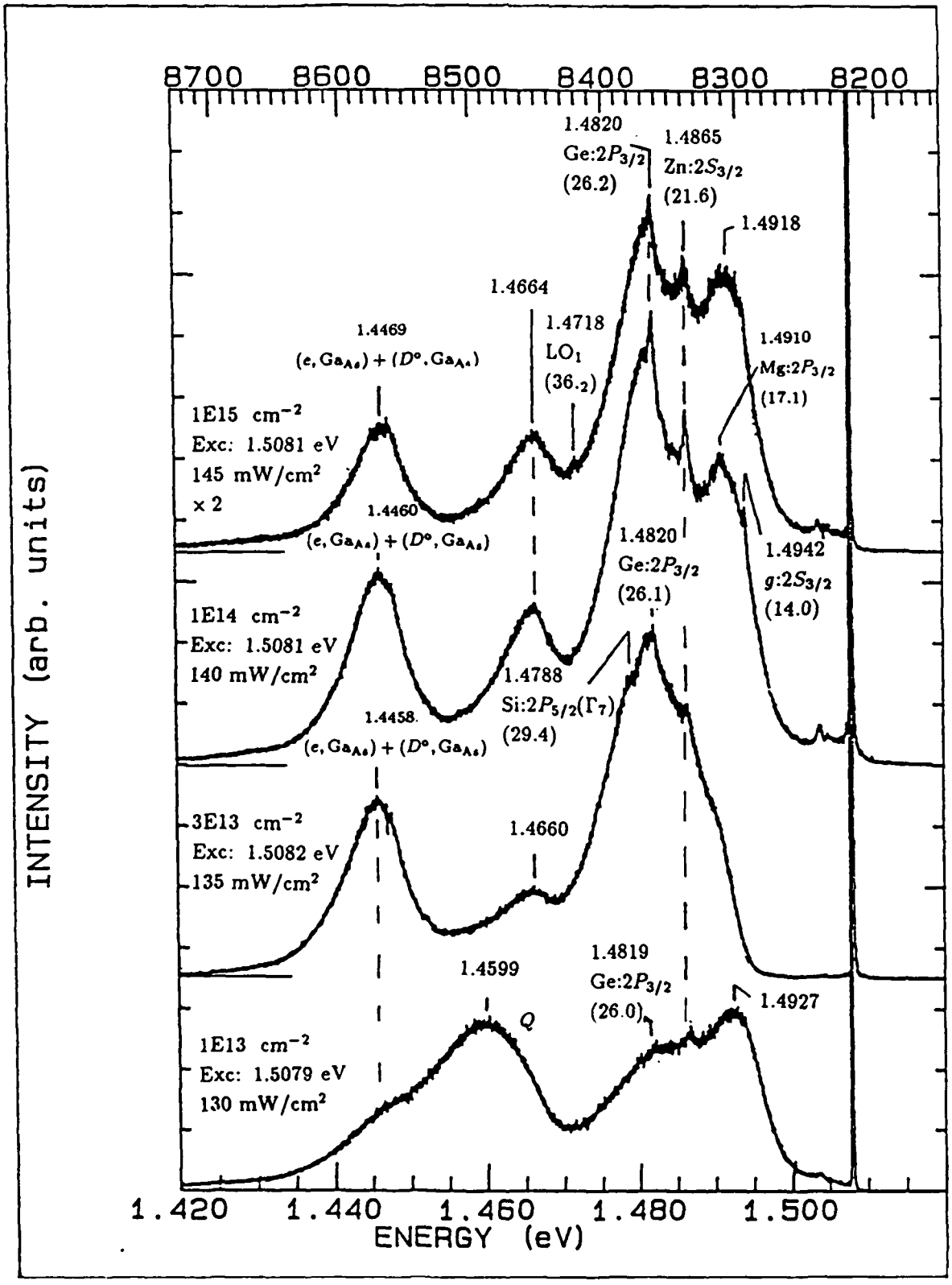

Figure 4.44. GaAs:{Ge+Ga}, ϕ=1E13-1E15 cm^{-2} Spectra, Exc: 1.5079-1.5082 eV, T=2.1K

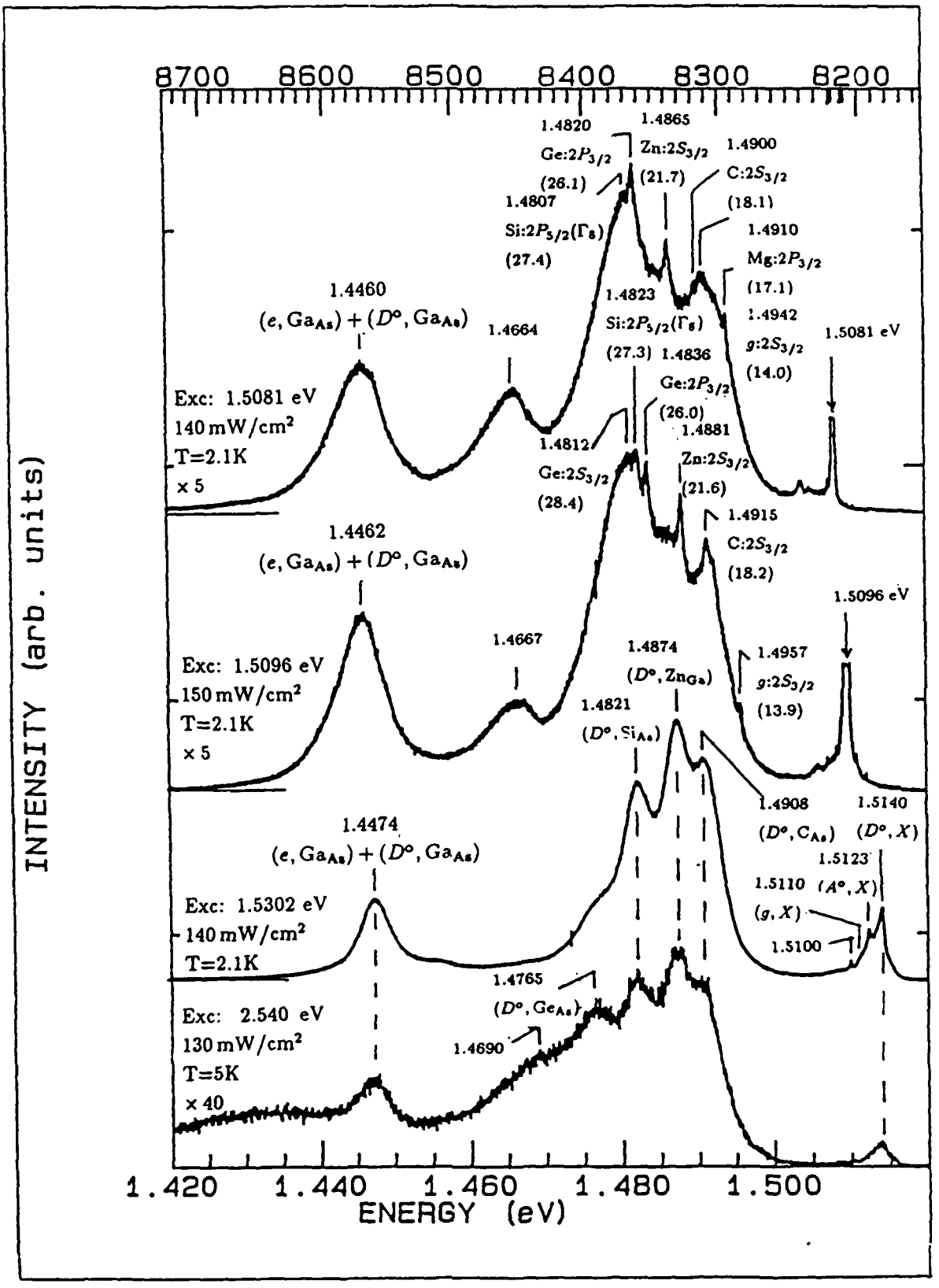

Figure 4.45. GaAs:{Ge+Ga}, ϕ=1E14 cm^{-2} Spectra, Exc: 2.5400–1.5081 eV, T Mainly 2.1K

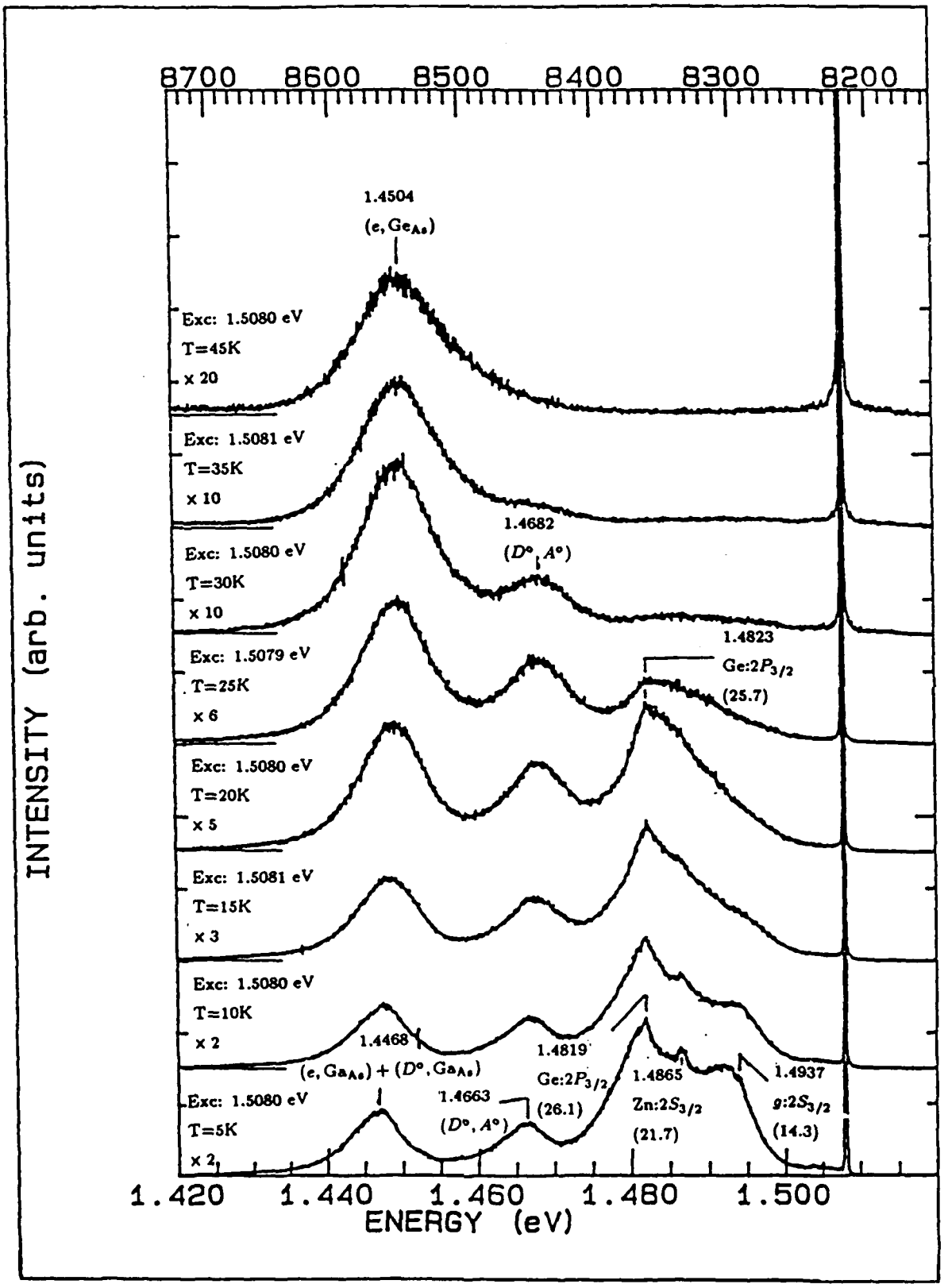

Figure 4.46. GaAs:{Ge+Ga}, ϕ=1E14 cm^{-2} Spectra, Exc: 1.5079–1.5081 eV at 135–140 mW/cm^2, T=5–45K

conclusion. A similar conclusion can be drawn for the 1.4468 eV peak shown in Figure 4.46. The Ga_{As}-related peak also shifts slightly to higher energy with increasing temperature, supporting its assignment as (D^o, Ga_{As}) at the lower temperatures. Additional contributions from (e, Ga_{As}) transitions are verified by the peak's existence at temperatures as high as 45K. The temperature dependence of the signals assigned to the $2S_{3/2}$ and $2P_{3/2}$ states of the hole bound to the g and Ge_{As} acceptors, respectively, are also shown in Figure 4.46. Such results substantiate the identification of these signals as SPL. Finally, referring back to Figure 4.44, the peak at $\sim$1.446–1.447 eV, which is assigned to (e, Ge_{As}) and (D^o, Ga_{As}) transitions, continues to be observed at the higher doses.

GaAs:Ge+As

The luminescence for samples implanted with Ge and As in the range 1E13–1E15 cm^{-2} is presented below. All samples were annealed following implantation at 900°C for 15 minutes. Stoichiometrically, these samples are As-rich relative to the as-grown and Ge-implanted samples. Thus, lower concentrations of V_{As} sites are assumed available for for Ge and/or Ga activation. On the other hand, higher concentrations of V_{Ga} sites are assumed available for Ge activation.

1E13-1E15 cm^{-2} Implants. Figure 4.47 shows the cumulative dose-dependent PL for the {Ge+As}-implanted samples. The dominant feature at all dose levels is a peak at $\sim$1.475–1.477 eV due to (e, Ge_{As}) and (D^o, Ge_{As}) recombinations. The peak's relative intensity seems to decrease as the dose increases. It is significant that the intense Q band is not observed in these samples, even at the lowest doses. At the 1E13 cm^{-2} dose, a peak is observed at 1.4476 eV which closely coincides to the spectral position for luminescence previously assigned to the Ga_{As} double acceptor. However, in consideration of the sample's As-rich stoichiometry, the Ga_{As} double acceptor is not expected to be present. The peak does have a very low intensity and may, in fact, be due to an LO phonon replica of a higher-energy

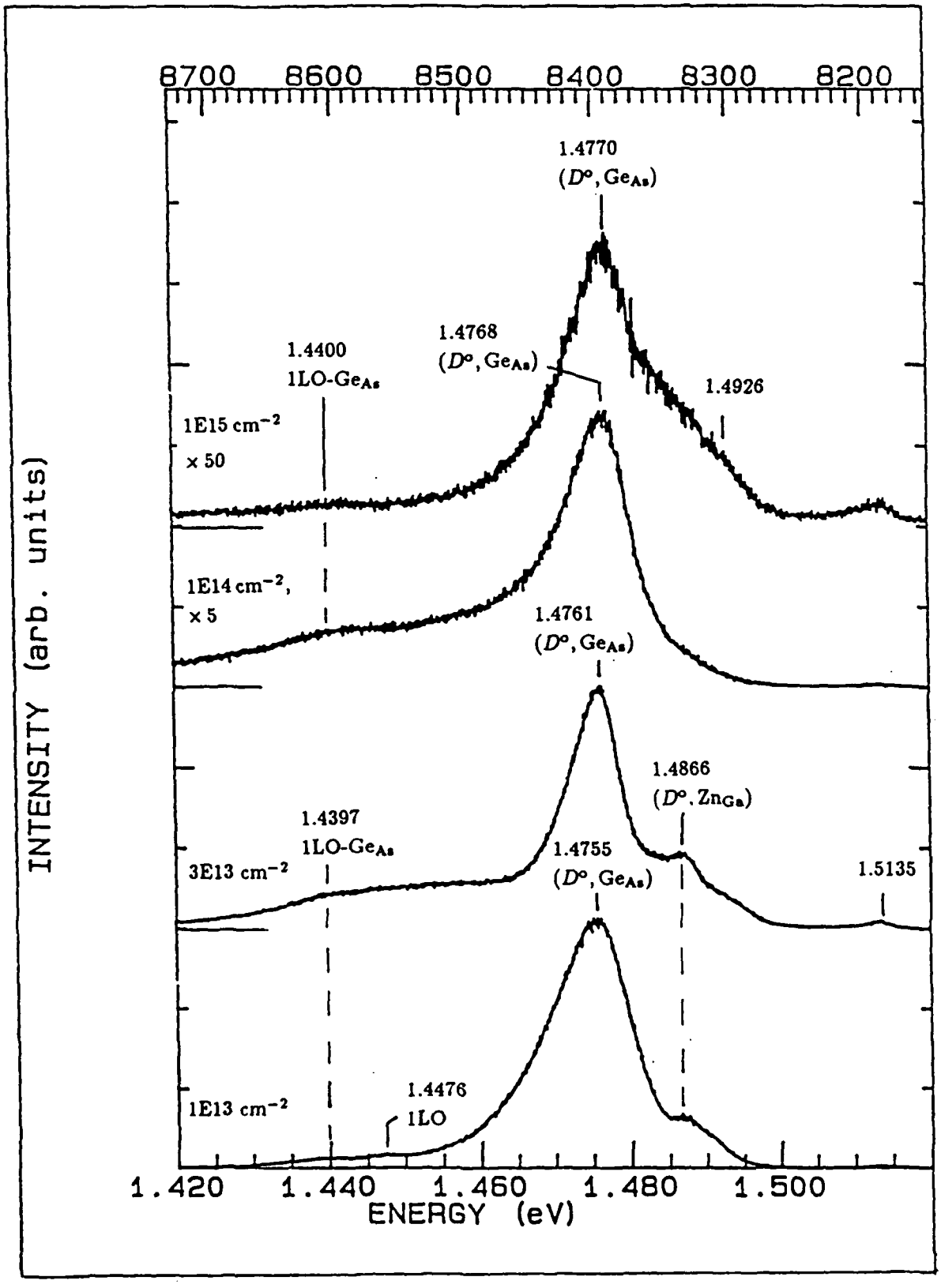

Figure 4.47. GaAs:{Ge+As}, ϕ=1E13-1E15 cm^{-2} Spectra, Exc: 2.5400 eV at 135 mW/cm^2, T=5K

unresolved Si_{As} acceptor-related peak at $\sim$1.484 eV. This assignment is consistent with that made earlier for the As-implanted samples (see Figure 4.4 and associated discussion) which act as a control for this set of dually implanted samples. It is also noted that the $\sim$ 1.475–1.477 eV peak exhibits a relatively long, low-energy luminescence tail. Excitation below the bandgap helps to resolve contributing recombination paths.

Excitation of the higher dose implants at 1.5082 eV is shown in Figure 4.48. It is observed that underlying the long, low-energy tail described above (especially for that of the samples implanted at a dose of 3E13 and 1E14 cm^{-2}), there are small contributions from the $\sim$ 1.466 and 1.447 eV peaks. The latter have been tentatively assigned to LO replicas. It is also significant that the SPL associated with the Ge_{As} acceptor is absent, in spite of the presence of (D^o, Ge_{As}) PL peaks. Coincidentally, and consistent with prior observations, there is no strong background luminescence associated with (D^o, Si_{As}) transitions at $\sim$ 1.482 eV upon, which such a signal may be superimposed.

The {Ge+As}-implanted samples do not exhibit the Q band. In addition, other luminescence originating from the Ga_{As} double acceptor (such as that associated with (ϵ, Ga_{As}) transitions and (D^o, Ga_{As}) transitions occurring amongst distant pairs) is very weak, if at all present. This is expected based on stoichiometric arguments and helps to confirm earlier assignments.

Summary Observations on the Q Band and Associated Ga_{As}

It is useful to present some of the previously shown results in a different format to open the conclusion section of this study. This involves displaying the luminescence arising from samples implanted with various ion species with respect to a constant implant dose.

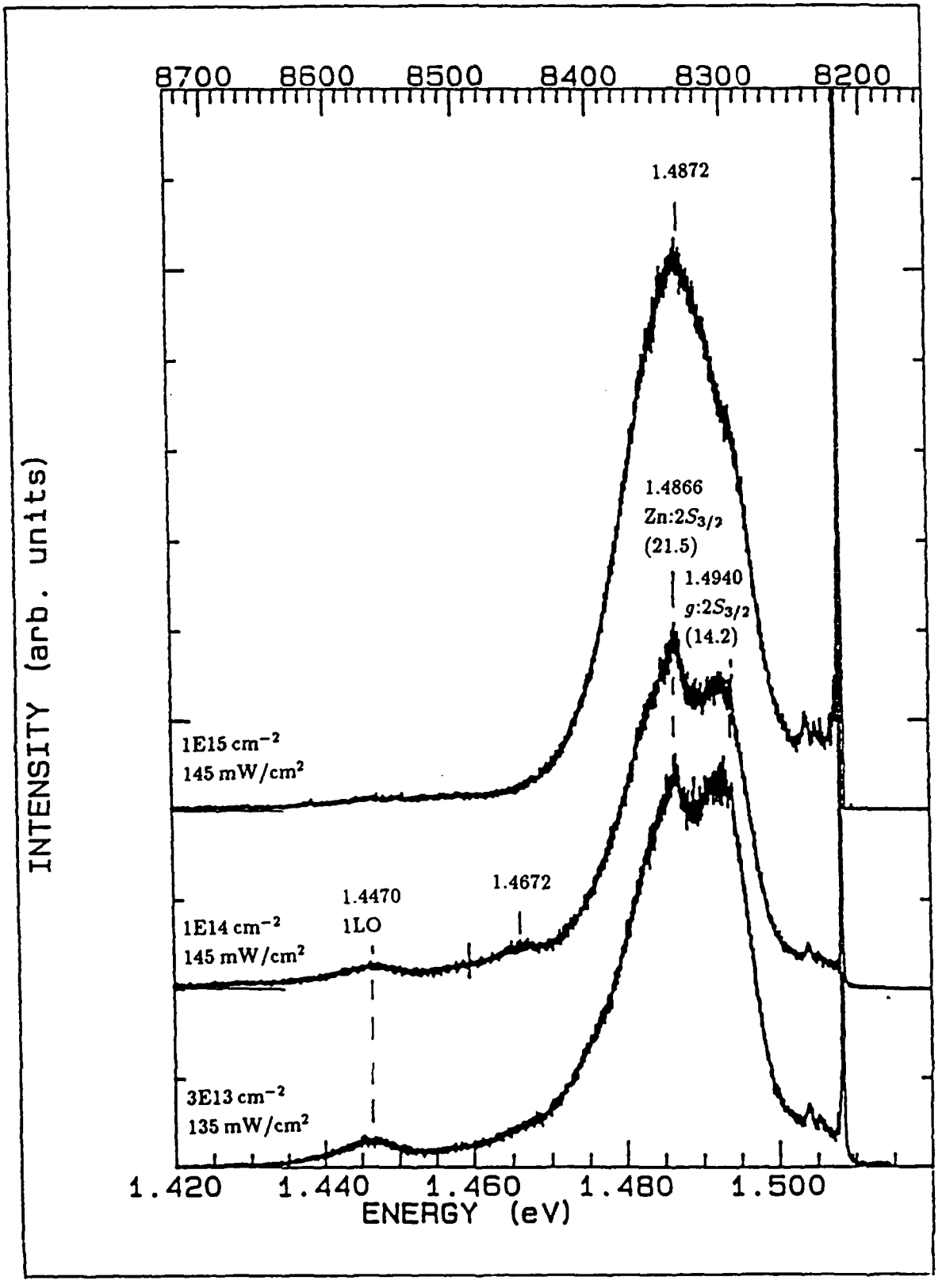

Figure 4.48. GaAs:{Ge+As}, ϕ=3E13–1E15 cm^{-2} Spectra, Exc: 1.5082 eV at 135–145 mW/cm^2, T=2.1K

Ion Dependence: 1E13 cm^{-2} Implants. The PL resulting from samples implanted with various elements at a dose of 1E13 cm^{-2} is shown in Figure 4.49. The Q band's dependence on V_{As} and Ge for its activation is clearly seen in the figure (by the lack of the Q band's observation in the as-grown, As-, Ga- and {Ge+As}-implanted samples). It is also noted that the Q band shifts to higher energy with the {Ge+Ga} dual implant. In terms of the close pairs model, this observation corresponds to an increase of Ga_{As} double acceptor concentration to allow for closer pairs and, therefore, higher (D^o, Ga_{As}) transition energies. The increase of Ga_{As} double acceptors is expected from the non-stoichiometry presented by the implant of Ga.

Ion Dependence: 3E13 cm^{-2} Implants. The PL resulting from samples implanted with various elements at a dose of 3E13 cm^{-2} is shown in Figure 4.50. These spectra support the general conclusions drawn from the PL of samples implanted at a dose of 1E13 cm^{-2}. The Q band peak energy is not as sensitive to dual implanted {Ge+Ga} for the dose of 3E13 cm^{-2} relative to that of 1E13 cm^{-2} implant dose.

Ion Dependence: 1E14 cm^{-2} Implants. The PL resulting from samples implanted with various elements at a dose of 1E14 cm^{-2} is shown in Figure 4.51. Perhaps the most notable feature of this figure is the absence of the Q band in all spectra. Nevertheless, the {Ge+Ga} dual implanted sample does indicate the presence of (e, Ga_{As}) transitions and (D^o, Ga_{As}) transitions occurring predominantly amongst distant pairs.

Ion Dependence: 1E15 cm^{-2} Implants. The PL resulting from samples implanted with various elements at a dose of 1E15 cm^{-2} is shown in Figure 4.52. Again, the Q band is not observed in these high dose samples. It is seen that a low-energy tail is associated with the (D^o, Ge_{As}) peak in both the Ge-only and

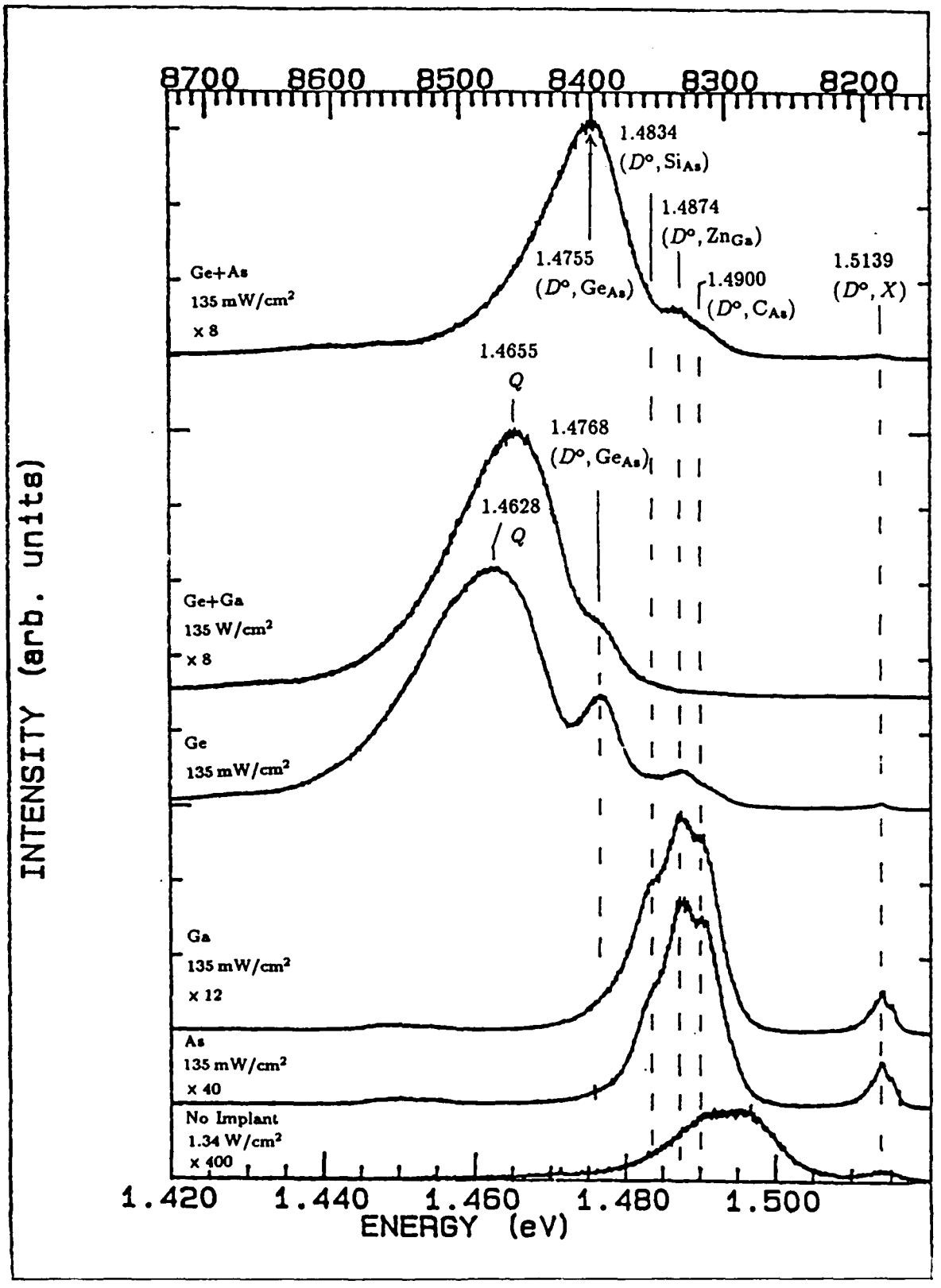

Figure 4.49. Ion Dependence: ϕ=1E13 cm^{-2} Spectra, Exc: 2.5409 eV, T=5K

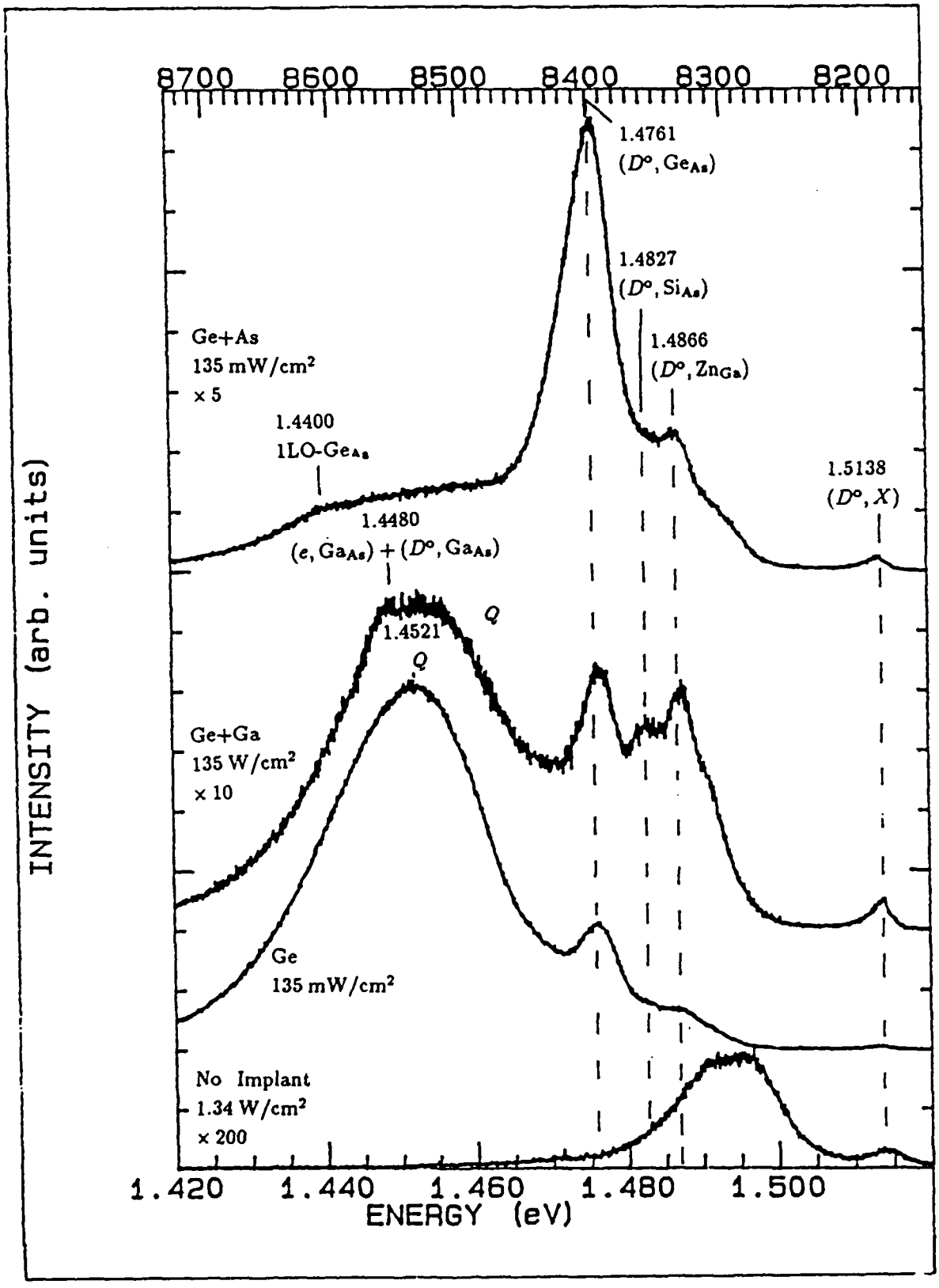

Figure 4.50. Ion Dependence: ϕ=3E13 cm^{-2} Spectra, Exc: 2.5400 eV, T=5K

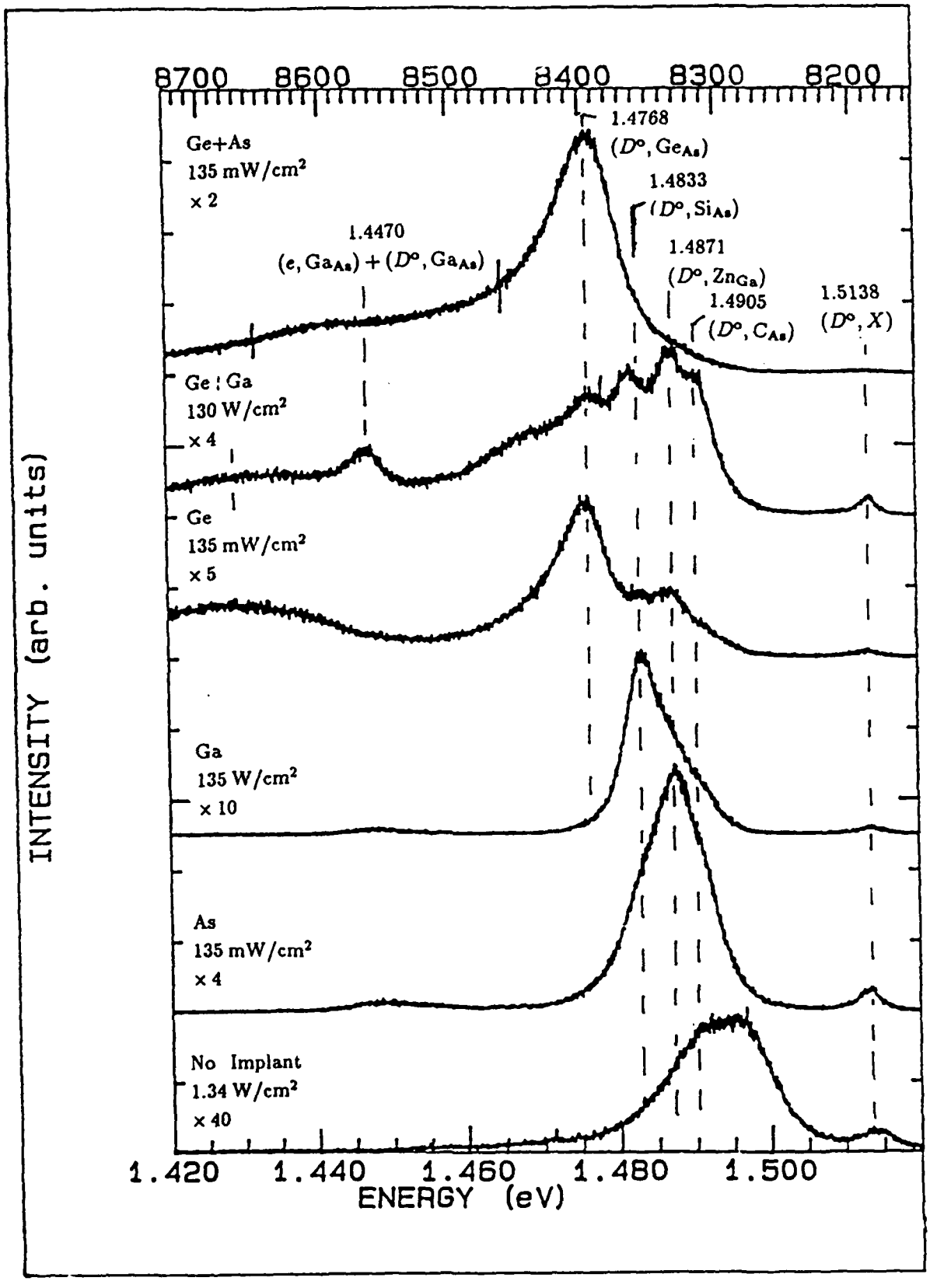

Figure 4.51. Ion Dependence: ϕ=1E14 cm^{-2} Spectra, Exc: 2.5400 eV, T=5K

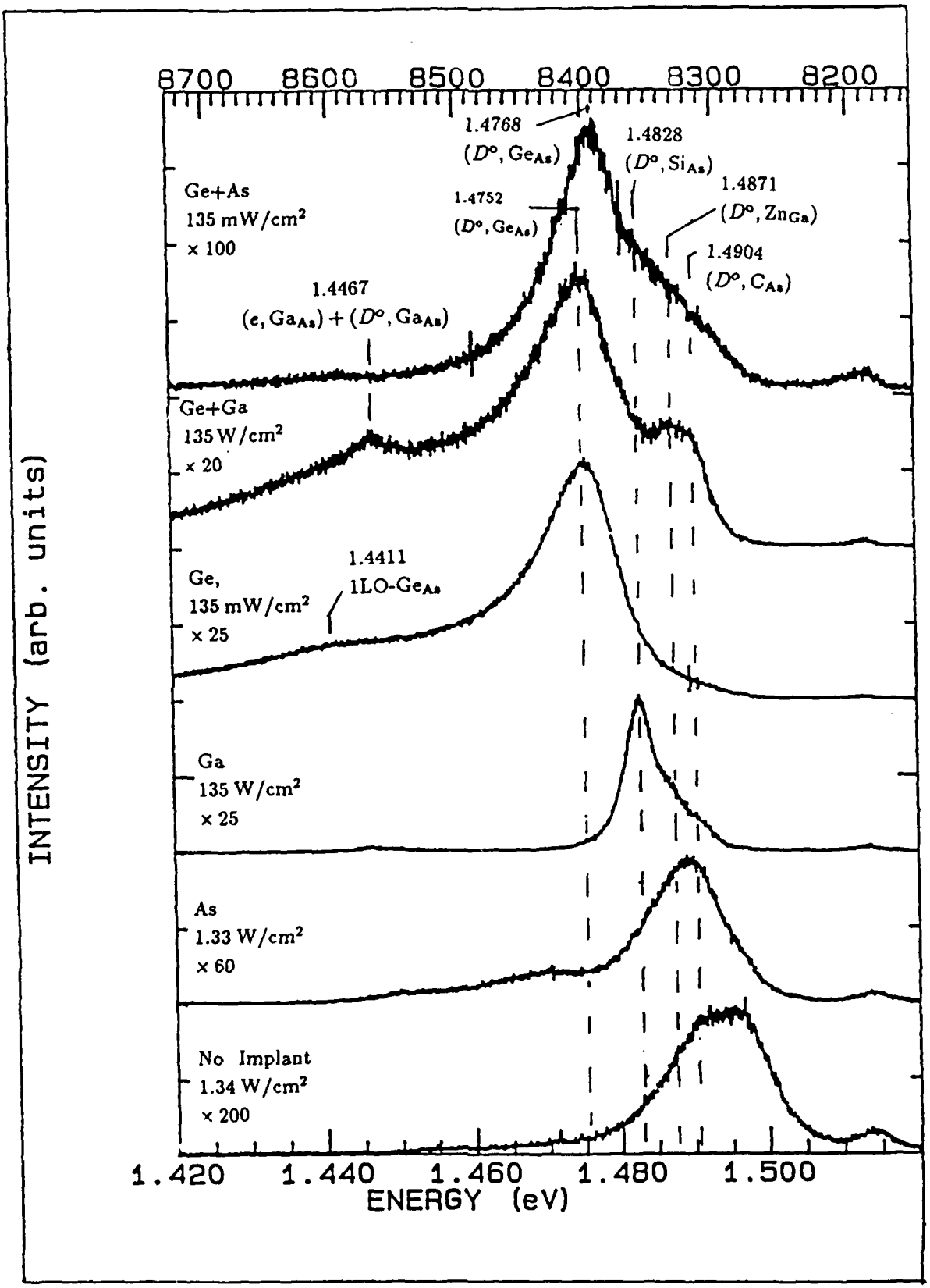

Figure 4.52. Ion Dependence: ϕ=1E15 cm^{-2} Spectra, Exc: 2.5400 eV, T=5K

{Ge+Ga}-implanted samples, making spectral analysis difficult. Nevertheless, a peak associated with $(e, \mathrm{Ga_{As}})$ transitions and $(D^{\circ}, \mathrm{Ga_{As}})$ transitions occurring predominantly amongst distant pairs is resolved for the {Ge+Ga}-implanted sample. As expected from stoichiometric considerations, the {Ge+As}-implanted sample shows no evidence at all for these $\mathrm{Ga_{As}}$-related transitions. This observation, in fact, can be consistently drawn from the {Ge+As}-implanted samples' luminescence.

V. Summary and Conclusions

Above- and below-gap excitation of GaAs, implanted with Ge, has been performed. In addition, dual implanted GaAs layers ({Ge+Ga} and {Ge+As}) were also investigated. The latter is significant for two reasons. To the best of my knowledge, this is the first luminescence characterization of such dual implanted layers. Also, by implanting the Ga or As with the Ge, the role of crystal stoichiometry could be better assessed and included in the analysis of the results obtained from the Ge-only implanted layers.

The PL (above gap excitation) of the Ge-only implanted layers was seen to be very dose-dependent. At doses of 1E13–3E13 cm^{-2}, a broad band in the 1.47–1.42 eV range dominated the PL spectrum and was assigned as the Q band. This band behaved (its PL excitation intensity-, temperature-, and Ge dose-dependent spectral shift) similarly to the original Q band characterized in PL studies of annealed GaAs:Si. Significantly, PL studies of the control samples (unimplanted, not annealed; Ga-implanted, annealed; As-implanted, annealed) did not show the Q band. This highlights the fact that the Group IV element Ge must be present for the Q band to occur. (similar to earlier GaAs studies in which it was discovered that Si, also a group IV element, was required for the emergence of the Q band [54, 72]). At these doses of 1E13–3E13 cm^{-2} , unresolved peaks due to the (e,Ge_{As}) and (D^o,Ge_{As}) recombinations were present, indicating that the Ge_{As} acceptor was optically active. At higher doses (1E14–1E15 cm^{-2}), these recombinations continued, but the Q band was no longer observed. Correspondingly, the electrical character of these layers was changing from p- to n-type at approximately these optical thresholds [80].

The PL results for the dual implanted layers supplemented the above data well. The PL features of the low dose (1E13–3E13 cm^{-2}) {Ge+Ga}-implants were similar to those of the low dose Ge-only implants. The Q band, located in the 1.47–

1.42 eV region, shifted, as in the Ge-only implants, to lower energy with increasing sample temperature and to higher energy with increasing excitation intensity. This behavior is atypical of D°-A° pair recombination. Significantly, at higher doses (1E14–1E15 cm^{-2}), the PL in the 1.47–1.42 eV region was very different from that of lower doses. All that remained in this region was a lower intensity peak which was assigned to transitions involving the Ga_{As} double acceptor. Such an assignment was supported by the fact that Ga was implanted into the layers. Interestingly, the Ga_{As} double acceptor was not optically activated in the control samples implanted with Ga-only. It suggests that the presence of the Ge encourages either the formation of the Ga_{As} double acceptor or increases the oscillator strength of transitions involving the double acceptor.

Finally, the {Ge+As}-implanted GaAs PL strengthens the above analysis. At all doses, the Ge_{As} acceptor was seen to be optically active (with the presence of the (e,Ge_{As}) and (D°,Ge_{As}) related peak in the PL). Most notably, there was no indication of the Q band. In addition, these samples did not exhibit clear evidence for the existence of PL that was observed in the 1.47–1.42 eV range of the higher dose {Ge+Ga}-implanted samples' spectra and assigned to the Ga_{As} double acceptor (as mentioned in the previous paragraph). Stoichiometrically, As-implantation would be expected to inhibit V_{As} defect formation, whereas Ga-implantation would favor it. This not only supports the Ga_{As} double acceptor assignment in the previous paragraph, but also indicates that the V_{As} plays a role in the Q band formation. Thus, the V_{As} and Ge_{As} acceptor seem to be required for the onset of the Q band. In addition, the dose-dependent PL of the Ge- and {Ge+Ga}-implants suggest that only certain concentrations of the V_{As} and Ge_{As} acceptor will give rise to the Q band.

The below-gap excitation was crucial in improving the understanding of the underlying recombination processes giving rise to the Q band. This was most assuredly seen in the data taken at different sample temperatures. With appropriate

excitation energy and intensity, the Q band in the Ge- and {Ge+Ga}-implanted samples was resolved into at least two components. The low-energy component peaked at $\sim$1.447 eV and were seen to shift slightly to higher energy with increasing temperature, especially between 20 and $\sim$30K. This behavior is to be expected for D^o-A^o pair recombinations. The low-energy component remained to temperatures as high as 45K, indicating that they originated from (e, A^o) recombinations as well. The low-energy component (at low temperatures), then, was believed to be made up of unresolved D^o-A^o pair and (e, A^o) recombinations. The acceptor was assigned as the Ga_{As}. The slightly higher-energy component, which peaked at $\sim$1.456–1.458 eV, disappeared quite rapidly with increasing temperature, such that at 20K, it was no longer observed. This data explained the Q band's seemingly contradictory temperature- and intensity-dependent PL behavior. That is, the intensity-dependent PL data indicated D^o-A^o pair recombination. On the other hand, temperature-dependent PL data did not. Now it is seen that the band's abnormal temperature-dependent PL data was caused by the rapid decrease in oscillator strength (with increasing temperature) of contributing higher-energy recombination paths.

The higher-energy recombination paths were also assigned to (D^o,Ga_{As}) transitions via the close pairs model. This model presumed that the relatively large ionization energy associated with the Ga_{As} double acceptor would allow closer pair recombination than typical for D^o-A^o pair recombinations involving the conventional shallow acceptors in GaAs. Indeed, the temperature dependence of the higher-energy transitions supported their assignment to (D^o,Ga_{As}) recombinations as well. Thus, it was determined that the (D^o,Ga_{As}) pair luminescence could be taking place over a sufficiently broad energy range (originating from the distant D^o-A^o pair recombination *and* relatively close pair recombination, as well) such that its peak could, in fact, occur at higher energies than the associated (e, Ga_{As}) luminescence (which contributed to the low-energy component mentioned above).

The close pairs model provides a good framework for understanding the Q band. The model can also be applied to the Q band found in Si-doped GaAs [54, 72]. However, a review of the results for the Si-doped layers does present two discrepancies. First, the Q band, in the Si-doped layers, is found at energies less than 1.44 eV, which is the energy typically noted for transitions involving the Ga_{As} double acceptors. The close pairs model, on the other hand, implicitly assumes that the Q band originates mainly from the Ga_{As} double acceptors. This discrepancy may arise from the fact that the band in those studies received contributions from transitions involving other defects. It is notable that the lowest energies reported were seen for the Q band arising from the surface of the Si-doped layers. In fact, Pomrenke *et al.* [54] postulated that the band at the surface results from V_{As} defects. The second discrepancy arises from the temperature-dependent data collected by Swaminathan *et al.* [72]. Specifically, a higher-energy peak evolved from the Q band at 60K (so that at 80K the new peak's position was 1.470 eV) and was assigned to Q-related F-B transitions. This interpretation, however, is not conclusive. Close inspection of the data does allow for a different interpretation. For example, taking into account the GaAs bandgap at the higher temperatures and the fact that the samples were heavily Si-doped, it is discovered that the higher temperature peaks may arise, instead, from (e, Si_{As}) transitions.

This work has shown that the Ga_{As}, V_{As} and Ge_{As} acceptor (which is similar to the Si_{As} acceptor in that both derive from group IV elements that are amphoteric in GaAs) all play a role in the formation of the Q band. However, the sensitivity of the Q band's intensity and its spectral position to the dose of either Ge or {Ge+Ga} appears to be ultimately determined by the relative concentrations of Ga_{As} double acceptors. It is plausible that as the concentration of Ge_{As} acceptors increases, that of Ga_{As} double acceptors decreases. Thus, although relatively close pair recombinations still are possible (according to the discussion that accompanied the development of the close pairs model), the relative numbers of these close

pair recombinations decreases and the typical pair separation begins to increase. Subsequently, the peak of the (D^o,Ga_{As}) pair luminescence band will begin to shift to lower energies (ultimately positioned at slightly lower energies than the associated (e, Ga_{As}) luminescence).

The below-gap excitation provided other supplementary pieces of information about the samples under investigation.

1. Acceptor SPL due to the implanted Ge was definitely observed. Notably, the best signal occurred for those samples which apparently had a sufficient Si_{As} acceptor activation (the Si impurity originating from the Si_3N_4 cap used during the anneal) for (D^o,Si_{As}) pair recombination luminescence upon which the Ge_{As} excited state was superimposed.

2. SPL, apparently associated with the g-acceptor, has been observed for the first time. The $1S_{3/2}-2S_{3/2}$ energy splitting was determined to be about 13.9 meV, in close agreement with results obtained from two-hole spectroscopy [18, 70]. This is also the first data to confirm the existence of the g-acceptor in bulk grown, Cr-doped GaAs.

3. SPL associated with the Mn_{Ga} acceptor also seems to have been observed. The sharp structure was separated from the laser line by about 87.4 meV and assigned as due to the $2S_{3/2}$ hole state. The data is significant because it would be the first observed SPL for the Mn_{Ga} acceptor, and the first known data for the acceptor's $1S_{3/2} - 2S_{3/2}$ energy splitting. Also, it would confirm others' conclusions that this acceptor acts more like the shallower, hydrogenic acceptors than a tight-binding $3d$ transition-metal that it is. To verify the data, it would be advantageous to perform an in-depth study of bulk grown GaAs which contains no Mn and compare the results to those of the same bulk material which is intentionally doped with various concentrations of Mn.

4. A relatively new peak at ~ 1.467 eV was observed, especially with the below-gap excitation. Recently, the peak was speculated to be due to Cu_{Ga}-As_{Ga} or Cu_{Ga}-As_i complexes [75]. Significantly, for the present work, the peak has also been observed in conjunction with the presence of the g-acceptor [57]. Temperature-dependent measurements indicated contribution from D^o-A^o pair recombinations. This determination was a first and supports the observation that the ~ 1.467 eV peak originates from transitions involving the g-acceptor rather than more complex centers such as Cu_{Ga}-As_{Ga} or Cu_{Ga}-As_i.

Appendix A. *Close Pairs Recombination*

The close pairs model provides a basic framework from which the Q band luminescence may be understood. The purpose of the following paragraphs is to quantitatively assess the models' reasonableness taking into account the data collected on the Q band in this research.

Coulomb Term

Because the Coulomb term of Eq (4.1) is of such great importance to D^o-A^o pair recombination in general, and the close pairs model in particular, it is instructive to first consider the magnitude of the term. (The higher-order, non-coulombic term, $J(R)$, of Eq (4.1) is not included in this analysis since it is relatively small [59:2512]). The Coulomb term may be re-written such that

$$\frac{e^2}{\epsilon R} = \frac{1161.3}{R} \text{ meV}$$

where ϵ was taken as 12.40 from Table 1.1 and R is in terms of angstroms. It should be recalled, from the discussion in Chapter II, that R takes on discrete values. For Type II pair recombination (which is a reasonable assumption for D^o-A^o pair recombination involving the Ga_{As} double acceptor), the discrete values were given by Eq (2.18)

$$R_m = a_o \left(\frac{m}{2} - \frac{5}{16} \right)^{1/2}$$

Table A.1 tabulates the magnitude of the Coulomb term as a function of discrete pair separations.

Other Considerations

The basic premise of the close pairs model, discussed in Chapter IV, is that close pair recombination can be dominant for the relatively deep Ga_{As} double

Table A.1. Magnitude of Coulomb Term as a Function of Pair Separation

Shell Number, m	Pair Separation, R_m (Å)	Coulomb Term (meV)
1	2.45	474.4
10	12.24	94.9
25	19.74	58.8
50	28.09	41.3
75	34.47	33.7
100	39.85	29.1
125	44.58	26.0
150	48.86	23.8
175	52.79	22.0
200	56.44	20.6
250	63.13	18.4
300	69.16	16.8
400	79.89	14.5
500	89.33	13.0
750	109.43	10.6
1000	126.37	9.2
1500	154.79	7.5
2000	178.74	6.5
2500	199.85	5.8
5000	282.64	4.1
10000	399.73	2.9

acceptor. The larger acceptor ionization energy is able to offset the larger Coulomb term associated with the closer pairs. Thus, the Q band, which peaked at energies as high as 1.4655 eV in PL (as shown in Figure 4.35), was assigned to $(D^{\circ}, \mathrm{Ga_{As}})$ transitions; many of which occurred amongst relatively close pairs and at energies higher than the $(e, \mathrm{Ga_{As}})$ transition. The peak energy of 1.465 eV is relatively large compared to that already reported of 1.441 eV for the $(D^{\circ}, \mathrm{Ga_{As}})$ transition [84]. The pair separations associated with the high-energy $(D^{\circ}, \mathrm{Ga_{As}})$ transitions can be determined using the above equations and Eq (4.1) (neglecting the non-coulombic term)

$$\hbar\omega_l = \hbar\omega_{D^{\circ}-A^{\circ}} = \mathrm{E_g} - (\mathrm{E_A} + \mathrm{E_D}) + \frac{e^2}{\epsilon R}$$

Assuming $\mathrm{E_D}$ is approximately 6 meV and recalling that $\mathrm{E_A}$ is 78 meV for the $\mathrm{Ga_{As}}$ double acceptor (see references [46] and [63]), the pair separation associated with the $(D^{\circ}, \mathrm{Ga_{As}})$ recombinations giving rise to the 1.4655 eV peak is calculated to be about 38.1Å. From Table A.1, this pair separation corresponds to approximately shell number 100. Thus, there is a distribution of shell numbers (pair separations) on either side of the peak, though obviously asymmetric (which seems to qualitatively explain the spectra that show asymmetric Q band luminescence). For there to be gradually decreasing luminescence intensity as one moves away from the band's peak, one expects there to be a reasonable distribution of shell numbers on both sides of the peak. If the pair separation at the peak had corresponded to shell numbers one or two, the luminescence intensity on the high-energy side of the peak would be expected to drop almost immediately to zero, which would be unrealistic. Finally, it can be argued that shallower acceptors in GaAs would not be as likely to produce D°-A° pair luminescence occurring over as broad an energy range (such that the D°-A° pair luminescence could be peaked at higher energies than the corresponding (e, A°) luminescence) as that exhibited by the $\mathrm{Ga_{As}}$ double acceptor. From Table A.1, the magnitude of the Coulomb term, corresponding to the D°-A° pair separation of 38.1Åat the peak of the Q band, is $\sim$30 meV. This

is already on the order of the ionization energies for many of the shallow acceptors in GaAs. Thus, D°-A° pairs involving these shallow acceptors will not be as likely to be involved in such close pair recombination (that creates the relatively high-energy D°-A° luminescence).

One of the ancillary features of D°-A° pair recombination that may be observed, as was discussed in Chapter II, is discrete lines corresponding to the discrete pair separations. As mentioned before, typical donor and acceptor ionization energies in GaAs are so small that D°-A° pair transitions occur for relatively large pair separations, where the interval between discrete peaks may become smaller than 0.1 meV, and therefore, are not easily resolved [22:119]. The question becomes whether the close pair transitions, thought to give rise to the Q band, have adequately small characteristic pair separation to see the discrete D°-A° pair lines. From the previous paragraph, the largest contribution to the 1.4655 eV Q band seems to come from $(D^{\circ}, \mathrm{Ga}_{\mathrm{As}})$ pairs having an R of about 38.1Å. From Eq (2.18), one can determine (rather than estimating from Table A.1) that this pair separation actually corresponds to a shell number of about 91. For the discrete structure to be observed, luminescence that originates from the D°-A° pairs having a pair separation corresponding to shell 90 should be resolved. Again, using Eq (2.18), the pair separation associated with a shell number of 90 is about 37.8Å. It then can be determined that the $(D^{\circ}, \mathrm{Ga}_{\mathrm{As}})$ luminescence originating from pairs of shell number 90 occurs at about 1.4659 eV. Thus, the discrete lines are still fairly close to one another (separated by about 0.4 meV), although probably resolvable using the current experimental set-up. The limiting factors which might make observation of the discrete structure more difficult, if not impossible, include mechanisms such as hopping transfer between neighboring donors before D°-A° pair recombination occurs.

Bibliography

1. Ai-zhen, L. *et al.* "Germanium Incorporation in Heavily Doped Molecular Beam Epitaxy Grown GaAs:Ge," *Journal of Vacuum Science and Technology B*, **3**: 629–633 (March/April 1985).
2. Anderson, W. J. and Y. S. Park. "Flux and Fluence Dependence of Implantantion Disorder in GaAs Substrates," *Journal of Applied Physics*, **49**: 4568–4570 (August 1978).
3. Ashcroft, N. W. and N. D. Mermin. *Solid State and Semiconductor Physics.* Philadelphia: Saunders College, 1976.
4. Ashen, D. J. *et al.* "The Incorporation and Characterization of Acceptors in Epitaxial GaAs," *Journal of Physics and Chemistry of Solids*, **36**: 1041–1053 (1975).
5. Bafleur, M. *et al.* "Photoluminescence of Molecular Beam Epitaxially Grown Ge-doped GaAs," *Journal of Applied Physics*, **54**: 2630–2634 (May 1983).
6. Baldereschi, A. and N. Lipari. "Spherical Model of Shallow Acceptor States in Semiconductors," *Physical Review B*, **8**: 2697–2709 (September 1973).
7. Baldereschi, A. and N. Lipari. "Cubic Contributions to the Spherical Model of Shallow Acceptor States," *Physical Review B*, **9**: 1525–1539 (February 1974).
8. Bassani, F. *et al.* "Electronic Impurity Levels in Semiconductors," *Reports on Progress in Physics*, **37**: 1099–1210 (1974).
9. Bebb, H. and E. W. Williams. "Photoluminescence I: Theory," *Semiconductors and Semi-metals, Volume 8*, edited by R. K. Willardson and A. C. Beer. New York: Academic Press, 1967.
10. Bishop, S. G. *et al.* "Photoluminescence and Infrared Spectroscopy of Acceptors in GaAs," *Journal of Applied Physics*, **56**: 1785–1790 (September 1984).
11. Blakemore, J. S. "Semiconducting and Other Major Properties of Gallium Arsenide," *Journal of Applied Physics*, **53**: R123–R181 (October 1982).
12. Cavins, Capt J. R. *Selective Pair Luminescence of Magnesium in Gallium Arsenide.* PhD dissertation. School of Engineering, Air Force Institute of Technology (AU), Wright-Patterson AFB OH, December 1988.
13. Cavins, J. R. *et al.* "Excited States of the Mg Acceptor in GaAs," *Journal of Applied Physics*, **64**: 6761–6766 (December 1988).
14. Cavins, J. R. *et al.* "Characterization of Residual Acceptors in Semi-Insulating and VPE GaAs by Selective Pair Luminescence and Photoluminescence Methods," *Journal of the Electrochemical Society*, **136**: 2113–2119 (July 1989).
15. Chan, S. S. *et al.* "Electrical Properties and Photoluminescence Studies of Ge-Implanted GaAs," *Journal of Electronic Materials*, **10**: 213–238 (1981).

16. Chapman, R. A. and W. G. Hutchinson. "Photoexcitation and Photoionization of Neutral Manganese Acceptors in Gallium Arsenide," *Physical Review Letters*, **18**: 443–445, 822 (March 1967).

17. Christel, L. A. and J. F. Gibbons. "Stoichiometric Disturbances in Ion Implanted Compound Semiconductors," *Journal of Applied Physics*, **52**: 5050–5055 (August 1981).

18. Contour, J. P. *et al.* "Optical Characterization of Defect Levels Induced by MBE Growth of GaAs," *Journal of Vacuum Science and Technology B*, **1**: 811–815 (July–September 1983).

19. Dansas, P. and J-P. Charlec. "Existence of $\simeq$ 64-meV Deep Acceptor in Se-implanted GaAs After Close-contact Annealing," *Journal of Applied Physics*, **55**: 3617–3623 (May 1984).

20. Dansas, P. "Existence of Deep Acceptors in Ga- and B-Implanted GaAs After Close-Contact Annealing," *Journal of Applied Physics*, **58**: 2212–2216 (September 1985).

21. Dean, P. J. "Inter-Impurity Recombinations in Semiconductors," *Progress in Solid State Chemistry, Volume 8*, edited by J. O. McCaldin and G. Somorjai. Oxford: Pergamon Press, 1973.

22. Dean, P. J. "Photoluminescence as a Diagnostic of Semiconductors," *Progress in Crystal Growth and Characterization*, **5**: 89–174 (1982).

23. Gibbons, J. F. *et al. Projected Range Statistics* (Second Edition). Stroudsburg PA: Dowden, Hutchinson and Ross, 1975.

24. Henning, J. C. M. "Selective Pair Luminescence in Semiconductors," *Excited-State Spectroscopy in Solids*, edited by U. M. Grassano and N. Terzi. Amsterdam: North-Holland Physics Publishing, 1987.

25. Hopkins, C. G. *et al.* "Incorporation of Boron During the Growth of GaAs Single Crystals," *Applied Physics Letters*, **36**: 989–990 (June 1980).

26. Hunter, A. T. and T. C. McGill. "Selective Excitation Luminescence in Bulk-Grown GaAs," *Applied Physics Letters*, **40**: 169 (1982).

27. Hwang, C. J. "Evidence for Luminescence Involving Arsenic Vacancy-Acceptor Centers in p-Type GaAs," *Physical Review*, **180**: 827–832 (April 1969).

28. Imbusch, G. F. "Inorganic Luminescence," *Luminescence Spectroscopy*, edited by M. D. Lumb. London: Academic Press, 1978.

29. Itoh, T. and M. Takeuchi. "Arsenic Vacancy Formation in GaAs Annealed in Hydrogen Gas Flow," *Japanese Journal of Applied Physics*, **16**: 227–232 (February 1977).

30. Jam, J. F. and R. S. Stermberg. *The Design of Optical Spectrometers*. London: Butler and Tanner, Ltd., 1969.

31. Jeong, M. *et al.* "Photoluminescence in Si-Doped GaAs," *Japanese Journal of Applied Physics,* **12**: 109–119 (January 1973).

32. Kisker, D. W. *et al.* "Luminescence Studies of C, Zn, Si, and Ge Acceptors in GaAs," *Journal of Applied Physics,* **54**: 1332–1336 (March 1983).

33. Kittel, C. and A. H. Mitchell. "Theory of Donor and Acceptor States in Silicon and Germanium," *Physical Review,* **96**: 1488–1493 (December 1954).

34. Koteles, E. S. *et al.* "Excited States of Shallow Acceptors in GaAs," *Proceedings of the International Conference on the Physics of GaAs and Related Compounds, Karuizawa, 1985.* Bristol: Institute of Physics, 1986.

35. Kressel, H. *et al.* "Luminescence in Silicon-Doped GaAs Grown by Liquid-Phase Epitaxy," *Journal of Applied Physics,* **39**: 2006–2011 (March 1968).

36. Kressel, H. *et al.* "Luminescence Due to Ge Acceptors in GaAs," *Journal of Applied Physics,* **39**: 4059–4066 (August 1968).

37. Kroger, F. A. *The Chemistry of Imperfect Crystals, Vol 2.* Amsterdam: North-Holland Publishing Co., 1974.

38. Kunzel, H. and K. Ploog. "The Effect of As_2 and As_4 Molecular Beam Species on Photoluminescence of Molecular Beam Epitaxially Grown GaAs," *Applied Physics Letters,* **37**: 416–418 (August 1980).

39. Kunzel, H. and K. Ploog. "Sharp-Line Luminescence Transitions Due to Growth Induced Point Defects in MBE GaAs," *GaAs and Related Compounds, 1980,* Conference Series No. 56, edited by H. W. Thim. Bristol: Institute of Physics, 1981.

40. Lipari, N. O. and A. Baldereschi. "Angular Momentum Theory and Localized States in Solids. Investigation of Shallow Acceptor States in Semiconductors," *Physical Review Letters,* **25**: 1660–1664 (December 1970).

41. Luttinger, J. M. "Quantum Theory of Cyclotron Resonance in Semiconductors: General Theory," *Physical Review,* **102**: 1030–1041 (May 1956).

42. Luttinger, J. M. and W. Kohn. "Motion of Electrons and Holes in Perturbed Periodic Fields," *Physical Review,* **97**: 869–883 (February 1955).

43. Magee, T. J. *et al.* "Stoichiometric Disturbances in Ion Implanted GaAs and Redistribution of Cr During Annealing," *Applied Physics Letters,* **39**: 906–908 (December 1981).

44. Metze, G. M. *et al.* "An Investigation of GaAs Films Grown by MBE at Low Substrate Temperatures and Growth Rates," *Journal of Vacuum Science and Technology B,* **1**: 166–169 (April–June 1983).

45. Mihara, M. *et al.* "Photoluminescence of the 78 meV Acceptor in GaAs Layers Grown by Molecular Beam Epitaxy," *Japanese Journal of Applied Physics,* **25**: L611–L613 (July 1986).

46. Moore, W. J. *et al.* "Properties of the 78 meV Acceptor in GaAs," *Physica B*, **146**: 65–74 (1987).

47. Morgan, D. V. *et al.* "Prospects for Ion Bombardment and Ion Implantation in GaAs and InP Device Fabrication," *IEE Proceedings I: Solid-State and Electron Devices* **128**: 109–130 (August 1981).

48. Myles, C. W. and O. F. Sankey. "Deep Levels Associated with (Vacancy, Impurity) Pairs in Covalent Semiconductors," *Physical Review B*, **29**: 6810–6823 (June 1984).

49. Nam, S. B. *et al.* "Free-exciton Energy Spectrum in GaAs," *Physical Review B*, **13**: 761–767 (January 1976).

50. Paget, D. and P. B. Klein. "Shallow Donors in Semi-insulating GaAs and Their Role in the Excitation of the 0.64 eV Photoluminescence," *Physical Review B*, **34**: 971–978 (July 1986).

51. Pankove, J. I. *Optical Processes in Semiconductors*. Englewood Cliffs: Prentice-Hall, Inc., 1971.

52. Pantelides, S. T. "The Electronic Structure of Impurities and Other Point Defects in Semiconductors," *Reviews of Modern Physics*, **50**: 797–858 (October 1978).

53. Pedrotti, F. L. *et al.* "Dual Implantation of Ga and Ge into GaAs," *Journal of Applied Physics*, **51**: 5781–5784 (November 1980).

54. Pomrenke, G. S. *et al.* "Luminescence Characteristics of the 1.4 eV Silicon Related Complex in Gallium Arsenide," *Physica B+C*, **116**: 414–419 (1983).

55. Pronko, P. P. *et al.* "Ion Implantation in III-V Compound Semiconductors." Final Report to Avionics Laboratory, Air Force Systems Command. Contract F33615-80-C-1108 with Universal Energy Systems, Inc. Wright-Patterson AFB OH. (September 1984).

56. *Properties of Gallium Arsenide*. Foreward by J. S. Blakemore. London: INSPEC, 1986.

57. Rao, E. V. K. *et al.* "Low-Temperature Photoluminescence Properties of High-Quality GaAs Layers Grown by Molecular-Beam Epitaxy," *Journal of Applied Physics*, **57**: 503–508 (January 1985).

58. RCA Corporation. *Photomultiplier Tubes, Photodiodes and Electron Multipliers*. Product Catalog. RCA Commercial Engineering, Harrison NJ, December 1971.

59. Reynolds, D. C. *et al.* "Lifetimes, Ionization Energies, and Discussion of the Emission Lines in the 1.5040–1.5110-eV Range in GaAs," *Journal of Applied Physics*, **60**: 2511–2516 (October 1986).

60. Schneider, J. *et al.* "Electronic Structure of the Neutral Manganese Acceptor in Gallium Arsenide," *Physical Review Letters,* **59**: 240–243 (July 1987).

61. Sell, D. D. "Resolved Free-Exciton Transitions in the Optical-Absorption Spectrum of GaAs," *Physical Review B,* **6**: 3750–3753 (November 1973).

62. Seraphin, B. O. and H. E. Bennett. "Optical Constants," *Semiconductors and Semi-metals, Volume 3,* edited by R. K. Willardson and A. C. Beer. New York: Academic Press, 1967.

63. Shanabrook, B. V. *et al.* "Model for the ~1.28-eV Double-Acceptor Luminescence in GaAs," *Journal of Applied Physics,* **59**: 2535–2537 (April 1986).

64. Sharma, R. S. and S. Rodriguez. "Theory of Excitons Bound to Ionized Impurities in Semiconductors," *Physical Review,* **153**: 823–827 (January 1967).

65. Sharma, R. S. and S. Rodriguez. "Exciton-Donor Complexes in Semiconductors," *Physical Review,* **159**: 649–651 (July 1967).

66. Shklovskii, B. I. and A. L. Efros. *Electronic Properties of Doped Semiconductors.* Berlin: Springer-Verlag, 1984.

67. Smith, K. K. "Photoluminescence of Semiconductor Materials," *Thin Solid Films,* **84**: 171–182 (1981).

68. Spectra-Physics. *Continuous Wave Dye Lasers Propagation and Performance Reports.* Spectra Physics, Mountain View, CA.

69. Spitzer, W. G. "Multiphonon Lattice Absorption," *Semiconductors and Semimetals. Volume 3,* edited by R. K. Willardson and A. C. Beer. New York: Academic Press, 1967.

70. Steiner, T. *et al.* "Time-Resolved Photoluminescence Study of Molecular Beam Epitaxial Growth Induced Defect Lines in GaAs," *Applied Physics Letters,* **47**: 257–259 (August 1985).

71. Sturge, M. "Optical Absorption of Gallium Arsenide Between 0.6 and 2.75 eV," *Physical Review,* **127**: 768–773 (August 1962).

72. Swaminathan, V. *et al.* "Photoluminescence of Thermally Treated n^+ Si-Doped and Semi-Insulating Cr-Doped GaAs Substrates," *Journal of Luminescence,* **22**: 153–170 (1981).

73. Tews, H. *et al.* "Excited States of Shallow Acceptors in ZnSe," *Physical Review B,* **19**: 5178 (1979).

74. Thorn EMI. *Photomultipliers.* Product Catalog. Thorn EMI Gencom Inc., Fairfield NJ, 1986.

75. van de Ven, J. *et al.* "Photoluminescence Studies of Defects and Impurities in Annealed GaAs," *Journal of Applied Physics,* **60**: 3735–3745 (November 1986).

76. Wagner, J. and M. Ramsteiner. "Binding Energies of Shallow Donors in Semi-insulating GaAs," *Journal of Applied Physics*, **62**: 2148–2150 (September 1987).

77. White, G. K. *Experimental Techniques in Low-Temperature Physics*. London: Oxford University Press, 1968.

78. Williams, E. W. and H. B. Bebb. "Photoluminescence II: Gallium Arsenide," *Semiconductors and Semi-metals, Volume 8*, edited by R. K. Willardson and A. C. Beer. New York: Academic Press, 1967.

79. Williams, E. W. and C. T. Elliott. "Luminescence Studies of a New Line Associated With Germanium in GaAs," *Journal of Physics D*, **2**: 1657–1665 (1969).

80. Yeo, Y. K. *et al.* "Amphoteric Behavior of Ge Implants in GaAs," *Applied Physics Letters*, **35**: 197–199 (July 1979).

81. Yeo, Y. K. *et al.* "Modification of the Amphoteric Activity of Ge Implants in GaAs by Dual Implantation of Ge and As," *Journal of Applied Physics*, **51**: 5785–5788 (November 1980).

82. Yu, P. W. "Excitation-Dependent Emission in Mg-, Be-, Cd-, and Zn-Implanted GaAs," *Journal of Applied Physics*, **48**: 5043–5051 (December 1977).

83. Yu, P. W. "Deep Emission Centers in Ge-Implanted GaAs," *Journal of Applied Physics*, **50**: 7165–7167 (November 1979).

84. Yu, P. W. and D. C. Reynolds. "Photoluminescence Identification of ~ 77-meV Deep Acceptor in GaAs," *Journal of Applied Physics*, **53**: 1263–1265 (February 1982).

Vita

Kevin J. Keefer [redacted] He graduated in 1977 from Lyons Township High School of LaGrange, Illinois, and subsequently entered the United States Air Force Academy. He graduated in 1981 with a Bachelor of Science degree in Atmospheric Physics. During his first assignment, as a project officer at the Ballistic Missile Office, Norton Air Force Base, California, he attained a Master of Science degree in Systems Management from the University of Southern California in 1983. In 1984 he entered the Air Force Institute of Technology at Wright-Patterson Air Force Base, Ohio, to pursue graduate studies in Physics. He received a Master of Science degree in Engineering Physics in 1985 and continued study for his doctorate. He has been assigned to the Air Force Weapons Laboratory at Kirtland Air Force Base, New Mexico.

[redacted]

REPORT DOCUMENTATION PAGE

Form Approved
OMB No. 0704-0188

1a. REPORT SECURITY CLASSIFICATION UNCLASSIFIED	1b. RESTRICTIVE MARKINGS
2a. SECURITY CLASSIFICATION AUTHORITY	3. DISTRIBUTION/AVAILABILITY OF REPORT Approved for public release; distribution unlimited.
2b. DECLASSIFICATION/DOWNGRADING SCHEDULE	
4. PERFORMING ORGANIZATION REPORT NUMBER(S) AFIT/DS/ENP/90-1	5. MONITORING ORGANIZATION REPORT NUMBER(S)
6a. NAME OF PERFORMING ORGANIZATION School of Engineering 6b. OFFICE SYMBOL (*If applicable*) AFIT/ENP	7a. NAME OF MONITORING ORGANIZATION
6c. ADDRESS (*City, State, and ZIP Code*) Air Force Institute of Technology (AU) Wright-Patterson AFB, Ohio 45433-6583	7b. ADDRESS (*City, State, and ZIP Code*)
8a. NAME OF FUNDING/SPONSORING ORGANIZATION 8b. OFFICE SYMBOL (*If applicable*)	9. PROCUREMENT INSTRUMENT IDENTIFICATION NUMBER
8c. ADDRESS (*City, State, and ZIP Code*)	10. SOURCE OF FUNDING NUMBERS PROGRAM ELEMENT NO. / PROJECT NO. / TASK NO. / WORK UNIT ACCESSION NO.

11. TITLE (*Include Security Classification*)
See Box 19

12. PERSONAL AUTHOR(S)
Kevin J. Keefer, B.S., M.S., M.S., Capt, USAF

13a. TYPE OF REPORT	13b. TIME COVERED	14. DATE OF REPORT (*Year, Month, Day*)	15. PAGE COUNT
PhD Dissertation	FROM _____ TO _____	1990 June	183

16. SUPPLEMENTARY NOTATION

17. COSATI CODES			18. SUBJECT TERMS (*Continue on reverse if necessary and identify by block number*)
FIELD	GROUP	SUB-GROUP	Gallium Arsenides, Photoluminescence, Germanium, Ion Implantation
07	02		
20	12		

19. ABSTRACT (*Continue on reverse if necessary and identify by block number*)

Title: DEFECTS ASSOCIATED WITH THE INCORPORATION OF GERMANIUM IN GALLIUM ARSENIDE

Dissertation Chairman: Yung Kee Yeo, PhD
Professor of Physics

20. DISTRIBUTION/AVAILABILITY OF ABSTRACT ☐ UNCLASSIFIED/UNLIMITED ☒ SAME AS RPT. ☐ DTIC USERS	21. ABSTRACT SECURITY CLASSIFICATION UNCLASSIFIED
22a. NAME OF RESPONSIBLE INDIVIDUAL Yung Kee Yeo, PhD	22b. TELEPHONE (*Include Area Code*) (513)255-2012 22c. OFFICE SYMBOL AFIT/ENP

Above and below bandgap excitation studies were performed on GaAs samples implanted with Ge, {Ge+Ga}, and {Ge+As} to characterize the nature of impurities and defects associated with the incorporation of Ge.

The above-gap excitation luminescence of Ge-only and {Ge+Ga}-implanted layers was seen to be critically dose-dependent. At doses of 1E13–3E13 cm^{-2}, a broad band dominated the luminescence spectrum in the 1.47–1.42 eV range, and it was assigned as the Q band. At higher doses (1E14–1E15 cm^{-2}), however, the Q band was no longer observed for the Ge-only implanted samples, whereas evidence for transitions involving the Ga_{As} double acceptor at $\sim$1.445 eV was collected for the {Ge+Ga}-implanted samples. The luminescence resulting from {Ge+As} dual implanted samples showed neither the Q band nor the Ga_{As}-related transitions.

Below-gap excitation, in conjunction with temperature-dependent studies, enabled resolution of the broad Q band into high- and low-energy components, which peaked at $\sim$ 1.457 and 1.447 eV, respectively. The luminescence was described according to a close (D°, A°) pairs model. This newly derived model assumed that the relatively strong binding energy of the Ga_{As} double acceptor allowed increased numbers of (D°, Ga_{As}) transitions to occur amongst relatively close pairs. Thus, the (D°, Ga_{As}) pair luminescence was able to take place over a sufficiently broad energy range such that its peak (at $\sim$1.457 eV) could, in fact, occur at higher energy than the (e, Ga_{As}) luminescence (which peaked in the vicinity of 1.447 eV).

The study provided new evidence for the Ga_{As} double acceptor's major role in the creation of the Q band in Ge-implanted GaAs. In addition, the atypical relative spectral positions of the (D°, Ga_{As}) and (e, Ga_{As}) transitions were explained using a close pairs model.